Electronic Deactivation Dynamics of DNA Model Systems and Solvation Dynamics of a Natural Antioxidant by Femtosecond Fluorescence and Absorption Spectroscopy

Dissertation
zur Erlangung des Doktorgrades
der Mathematisch-Naturwissenschaftlichen Fakultät
der Christian-Albrechts-Universität zu Kiel

vorgelegt von
Mayra Christina Stuhldreier

Institut für Physikalische Chemie
der Christian-Albrechts-Universität zu Kiel

Kiel, im Mai 2013

Erster Gutachter:	Prof. Dr. Friedrich Temps
Zweiter Gutachter:	Prof. Dr. Bernd Hartke
Tag der mündlichen Prüfung:	2. Juli 2013
Zum Druck genehmigt:	2. Juli 2013

gez. Prof. Dr. Wolfgang J. Duschl, Dekan

Erklärung

Hiermit erkläre ich an Eides Statt, dass die vorliegende Abhandlung - abgesehen von der Beratung durch meinen Betreuer Prof. Dr. Friedrich Temps - nach Inhalt und Form meine eigene Arbeit ist.

Diese Arbeit hat weder in Auszügen noch in ganzer Form einer anderen Stelle im Rahmen eines Prüfungsverfahrens vorgelegen. Sie wurde in ihrer Gesamtheit nicht veröffentlicht und auch nicht zur Veröffentlichung eingereicht.

Teile dieser Arbeit wurden in fachwissenschaftlichen Zeitschriften veröffentlicht. Dies bezieht sich auf die folgenden Kapitel:

Kapitel 3
Mayra Stuhldreier, Carmen Schüler, Joscha Kleber, and Friedrich Temps, Femtosecond Fluorescence Measurements of the Adenine Dinucleotide: Direct Observation of the Excimer State, *Ultrafast Phenomena XVII*, pp. 553 – 555, M. Chergui, D. M. Jonas, E. Riedle, R. W. Schoenlein, A. J. Taylor (Eds.), Oxford University Press, New York, U.S.A., **2011**.

Kapitel 5
Mayra C. Stuhldreier and Friedrich Temps, Ultrafast Photo-Initiated Molecular Quantum Dynamics in the DNA Dinucleotide d(ApG) Revealed by Broadband Transient Absorption Spectroscopy, *Faraday Disc., doi:10.1039/C3FD00003F*, **2013**.

Die Arbeit ist unter Einhaltung der Regeln guter wissenschaftlicher Praxis der Deutschen Forschungsgemeinschaft entstanden.

Kiel, im Mai 2013

Mayra Stuhldreier

Abstract

In the first part of the present Thesis, femtosecond time-resolved transient absorption and fluorescence investigations on small DNA building blocks have been performed to disentangle the contributions and interplay of π-stacking, hydrogen bonding and base sequence to the overall electronic deactivation dynamics of natural DNA strands. The influence of base stacking interactions and base sequence was studied with two of the simplest possible model systems, the adenine homo-dinucleotide d(ApA) and the hetero-dinucleotide d(ApG). The deactivation dynamics differ substantially from those of the constituent monomers and showcase an intricate hierarchy of dynamical processes on vastly differing time scales, from $\tau \lesssim 100$ fs, *via* $\tau = 0.30 - 0.40$ ps and $\tau \approx 6 - 8$ ps, to $\tau > 100$ ps. This led to a comprehensive picture for the overall electronic deactivation dynamics from the population of the initially excited bright $\pi\pi^*$ states *via* relaxed Franck-Condon states to either 'perturbed-monomer-like' dynamics or a long-lived excimer state back to the electronic ground state. For d(ApA), the excimer state exhibits a longer lifetime than that found for d(ApG) ($\tau = 380 \pm 40$ ps *vs.* $\tau = 124 \pm 4$ ps), possibly due to imperfect orbital overlap in the hetero-dinucleotide. Of special interest is the identification of a spectral feature associated with the long-lived excimer state for both dinucleotides, namely a narrow excited-state absorption band around $\lambda \approx 340$ nm.

The short oligonucleotide hairpin d[5'-GpGpGp-HEG-pCpCpC-3'] served as model system to investigate the influence of hydrogen bonding on the excited-state lifetime of DNA base pairs and double strands. This self-complementary DNA loop forms a stable, albeit quite flexible B-DNA double helix in aqueous solution, which was confirmed by a thorough NMR study together with static absorption, fluorescence and circular dichroism spectroscopy and molecular mechanics simulations. Hydrogen-bonding seems to lead to a new excited-state deactivation pathway through which the molecule returns to the ground state even faster than its constituent trimers, as confirmed by femtosecond fluorescence spectroscopy.

The shorter second part of this Thesis deals with the ultrafast solvation dynamics of the natural antioxidant ferulic acid. The influence of steric restraints, modelled by embedding the molecular probe into the palisade layer of micelles leads to an alteration of the electronic deactivation pathways. On the one hand, the fluorescence lifetime at the micellar surface is prolonged compared to that found for FA bulk water ($\tau = 33 \pm 7$ ps *vs.* $\tau = 19 \pm 2$ ps). This finding may be rationalised by assuming an electronic deactivation pathway involving the $E \rightarrow Z$ isomerisation of the vinylic double bond. On the other hand, the initial as well as the overall solvation dynamics monitored by time-dependent Stokes shift are decelerated in a constrained environment. Most likely, the mobility of the water molecules is hindered by electrostatic interactions with the polar headgroups of emulsifier molecules.

Zusammenfassung

Im ersten Teil der vorliegenden Dissertation wurde die ultraschnelle elektronische Desaktivierung von kleinen DNS-Bausteinen mithilfe Femtosekunden-zeitaufgelöster Absorptions- und Fluoreszenzspektroskopie verfolgt, um den Einfluss von π-Stapel-Wechselwirkungen, Wasserstoffbrücken und Basensequenz auf die angeregten elektronischen Zustände und Desaktivierungsmechanismen natürlicher DNS-Stränge zu untersuchen. Der Effekt von Basenstapel-Wechselwirkungen sowie der Basensequenz wurde mithilfe der beiden einfachen Modellsysteme d(ApA) und d(ApG) analysiert. Deren Desaktivierungsmechanismen unterscheiden sich grundlegend von denen der jeweiligen Monomere und zeigen eine komplexe Abfolge dynamischer Prozesse, deren Zeitskalen von $\tau \lesssim 100$ fs über $\tau = 0.30 - 0.40$ ps und $\tau \approx 6 - 8$ ps bis hin zu $\tau > 100$ ps reichen. Daraus ergab sich ein weitgehend vollständiges Bild der elektronischen Desaktivierungspfade von den zunächst bevölkerten optisch hellen $\pi\pi^*$ Zuständen über relaxierte Franck-Condon Zustände bis hin zu entweder „verzerrt-monomerartiger“ Desaktivierung oder zu einem stabilen Excimer-Zustand. Dieser ist für d(ApA) langlebiger als für d(ApG) ($\tau = 380 \pm 40$ ps *vs.* $\tau = 124 \pm 4$ ps), vermutlich da im Hetero-Dinukleotid kein idealer Orbitalüberlapp möglich ist. Von besonderem Interesse ist die Beobachtung einer schmalen transienten Absorptionsbande der langlebigen Excimer-Zustände bei $\lambda \approx 340$ nm für beide Dinukleotide.

Das kurze Oligonukleotid d[5'-GpGpGp-HEG-pCpCpC-3'] erlaubte die Untersuchung des Einflusses von Wasserstoffbrücken auf die Lebenszeit des elektronisch angeregten Zustands von DNS Basenpaaren und Doppelsträngen. Dieses selbstkomplementäre Molekül liegt in wässriger Lösung als stabile, wenn auch flexible B-DNS Doppelhelix vor. Die Struktur wurde durch eine gründliche NMR-spektroskopische Untersuchung sowie statische Absorptions-, Fluoreszenz- und Zirkulardichroismus-Messungen und Molekularmechanik-Simulationen bestätigt. Zeitaufgelöste Fluoreszenzdaten lassen darauf schließen, dass Wasserstoffbrücken-Bindungen möglicherweise zu einem neuen Desaktivierungspfad im elektronisch angeregten Zustand führen, durch welchen das selbstkomplementäre Oligonukleotid schneller in den Grundzustand zurückkehren kann als seine Einzelbausteine.

Der zweite Teil der Dissertation beschäftigt sich mit der ultraschnellen Solvatationsdynamik des natürlichen Antioxidans Ferulasäure. Sterische Beschränkungen, die durch Einbringen des Moleküls in die Palisadenschicht von Mizellen realisiert wurden, änderten die elektronischen Desaktivierungspfade. Einerseits verlängerte sich die Fluoreszenz-Lebenszeit an der Mizellenoberfläche verglichen mit der in reinem Wasser ($\tau = 33 \pm 7$ ps *vs.* $\tau = 19 \pm 2$ ps). Dieser Effekt kann dadurch erklärt werden, dass die elektronische Desaktivierung mit der $E \rightarrow Z$ Isomerisierung der Seitenketten-Doppelbindung einhergeht. Andererseits werden an der Mizellenoberfläche sowohl die anfängliche als als die Gesamt-Solvatationsdynamik verlangsamt. Dies ist wahrscheinlich darauf zurückzuführen, dass die Wassermoleküle durch elektrostatische Wechselwirkungen mit den polaren Kopfgruppen der Tensidmoleküle in ihrer Bewegung gehindert sind.

Contents

List of Figures

List of Tables

1

Introduction

The main focus of this Thesis lies on the ultrafast deactivation dynamics of small DNA building blocks. In this Chapter, a short introduction to the conformational structure of DNA molecules and consequently their model building blocks will be given. This part will be followed by a more detailed summary of former work, both experimentally and theoretically, on the ultrafast deactivation dynamics of DNA monomers and small multimers. Special attention will be paid to the influence of hydrogen bonding and the controversial discussion about the nature and extent of π-stacking interactions to the overall electronic deactivation dynamics, as these two topics are closely related to the model systems which were investigated throughout this Thesis. As the influence of a water solvent shell around biomolecules has to be considered to understand their dynamics in aqueous solution, a second part of the present Thesis deals with the ultrafast solvation dynamics of a natural antioxidant. A brief summary is given of the theoretical background of both solvation dynamics and the investigated molecule ferulic acid in a micellar environment.

1.1 Structural Properties of DNA

As the encoder of the genetic information of life,[1,2] deoxyribonucleic acid (DNA) has been studied extensively for the last decades. DNA is a huge biopolymer which generally exists as a double-stranded helix, whereupon the two constituent single strands are composed of four monomers, the nucleobases, attached to a deoxyribose-phosphate backbone. Each of the nucleobases pairs with a specific partner *via* hydrogen bonds, thus forming a double helix of two complementary single strands (see Figure 1.1). The sequence of nucleobases within a DNA strands carries the genetic information and may be read out and converted to proteins *via* the processes of transcription and translation. Details of these highly

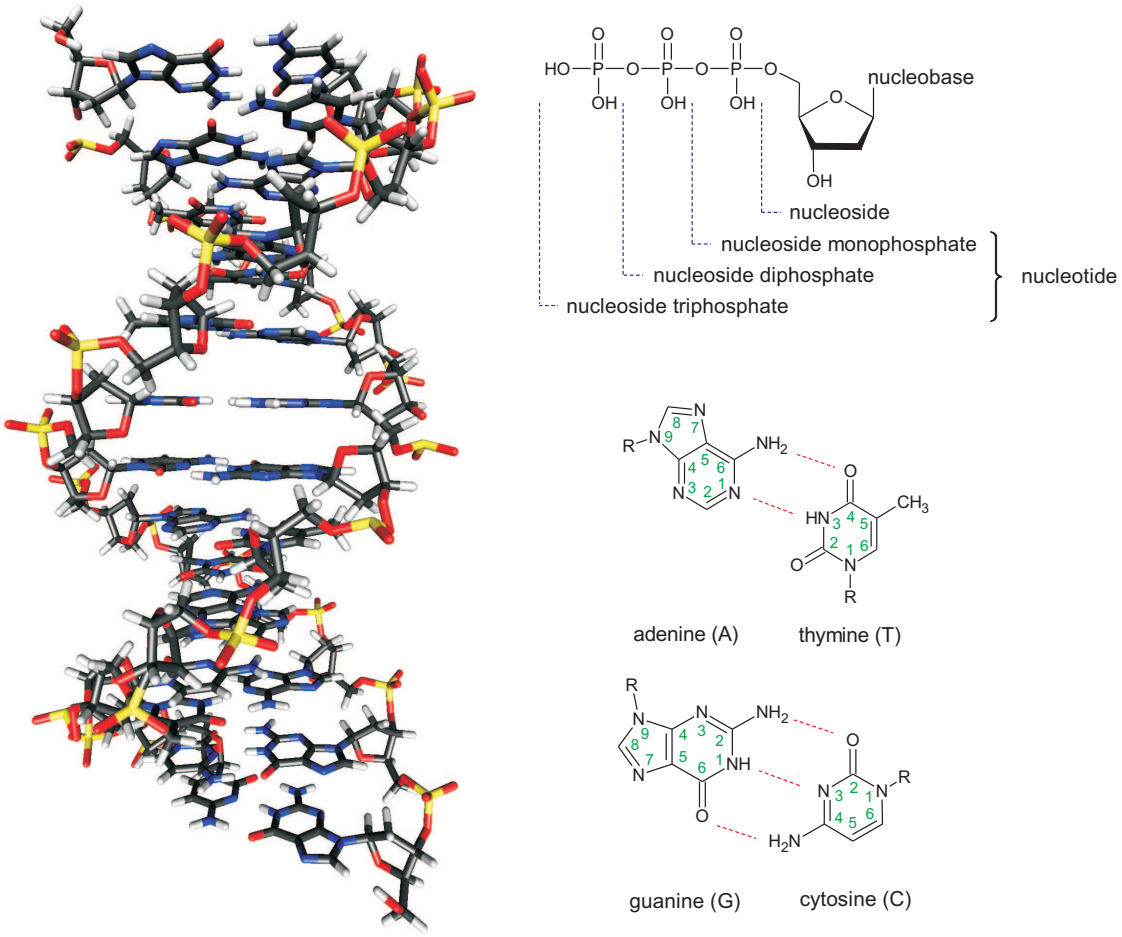

Fig. 1.1: Left: Structure of a B-DNA double stranded helix. The two single strands are connected *via* hydrogen bonds between the constituent nucleobases. Upper right corner: Generalised molecular structure of DNA nucleosides and nucleotides. Lower right corner: Base pairing geometry and atom numbering of the four DNA nucleobases, R stands for the deoxyribose-phosphate backbone.

complex processes can be found in common biochemistry textbooks.[3,4]

In Figure 1.1, the physiologically most common conformation of DNA strands is displayed, the so-called B-DNA form. Dependent on counter cation type and concentration, solvent, temperature and base sequence, other helical motifs are possible, namely the A- and Z-form.[5,6] Whereas Z-DNA is conformationally well-defined and relatively rigid, it has to be kept in mind that the A- and B-family themselves possess a high, sequence-dependent conformational variability.[7] These helical conformations may also be adopted by single strands. If the deoxyribose in the sugar-phosphate backbone is replaced by ribose, ribonucleic acid (RNA) emerges. This biomolecule, which generally is single-stranded, features the nucleobase monomer uracil instead of thymine. The hydroxy group in 2' position of the sugar ring hinders the formation of a B-type helix, but allows for an A-type helical form and rarely the Z-conformation. RNA often adopts other secondary structures such as hairpins and loops. For a detailed insight into the structural properties of DNA and RNA

molecules, see standard biochemistry textbooks.[3,5,6] Under the experimental conditions throughout this Thesis, only the B-DNA helix conformation matters. A powerful and at the same time straightforward tool to determine the geometrical structure of DNA/RNA is circular dichroism (CD) spectroscopy.[8–14] CD spectra are conformation-sensitive, and they can be calculated theoretically from a proposed structure.[15] This even allows for the determination of structural parameters such as helical angles.[16] Although CD spectroscopy is the appropriate method to determine the overall helix conformation of large oligonucleotides in solution, it cannot reach the precision of nuclear magnetic resonance (NMR) spectroscopy. Proton-proton coupling through bonds and space is revealed by 2D-^{1}H-NMR spectra and allows for exact structural determination of the solution conformation and even structural dynamics on a time scale of milliseconds. An outstanding example is the investigation of structure, dynamics and interactions of G-quadruplexes in a number of biologically important conformations.[17,18] However, disentangling the complex coupling patterns for oligonucleotides is challenging and often only achieved by site-specific deuteration of the investigated macromolecule.[17–20] Furthermore, ^{13}C- and ^{15}N-NMR spectroscopy provides even deeper insight in the structure of the DNA backbone. The respective studies are complicated by the low natural occurrences of this NMR-active isotopes, unless they are artificially enriched in the investigated sample.

The nucleobase monomers are planar chromophores with a delocalised π-system over the heterocyclic aromatic ring system, they consequently absorb UV light. Astonishingly, DNA possesses an exceptional high photostability after being exposed to UV radiation as in sunlight. This is partly explained by efficient cellular repair mechanisms after photodamage has taken place, but is largely due to inherent molecular properties of the constituent nucleobases.[21] Despite being excited to higher electronic states after UV absorption, the molecules dissipate the absorbed energy very fast *via* non-radiative decay mechanisms. This is reflected by the very low fluorescence quantum yields of nucleobase monomers of $\approx 10^{-4}$.[22–24] The observation of these extremely short excited-state lifetimes in real time only became possible about 15 years ago after the development of femtosecond laser sources.[21] A. Zewail is known as the pioneer in their application in pump-probe spectroscopy and received the Nobel Prize in chemistry for his work in 1999.[25–28]

However, the excited-state dynamics change dramatically when going from single nucleobases over small building blocks to natural DNA strands. Two review articles in 2004 and 2009 give an extensive overview over experimental and theoretical work on DNA single nucleobases and small DNA multimers.[21,29] In the following, a short summary on the deactivation dynamics of the nucleoside monomers and small multimers according to literature is given. A more detailed discussion with regard to the experimental results obtained in this Thesis can be found in the Chapters 4, 5 and 6.

In principle, nucleobases can exist in different tautomers. However, in the natural DNA double helix the nucleobase chromophores are connected to the sugar-phosphate backbone *via* an *N*-glycosidic bond, thus tautomers involving the connecting nitrogen atom are not

present. The pyrimidine bases cytosine, thymine and uracil are attached *via* the N^1-atom, the purine bases adenine and guanine *via* the N^9-atom. This is especially important for adenine, which exists in two tautomeric forms in aqueous solution, namely $7H$-adenine and $9H$-adenine. The $9H$-tautomer corresponds to the physiologically important nucleoside/nucleotide, in aqueous solution at room temperature its fraction is about 78%.[30,31] In the following chapters, only the biologically relevant (canonical) tautomers will be discussed. Since the canonical tautomers, DNA and RNA nucleosides and nucleotides show similar excited-state behaviour, they will be summarised where appropriate.

1.2 Single Nucleobases

The five natural single nucleobases possess very short excited-state lifetimes (a few hundreds of femtoseconds) after photo-excitation. Due to their size they are accessible to theoretical calculations and they have been extensively studied experimentally. For $9H$-adenine, the deactivation pathway has been investigated theoretically in detail and seems to be generally agreed upon.[32–45] The first three excited states are found to possess $n\pi^*$, $\pi\pi^*(L_b)$ and $\pi\pi^*(L_a)$ character, whereupon the latter carries most of the oscillator strength from S_0. The exact ordering of the states is disputed and changes when going from the gas phase to aqueous solution. In particular, the $n\pi^*$ state is less well stabilised in a polar environment and lies energetically higher than or between the $\pi\pi^*$ states at vertical excitation.[32,42] Directly after photo-excitation to the $\pi\pi^*(L_a)$ state, the wavepacket leaves the Franck-Condon region within $\tau \leq 0.1$ ps.[24,46–48] In gas phase calculations, deactivation pathways include conical intersections (CI) between $\pi\pi^*(L_a)/\pi\pi^*(L_b)$, $\pi\pi^*(L_a)/n\pi^*$ and even $\pi\pi^*(L_a)/\pi\sigma^*$. The molecule eventually returns to the ground state through two CIs, either $(\pi\pi^*(L_a)/gs)_{CI}$ or $(n\pi^*/gs)_{CI}$. The $(\pi\pi^*(L_a)/gs)_{CI}$ is characterised by a ring puckering at C^2, the $(n\pi^*/gs)_{CI}$ features a molecular geometry where the C^6 atom together with the NH_2 group is bent out-of-plane.[32–40,49] In aqueous solution, the direct pathway without crossing any states other than the initially excited $\pi\pi^*(L_a)$ is widely assumed to be the most common electronic deactivation and takes place within $\tau \approx 0.3 - 0.4$ ps.[24,31,32,44–47,50] Yamazaki *et al.* found the $\pi\pi^*(L_a)$ and $\pi\pi^*(L_b)$ state to be strongly vibronically coupled in aqueous solution, thus the direct deactivation *via* $(\pi\pi^*(L_a)/gs)_{CI}$ becomes dominant and the energetically blue-shifted pathway involving the $n\pi^*$ state is suppressed.[44] In contrast, Lan *et al.* performed QM/MM simulations of $9H$-adenine in solution. They found excitation into both $\pi\pi^*(L_a)$ and $n\pi^*$ to contribute to the absorption band, followed by a step-wise relaxation $\pi\pi^*(L_a) \rightarrow n\pi^* \rightarrow gs$. The respective deactivation times are $\tau_{La \rightarrow n\pi^*} = 40$ fs and $\tau_{n\pi^* \rightarrow gs} = 410$ fs.[49] Photoelectron and photoion spectroscopy on adenine in water clusters suggested the direct $\pi\pi^*(L_a) \rightarrow gs$ pathway to compete with a step-wise deactivation including the $n\pi^*$ state like in the isolated base.[41] Subsequent vibrational cooling of molecules returning to the ground state with a high amount of excess energy is completed in only a few picoseconds in aqueous solution.[51]

The second purine base guanine shows very similar excited-state dynamics.[45,52–60] As was discussed for 9*H*-adenine, the first three excited states possess $\pi\pi^*(L_a)$, $n\pi^*$ and $\pi\pi^*(L_b)$ character. Both $\pi\pi^*$ states carry similar oscillator strengths from S_0 at wavelengths $\lambda \leq 267$ nm, which leads to two spectrally resolved UV absorption bands. The ensuing photodynamics include a fast, barrierless deactivation from $\pi\pi^*(L_a)$ *via* a conical intersection with the ground state. The molecular geometry at $(\pi\pi^*(L_a)/gs)_{CI}$ resembles the one found for the respective CI in adenine, namely a deformation of the six-membered ring *via* puckering at C^2 and bending of the amino group. A second, slower deactivation pathway involves a transition to the $n\pi^*$ state, from where the molecule may reach a conical intersection $(n\pi^*/gs)_{CI}$ after passing a small energy barrier. The molecular geometry at $(n\pi^*/gs)_{CI}$ again resembles that found for adenine, the C^6 atom is puckered out-of-plane and the oxygen atom stands perpendicular to the ring.[52,54,56,58,59] The guanine molecule may also return to the $\pi\pi^*(L_a)$ state *via* $(n\pi^*/\pi\pi^*(L_a))_{CI}$ and than follow the above mentioned deactivation pathway through $(\pi\pi^*(L_a)/gs)_{CI}$. The experimentally observed time constants are $\tau \approx 0.15 - 0.3$ ps and $\tau \approx 0.4 - 1.3$ ps, respectively, whereas the fast component could not always be observed due to the experimental time resolution.[24,50,53,55,61–64] In summary, the electronic deactivation pathways and CI geometries closely resemble those of adenine, the most pronounced difference lies in the longer lifetime of guanine. Due to the more planar $\pi\pi^*(L_a)$ surface of the latter, the excited-state population sort of 'spreads out', thus leading to a more complex and slower deactivation.[53,55,57] Again an aqueous environment suppresses the deactivation pathways involving the $n\pi^*$ state.[60] The vibrational cooling in the ground state is completed in only a few picoseconds in aqueous solution.[55]

The picture for the pyrimidine base cytosine seems somewhat less clear. The main pathway on the surface of the initially excited $\pi\pi^*$ state towards a conical intersection with the ground state is assumed to be fairly barrierless, although including a shallow minimum, and accounts for a *sub*-picosecond decay channel.[65–72] The conical intersection, through which the excited-state population quickly returns to the ground state may also be a three-state CI, caused by degeneracy of a $\pi\pi^*$, a $n\pi^*$ and the ground state.[69,70,72,73] Experimentally, a monoexponential decay with $\tau \approx 0.5 - 1$ ps or a biexponential behaviour with $\tau \approx 0.2$ ps and $\tau \approx 1 - 2$ ps was observed and may be attributed to this deactivation pathway.[24,50,61,63,74–78] Zgierski *et al.* propose the $(\pi\pi^*/gs)_{CI}$ to possess a biradical character and a ring-distorted geometry, where C^5 and C^6 are both bent out-of-plane, one above and one below the ring plane.[79–81] A CI with a C^5-C^6 twist geometry, also called ethylenic CI, was also found by other authors, but the biradical character was not confirmed.[65,68,71,82] Blancafort *et al.*, however, observed a zwitterionic nature for the ethylenic CI.[83] A second conical intersection of the $\pi\pi^*$ state with the ground state has been found to show a 'sofa' geometry, where the N^3 atom is displaced out-of-plane.[68,84] In some femtosecond time-resolved experiments, a contribution with $\tau \approx 20 - 30$ ps was found to add to the overall decay dynamics of cytosine.[75,76] Regarding theoretical inves-

tigations, there is some reluctance in assigning such a long-lived contribution to a specific deactivation channel. One possibility is the population of a $n\pi^*$ state with a shallow minimum *via* a $(\pi\pi^*/n\pi^*)_{CI}$.[66,85] Furthermore, a triplet state may play a role in the electronic deactivation.[67,75,86] In the vicinity of the shallow minimum on $\pi\pi^*(S_1)$, a S_1/T_1 degeneracy region is supposed to allow intersystem crossing (ISC) to a triplet state with $^3\pi\pi^*$ character.[67] This close degeneracy leads to very efficient ISC within tens of femtoseconds, which therefore competes successfully with the spin-conserving internal conversion pathway.[86] It might be speculated that an aqueous environment shortens the excited-state lifetime, as the shallow barrier towards the ethylenic CI is lowered, due to its zwitterionic character. Additionally, the assumed $n\pi^*$ deactivation pathway is found to be destabilised in water, although still accessible,[83] as the $n\pi^*$ state is shifted above the $\pi\pi^*$ states upon solvation.[87] On the other hand, no preference for one of the pathways including either 'sofa' or 'twist' CI upon water solvation could be detected.[88]

The fourth nucleobase thymine shows the longest gas-phase excited-state lifetime of the four DNA bases. Experiments in aqueous solution report a biexponential decay behaviour with $\tau \approx 0.1 - 0.2$ ps and $\tau \approx 1$ ps, whereupon in some cases the fast component was not observed, probably due to poor time resolution.[24,50,63,89–92] On the other hand, Hare *et al.* observed $\tau \approx 0.4 - 0.7$ ps, $\tau \approx 2 - 3$ ps, and $\tau \approx 30 - 130$ ps with transient absorption measurements of thymine and TMP in aqueous solution.[75] In the gas phase the deactivation dynamics feature three contributions with $\tau \approx 0.1 - 0.2$ ps, $\tau \approx 5$ ps, and $\tau \approx 300$ ns.[61,62,93,94] From a theoretical point of view, two major deactivation pathways for thymine in the gas phase seem to be generally accepted.[65,71,95–103] After excitation to the S_2 state with $\pi\pi^*$ character, the molecule may deactivate directly or *via* an $n\pi^*$ intermediate. The direct pathway on the $\pi\pi^*$ surface towards a $(\pi\pi^*/gs)_{CI}$ passes a flat region, or even a shallow minimum, which contributes to the picosecond decay channel.[97–99,104] The $(\pi\pi^*/gs)_{CI}$ is characterised by a ring distortion and the C^5-methyl group standing perpendicular to the ring plane.[95,99,101,102] The indirect pathway follows a step-wise relaxation from $\pi\pi^*$ *via* $(\pi\pi^*/n\pi^*)_{CI}$ to $n\pi^*$ and finally to the electronic ground state *via* $(n\pi^*/gs)_{CI}$. The latter conical intersection again shows a ring-distorted geometry, with the methyl group slightly bent out-of-plane.[95,99,101,102] The $n\pi^*$ state, which is populated in ≤ 1 ps is found to be a precursor state to a triplet state with $^3\pi\pi^*$ character.[75,100,105] In contrast to the other three DNA nucleobases, the triplet state plays a significant role in the electronic dynamics of thymine. The most common DNA photolesion, the formation of a cyclopyrimidine dimer (CPD) between two neighbouring thymine chromophores, is assumed to take place from either the singlet $n\pi^*$ state[106,107] or the $^3\pi\pi^*$ T_1 state.[89] In both cases the pre-orientation of the two thymine moieties in the electronic ground state is crucial for the CPD yield.[106–111] As well the triplet state as the $n\pi^*$ population is quenched in aqueous solution, thus leading to a decrease in excited-state lifetime and CPD formation and consequently to an increased photostability.[94,95,112]

In summary, it can be stated that all five naturally occurring nucleobases exhibit barri-

erless, or nearly barrierless, pathways from the initially excited bright $\pi\pi^*$ states back to the ground state and therefore short excited-state lifetimes, whereas nucleobase isomers or slightly modified nucleobases display energy barriers along this path.[113]

1.3 Hydrogen Bonded Nucleobase Pairs

As mentioned above, hydrogen bonds between nucleobases allow for the formation and stability of the DNA double helical structure. The two strands are held together by the selective pairing patterns A·T (two hydrogen bonds) and G·C (three hydrogen bonds).[114,115] The photodynamics are significantly affected by hydrogen bonding, as the 'sharing' of an H atom between two nucleobases naturally influences the excited electronic states. Of course, nucleobases as heterocyclic ring system with a number of accepting (O, N) and donating (OH, NH) atoms may form a huge number of homo- and heterodimers with different geometries, and even larger assemblies such as ribbons.[116–122] Nucleobase-water complexes, formed by hydrogen-bonding of the investigated bases to one or several water molecules, already alter the electronic deactivation dynamics of single nucleobases significantly (see Section 1.2). They mainly lead to a reordering of the excited states and often to a shorter excited-state lifetime. Usually, the direct $\pi\pi^*$ pathway becomes dominant in aqueous solution. In the following, a short comment on the photodynamics of natural occurring base pairs with Watson-Crick (WC) conformation will be given. The Watson-Crick base pairing geometry is shown in Figure 1.1.

The Watson-Crick G·C base pair shows a very fast electronic deactivation time after photo-excitation.[123–125] Theoretical investigations assigned this to the possibility of an interbase electron-driven proton-transfer (EDPT), which opens a barrierless pathway from the initially excited $\pi\pi^*$ state to the ground state.[126–130] In particular, an electron from the highest occupied molecular orbital (HOMO) of the photo-excited guanine is transferred to the lowest unoccupied molecular orbital (LUMO) of cytosine, directly followed by a proton transfer from G-N^{1}H to C-N^3 (middle hydrogen bond). Thus, the charge transfer (CT) state is stabilised and the molecule can follow a barrierless pathway towards a conical intersection of the CT state with $\pi\pi^*$ character with the ground state. After passing the $(\pi\pi^*(\mathrm{CT})/\mathrm{gs})_{\mathrm{CI}}$, electron and proton are transferred back to guanine. This happens faster than the intrabase deactivation processes, possibly on the time scale of $\tau = 0.3$ ps.[124,125,128] The same picture was recently found for the 8-oxo-G·C base pair with WC conformation.[131] In contrast, Biemann *et al.* did not find any evidence of this EDPT after photo-excitation, they claimed that the deactivation occurs *via* 'monomer' pathways. However, they excited the base pair with $\lambda_{\mathrm{pump}} = 284$ nm, which results mainly in photo-excitation of cytosine. As the EDPT process described above starts from guanine, this may explain the only small differences between base pair and constituent monomers. Moreover, recent experimental data reported in another transient absorption study at the CAU Kiel found evidence for the formation of an intermediate (G-H)$^\bullet$·(C+H)$^\bullet$ radical state, which

supports the assumption of an EDPT deactivation pathway.[132]

For A·T the picture is less clear, as not much work has been performed on this base pair. Femtosecond time-resolved ionisation in the gas phase suggested that only intrabase deactivation mechanism play a role after photo-excitation.[133] Tentatively a $\tau \approx 40$ ps component observed for the A·T base pair and the T·T homodimer was assigned to some sort of proton transfer reaction channel. However, these findings should not be valued too high, as the experiments were performed in the gas phase where the Watson-Crick pairing geometry is not the energetically lowest. Perun *et al.* on the other hand investigated the A·T base pair in WC and non-WC conformation theoretically and suggest a deactivation pathway including a CT state and possibly an EDPT proton transfer.[134] The investigated non-WC conformation was the most stable (MS) in the gas phase. After photo-excitation to a bright $\pi\pi^*$ state, the excited-state dynamics of both base pairs include conical intersections to a $n\pi^*$ state and a CT state with $\pi\pi^*$ character. The CT state is characterised by electron transfer from A to T and can be stabilised by a subsequent proton transfer from A-N^6H $\rightarrow$ T-O^4 (WC) or A-N^9H $\rightarrow$ T-O^2 (MS). Along the A-NH stretching mode, a barrierless pathway towards a conical intersection of the CT state with the ground state allows for an ultrafast deactivation for the WC base pair. Remarkably, in the MS conformation this pathway is not accessible, no $(\pi\pi^*(\mathrm{CT})/\mathrm{gs})_{\mathrm{CI}}$ was found along the A-NH stretching mode. The pathway for the WC A·T base pair was confirmed by CASSCF/CASPT2 calculations recently.[135]

The general importance of the EDPT process in electronic deactivation processes is further supported by theoretical investigations of the 2-aminopyridine homodimer[136–140] and short polypeptides.[141] They also revealed a deactivation process which includes the population of a CT state stabilised by a single proton transfer (SPT) out of the initially excited $\pi\pi^*$ state, and a subsequent electron and proton back transfer process when returning to the ground state. The corresponding excited-state lifetimes decreased considerably.

Between two pairing nucleobases in electronically excited states, a double proton transfer (DPT) may occur, which is not feasible in the electronic ground state.[130] This leads to a non-WC conformation, or the pairing of non-canonical nucleobase tautomers and can eventually lead to DNA photolesions. The energetic barriers leading to such a DPT are significantly higher than those for SPT, thus DPT processes are not supposed to play an important role in electronic deactivation dynamics.[142]

To summarise, base pairing *via* hydrogen bonds influences the electronic deactivation dynamics in DNA double strands. It has been speculated that this may mainly be due to the fixation of the chromophores, inhibiting the ring puckering modes connected with barrierless deactivation pathways.[143] However, the investigations summarised above suggest that this point of view is oversimplified. Regarding the fixation of nucleobase chromophores, it should be carefully considered whether base stacking or hydrogen bonding, which both lock the nucleobase geometry in a DNA strands, are responsible for altered excited-state

deactivation dynamics, and to which extent.

1.4 π-Stacking Interactions

When going from the single nucleobases to longer DNA single and double strands, the excited-state lifetimes increase by several orders of magnitude.[144–148] This effect is mainly due to π-stacking interactions of the aromatic ring systems of the nucleobase chromophores, whose delocalised π-electron clouds above and below the ring plane overlap partially. In Figure 1.2, the base stacking geometry in a $d(A)_4$ strand with B-DNA helical geometry is shown, whereupon the adenine subunits are coloured and the sugar-phosphate backbone is shown in dark grey. The depicted B-DNA helical structure naturally exhibits a quite different amount of overlap compared with, e.g., A- and Z-DNA due to differences in the interbase distance, helical diameter and helical winding angle. It is immediately obvious that the overlap and therefore the amount of π-stacking is highly sensitive to the overall strand conformation, which is quite flexible - especially for short oligonucleotides and DNA single strands.

Fig. 1.2: Structure of a $d(A)_4$ single strand from a sideways view (left) and the top view along the helical axis (right). The adenine subunits are coloured, the sugar-phosphate backbone is depicted in dark grey.

The huge influence of π-stacking between adjacent nucleobases on the excited electronic states has been observed and discussed already in the $1960-1980$s based on static emission spectra.[149,150,150–156] In particular, emission after UV excitation of dinucleotides and, to a lesser extent, of DNA strands was hugely red-shifted compared to single nucleobases or nucleotides. This red-shifted fluorescence was attributed to originate from a base-stacked excimer state.[149–157] In this context, Daniels *et al.* found the excimer fluorescence of ApC and CpA to differ considerably.[156] This observation can be rationalised from the geometrical implications of the right-handed B-DNA helix, which lead to base-sequence dependent differences of the π-overlap extent. Optical rotatory dispersion (ORD)[158–160]

and circular dichroism (CD) spectra[160,161] of all possible DNA and RNA dinucleotides also observed base stacking and confirm the sequence dependence of excimer formation. The connection between the two subunits may be ruptured by protonation of the dinucleotide, which leads to coulombic repulsion, de-stacking and finally monomer-like static emission spectra[149] and excited-state lifetimes.[162]

However, within the last decade an intense debate about the experimentally observed long-lived electronically excited states states in π-stacked oligonucleotides upon UV excitation arose.[29,145–148,163–171] The current discussion is nicely summarised in a recent review article, which addresses the nature and extent of electronic coupling between nucleobases, especially in the initially excited bright states.[172] Two major points of view regarding the assignment of the observed long-lived states can be distinguished. On the one hand, a Frenkel exciton[173,174] model is assumed, where the delocalisation spreads over several adjacent nucleobases.[146,147,163–167] On the other hand, the formation of excimer states which consist of only two nucleobases sharing the UV excitation energy is postulated, possibly with a (partial) CT character.[29,145,148,168–171] These two pictures are hard to reconcile. The implications of both approaches with a focus on the adenine dinucleotide are summarised in more detail in Chapter 4.

In a nutshell, the differences between the exciton and the excimer model can be summarised as follows: A Frenkel exciton consists of an electron-hole pair created by the UV excitation energy, which may move freely over several adjacent nucleobases in an oligonucleotide strand.[167] Its delocalisation length is limited by imperfections in the molecular succession, in DNA these result mainly from structural fluctuations. In contrast, an excimer (*exci*ted di*mer*) describes the case of attraction of two subunits in the excited electronic state, whereas there is no association in the electronic ground state. It has to be noted that throughout this Thesis the term 'excimer' will be used for both homo- and heterodimers. Strictly speaking, the latter are denoted as 'exciplex' (*exci*ted du*plex*), but this is mainly due to historic reasons and the important characteristics and properties of excimers and exciplexes are the same. In the electronically excited state, the two subunits are bound due to shared electron density and are closer than in the ground state. The stability of a nucleobase excimer is highly dependent on the relative conformation of the two monomers.[171] The data obtained in the present Thesis for the dinucleotides d(ApA) and d(ApG) support the excimer model (cf. Chapters 4 and 5).

1.5 Effects of a 'Natural' DNA Environment on Excited-State Dynamics

The broad range of conformations a natural DNA strand can adopt due to its flexibility, its strand length and base sequence complicate and blur its excited-state dynamics after photo-excitation.[148,162,165,170,175–181] The single nucleobase deactivation pathways presented in Section 1.2 involve a ring deformation coordinate, mostly puckering of a ring atom and/or out-of-plane bending of substituents. These motions are of course hindered

in the higher order structure of a DNA single or double strand. Additionally, alterations in the electronically excited states due to π-stacked adjacent chromophores and hydrogen-bonds have to be taken into account - but both of these effects are crucially dependent on the exact structure, which changes dynamically in solution at room temperature.

Only a few theoretical calculations on DNA excited-state characteristics are available, as oligonucleotides are simply too large. A reasonable compromise to overcome this obstruction is the combination of quantum mechanical (QM) calculations on a single nucleobase or base pair embedded in a DNA strand, which is calculated on a molecular dynamics (MD) or molecular mechanics (MM) level.[143,182–187] In summary, these calculations suggest a slow-down of the 'single nucleobase pathways' due to the steric restraints introduced by the DNA environment. An example was given by Lu *et al.*, who performed QM/MM simulations on a single adenine and the adenine-thymine base pair embedded in a DNA single or double stranded decamer and found the deactivation time to increase by one order of magnitude to 5.7/4.1 ps.[182] In the single stranded case, the deactivation pathway along the C^6 puckering/NH_2 bending mode is dominant, while the C^2 puckering channel coexists. For the A·T base pair the C^6 puckering pathway is completely suppressed, as the C^6-NH_2 group is engaged in the hydrogen bond, and the deactivation occurs only *via* the C^2 puckering channel. Conti *et al.* performed calculations on a single adenine treated on a quantum mechanical level embedded in a $d(A)_{10}$·$d(T)_{10}$ strand (MM level of theory) and found the $\pi\pi^*(L_a)$ relaxation pathway to be flatter than in vacuo.[183] They concluded that intramonomer dynamics may account for the experimentally observed multi-exponential decay behaviour in DNA strands, including long time constants $\tau > 100$ ps. Additionally they declared the intramonomer dynamics to compete successfully with excimer formation. This interpretation has to be considered with caution, as it is not likely to detect excimer formation between the QM subsystem adenine and the DNA environment treated by MM methods (cf. also Section 1.4). The G·C base pair embedded in a double stranded DNA dodecamer treated with QM/MM methods revealed a different influence on the electronic dynamics for cytosine and guanine, respectively.[143] The intramonomer deactivation of cytosine is hardly affected due to the small ring puckering motion along the monomer deactivation pathway. The deactivation time of guanine, on the other hand, is severely altered, since the electronic deactivation of the guanine monomer includes an out-of-plane bending of the C^2-NH_2 group, which is engaged in the hydrogen bonding to cytosine.

The above mentioned difficulties emphasise the need for developing shorter DNA model system to disentangle the various contributions to the excited-state dynamics. Especially the influence of hydrogen bonding and π-stacking needs to be distinguished and interpreted with care. Both interactions restrict structural movements of the investigated systems, but simultaneously alter the electronic state geometry considerably. On the other hand the questions arise, whether solvent and oligonucleotide environment can be accounted for in experimental measurements. The interplay of solvent and DNA strand geometry regarding (de-)solvation and the resulting entropy-enthalpy balance is rather complicated

and highly sensitive to local conformations.[6] An interesting example is given by Dallmann *et al.*, who followed the solvent mobility around a dye molecule embedded in a 13mer DNA duplex by transient absorption spectroscopy and quantified the mobility of bound H_2O and D_2O solvent molecules.[188] A possibility to gain insight into the solvent behaviour after electronic excitation is given in the following Section.

1.6 Solvation Dynamics

The dipole moment of many molecules changes hugely upon excitation due to the electron displacement, in most cases it increases. A solvent shell around such a photo-excited molecule consequently needs to rearrange itself according to the new dipole moment. The photo-excitation takes place much faster than the molecular movement in solution, and the solvent shell rearrangement can be followed with femtosecond time-resolved spectroscopy. The emitted fluorescence shifts spectrally to the red (dynamic Stokes shift), as the potential energy surfaces come closer when the excited molecule becomes better stabilised by the solvent molecules. Fluorophores normally used for this kind of spectroscopy emit quite a long time after reaching the new, energetically favourable solvent shell arrangement, thus allowing one to determine the pathway to said equilibrium quite directly. A simplified visualisation of the origin of the fluorescence band shift is illustrated in Figure 1.3, more details can be found in textbooks.[189]

The spectro-temporal evolution can be quantified by the so-called solvation-correlation

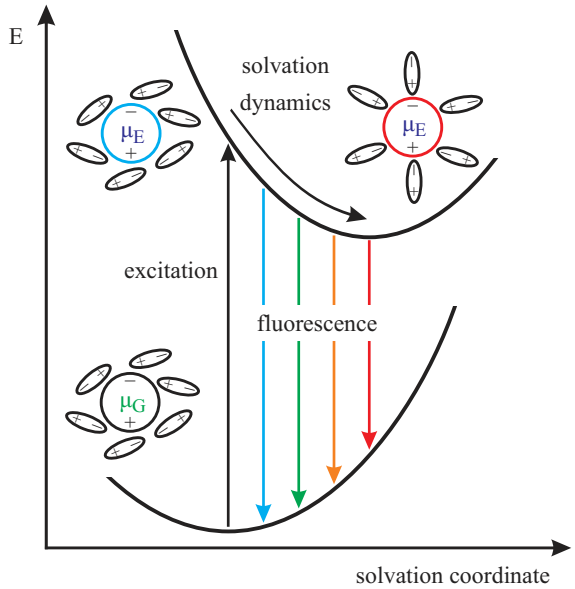

Fig. 1.3: Visualisation of the red-shift in emission due to solvation dynamics of polar solvent molecules around a photo-excited fluorophore. The initial solvent shell rearranges itself after the sample molecule changed its dipole moment after the photo-excitation. The coloured arrows symbolise the wavelength-shift in emission due to the decreasing gap between the potential energy surfaces.

function $C(t)$:[190–192]

$$C(t) = \frac{\tilde{\nu}(t) - \tilde{\nu}(\infty)}{\tilde{\nu}(0) - \tilde{\nu}(\infty)} \tag{1.1}$$

Here, $\tilde{\nu}$ refers to a specific signature of an emission spectrum - generally the emission maximum - directly after excitation ($\tilde{\nu}(0)$), after a certain time delay t ($\tilde{\nu}(t)$) and after completion of the solvent rearrangement ($\tilde{\nu}(\infty)$). The transient emission spectrum directly after excitation with its maximum at $\tilde{\nu}(0)$ is very hard to determine, as all time-resolved measurements have a certain time resolution. Fee and Maroncelli presented a possibility to calculate $\tilde{\nu}(0)$ using steady-state spectra of the respective molecule in non-polar solvents.[193] The emission spectrum after completion of the solvent shell rearrangement with its maximum $\tilde{\nu}(\infty)$ corresponds in most cases to the static fluorescence spectrum. The fluorescence lifetime of most fluorophores lies in the range of nanoseconds, whereas the solvent molecules move considerably faster. Namely in aqueous solution the solvent shell rearrangement is completed in ≤ 1 ps to several picoseconds.[194–207] However, in the case of short-lived fluorophores, which emit only up to a few tens of picoseconds after excitation, the quantitative analysis of the dynamic Stokes shift is complicated. This is explained in more detail in Chapter 7. In such cases, the asymptotic baseline of $C(t)$ may be taken as an approximation for $\tilde{\nu}(\infty)$.[208] Variations in this value only alter the determination of long-lived components in $C(t)$, the initial dynamics are not affected.[209]

An interesting example for the insights solvation dynamics can grant is given by Zhong and co-workers, who investigated the hydration dynamics of intrinsic tryptophan (Trp) in a series of small proteins with femtosecond time-resolved fluorescence up-conversion spectroscopy.[210–214] Tryptophan turned out to be an excellent local probe, which could even monitor conformational changes of a protein. The protein melittine for example adopts different structures under certain environmental conditions, which leads to a stronger or weaker incorporation of the Trp residue in the peptide and therefore differently constrained water molecules.[210] Molecular dynamics simulations confirmed the strong coupling of water and protein dynamics.[215] In human thioredoxin, a Trp residue is located near the active site. Comparison of different site-directed mutations and the wild-type gave insight into the structure of the active site, the time scales of electron and charge transfer reactions in the vicinity and the ns fluctuations of the whole protein.[212] The softness of a protein binding pocket and the large plasticity of the native structure was observed for human serum albumin, which features an intrinsic tryptophan in a crevice of the 3D structure.[211]

These promising examples encourage the investigation of other molecular probes in a defined environment. In the course of this Thesis, the solvation dynamics of the natural antioxidant ferulic acid were used to monitor the mobility of solvent molecules in bulk aqueous phase and in a constrained micellar environment. The time-resolved measurements can be found in Chapter 7, in the following section the investigated system is described briefly.

1.7 The Natural Antioxidant Ferulic Acid and its Incorporation in Micelles

Cinnamic acid derivatives are frequently found in plant cells, where they play a role in building cell wall material (lignin)[216] and act as radical catchers to protect against oxidation processes.[217] 4-Hydroxy-3-methoxycinnamic acid (ferulic acid, FA, Figure 1.4) is such a natural antioxidant, especially distributed in grain[218] and edible beans,[219] which even possesses antibacterial properties.[218,220,221] The molecule features a vinylic double bond, which may undergo $E \rightarrow Z$ isomerisation upon UV irradiation.[222,223] This large-scale motion may be utilised by nature: the structurally related *p*-coumaric acid (4-hydroxy-cinnamic acid) acts as chromophore in the photoactive yellow protein (PYP). The polypeptide unfolds upon UV irradiation and is responsible for the negative phototactic response of some purple bacteria. Its photosensitivity has been demonstrated to originate from $E \rightarrow Z$ isomerisation of the chromophore, which initiates the de-folding upon UV irradiation.[224–228] Lewis *et al.* suggested two competing $\pi\pi^*$ states in cinnamic acid derivatives, only one leading to photoisomerisation, and held their relative configuration responsible for the observed dependence of photoisomerisation efficiency on excitation wavelength, substitution pattern, solvent and complexation with BF_3.[229] The relatively short lifetime of FA in the excited state was determined to $\tau \approx 19$ ps by following the ground state recovery.[230] The deactivation pathway probably involves the $E \rightarrow Z$ isomerisation of the vinylic double bond, as the lifetime of *p*-coumaric acid has been found to increase more than two orders of magnitude if the respective degree of freedom is blocked.[231]

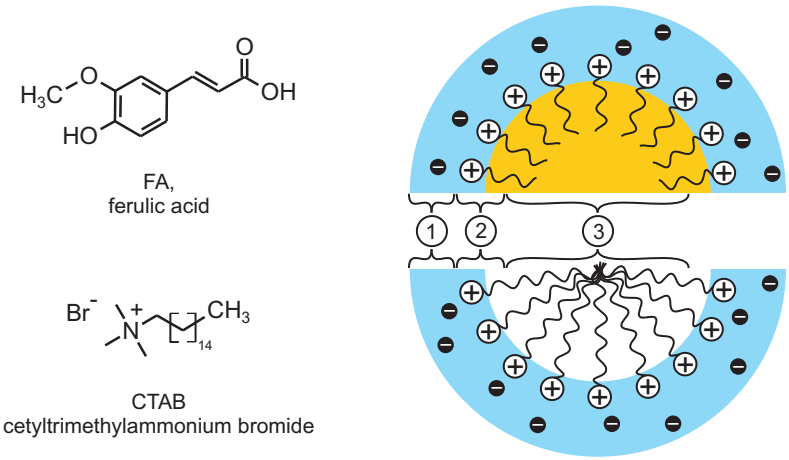

Fig. 1.4: Left: Chemical structure of ferulic acid (FA, top) and cetyltrimethylammonium bromide (CTAB, bottom). Right: Schematic visualisation of an o/w emulsion droplet stabilised by emulsifier molecules (top) and a micelle formed of amphiphilic molecules (bottom). The numbering reflects the layer structure of both emulsion droplet and micelle: 1 = Stern layer, 2 = palisade layer, 3 = hydrophobic core (oil or alkyl chain region).

The antioxidant activity of a biomolecule like ferulic acid depends on its location inside the considered system. Of special interest in this context are oil-in-water (o/w) emulsions, which consist of finely dispersed oil/fat droplets in an aqueous environment. As the two liquids are immiscible, such a mixture would normally segregate quite rapidly. Stable emulsions are stabilised by surfactant molecules, so-called emulsifiers. These are amphiphilic molecules with a hydrophilic head group (often charged) and a hydrophobic/lipophilic tail, mostly a long alkyl chain. The molecules arrange themselves in a way that all tails point into the oil phase droplets and the hydrophilic headgroups lie on the o/w surface. A visualisation is sketched in Figure 1.4, together with the structure of the emulsifier cetyltrimethylammonium bromide (CTAB). If the droplet surface is saturated with tenside molecules or they are dissolved in pure water, they start to form micelles upon reaching the critical micelle concentration (cmc). In a micelle, all hydrophobic chains are gathered in the core, the headgroups are on the outside and well solvated by the aqueous environment. The comparison of emulsion droplet and micelle sketched in Figure 1.4 shows their similar structure. Especially the Stern layer of counter ions around the charged headgroups and the so-called palisade layer are fairly identical. The palisade layer consists of the o/w interface and the hydrophilic headgroups. The respective core - oil or just the alkyl chain aggregate - obviously differs. When regarding the Stern layer and the palisade layer, micelles can consequently be used to model o/w emulsion droplets. Emulsions themselves are hardly accessible by UV/vis spectroscopy as their size is often comparable to visible wavelengths, which causes a huge amount of scattering (as in milk).

In food and pharmaceutical formulations the protection of unsaturated fatty acids in o/w emulsions is of interest. In these cases, the location and mobility of antioxidant molecules affect its activity,[232–236] as radicals often come from the aqueous phase and oxidise the lipids. Ferulic acid has been shown to be located in the palisade layer of CTAB micelles,[237] its concentration in the surrounding bulk aqueous phase is negligible.[238] The CTAB micelles consist of $90-120$ molecules,[239,240] in the palisade layer is therefore still enough room for a water solvent shell around FA. Nevertheless, the mobility of both FA and water molecules in the palisade layer is assumed to be hindered compared with the bulk water environment.

1.8 Contents of this Thesis

Within the course of this Thesis, two major tasks can be distinguished. In the first part of the present Thesis (Chapters 3, 4, 5 and 6), investigations on small DNA building blocks have been performed to disentangle some of the features observed in natural DNA strands. As has been summarised above, the photophysics and electronic deactivation dynamics of DNA are very complex and the nature and extent of different contributions are still under discussion. Here, special attention is dedicated to the influence of π-stacking of adjacent nucleobases. Towards this end, the electronic deactivation after UV excitation of the DNA

dinucleotides d(ApA) (Chapters 3 and 4) and d(ApG) (Chapter 5) are investigated and compared with their constituent monomers. These very basic model systems allow for the direct observation of cooperative effects between neighbouring nucleobases and the influence of base sequence on π-stacking interactions. Femtosecond time-resolved absorption and fluorescence spectroscopy reveal the astonishing contributions of an excimer state formed upon UV excitation to the overall deactivation dynamics. In particular, the excimer state is remarkably long-lived and gives rise to a specific excited-state absorption band, which is reported for the first time in this Thesis. On the other hand, hydrogen bonds are an important factor for DNA photodynamics. This contribution is more difficult to separate from other effects. In aqueous solution at least $10 - 20$ bases are necessary to hold a DNA double strand together, which inevitably leads to a considerable amount of base stacking. To overcome this obstruction, a short, self-complementary DNA hairpin is presented and thoroughly characterised by static and femtosecond time-resolved spectroscopy (Chapter 6). The oligonucleotide loop d[5'-GpGpGp-HEG-pCpCpC-3'] consists of two oligonucleotide 'arms' linked by a hexaethylene glycol chain. This molecule turned out to be an excellent model system for a hydrogen bonded double strand.

The smaller second part of this Thesis (Chapter 7) deals with the ultrafast solvation dynamics of the natural antioxidant ferulic acid. The influence of a solvent shell and its response to electronic modification, which UV excitation implies, is of high impact regarding reactivity in the excited state and electronic deactivation pathways. Therefore, the rearrangement of the water solvent shell around ferulic acid in solution and in a constrained environment has been followed by means of femtosecond time-resolved broadband fluorescence spectroscopy. The steric restraints are modelled by embedding the molecular probe into the palisade layer of micelles, where a solvent shell around the investigated molecule is still present but its mobility is clearly hindered. The employed Kerr gating setup was confirmed as powerful method to follow the solvent mobility even on a *sub*-picosecond time scale, and the implications of steric hindrances to the electronic deactivation pathways could unambiguously be demonstrated.

The experimental details for all measurements performed in the course of this Thesis are presented in Chapter 2. A summary regarding the implications of and the deductions from the presented data together with a short outlook can be found in Chapter 8.

References

[1] O. T. Avery, C. M. MacLeod, M. McCarty, *J. Exp. Med.* **79**, 137 (1944).

[2] J. D. Watson, F. H. C. Crick, *Nature* **171**, 737 (1953).

[3] G. M. Blackburn, M. J. Gait, Eds., *Nucleic Acids in Chemistry and Biology* (Oxford University Press, 1990).

[4] T. A. Brown, *Genomes 3* (Garland Science Publishing, 2007).

[5] W. Saenger, *Principles of Nucleic Acid Structure* (Springer, New York, 1984).

[6] I. T. J. Victor A. Bloomfield, Donald M. Crothers, *Nucleic Acids: Structures, Properties, and Functions* (University Science Books, 2000).

[7] Z. Shakked, D. Rabinovich, *Prog. Biophys. Mol. Biol.* **47**, 159 (1986).

[8] J. T. Yang, T. Samejima, *Biochem. Biophys. Res. Commun.* **33**, 739 (1968).

[9] V. I. Ivanov, L. E. Minchenkova, A. K. Schyolkina, A. I. Poletayev, *Biopolymers* **12**, 89 (1973).

[10] J. H. Riazance, W. A. Baase, J. W. Curtis Johnson, K. Hall, P. Cruz, J. Ignacio Tinoco, *Nucleic Acids Res.* **13**, 4983 (1985).

[11] J. Kypr, I. Kejnovska, D. Renciuk, M. Vorlickova, *Nucleic Acids Res.* **37**, 1713 (2009).

[12] M. F. Maestre, *J. Mol. Biol.* **52**, 543 (1970).

[13] M. J. B. Tunis-Schneider, M. F. Maestre, *J. Mol. Biol.* **52**, 521 (1970).

[14] L. Trantírek, R. Štefl, M. Vorlíčková, J. Koča, V. Sklenár, J. Kypr, *J. Mol. Biol.* **297**, 907 (2000).

[15] W. Johnson, I. Tinoco, *Biopolymers* **7**, 727 (1969).

[16] W. A. Baase, J. Johnson, W. Curtis, *Nucleic Acids Res.* **6**, 797 (1979).

[17] M. Adrian, B. Heddi, A. T. Phan, *Methods (Amsterdam, Neth.)* **57**, 11 (2012).

[18] M. Webba da Silva, *Methods (Oxford, U. K.)* **43**, 264 (2007).

[19] D. MacDonald, P. Lu, *J. Am. Chem. Soc.* **124**, 9722 (2002).

[20] J. Yang, K. McAteer, L. A. P. Silks, R. Wu, N. G. Isern, C. J. Unkefer, M. A. Kennedy, *J. Magn. Reson.* **146**, 260 (2000).

[21] C. E. Crespo-Hernández, B. Cohen, P. M. Hare, B. Kohler, *Chem. Rev.* **104**, 1977 (2004).

[22] M. Daniels, W. W. Hauswirth, *Science* **171**, 675 (1971).

[23] P. R. Callis, *Annu. Rev. Phys. Chem.* **34**, 329 (1983).

[24] D. Onidas, D. Markovitsi, S. Marguet, A. Sharonov, T. Gustavsson, *J. Phys. Chem. B* **106**, 11367 (2002).

[25] M. Dantus, M. J. Rosker, A. H. Zewail, *J. Chem. Phys.* **87**, 2395 (1987).

[26] A. H. Zewail, *Femtochemistry: Ultrafast Dynamics of the Chemical Bond.* (World Scientific, 1994).

[27] J. Manz, *Femtosecond Chemistry.* (VCH Verlagsgesellschaft mbH, Weinheim, 1995).

[28] A. H. Zewail, *J. Chem. Phys. A* **104**, 5660 (2000).

[29] C. T. Middleton, K. de La Harpe, C. Su, Y. K. Law, C. E. Crespo-Hernández, B. Kohler, *Annu. Rev. Phys. Chem.* **60**, 217 (2009).

[30] M. Dreyfus, G. Dodin, O. Bensaude, J. E. Dubois, *J. Am. Chem. Soc.* **97**, 2369 (1975).

[31] B. Cohen, P. M. Hare, B. Kohler, *J. Am. Chem. Soc.* **125**, 13594 (2003).

[32] L. Serrano-Andrés, M. Merchán, A. C. Borin, *Chem. Eur. J.* **12**, 6559 (2006).

[33] L. Blancafort, *J. Am. Chem. Soc.* **128**, 210 (2006).

[34] W. M. I. Hassan, W. C. Chung, N. Shimakura, S. Koseki, H. Kono, Y. Fujimura, *Phys. Chem. Chem. Phys.* **12**, 5317 (2010).

[35] S. Perun, A. L. Sobolewski, W. Domcke, *J. Am. Chem. Soc.* **127**, 6257 (2005).

[36] C. M. Marian, *J. Chem. Phys.* **122**, 104314 (2005).

[37] I. Conti, M. Garavelli, G. Orlandi, *J. Am. Chem. Soc.* **131**, 16108 (2009).

[38] M. Barbatti, H. Lischka, *J. Am. Chem. Soc.* **130**, 6831 (2008).

[39] M. Barbatti, A. J. A. Aquino, J. J. Szymczak, D. Nachtigallovà, P. Hobza, H. Lischka, *Proc. Natl. Acad. Sci. U.S.A.* **107**, 21453 (2010).

[40] M. Barbatti, Z. Lan, R. Crespo-Otero, J. J. Szymczak, H. Lischka, W. Thiel, *J. Chem. Phys* **137**, 22A503 (2012).

[41] C. Canuel, M. Elhanine, M. Mons, F. Piuzzi, B. Tardivel, I. Dimicoli, *Phys. Chem. Chem. Phys.* **8**, 3978 (2006).

[42] V. Ludwig, Z. M. da Costa, M. S. do Amaral, A. C. Borin, S. Canuto, L. Serrano-Andrés, *Chem. Phys. Lett.* **492**, 164 (2010).

[43] H. Chen, S. Li, *J. Phys. Chem. A* **109**, 8443 (2005).

[44] S. Yamazaki, S. Kato, *J. Am. Chem. Soc.* **129**, 2901 (2007).

[45] B. Kohler, *J. Phys. Chem. Lett.* **1**, 2047 (2010).

[46] T. Gustavsson, A. Sharonov, D. Onidas, D. Markovitsi, *Chem. Phys. Lett.* **356**, 49 (2002).

[47] T. Pancur, N. K. Schwalb, F. Renth, F. Temps, *Chem. Phys.* **313**, 199 (2005).

[48] N. L. Evans, S. Ullrich, *J. Phys. Chem. A* **114**, 11225 (2010).

[49] Z. Lan, Y. Lu, E. Fabiano, W. Thiel, *ChemPhysChem* **12**, 1989 (2011).

[50] J.-M. L. Pecourt, J. Peon, B. Kohler, *J. Am. Chem. Soc.* **122**, 9348 (2000).

[51] J.-M. L. Pecourt, J. Peon, B. Kohler, *J. Am. Chem. Soc.* **123**, 10370 (2001).

[52] L. Serrano-Andrés, M. Merchán, A. C. Borin, *J. Am. Chem. Soc.* **130**, 2473 (2008).

[53] F.-A. Miannay, T. Gustavsson, A. Banyasz, D. Markovitsi, *J. Phys. Chem. A* **114**, 3256 (2010).

[54] C. M. Marian, *J. Phys. Chem. A* **111**, 1545 (2007).

[55] V. Karunakaran, K. Kleinermanns, R. Improta, S. A. Kovalenko, *J. Am. Chem. Soc.* **131**, 5839 (2009).

[56] S. Yamazaki, W. Domcke, A. L. Sobolewski, *J. Phys. Chem. A* **112**, 11965 (2008).

[57] H. Chen, S. Li, *J. Chem. Phys.* **124**, 154315 (2006).

[58] Z. Lan, E. Fabiano, W. Thiel, *ChemPhysChem* **10**, 1225 (2009).

[59] M. Barbatti, J. J. Szymczak, A. J. A. Aquino, D. Nachtigallová, H. Lischka, *J. Chem. Phys.* **134**, 014304 (2011).

[60] B. Heggen, Z. Lan, W. Thiel, *Phys. Chem. Chem. Phys.* **14**, 8137 (2012).

[61] C. Canuel, M. Mons, F. Piuzzi, B. Tardivel, I. Dimicoli, M. Elhanine, *J. Chem. Phys.* **122**, 074316 (2005).

[62] H. Kang, K. T. Lee, B. Jung, Y. J. Ko, S. K. Kim, *J. Am. Chem. Soc.* **124**, 12958 (2002).

[63] J. Peon, A. H. Zewail, *Chem. Phys. Lett.* **348**, 255 (2001).

[64] C. C. Chan-Wut, C. Ma, C. T.-L. Chan, H. K. Yat-Fung, W.-M. Kwok, *Photochem. Photobiol. Sci.* doi:10.1039/C3PP25450J (2013).

[65] M. Merchán, R. González-Luque, T. Climent, L. Serrano-Andrés, E. Rodríguez, M. Reguero, D. Peláez, *J. Phys. Chem. B* **110**, 26471 (2006).

[66] M. Merchán, L. Serrano-Andrés, *J. Am. Chem. Soc.* **125**, 8108 (2003).

[67] M. Merchán, L. Serrano-Andrés, M. A. Robb, L. Blancafort, *J. Am. Chem. Soc.* **127**, 1820 (2005).

[68] K. A. Kistler, S. Matsika, *J. Phys. Chem. A* **111**, 2650 (2007).

[69] J. González-Vázquez, L. González, *ChemPhysChem* **11**, 3617 (2010).

[70] L. Blancafort, M. A. Robb, *J. Phys. Chem. A* **108**, 10609 (2004).

[71] Z. Lan, E. Fabiano, W. Thiel, *J. Phys. Chem. B* **113**, 3548 (2009).

[72] M. Barbatti, A. J. A. Aquino, J. J. Szymczak, D. Nachtigallova, H. Lischka, *Phys. Chem. Chem. Phys.* **13**, 6145 (2011).

[73] K. A. Kistler, S. Matsika, *J. Chem. Phys.* **128**, 215102 (2008).

[74] A. Sharonov, T. Gustavsson, V. Carre, E. Renault, D. Markovitsi, *Chem. Phys. Lett.* **380**, 173 (2003).

[75] P. M. Hare, C. E. Crespo-Hernández, B. Kohler, *Proc. Natl. Acad. Sci. U.S.A.* **104**, 435 (2007).

[76] K. Kosma, C. Schroeter, E. Samoylova, I. V. Hertel, T. Schultz, *J. Am. Chem. Soc.* **131**, 16939 (2009).

[77] N. K. Schwalb, F. Temps, *J. Photochem. Photobiol., A* **208**, 164 (2009).

[78] R. J. Malone, A. M. Miller, B. Kohler, *Photochem. Photobiol.* **77**, 158 (2003).

[79] M. Z. Zgierski, S. Patchkovskii, E. C. Lim, *J. Chem. Phys.* **123**, 081101 (2005).

[80] M. Z. Zgierski, S. Patchkovskii, T. Fujiwara, E. C. Lim, *J. Phys. Chem. A* **109**, 9384 (2005).

[81] M. Z. Zgierski, S. Alavi, *Chem. Phys. Lett.* **426**, 398 (2006).

[82] K. Tomic, J. Tatchen, C. M. Marian, *J. Phys. Chem. A* **109**, 8410 (2005).

[83] L. Blancafort, A. Migani, *J. Photochem. Photobiol. A* **190**, 283 (2007).

[84] M. Kotur, T. C. Weinacht, C. Zhou, K. A. Kistler, S. Matsika, *J. Chem. Phys.* **134**, 184309 (2011).

[85] H. R. Hudock, T. J. Martinez, *ChemPhysChem* **9**, 2486 (2008).

[86] M. Richter, P. Marquetand, J. González-Vázquez, I. Sola, L. González, *J. Phys. Chem. Lett.* **3**, 3090 (2012).

[87] P. G. Szalay, T. Watson, A. Perera, V. Lotrich, G. Fogarasi, R. J. Bartlett, *J. Phys. Chem. A* **116**, 8851 (2012).

[88] K. A. Kistler, S. Matsika, *Phys. Chem. Chem. Phys.* **12**, 5024 (2010).

[89] W.-M. Kwok, C. Ma, D. L. Phillips, *J. Am. Chem. Soc.* **130**, 5131 (2008).

[90] T. Gustavsson, A. Sharonov, D. Markovitsi, *Chem. Phys. Lett.* **351**, 195 (2002).

[91] T. Gustavsson, A. Banyasz, E. Lazzarotto, D. Markovitsi, G. Scalmani, M. J. Frisch, V. Barone, R. Improta, *J. Am. Chem. Soc.* **128**, 607 (2006).

[92] A. Reuther, H. Iglev, R. Laenen, A. Lauberau, *Chem. Phys. Lett.* **325**, 360 (2000).

[93] M. Kunitski, Y. Nosenko, B. Brutschy, *ChemPhysChem* **12**, 2024 (2011).

[94] Y. He, C. Wu, W. Kong, *J. Phys. Chem. A* **107**, 5145 (2003).

[95] S. Perun, A. L. Sobolewski, W. Domcke, *J. Phys. Chem. A* **110**, 13238 (2006).

[96] M. Schneider, R. Maksimenka, F. J. Buback, T. Kitsopoulos, L. R. Lago, I. Fischer, *Phys. Chem. Chem. Phys.* **8**, 3017 (2006).

[97] J. J. Szymczak, M. Barbatti, J. T. Soo Hoo, J. A. Adkins, T. L. Windus, D. Nachtigallova, H. Lischka, *J. Phys. Chem. A* **113**, 12686 (2009).

[98] D. Picconi, V. Barone, A. Lami, F. Santoro, R. Improta, *ChemPhysChem* **12**, 1957 (2011).

[99] G. Zechmann, M. Barbatti, *J. Phys. Chem. A* **112**, 8273 (2008).

[100] M. Etinski, T. Fleig, C. M. Marian, *J. Phys. Chem. A* **113**, 11809 (2009).

[101] D. Asturiol, B. Lasorne, M. A. Robb, L. Blancafort, *J. Phys. Chem. A* **113**, 10211 (2009).

[102] D. Asturiol, B. Lasorne, G. A. Worth, M. A. Robb, L. Blancafort, *Phys. Chem. Chem. Phys.* **12**, 4949 (2010).

[103] X.-M. Zhu, H.-g. Wang, X. Zheng, D. L. Phillips, *J. Phys. Chem. B* **112**, 15828 (2008).

[104] H. R. Hudock, B. G. Levine, A. L. Thompson, H. Satzger, D. Townsend, N. Gador, S. Ullrich, A. Stolow, T. J. Martinez, *J. Phys. Chem. A* **111**, 8500 (2007).

[105] P. M. Hare, C. T. Middleton, K. I. Mertel, J. M. Herbert, B. Kohler, *Chem. Phys.* **347**, 383 (2008).

[106] W. J. Schreier, T. E. Schrader, F. O. Koller, P. Gilch, C. E. Crespo-Hernández, V. N. Swaminathan, T. Carell, W. Zinth, B. Kohler, *Science* **315**, 625 (2007).

[107] W. J. Schreier, J. Kubon, N. Regner, K. Haiser, T. E. Schrader, W. Zinth, P. Clivio, P. Gilch, *J. Am. Chem. Soc.* **131**, 5038 (2009).

[108] M. Hariharan, F. D. Lewis, *J. Am. Chem. Soc.* **130**, 11870 (2008).

[109] M. Boggio-Pasqua, G. Groenhof, L. V. Schaefer, H. Grubmueller, M. A. Robb, *J. Am. Chem. Soc.* **129**, 10996 (2007).

[110] L. Blancafort, A. Migani, *J. Am. Chem. Soc.* **129**, 14540 (2007).

[111] M. Hariharan, M. McCullagh, G. C. Schatz, F. D. Lewis, *J. Am. Chem. Soc.* **132**, 12856 (2010).

[112] M. Etinski, C. M. Marian, *Phys. Chem. Chem. Phys.* **12**, 4915 (2010).

[113] L. Serrano-Andrés, M. Merchán, *J. Photochem. Photobiol. C* **10**, 21 (2009).

[114] F. H. C. Crick, J. D. Watson, *Proc. R. Soc. London, Ser. A* **223**, 80 (1954).

[115] E. Chargaff, *Experientia* **6**, 201 (1950).

[116] K. Röttger, N. K. Schwalb, F. Temps, *J. Phys. Chem. A* **117(12)**, 2469 (2013).

[117] G. Gottarelli, S. Masiero, E. Mezzina, G. P. Spada, P. Mariani, M. Recanatini, *Helv. Chim. Acta* **81**, 2078 (1998).

[118] J. L. Sessler, M. Sathiosatham, K. Doerr, V. Lynch, K. A. Abboud, *Angew. Chem., Int. Ed.* **39**, 1300 (2000).

[119] T. Giorgi, F. Grepioni, I. Manet, P. Mariani, S. Masiero, E. Mezzina, S. Pieraccini, L. Saturni, G. P. Spada, G. Gottarelli, *Chem. Eur. J.* **8**, 2143 (2002).

[120] R. Rinaldi, G. Maruccio, A. Biasco, V. Arima, R. Cingolani, T. Giorgi, S. Masiero, G. P. Spada, G. Gottarelli, *Nanotechnology* **13**, 398 (2002).

[121] J. T. Davis, G. P. Spada, *Chem. Soc. Rev.* **36**, 296 (2007).

[122] K. Hunger, L. Buschhaus, L. Biemann, M. Braun, S. Kovalenko, R. Improta, K. Kleinermanns, *Chem. Eur. J.* **19**, 5425Ű5431 (2013).

[123] A. Abo-Riziq, L. Grace, E. Nir, M. Kabeláč, P. Hobza, M. S. de Vries, *Proc. Natl. Acad. Sci. U.S.A.* **102**, 20 (2005).

[124] N. K. Schwalb, F. Temps, *J. Am. Chem. Soc.* **129**, 9272 (2007).

[125] N. K. Schwalb, T. Michalak, F. Temps, *J. Phys. Chem. B* **113**, 16365 (2009).

[126] A. L. Sobolewski, W. Domcke, *Phys. Chem. Chem. Phys.* **6**, 2763 (2004).

[127] A. L. Sobolewski, W. Domcke, C. Hättig, *Proc. Natl. Acad. Sci. U.S.A.* **102**, 17903 (2005).

[128] G. Groenhof, L. V. Schäfer, M. Boggio-Pasqua, M. Goette, H. Grubmüller, M. A. Robb, *J. Am. Chem. Soc.* **129**, 6812 (2007).

[129] S. Yamazaki, T. Taketsugu, *Phys. Chem. Chem. Phys.* **14**, 8866 (2012).

[130] V. Guallar, A. Douhal, M. Moreno, J. M. Lluch, *J. Phys. Chem. A* **103**, 6251 (1999).

[131] A. Kumar, M. D. Sevilla, *Photochem. Photobiol. Sci.* doi:10.1039/C3PP25430E (2013).

[132] K. Röttger, *unpublished results* .

[133] E. Samoylova, H. Lippert, S. Ullrich, I. V. Hertel, W. Radloff, T. Schultz, *J. Am. Chem. Soc.* **127**, 1782 (2005).

[134] S. Perun, A. Sobolewski, W. Domcke, *J. Phys. Chem. A* **110**, 9031 (2006).

[135] J. P. Gobbo, V. Saurí, D. Roca-Sanjuán, L. Serrano-Andrés, M. Merchán, A. C. Borin, *J. Phys. Chem. B* **116**, 4089 (2012).

[136] A. L. Sobolewski, W. Domcke, *Chem. Phys.* **294**, 73 (2003).

[137] T. Schultz, E. Samoylova, W. Radloff, I. V. Hertel, A. L. Sobolewski, W. Domcke, *Science* **306**, 1765 (2004).

[138] E. Samoylova, V. R. Smith, H.-H. Ritze, W. Radloff, M. Kabelac, T. Schultz, *J. Am. Chem. Soc.* **128**, 15652 (2006).

[139] E. Samoylova, W. Radloff, H.-H. Ritze, T. Schultz, *J. Phys. Chem. A* **113**, 8195 (2009).

[140] Y.-J. Ai, F. Zhang, G.-L. Cui, Y. Luo, W.-H. Fang, *J. Chem. Phys.* **133**, 064302 (2010).

[141] A. L. Sobolewski, W. Domcke, *ChemPhysChem* **7**, 561 (2006).

[142] S. Xiao, L. Wang, Y. Liu, X. Lin, H. Liang, *J. Chem. Phys.* **137**, 195101 (2012).

[143] T. Zeleny, M. Ruckenbauer, A. J. A. Aquino, T. Muller, F. Lankas, T. Drsata, W. L. Hase, D. Nachtigallova, H. Lischka, *J. Am. Chem. Soc.* **134**, 13662 (2012).

[144] C. E. Crespo-Hernández, B. Cohen, B. Kohler, *Nature* **436**, 1141 (2005).

[145] W.-M. Kwok, C. Ma, D. L. Phillips, *J. Am. Chem. Soc.* **128**, 11894 (2006).

[146] D. Markovitsi, D. Onidas, T. Gustavsson, F. Talbot, E. Lazzarotto, *J. Am. Chem. Soc.* **127**, 17130 (2005).

[147] D. Markovitsi, F. Talbot, T. Gustavsson, D. Onidas, E. Lazzarotto, S. Marguet, *Nature* **441**, E7 (2006).

[148] N. K. Schwalb, F. Temps, *Science* **322**, 243 (2008).

[149] J. Eisinger, M. Guéron, R. G. Shulman, T. Yamane, *Proc. Natl. Acad. Sci. U.S.A.* **55**, 1015 (1966).

[150] J. Eisinger, *Photochem. Photobiol.* **7**, 597 (1968).

[151] M. Daniels, J. P. Morgan, *Chem. Phys. Lett.* **58**, 283 (1978).

[152] M. Daniels, J. P. Morgan, *J. Luminescence* **18/19**, 593 (1979).

[153] J. P. Morgan, M. Daniels, *Photochem. Photobiol.* **31**, 207 (1980).

[154] J. P. Morgan, M. Daniels, *Photochem. Photobiol.* **31**, 101 (1980).

[155] C. S. Shaar, J. P. Morgan, M. Daniels, *Photochem. Photobiol.* **39**, 747 (1984).

[156] M. Daniels, C. S. Shaar, J. P. Morgan, *Biophys. Chem.* **32**, 229 (1988).

[157] J. Eisinger, R. G. Shulman, *Science* **161**, 1311 (1968).

[158] M. M. Warshaw, I. T. Jr., *J. Mol. Biol.* **13**, 54 (1965).

[159] M. Y. Warshaw, I. Tinoco, *J. Mol. Biol.* **20**, 29 (1966).

[160] M. M. Warshaw, C. R. Cantor, *Biopolymers* **9**, 1079 (1970).

[161] C. R. Cantor, M. M. Warshaw, H. Shapiro, *Biopolymers* **9**, 1059 (1970).

[162] C. Su, C. T. Middleton, B. Kohler, *J. Phys. Chem. B* **116**, 10266 (2012).

[163] B. Bouvier, J.-P. Dognon, R. Lavery, D. Markovitsi, P. Millie, D. Onidas, K. Zakrzewska, *J. Phys. Chem. B* **107**, 13512 (2003).

[164] B. Bouvier, T. Gustavsson, D. Markovitsi, P. Millié, *Chem. Phys.* **275**, 75 (2002).

[165] I. Buchvarov, Q. Wang, M. Raytchev, A. Trifonov, T. Fiebig, *Proc. Natl. Acad. Sci. U.S.A.* **104**, 4794 (2007).

[166] E. Emanuele, D. Markovitsi, P. Millié, K. Zakrewska, *ChemPhysChem* **6**, 1387 (2005).

[167] A. Czader, E. R. Bittner, *J. Chem. Phys* **128**, 035101 (2008).

[168] C. E. Crespo-Hernández, B. Cohen, B. Kohler, *Nature* **441**, E8 (2006).

[169] E. B. Starikov, G. Cuniberti, S. Tanaka, *J. Phys. Chem. B* **113**, 10428 (2009).

[170] T. Takaya, C. Su, K. de La Harpe, C. E. Crespo-Hernández, B. Kohler, *Proc. Natl. Acad. Sci. U.S.A.* **105**, 10285 (2008).

[171] G. Olaso-González, M. Merchán, L. Serrano-Andrés, *J. Am. Chem. Soc.* **131**, 4368 (2009).

[172] L. M. Nielsen, S. V. Hoffmann, S. B. Nielsen, *Photochem. Photobiol. Sci.* doi:10.1039/C3PP25438K (2013).

[173] J. Frenkel, *Phys. Rev.* **37**, 17 (1931).

[174] J. Frenkel, *Phys. Rev.* **37**, 1276 (1931).

[175] S. O. Konorov, H. G. Schulze, C. J. Addison, C. A. Haynes, M. W. Blades, R. F. B. Turner, *Open Spectrosc. J.* **3**, 9 (2009).

[176] S. O. Konorov, H. G. Schulze, C. J. Addison, C. A. Haynes, R. F. B. Turner, M. W. Blades, *Open Spectrosc. J.* **3**, 43 (2009).

[177] K. de La Harpe, B. Kohler, *J. Phys. Chem. Lett.* **2**, 133 (2011).

[178] D. Markovitsi, T. Gustavsson, I. Vayá, *J. Phys. Chem. Lett.* **1**, 3271 (2010).

[179] I. Vayá, T. Gustavsson, T. Douki, Y. Berlin, D. Markovitsi, *J. Am. Chem. Soc.* **134**, 11366 (2012).

[180] I. Vayá, J. Brazard, T. Gustavsson, D. Markovitsi, *Photochem. Photobiol. Sci.* **11**, 1767 (2012).

[181] I. Vayá, T. Gustavsson, F.-A. Miannay, T. Douki, D. Markovitsi, *J. Am. Chem. Soc.* **132**, 11834 (2010).

[182] Y. Lu, Z.-G. Lan, W. Thiel, *Angew. Chem., Int. Ed.* **50**, 6864 (2011).

[183] I. Conti, P. Altoè, M. Stenta, M. Garavelli, G. Orlandi, *Phys. Chem. Chem. Phys.* **12**, 5016 (2010).

[184] M. Valiev, K. Kowalski, *J. Chem. Phys.* **125**, 211101 (2006).

[185] D. Roca-Sanjuán, G. Olaso-González, M. Rubio, P. B. Coto, M. Merchán, N. Ferré, V. Ludwig, L. Serrano-Andrés, *Pure Appl. Chem.* **81**, 743 (2009).

[186] E. Cauët, M. Valiev, J. H. Weare, *J. Phys. Chem. B* **114**, 5886 (2010).

[187] E. Cauët, M. Valiev, J. H. Weare, J. Liévin, *J. Phys.: Conf. Ser.* **373**, 012003 (2012).

[188] A. Dallmann, M. Pfaffe, C. Mugge, R. Mahrwald, S. A. Kovalenko, N. P. Ernsting, *J. Phys. Chem. B* **113**, 15619 (2009).

[189] J. R. Lakowicz, *Principles of Fluorescence Spectroscopy, 3rd edition* (Springer, 2006).

[190] G. Van der Zwan, J. T. Hynes, *J. Phys. Chem.* **89**, 4181 (1985).

[191] B. Bagchi, D. W. Oxtoby, G. R. Fleming, *Chem. Phys.* **86**, 257 (1984).

[192] M. Maroncelli, J. MacInnis, G. R. Fleming, *Science* **243**, 1674 (1989).

[193] R. S. Fee, M. Maroncelli, *Chem. Phys.* **183**, 235 (1994).

[194] W. Jarzeba, G. C. Walker, A. E. Johnson, M. A. Kahlow, P. F. Barbara, *J. Phys. Chem.* **92**, 7039 (1988).

[195] R. Jimenez, G. R. Fleming, P. V. Kumar, M. Maroncelli, *Nature* **369**, 471 (1994).

[196] R. E. Riter, D. M. Willard, N. E. Levinger, *J. Phys. Chem. B* **102**, 2705 (1998).

[197] D. Pant, R. E. Riter, N. E. Levinger, *J. Chem. Phys.* **109**, 9995 (1998).

[198] A. V. Benderskii, K. B. Eisenthal, *J. Phys. Chem. B* **104**, 11723 (2000).

[199] X. Shen, J. R. Knutson, *J. Phys. Chem. B* **105**, 6260 (2001).

[200] D. Zhong, S. K. Pal, D. Zhang, S. I. Chan, A. H. Zewail, *Proc. Natl. Acad. Sci. U.S.A.* **99**, 13 (2002).

[201] W. Lu, J. Kim, W. Qiu, D. Zhong, *Chem. Phys. Lett.* **388**, 120 (2004).

[202] R. K. Mitra, S. S. Sinha, S. K. Pal, *Langmuir* **24**, 49 (2008).

[203] Y. Rao, N. J. Turro, K. B. Eisenthal, *J. Phys. Chem. C* **114**, 17703 (2010).

[204] M. Sajadi, M. Weinberger, H.-A. Wagenknecht, N. P. Ernsting, *Phys. Chem. Chem. Phys.* **13**, 17768 (2011).

[205] M. Maroncelli, G. R. Fleming, *J. Chem. Phys.* **89**, 5044 (1988).

[206] S. Roy, B. Bagchi, *J. Chem. Phys.* **99**, 9938 (1993).

[207] N. Nandi, S. Roy, B. Bagchi, *J. Chem. Phys.* **102**, 1390 (1995).

[208] K. Hara, H. Kuwabara, O. Kajimoto, *J. Phys. Chem. A* **105**, 7174 (2001).

[209] M. Maroncelli, G. R. Fleming, *J. Chem. Phys.* **86**, 6221 (1987).

[210] W. Qiu, L. Zhang, Y.-T. Kao, W. Lu, T. Li, J. Kim, G. M. Sollenberger, L. Wang, D. Zhong, *J. Phys. Chem. B* **109**, 16901 (2005).

[211] W. Qiu, L. Zhang, O. Okobiah, Y. Yang, L. Wang, D. Zhong, A. H. Zewail, *J. Phys. Chem. B* **110**, 10540 (2006).

[212] W. Qiu, L. Wang, W. Lu, A. Boechler, D. A. R. Sanders, D. Zhong, *Proc. Natl. Acad. Sci. U. S. A.* **104**, 5366 (2007).

[213] T. Li, A. A. Hassanali, Y.-T. Kao, D. Zhong, S. J. Singer, *J. Am. Chem. Soc.* **129**, 3376 (2007).

[214] L. Zhang, Y.-T. Kao, W. Qiu, L. Wang, D. Zhong, *J. Phys. Chem. B* **110**, 18097 (2006).

[215] A. A. Hassanali, T. Li, D. Zhong, S. J. Singer, *J. Phys. Chem. B* **110**, 10497 (2006).

[216] A. Gossauer, *Struktur und Reaktivität der Biomoleküle: eine Einführung in die organische Chemie* (Helvetica Chimica Acta, 2006).

[217] H. Yin, L. Xu, N. A. Porter, *Chem. Rev.* **111**, 5944 (2011).

[218] T. Masuda, K. Yamada, T. Maekawa, Y. Takeda, H. Yamaguchi, *J. Agric. Food Chem.* **54**, 6069 (2006).

[219] D. L. Luthria, M. A. Pastor-Corrales, *J. Food Compos. Anal.* **19**, 205 (2005).

[220] E. van der Watt, J. C. Pretorius, *J. Ethnopharmacol.* **76**, 87 (2001).

[221] B. Ibtissem, C. Abdelly, S. Sfar, *Adv. Chem. Eng. Sci.* **2**, 359 (2012).

[222] G. Kahnt, *Phytochemistry* **6**, 755 (1967).

[223] A. M. Brouwer, S. M. Fazio, N. Haraszkiewicz, D. A. Leigh, C. M. Lennon, *Photochem. Photobiol. Sci.* **6**, 480 (2007).

[224] M. Baca, G. E. O. Borgstahl, M. Boissinot, P. M. Burke, D. R. Williams, K. A. Slater, E. D. Getzoff, *Biochemistry* **33**, 14369 (1994).

[225] G. E. O. Borgstahl, D. R. Williams, E. D. Getzoff, *Biochemistry* **34**, 6278 (1995).

[226] R. Kort, H. Vonk, X. Xu, W. D. Hoff, W. Crielaard, K. J. Hellingwerf, *FEBS Lett.* **382**, 73 (1996).

[227] G. Groenhof, M. F. Lensink, H. J. C. Berendsen, J. G. Snijders, A. E. Mark, *Proteins: Struct., Funct., Genet.* **48**, 202 (2002).

[228] Y. Imamoto, M. Kataoka, *Photochem. Photobiol.* **83**, 40 (2007).

[229] F. D. Lewis, J. E. Elbert, A. L. Upthagrove, P. D. Hale, *J. Org. Chem.* **56**, 553 (1991).

[230] M. Vengris, D. S. Larsen, M. A. Van der Horst, O. F. A. Larsen, K. J. Hellingwerf, R. Van Grondelle, *J. Phys. Chem. B* **109**, 4197 (2005).

[231] M. Vengris, M. A. van der Horst, G. Zgrablic, I. H. M. van Stokkum, S. Haacke, M. Chergui, K. J. Hellingwerf, R. van Grondelle, D. S. Larsen, *Biophys. J.* **87**, 1848 (2004).

[232] K. Schwarz, E. N. Frankel, J. B. German, *Fett/Lipid* **98**, 115 (1996).

[233] H. Stockmann, K. Schwarz, T. Huynh-Ba, *J. Am. Oil Chem. Soc.* **77**, 535 (2000).

[234] W. A. Pryor, J. A. Cornicelli, L. J. Devall, B. Tait, B. K. Trivedi, D. T. Witiak, M. Wu, *J. Org. Chem.* **58**, 3521 (1993).

[235] S. S. Pekkarinen, H. Stoeckmann, K. Schwarz, I. M. Heinonen, A. I. Hopia, *J. Agric. Food Chem.* **47**, 3036 (1999).

[236] A. Heins, D. B. McPhail, T. Sokolowski, H. Stoeckmann, K. Schwarz, *Lipids* **42**, 573 (2007).

[237] A. Heins, T. Sokolowski, H. Stoeckmann, K. Schwarz, *Lipids* **42**, 561 (2007).

[238] K. Oehlke, A. Heins, H. Stöckmann, K. Schwarz, *Food Chemistry* **118(1)**, 48 (2009).

[239] K. Kuperkar, L. Abezgauz, K. Prasad, P. Bahadur, *J. Surfactants Deterg.* **13**, 293 (2010).

[240] K. Oehlke, V. M. Garamus, A. Heins, H. Stoeckmann, K. Schwarz, *J. Colloid Interface Sci.* **322**, 294 (2008).

2

Experimental Methods

This Chapter deals with the experimental details of the spectroscopic methods used in this Thesis. The main focus lies on the applied femtosecond time-resolved spectroscopy setups, namely single-colour UV/vis fluorescence up-conversion, broadband UV/vis fluorescence Kerr gating and broadband UV/vis transient absorption together with single-colour transient absorption in the UV region. The broadband fluorescence Kerr gating is described more closely, as the details of the setup used in our work group have not yet been published. Furthermore, the data analysis methods are presented and a short comment is given how the investigated samples were handled and how static absorption, fluorescence and circular dichroism spectra were achieved.

2.1 Femtosecond Time-Resolved Spectroscopy

Femtosecond time-resolved spectroscopy is based on ultrashort (femto- to picoseconds) intense laser pulses. Non-linear optical processes can be applied to tune these pulses to the desired, spectroscopically needed wavelength and pulse duration. The following description of the employed spectroscopic techniques is focused on the application of these effects. A detailed theoretical description of the underlying non-linear effects can be found in non-linear optics textbooks.[1–3] The non-linear optics background specific for the single-colour up-conversion setup and the transient absorption spectroscopy can be found in some detail in former Theses written in our work group.[4–6]

Electronic detection such as CCD cameras and photon counters are too slow to resolve changes in the femtosecond region. To follow the ultrafast dynamics of photo-excited molecules, the pump-probe spectroscopy technique is appropriate. In short, a laser pulse optically excites the investigated molecules, whose response is recorded by a second laser

pulse. The time delay between the arrival of the two pulses in the sample cell can be changed by varying the path length of the laser beam, as the pulses move both with the speed of light. The selectable time delay between pump and probe pulse then allows to record the molecular response at a given time after excitation. By enhancing the time delay gradually, response-time profiles can be recorded, whose time resolution only depends on the temporal duration of the laser pulses.

Different types of transient spectroscopy can be distinguished, which mostly differ in the nature of the recorded molecular response. Examples are transient absorption and fluorescence spectroscopy, time-resolved mass spectrometry, photoelectron or ion imaging. The used excitation and probe wavelengths, as well as the nature of the environment (especially gas phase *vs.* condensed phase) further specialise the spectroscopic techniques. In the course of this work, UV/vis absorption and emission spectroscopy after UV excitation of molecules in solution have been performed.

2.1.1 Fluorescence Up-Conversion Setup

The setup used for recording time-resolved single-colour fluorescence-time profiles has been described in detail previously.[4,5] A schematic representation is sketched in Figure 2.1. As described in Section 2.1, at first a pump laser pulse is needed to optically excite the sample solution. This pulse is generated by a so-called non-linear optical parametric amplifier (NOPA) which converts the laser beam provided by a Ti:Sa laser system (Clark-MXR CPA2001, 775 nm, 160 fs (full width half maximum, FWHM), 1 mJ, 1 kHz) to pulses in the region from $450 - 700$ nm with a spectral width of $20 - 50$ nm. The NOPA process has been described in detail in former works within this work group.[5–8] The resulting pulses are then temporally compressed to $\approx 30 - 50$ fs duration (FWHM) by a prism compressor consisting of two BK7 glass prisms. For UV excitation, the generated visible light is frequency-doubled in a suitable BBO crystal (520 nm $\rightarrow$ 260 nm: $5 \times 5 \times 0.2$ mm^3, $\theta = 49.3°$, $\phi = 90°$; 640 nm $\rightarrow$ 320 nm: $5 \times 5 \times 0.2$ mm^3, $\theta = 38.9°$, $\phi = 90°$). The pump pulse is then focused in the sample cell, a flow cell with an optical path length of 1 mm between two quartz windows (0.2 mm thickness, fused silica). The sample is pumped through the cell with a peristaltic pump (Ismatec), to ensure that every pump pulse meets a new, unexcited ensemble of molecules. The induced fluorescence is collected, collimated and refocused on a 1 mm BBO crystal for type I sum frequency generation ($5 \times 5 \times 0.1$ mm^3, $\theta = 54.4°$, $\phi = 0°$) with a pair of off-axis aluminium coated parabolic mirrors (effective focal length $f_{\text{eff}} = 119$ mm, $\varnothing = 6.2$ cm). The pump beam was blocked by a beam stop after the sample cell, scattered pump light was filtered with a Schott filter (WG 290, WG 320, or WG 340, depending on pump and recorded fluorescence wavelength). A part of the laser fundamental at 775 nm (≈ 80 μJ) is used as gate pulses. The polarisation is rotated 90° to meet the *ooe* phase matching condition in the type I up-conversion BBO. The beam is then spatially overlapped with the fluorescence photons in the up-conversion

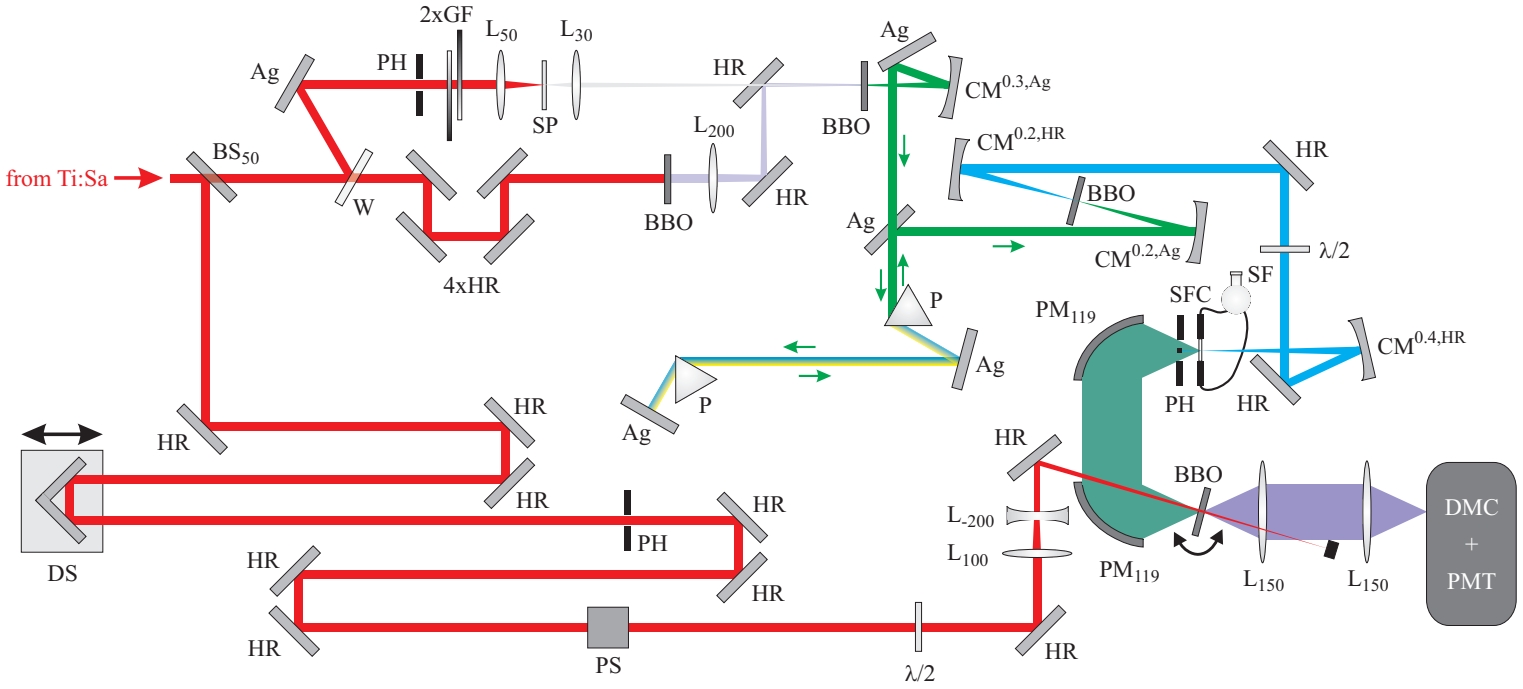

Ag	flat silver mirror	DMC	double monochromator	L_x	lens (x = focal length in mm)	PS	periscope
BS_x	beam splitter (x = reflectivity in %)	DS	delay stage with retroreflector	P	BK7 prism	SF	sample flask
BBO	β-BaB_2O_4 crystal	GF	gradient filter	PH	pin hole	SFC	sample flow cell
$CM^{x,y}$	concave mirror (x = rcc in m, y = coating)	HR	high reflective mirror	PMT	photomultiplier tube	SP	sapphire plate (d = 1 mm)
		λ/2	half-wave plate	PM_x	parabolic mirror (x = focal length in mm)	W	wedge (30°)

Fig. 2.1: Schematic representation of the UV/vis fluorescence up-conversion setup. All mirrors denoted as HR are high reflective mirrors suitable for the respective wavelength.

BBO crystal. Temporal overlap is achieved by ensuring that the path length of the two beams are equal. The gate beam path includes a delay stage carrying a retroreflector which can be electronically controlled and moved. The polarisation of the pump beam is set to the magic angle to avoid depolarisation effects. The up-converted fluorescence photons are collimated and refocused on the slit entrance of a double monochromator by a pair of quartz lenses ($f = 150$ mm) and detected by a photomultiplier tube and a photon counter. The 'time zero' of the experiment was defined by the simultaneous arrival of gate and pump pulse in the BBO crystal and determined by the cross correlation signal with scattered pump light. The FWHM of a Gaussian function describing the cross peak was determined to be ≈ 350 fs. This results in a standard deviation $\sigma \approx 150$ fs (cf. Eq. 2.4 below), which corresponds to the time resolution of the experiment. The lower bound for the time resolution is given by the relatively long laser fundamental pulse, which acts as the gate beam. The usage of reflective focusing optics instead of lenses (where possible) improved the time resolution of the setup notably compared to the former ≈ 230 fs.

During this Thesis, an exponential increase in the time delay between gate and pump beam has been implemented into the LabView routine which controls the experiment. In the beginning four sequential different linear step sizes, which changed after a desired time delay, were chosen. In later measurements, this was modified: after a certain time delay with linear step sizes, the displacement grew gradually longer, whereupon it satisfied an exponential prolongation. The fluorescence-time profiles presented herein originate from both above mentioned versions.

The phase-matching rotation angle of the up-conversion BBO has to be optimised for each emission wavelength, therefore no quantitative comparison is possible between the intensity of the recorded fluorescence-time profiles. Throughout this work, the given single-colour fluorescence intensities are normalised. Despite this drawback, the tremendous sensitivity of the fluorescence up-conversion setup is essential when investigating the very weakly fluorescing DNA nucleotides and building blocks.

2.1.2 Kerr Gating Setup

A different detection technique than presented above is necessary to collect broadband transient fluorescence spectra, as a non-linear crystal for sum-frequency generation with its wavelength-dependent phase-matching rotation angles distorts the fluorescence spectrum. The Kerr shutter itself, which allows here for femtosecond time-resolved broadband fluorescence detection, is based on the optical Kerr effect (OKE). A normally isotropic medium (gas, liquid or solid) may become anisotropic upon intense irradiation. The anisotropy induced from an external electric field E, as provided from an intense laser pulse, leads to birefringence of the Kerr medium, which in turn rotates the polarisation plane of incident (fluorescence) light by a few degrees. If the Kerr medium is placed between two crossed polarisers, the incident fluorescence light is transmitted and detected

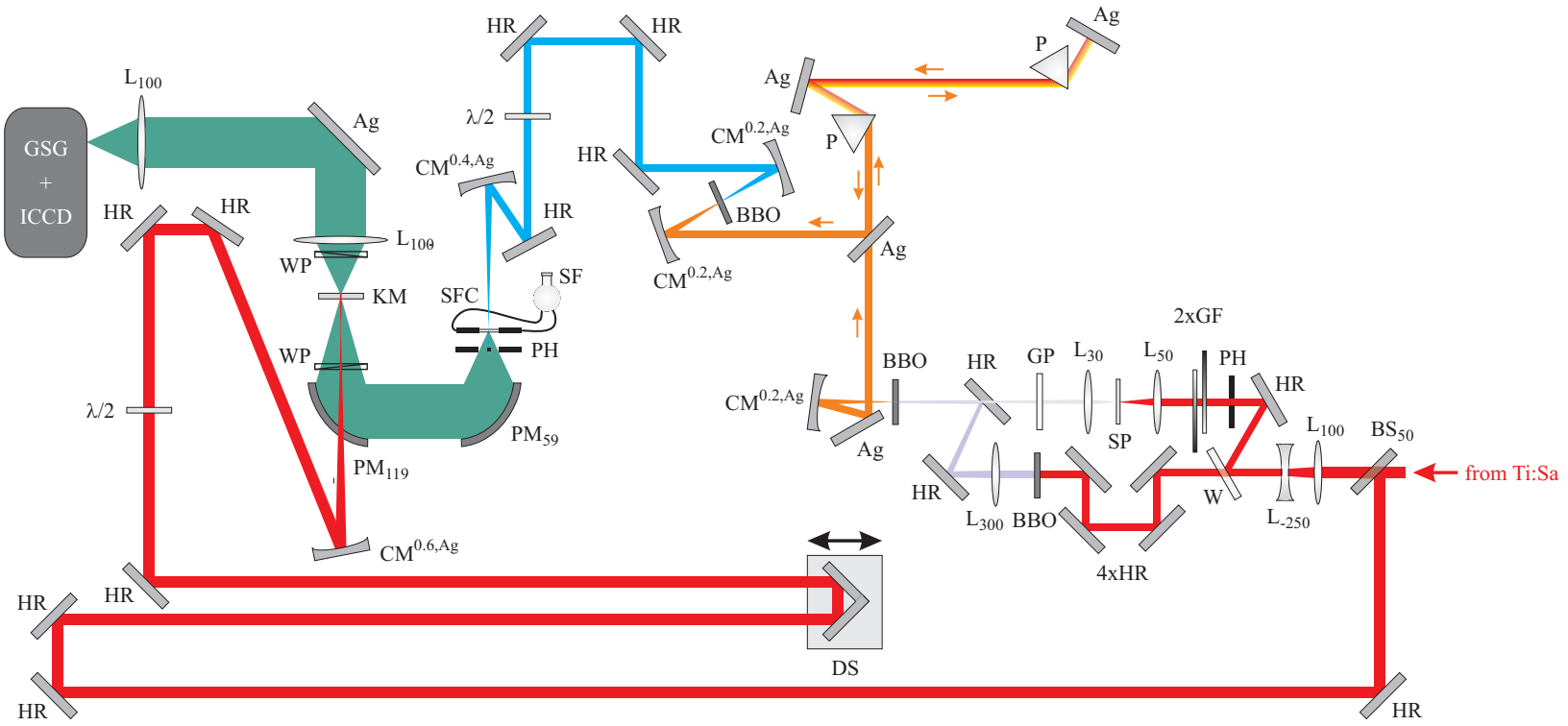

Ag	flat silver mirror	GF	gradient filter	λ/2	half-wave plate	SFC	sample flow cell
BS_x	beam splitter (x = reflectivity in %)	GP	glass plate (d = 1 cm)	L_x	lens (x = focal length in mm)	SP	sapphire plate (d = 1 mm)
BBO	β-BaB_2O_4 crystal	GSG	grating spectrograph	P	BK7 prism	W	wedge (30°)
$CM^{x,y}$	concave mirror (x = rcc in m, y = coating)	HR	high reflective mirror	PH	pin hole	WP	wire grid polariser
DS	delay stage with retroreflector	ICCD	camera	PM_x	parabolic mirror (x = focal length in mm)		
		KM	Kerr medium	SF	sample flask		

Fig. 2.2: Schematic representation of the UV/vis Kerr gating setup. All mirrors denoted as HR are high reflective mirrors suitable for the respective wavelength.

by a camera only during the presence of the intense gate pulse. The birefringence can be quantified by

$$\Delta n = n_{\parallel} - n_{\perp} = n_e - n_o = K \cdot \lambda \cdot E^2, \tag{2.1}$$

where K is the temperature- and wavelength-dependent Kerr constant. The largest transmittance is achieved if the intense gate beam is polarised at an angle of 45° with respect to the fluorescence beam. The Kerr gating technique allows the transmittance of light only during the presence of the gate beam, which makes it suitable for femtosecond time-resolved spectroscopy. Unfortunately, there is a restriction to this application: The induced anisotropy in some materials exhibits a quite long response time, which smudges the time resolution. Namely liquid benzene possesses a delayed response due to free molecular motion in solution. Solids such as flint glass react much faster, as only the electrons rearrange themselves in the intense electric field, but their Kerr constants K are $10 - 20$ times smaller. For the investigation of very weakly fluorescing samples we therefore chose benzene, despite the poor time resolution of ≈ 350 fs. Liquid carbon tetrachloride (CCl_4) provides a better time resolution if the emission is strong enough, its Kerr constant K is ≈ 10 times smaller than that of benzene.[9] The transmittance of light through the Kerr medium is not dependent on a rotation angle or other phase-matching conditions, it is only limited by the transmission properties of Kerr medium and polarisers.

In principle, the Kerr gating setup (see Figure 2.2) is the same as the up-conversion setup regarding the generation of pump and gate beam, although a different Ti:Sa laser system was employed (Coherent Libra HE, 800 nm, 100 fs FWHM, 3.6 mJ, 1 kHz). A small, but important alteration is the presence of a 1 cm glass plate (Schott WG 345 filter) in the NOPA white light continuum beam when generating the pump pulses for the ferulic acid (FA) measurements (cf. Chapter 7). Only with the induced additional temporal and spectral elongation of the seed pulses the desired wavelength of $\lambda = 640$ nm could be generated spectrally sufficiently narrow ($\Delta\lambda \approx 50$ nm) and with adequate intensity.

In the following, only the beam path after the sample flow cell (1 mm path length between two 0.2 mm fused silica windows) is described. Again a pair of aluminium coated off-axis parabolic mirrors ($f_{\mathrm{eff},1} = 59$ mm, $\varnothing_1 = 5.0$ cm; $f_{\mathrm{eff},2} = 119$ mm, $\varnothing_2 = 6.2$ cm) is used to collect, collimate and refocus the emitted fluorescence photons after UV excitation. A fluorescence cone which nearly fills the first parabolic mirror is cut out from the omnidirectional fluorescence with an adjustable pin hole. This facilitates the collimation and consequently the refocusing considerably. The first parabolic mirror has a shorter focal length than the second to collect as much fluorescence photons as possible. Attempts to realise the setup with two $f_{\mathrm{eff}} = 119$ mm parabolic mirrors failed due to insufficient emission intensity. The longer focal length of the second parabolic mirror is needed to place all the required optical components for the Kerr shutter. The collected and refocused fluorescence photons pass a pair of wire grid polarisers (Moxtek, UBB01) before being focused on the Kerr medium, in this case a 1 mm quartz cuvette with liquid benzene. A second

wire grid polariser pair, in cross configuration with respect to the first, is placed behind, so no fluorescence photons are transmitted through the crossed polarisers. The diameter of the emission beam is chosen to be as large as possible when passing the polarisers to ensure the most efficient polarisation. The pump beam polarisation is set to the magic angle with respect to the first polariser pair to avoid depolarisation effects. The gate beam (≈ 100 μJ) is focused on the Kerr medium as well (silver coated reflective mirror, $f = 300$ mm), spatially and temporally overlapping with the emission photons. To be more precise, the gate beam focus lies ≈ 3 cm before the Kerr medium. If it is focused directly into the benzene, the medium degrades and forms a black film on the quartz cuvette windows. If the focus lies behind the Kerr medium, the same can happen due to self-focusing in the liquid benzene. Additionally, a huge amount of white light might be generated by the intense gate beam in the Kerr medium if the focus lies to close, which leads to high background intensities on the camera. The gate beam comes from above the fluorescence beam path, so as not to cross the polarisers. The smallest possible angle is chosen which leads the beam over the second parabolic mirror and the first polariser pair. Nevertheless, the height of the reflective mirror over the optical table is about 25 cm. To ensure high stability, it is attached to a very stable post ($\varnothing = 2.54$ cm, Newport). A delay stage with retroreflector in the gate beam allows for recording time-dependent fluorescence spectra. The LabView routine controlling the experiment allowed for sequential linear step size changes (cf. Section 2.1.1) for the d(pApA) measurements (cf. Chapter 4) and exponentially increasing step sizes for the ferulic acid measurements (cf. Chapter 7).

To obtain fluorescence spectra with a good signal-to-noise ratio, one has to fulfil the following conditions:

- The position of the lens that focuses the fluorescence photons onto the spectrograph and the detector has to be chosen in a way that the wavelength-resolved fluorescence on the camera is as narrow as possible and no scattered pump light is visible. Although the camera is 256 pixel high, only $80 - 100$ pixel should be cut out from that. In Figure 2.3a, an optimally aligned fluorescence trace in a 1024×82 pixel^2 cut-out is displayed. This procedure should be performed with slightly detuned polarisers to observe a nice fluorescence trace and improves the signal-to-noise ratio of the transient measurement considerably, sometimes just over the detection limit. Often (especially for weakly fluorescing and/or long-lived molecules) the rise in fluorescence intensity cannot be observed with a full camera read-out, so one should search for 'time zero' with an appropriate cut-out.
- To achieve the best possible position of the fluorescence trace on the camera, it is often necessary to move the camera itself. The height can be adjusted with the four screw pedestals of the aluminium plate on which the camera stands (check the horizontal position with spirit level). The x- and y-displacement is done manually and requires some diligence.

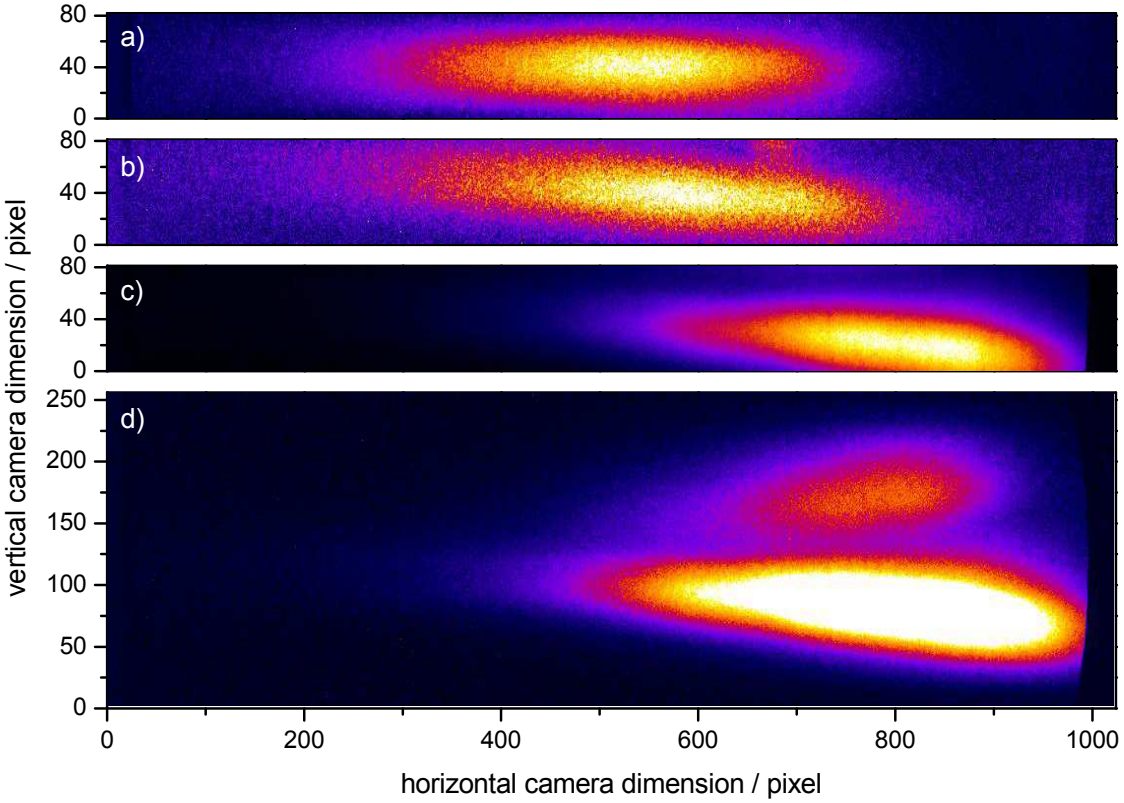

Fig. 2.3: False-colour pictures of spectrally resolved fluorescence light intensities on the Kerr gating CCD camera with arbitrary intensities. All pictures have been taken after excitation with $\lambda_{\mathrm{pump}} = 320$ nm. Pictures a) and b) show emission from two different ferulic acid/buffer measurements, pictures c) and d) emission from 2-aminopyridine/H_2O. a) 1024×82 pixel^2 cut-out from a well-aligned beam path geometry, as it should be strived for. b) 1024×81 pixel^2 cut-out from a slightly curved beam signature on the camera. Note the scattered light contribution around $\lambda = 400$ nm above the fluorescence trace. c) Badly chosen 1024×81 pixel^2 cut-out which clips the emission in the blue wavelength range. d) Full camera read-out, which shows a weak mirror image emission trace due to badly aligned optics.

- The fluorescence trace on the CCD might be slightly curved (see Figure 2.3b). This feature should be minimised to avoid distortion of the wavelength resolution. This is best done by carefully aligning the Ag mirror leading to the camera and ensuring all transmissive optics (lenses, polarisers) are scrupulously perpendicular to the beam path. Another factor may be that the camera is not exactly levelled.
- Scattered light occurs mostly around $\lambda = 400$ nm due to second harmonic generation of the gate pulses in the Kerr medium. As the gate beam pathway differs from that of the collected fluorescence, normally the scattered light contribution hits the camera at a different vertical position. With the curvature not being too strong, the cut-out can be chosen in a way that minimises the scattered light contribution to the transient spectrum. In Figure 2.3b some residual scattered 400 nm light can be seen above the desired emission curve. However, if the gate beam focus lies far enough from the Kerr medium, this feature can be avoided almost completely. Of course

this has to be balanced with the needed signal intensity.

- Every day, the position of the fluorescence trace on the camera should be checked to ensure no fluorescence is clipped due to some displacement in the alignment (see Figure 2.3c). For the same reason, the wavelength calibration with interference filters as well as the sensitivity calibration measurements of suitable dyes with slightly detuned polarisers have to be performed without changing the position of the camera or any other optics compared to the actual measurement.
- If the fluorescence trace seems to have an upside-down mirror image as shown in Figure 2.3d, the alignment should be checked as for the disposal of the curvature. To notice such a feature, always the whole camera picture should be considered, not only the chosen cut-out. Note that the intensity scale in Figure 2.3d is set to show the normally weak mirror image clearly.
- Depending on the lifetime of the investigated molecules, the signal-to-noise ratio is often poor. Therefore, one should take care to check the cross configuration of the polarisers daily and optimise it to the smallest possible emission leaking quantity.[1]
- At least 20 transient spectra before 'time zero' with $\Delta t = 100 - 500$ fs should be recorded to subtract the background reliably. One should take care to ensure that the fluorescence intensity has dropped to the background level for at least 10 transient spectra before the measurement is completed.
- Due to the chirp induced by the transmissive optics after the Kerr shutter, the fluorescence photons show a wavelength-dependent arrival time on the camera. The 'time zero' correction should accordingly be performed with a molecule whose fluorescence is known to rise immediately after excitation.
- The emission beam pathway is highly dependent on the sample solution, as the refractive index changes with the solvent. Therefore it should be aimed at using fluorophores for signal searching and sensitivity correction which can be dissolved in the same solvent as the sample molecule.

The obtained fluorescence spectra were spectrally calibrated with the help of up to six interference filters (Edmund Optics), depending on the emission wavelength range. They were placed in front of the camera and only let pass a specific part of the emission (with detuned polarisers). The resulting spectra were fitted with Lorentzian functions and the pixel positions of the maxima were used to generate a wavelength correction curve for each single measurement. As a grating spectrograph is used, the correction curve is a straight line. An intensity correction was necessary to account for the mentioned transmission properties of polarisers, Kerr medium and quartz cuvette and the wavelength-dependent

1 The quality of the polarisers is crucial for the S/N ratio. The polarisers used for the measurements presented in this Thesis have recently been replaced by new ones (WP25L-UB, Thorlabs), which resulted in an extinction ratio of ≥ 5000 at 500 nm.

sensitivity of the CCD camera. It was performed using a fluorometric calibration curve (FCC) generated by comparing static fluorescence spectra of suitable chromophores with the Kerr-cell polarisers slightly detuned from the cross-polarisation configuration with spectral profiles reported in the literature. In the case of the adenine dinucleotide (cf. Chapter 4), tryptophan in water and 1, 1, 4, 4-tetraphenyl-1, 3-butadiene in cyclohexane were used as chromophores excitable at $\lambda_{\mathrm{pump}} = 260$ nm and emitting in the range of $\lambda_{\mathrm{fl}} = 290 - 500$ nm. For ferulic acid (cf. Chapter 7), i.e., the excitation wavelength $\lambda_{\mathrm{pump}} = 320$ nm and the emission range $\lambda_{\mathrm{fl}} = 350 - 560$ nm, 2-aminopyridine in water was used. Exemplarily for the latter, fluorescence spectra and the resulting sensitivity calibration curve are shown in Figure 2.4. The fluorescence spectra were fitted with a sum of Gaussian functions, respectively, and the comparison of the fits gave the FCC. The fluorometric calibration curve itself was also smoothed in order not to insert artificial noise to the corrected fluorescence spectra. At $\lambda_{\mathrm{fl}} < 350$ nm, the emission detected by the CCD camera was too weak to allow for the unambiguous determination of the FCC. The transient fluorescence spectra of ferulic acid are accordingly shown and analysed at fluorescence wavelengths $\lambda_{\mathrm{fl}} \geq 350$ nm. The maximum value of the fluorometric calibration curve was 2.3 at 350 nm. In the wavelength range of the transient emission maximum of ferulic acid ($\lambda_{\mathrm{fl}} = 390 - 430$ nm), the applied correction factor ranged between $1.6 - 1.1$.

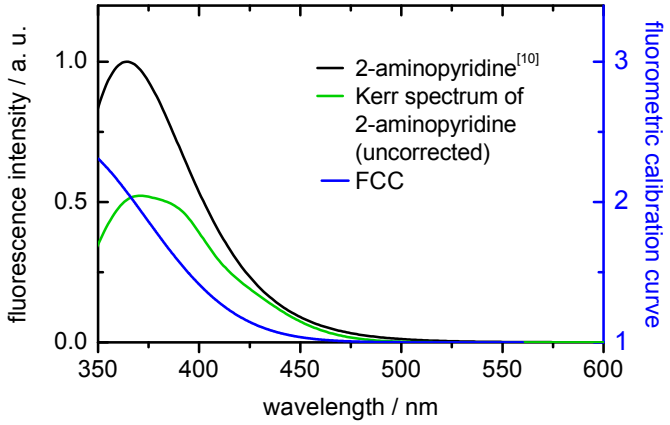

Fig. 2.4: Stationary fluorescence spectrum of 2-aminopyridine (2-AP) in water (literature spectrum [10], black), 2-AP fluorescence spectrum obtained in the Kerr gating setup with the polarisers slightly detuned before calibration (green) and the resulting fluorometric calibration curve (FCC, blue). The FCC could be applied at $\lambda_{\mathrm{fl}} \geq 350$ nm, its scale is given on the right-hand ordinate.

2.1.3 Transient Absorption Spectroscopy Setup

The transient absorption setup presented here is described in detail in the Thesis of Katharina Röttger.[11,12] The Ti:Sa laser system used was the same as for the fluorescence upconversion setup (Clark-MXR CPA2001). Analogous to the two described fluorescence

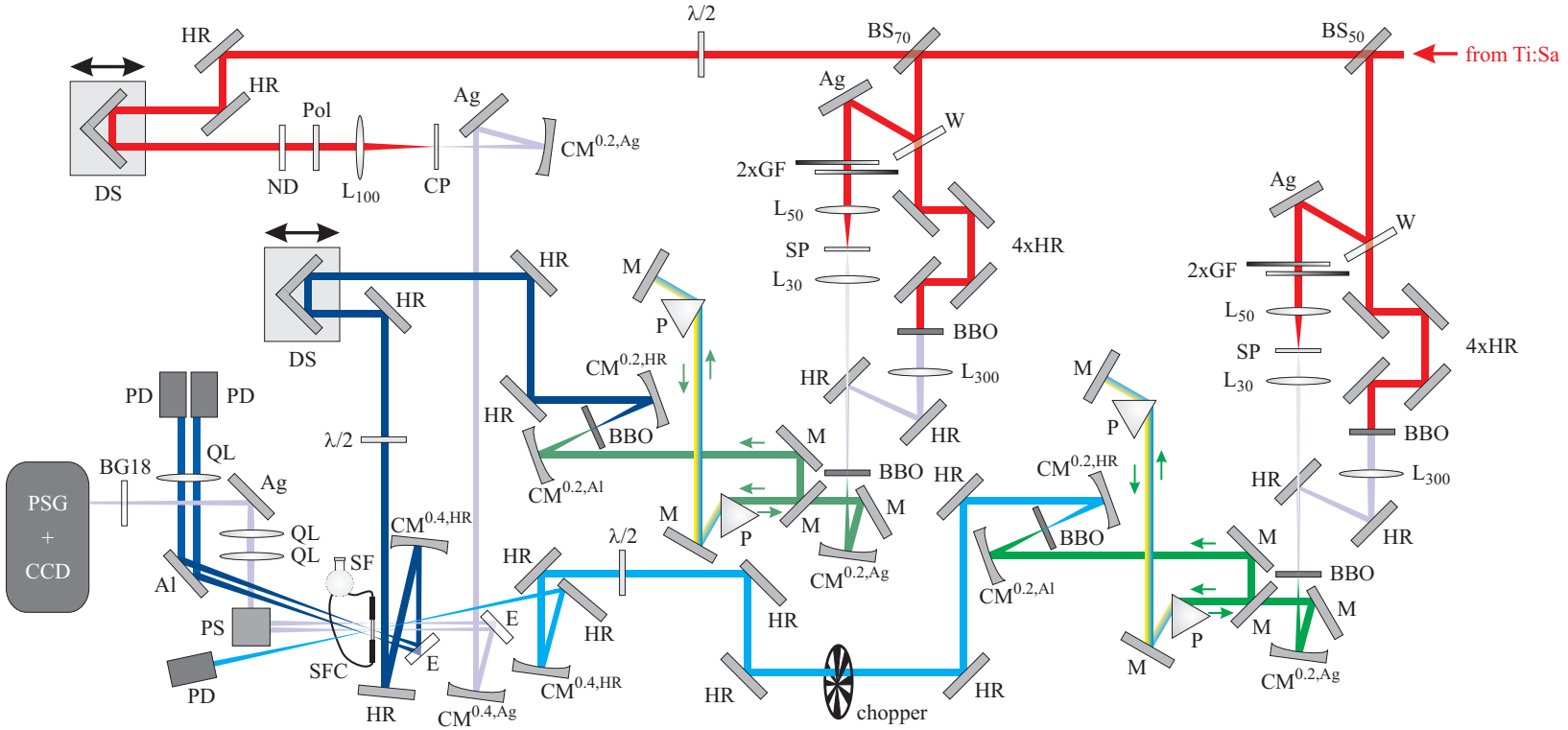

Ag	flat silver mirror	CP	CaF_2 plate (d = 2 mm)	M	flat Ag or Al mirror	PSG	prism spectrograph
Al	flat aluminium mirror	DS	delay stage with retroreflector	ND	neutral density filter	SF	sample flask
BS_x	beam splitter (x = reflectivity in %)	GF	gradient filter	P	BK7 prism	SFC	sample flow cell
BBO	β-BaB_2O_4 crystal	GP	glass plate (d = 5 mm)	PD	photodiode	SP	sapphire plate (d = 1 mm)
BG18	BG18 filter	HR	high reflective mirror	PH	pin hole	QL	quartz lens
CCD	CCD camera	λ/2	half-wave plate	Pol	polariser	W	wedge (30°)
$CM^{x,y}$	concave mirror (x = rcc in m, y = coating)	L_x	lens (x = focal length in mm)	PS	periscope		

Fig. 2.5: Schematic representation of the UV/vis transient absorption setup. All mirrors denoted as HR are high reflective mirrors suitable for the respective wavelength.

setups, the UV pump pulses to excite the sample were generated by a frequency-doubled NOPA, but the transient absorption setup naturally features a quite different detection unit. For the detection of broadband transient absorption, a white light continuum in the range of $\lambda = 320 - 780$ nm is generated in a moving calcium fluoride plate. To record only absorption induced by the pump pulse, i.e., absorption of excited molecules, the white light beam is split with a planar quartz plate ($d = 5$ mm) into probe and reference beam travelling parallel, which are both focused in the sample cell (path length 0.1 mm, 0.2 mm fused silica windows). The probe beam is overlapped spatially and temporarily with the pump beam, whereas the reference beam travels through an unexcited part of the sample cell. Both beams are then recorded wavelength-resolved on two CCD cameras after passing a quartz prism spectrograph. The wavelength calibration was performed with nine different bandpass filters. To correct for intensity differences between probe and reference beam and eventual background issues, transient absorption spectra without pump pulse are recorded. This is achieved *via* a chopper in the pump beam path, which blocks every second pulse. The correlation of recorded intensities with pump beam 'on' or 'off' is checked by a photodiode in the excitation beam path. A second, single-colour probe in the deep-UV is generated by an additional frequency-doubled NOPA. Again this beam is split with a planar glass plate into probe and reference beam and focused on the sample cell. The intensities of UV probe and reference are each recorded with a photodiode. The transient absorption is then calculated from the intensities of probe and reference beams according to

$$\Delta\mathrm{OD}(\lambda, t) = -\log\left(\frac{I^{pr}(\lambda, t) \cdot I_0^{ref}(\lambda, t)}{I_0^{pr}(\lambda, t) \cdot I^{ref}(\lambda, t)}\right). \tag{2.2}$$

I_0^{pr} and I_0^{ref} refer to the intensities of probe and reference beam, respectively, without excitation beam and I^{pr} and I^{ref} mean the measured intensities in presence of the excitation light.

The shot-to-shot readout of the transient absorption spectra leads to a signal to noise ratio of $\approx 10^{-5}$ (wavelength-dependent) for the white light probe beam. The signal-to-noise ratio for the deep-UV probe is $\approx 5{\cdot}10^{-6}$, as the photodiodes allow for a more sensitive detection of the intensities than the CCD cameras. The transient spectra were recorded with exponentially increasing time delays between pump and probe beam (cf. Section 2.1.1). The time resolution of the absorption setup was extracted from the parameter fitting and was found to be ≈ 60 fs for the broadband detection and ≈ 50 fs for the single-colour measurements. The polarisation of the excitation beam was again set to the magic angle to avoid depolarisation effects, which could feign faster deactivation dynamics.

2.2 Data Analysis

All measurements with all experimental setups were performed with several batches and repeated several times on each sample solution to ensure reproducibility and to check that

no photodamage had taken place during the experiments.

The single-colour transient fluorescence and absorption yielded intensity-time profiles at the given fluorescence/absorption wavelength. In the case of the broadband experiments, time profiles at different fluorescence/absorption wavelengths and transient spectra at different delay times were extracted from the recorded 2D maps. All fitting routines necessary for the description of the data were self-written with the MATHEMATICA software and used a non-linear least-squares routine based on the Levenberg-Marquardt algorithm.[13,14] All given errors throughout this Thesis correspond to 2σ standard deviations unless noted otherwise.

2.2.1 Single-Colour Fluorescence Spectroscopy

No data correction procedures were necessary, the intensity-time profiles were analysed exactly as recorded. Most obtained fluorescence-time profiles were described by a sum of decaying exponential functions, convoluted with a Gaussian $G_{IRF}(t)$ describing the instrument response function (IRF).

$$I_\lambda(t) = G_{IRF}(t) \otimes \sum_i A_i \cdot e^{-t/\tau_i} \tag{2.3}$$

The IRF accounts for the limited time resolution of the setup due to a certain duration of pump and gate pulses. The approximation of the IRF with a Gaussian function $G_{IRF}(t)$ is customary. Its most important parameter is the standard deviation σ, which is directly connected with the temporal resolution.

$$G_{IRF}(t) = \frac{1}{\sigma\sqrt{2\pi}} \cdot e^{-t^2/2\sigma^2} \tag{2.4}$$

This function peaks at $t = 0$, its width parameter σ is connected with the full width at half maximum (FWHM) of the Gaussian by

$$FWHM = 2 \cdot \sqrt{2 \cdot \ln 2} \cdot \sigma \approx 2.355 \cdot \sigma. \tag{2.5}$$

The single-colour fluorescence of ferulic acid was described a little differently, by a sum of two decaying exponential functions, one of them rising with τ_{rise}. Both are again convoluted with a Gaussian $G_{IRF}(t)$:

$$I_\lambda(t) = G_{IRF}(t) \otimes \left[A_1 \cdot e^{-t/\tau_1} + A_2 \cdot \left(e^{-t/\tau_2} - e^{-t/\tau_{\text{rise}}}\right)\right] \tag{2.6}$$

This was necessary to account for the delayed rise of the fluorescence, especially at longer emission wavelengths.

2.2.2 Broadband Fluorescence Spectroscopy

In the broadband fluorescence spectra, certain data processing procedures had to be performed on the raw data. The data file itself consists of a '1024×step number' matrix, the delay times of the single steps (vertical pixel) are known. The allocation of the horizontal pixel positions to the wavelength in nm was performed using a calibration curve generated separately for each measurement with the help of up to six interference filters as described above.

The data processing procedure was programmed in MATHEMATICA analogous to a transient absorption fitting routine of Ron Siewertsen.[6] The data itself were treated as follows:

(i) A background correction was performed, in which the transient spectra before 'time zero' were averaged over the time delay and this average background spectrum was fitted with a sum of Gaussian functions. The resulting fit function was then subtracted from every single transient spectrum.

(ii) The data quality was improved by compensating so-called 'baseline jumps'. The emission was averaged over all wavelengths and the resulting spectrally integrated 'time profile' fitted with a sum of Gaussian functions and an exponential function. The resulting fit function has no physical meaning at all, it should only describe the form of the data profile as good as possible. This way, an intensity displacement of a whole spectrum, i.e., due to pump intensity drops, can be accounted for and corrected by adding or subtracting the amount of displacement from the fit function as a baseline to or from the respective transient spectrum. One has to be careful not to smooth the data unreasonably.

(iii) The fluorometric correction had to be applied to ensure the correct intensity ratio and shape of the transient fluorescence spectra. The calibration curve was generated as described in 2.1.2, and multiplied with each transient spectrum.

(iv) The wavelength-dependent arrival time on the CCD camera had to be accounted for with a so-called 'time zero' correction. This was achieved by displacing every pixel column vertically until a common 'time zero' was achieved, using a suitably 'fast' fluorophore sample for calibration.

Due to the poor time resolution and lower sensitivity, no fluorescence-time profiles extracted from the broadband measurements are presented in this Thesis. However, total wavelength-integrated fluorescence lifetimes for FA/buffer and FA/CTAB were determined by integrating over all wavelengths and fitting the resulting time profile according to Section 2.2.1.

The broadband fluorescence setup was used mainly to monitor the time-dependence of the emission maximum, i.e., to follow the solvation dynamics (cf. Chapter 7). To follow the time-dependent shift in fluorescence, transient spectra were extracted from the recorded

2D map and described by a single log-normal function,[15] respectively (Eq. 2.7).

$$f(\lambda) = \frac{a \cdot b}{\lambda - \lambda_0} \cdot exp\left[-\left\{\frac{(\ln\frac{\lambda-\lambda_0}{b})^2}{2c^2} + c^2\right\}\right] \tag{2.7}$$

In the UV/vis spectrum, the use of log-normal functions rather than Gaussian functions is appropriate, as they account for the inherent asymmetry of broad absorption or emission bands when recording them as a function of the wavelength λ rather than cm^{-1}, s^{-1} or eV. The spectro-temporal evolution after excitation can then be quantified by calculating the dynamic Stokes shift. The respective fluorescence peak position as function of time can be described by the so-called solvation-correlation function[16–18]

$$C(t) = \frac{\tilde{\nu}(t) - \tilde{\nu}(\infty)}{\tilde{\nu}(0) - \tilde{\nu}(\infty)}. \tag{2.8}$$

The $\tilde{\nu}$'s may refer to every specific signature in the fluorescence spectrum, here we use the maximum of the time-dependent emission. The difficulty consists in determining precisely the transient spectrum at the time of excitation ('time zero'), to give the peak position $\tilde{\nu}(0)$ before any solvent shell reorganisation has taken place. One possibility to calculate this 'time-zero spectrum' has been described by Fee and Maroncelli.[19] Here, we extrapolated the values for $\tilde{\nu}(0)$ from the $C(t)$ curves. As the fluorescence shift is not completed within the fluorescence lifetime of FA/buffer and only hardly for FA/CTAB, the asymptotic baseline of $C(t)$ was taken as $\tilde{\nu}(\infty)$.[20] After calculating $C(t)$ according to Eq. 2.8, the obtained data were fitted biexponentially:

$$I_\lambda(t) = \sum_i A_i \cdot e^{-t/\tau_i}, \text{ here i} = 2. \tag{2.9}$$

2.2.3 Transient Absorption Spectroscopy

The spectro-temporal 2D transient absorption maps were treated as the broadband fluorescence Kerr gating maps regarding the background correction, compensation of baseline jumps and the 'time zero correction'. The wavelength calibration was done with a fitting curve generated from the peak positions of transmitted light with narrow bandpass filters placed before the CCD cameras. As the quartz prism spectrograph induces a non-linear wavelength resolution, as many as nine different filters were necessary.

For each sample measurement, a blank solvent measurement was performed with exactly the same beam pathway. This allowed for the subtraction of coherent artefacts induced by the intense pump pulse in the glass of the sample cell windows and the solvent contributions to the overall signal. The short optical path length of 0.1 mm in the sample flow cell resulted in smaller than usual contributions from cross-phase modulation (XPM) and very weak signal contributions from solvated electrons generated by multi-photon absorption of the pump pulses. A detailed description of the correction procedure for these artefacts can

be found elsewhere,[6,11] in the following only a short summary is given. From the recorded 2D maps, absorption-time profiles were extracted and fitted according to the procedure for single-colour fluorescence measurements described in Section 2.2.1. An important difference is the consideration of the solvent spectrum. This is achieved by describing the solvent absorption-time profiles at the respective wavelength with a sum of Gaussian and exponential functions and including the resulting overall fit function in the sample measurement fit. Contributions of XPM and solvated electrons are scaled each with a factor, which is implemented as a changeable parameter in the MATHEMATICA fitting routine.[6]

The presented spectro-temporal absorption maps shown in Chapters 4 and 5 are solvent corrected, i.e., the solvent measurement is subtracted from the sample measurement with the scaling factor determined by global fitting at up to 14 different wavelengths over the whole recorded range. From the solvent corrected 2D maps, transient spectra were extracted. In the case of d(ApA), these spectra were fitted by a sum of three log-normal functions[15] (cf. Section 2.2.2). The temporal evolution of the three different absorption bands regarding peak position and band integral was described by a sum of exponentially decaying functions, respectively (see Eq. 2.9).

2.3 Stationary Spectroscopy

2.3.1 Static Absorption Spectroscopy

Static UV absorption spectra have been recorded on a Shimadzu UV-2401 desktop spectrometer. Quartz cuvettes with an optical path length of 1 cm and 1 mm were used, depending on the respective sample concentration. As the used spectrometer is a two-channel spectrometer, the respective solvent contribution is automatically accounted for. Additionally, for each series of measurements the respective solvent was checked against an empty cuvette for eventual impurities or absorption bands in the region of interest.

2.3.2 Static Emission Spectroscopy

Static fluorescence spectra were taken on a Jobin-Yvon FluoroMax-4 spectrometer in 90° mode. The sample concentration was adjusted to an optical density of < 0.5 OD (1 cm path length) at the excitation wavelength. This resulted in an optical density of < 0.05 OD at the recorded emission wavelengths, which was necessary to avoid inner filtering effects. All emission spectra were corrected with internal correction functions and with the excitation energy, which depends on the excitation wavelength. The pure solvent was measured after the respective sample with exactly the same settings. The solvent spectrum was subsequently subtracted from the sample measurement taking the ratio of the water Raman peaks in both spectra as a scaling factor.

2.3.3 Static Circular Dichroism Spectroscopy

Circular dichroism spectra were recorded on a JASCO J-715 spectrometer in the group of Prof. Dr. J. Grötzinger (Institute of Biochemistry, CAU Kiel) with the help of Dr. Sascha Jung. The optical path length in the used quartz cuvettes was 1 cm. The respective solvent measurements were taken before and after the sample measurement and accordingly subtracted.

2.4 Nuclear Magnetic Resonance Spectroscopy

NMR spectra were recorded by Prof. Dr. F. D. Sönnichsen (Otto Diels Institute of Organic Chemistry, CAU Kiel) on a Bruker Avance 600 MHz spectrometer. Standard ^{1}H-NMR spectra as well as 2D spectra (Nuclear Overhauser Effect Spectroscopy, NOESY, and Total Correlation Spectroscopy, TOCSY) were recorded temperature-dependent with a cryostat sample holder. A detailed description of the spectra analysis is given in Chapter 6.

2.5 Sample Preparation and Handling

All investigated molecules were purchased and used without further purification. They were dissolved in aqueous buffer solution to give sample concentrations of < 0.5 OD for the static spectroscopy and the transient fluorescent measurements and about 1 OD for the transient absorption spectroscopy. The lower optical density in the fluorescence spectroscopy is important to avoid inner filtering effects. The molar concentrations depend on the optical path length and are given in the respective Chapter (cf. Chapters 4, 5, 6, and 7). The used buffer solution depended on the investigated molecule. For the DNA samples a pH 7.0 phosphate buffer was appropriate, for the ferulic acid samples a pH 5.0 acetic acid buffer solution was used. The integrity and purity of each solution was checked before and after each time-resolved experiment by static absorption/fluorescence spectroscopy.

2.5.1 DNA Samples

The investigated molecules were purchased from Sigma-Aldrich (dAMP, dGMP, dCMP), The Midland Certified Reagent Company (5'-d(pApA)-3'), and biomers.net (5'-d(ApA)-3', 5'-d(ApG)-3', d[5'-GpGpGp-HEG-pCpCpC-3'], $d(G)_3$, $d(C)_3$, $d(G)_{10}$, $d(C)_{10}$). They were dissolved in phosphate buffered ultrapure water (pH = 7.0, 16 mM NaH_2PO_4, 34 mM Na_2HPO_4, 117 mM NaCl) and the oligonucleotides were thermally annealed, i.e., heated at 90°C for ten minutes and then allowed to cool down to room temperature. Molecular concentrations ranged from $2-10$ mM in the transient absorption measurements (0.1 mm optical path length) and were about 0.2 mM in the transient fluorescence spectroscopy (1

mm optical path length). Static absorption, fluorescence, and circular dichroism spectra were performed in 0.1 or 1 cm cuvettes on tenfold/hundredfold diluted sample solutions.

2.5.2 Ferulic Acid Samples

The sample solutions of ferulic acid in acetic buffer solution (pH = 5.0, 140 mM CH_3COONa, 59 mM CH_3COOH in ultrapure water) were prepared by Kathleen Oehlke and Julia Keppler (Institute of Human Nutrition and Food Science, CAU Kiel) according to Oehlke *et al.*[21] The ferulic acid concentration was 50 μM for the fluorescence up-conversion measurements and the static spectroscopy, for the broadband transient fluorescence spectra an eightfold higher concentration of 400 μM was needed. In the latter case, the optical density in a 1 mm flow cell was $\approx$ 0.5 OD. The micellar solution was prepared by adding cetyltrimethylammonium bromide (CTAB) to the acetic buffer, the CTAB concentration was 30 mM in all cases.

References

[1] W. Demtröder, *Laserspektroskopie: Grundlagen und Techniken* (Springer, 2000).

[2] D. Meschede, *Optik, Licht und Laser* (B. G. Teubner, 2005).

[3] R. W. Boyd, *Nonlinear Optics Third Edition* (Elsevier Inc., 2008).

[4] T. Pancur, Untersuchung der Isomerisierungsdynamik von Azobenzolen und der strahlungslosen Desaktivierung von Nukleobasen mit Hilfe der Femtosekunden-Fluoreszenzspektroskopie, Ph.D. Thesis, Christian-Albrechts-Universität zu Kiel (2004).

[5] N. K. Schwalb, Ultrafast Electronic Deactivation Dynamics in DNA Model Systems by Femtosecond UV Fluorescence Spectroscopy, Ph.D. Thesis, Christian-Albrechts-Universität zu Kiel (2009).

[6] R. Siewertsen, Ultrafast Photochromic Reactions of Structurally Modified Furylfulgides and a Bridged Azobenzene, Ph.D. Thesis, Christian-Albrechts-Universität zu Kiel (2011).

[7] H. Studzinski, Aufbau und Charakterisierung eines nicht-linearen optisch-parametrischen Verstärkers, Diploma Thesis, Christian-Albrechts-Universität zu Kiel (2002).

[8] H. Studzinski, Ultrafast Radiationless Dynamics of Selected Electronically Excited Aromatic Molecules by Femtosecond Time-Resolved Mass Spectrometry and Photoelectron Imaging, Ph.D. Thesis, Christian-Albrechts-Universität zu Kiel (2007).

[9] Y. R. Shen, *Phys. Lett.* **20**, 378 (1966).

[10] W. H. Melhuish, *J. Res. Nat. Bur. Stand., Sect. A* **76**, 547 (1972).

[11] K. Röttger, Ultrafast Deactivation Dynamics of Structurally Modified and Hydrogen-Bonded DNA and RNA Building Blocks, Ph.D. Thesis, Christian-Albrechts-Universität zu Kiel (2013).

[12] K. Röttger, R. Siewertsen, F. Temps, *Chem. Phys. Lett.* **536**, 140 (2012).

[13] Wolfram Research, *Mathematica Edition: Version 7.0* (Wolfram Research, Inc., Champaign, Illinois, 2008).

[14] Wolfram Research, *Mathematica Edition: Version 8.0* (Wolfram Research, Inc., Champaign, Illinois, 2010).

[15] D. B. Siano, D. E. Metzler, *J. Chem. Phys.* **51**, 1856 (1969).

[16] G. Van der Zwan, J. T. Hynes, *J. Phys. Chem.* **89**, 4181 (1985).

[17] B. Bagchi, D. W. Oxtoby, G. R. Fleming, *Chem. Phys.* **86**, 257 (1984).

[18] M. Maroncelli, J. MacInnis, G. R. Fleming, *Science* **243**, 1674 (1989).

[19] R. S. Fee, M. Maroncelli, *Chem. Phys.* **183**, 235 (1994).

[20] K. Hara, H. Kuwabara, O. Kajimoto, *J. Phys. Chem. A* **105**, 7174 (2001).

[21] K. Oehlke, A. Heins, H. Stöckmann, K. Schwarz, *Food Chemistry* **118(1)**, 48 (2009).

3

Femtosecond Fluorescence Measurements of the Adenine Dinucleotide: Direct Observation of the Excimer State

Mayra Stuhldreier, Carmen Schüler, Joscha Kleber, and Friedrich Temps

Institut für Physikalische Chemie, Christian-Albrechts-Universität zu Kiel, Germany
E-mail: stuhldreier@phc.uni-kiel.de, temps@phc.uni-kiel.de

Ultrafast Phenomena XVII, pp. 553 – 555
M. Chergui, D. M. Jonas, E. Riedle, R. W. Schoenlein, A. J. Taylor (Eds.), Oxford University Press, New York, U.S.A., **2011**.

Own contributions presented in this paper:

- Femtosecond time-resolved fluorescence up-conversion spectroscopy
- Writing of the data analysis software and data analysis of all presented data
- Writing of the publication

3.1 Introduction

The effect of intrastrand π-stacking interactions among the nucleobase chromophores on the lifetimes and deactivation dynamics of the excited electronic states of DNA oligonucleotides has been a subject of substantial controversy in the last few years.[1–4] In the case of dinucleotides, it has been supposed based on static emission spectra[5] that the optically bright excited state subsequently forms an excimer state with partial charge transfer (CT) character, in which the excitation is delocalised to a certain extent over the two bases. This paper highlights and elucidates the role of excimer/CT states in the excited-state dynamics of the adenine dinucleotide d(pApA) by means of femtosecond time-resolved UV/vis fluorescence up-conversion measurements.

3.2 Experimental Methods

The experimental setup has been described previously.[6] In short, the investigated molecules in phosphate buffer solution contained in a 1 mm flow cell were excited with ≈ 50 fs pump pulses at $\lambda_{\text{pump}} = 261$ nm generated by a Ti:Sa-pumped frequency-doubled noncollinear optical parametric amplifier. The resulting fluorescence was monitored as function of time by frequency up-conversion using the Ti:Sa fundamental at $\lambda = 775$ nm as gate pulses. The excitation power was kept below 0.1 mW to avoid sample damage.

3.3 Results

Evidence for substantial differences in the excited electronic state structures of di- and oligonucleotides *vs.* mononucleotides is visible in the UV absorption and, especially, in the static fluorescence spectra of dAMP, d(pApA), and d[A(pA)$_{19}$] given in Figure 3.1.

The absorption spectra of both d(pApA) and d[A(pA)$_{19}$] are broader in the red wings compared to dAMP, and they also extend very weakly to longer wavelengths. In particular, the d(pApA) dinucleotide exhibits a weak residual absorption beyond $\lambda = 290$nm, which can arise due to an intramolecular excimer/CT state. The respective static fluorescence spectra differ much more dramatically. The dAMP mononucleotide shows only a very weak emission peaking around $\lambda_{\text{fl}} = 320$ nm. The dinucleotide exhibits weak fluorescence in the monomer region as well, but a stronger, red-shifted fluorescence band around $\lambda_{\text{fl}} = 430$nm is observed additionally. This second band points at an excimer state with certain charge separation. The much higher fluorescence intensity suggests a significantly longer lifetime of that state compared to dAMP. The emission spectrum of the longer d[A(pA)$_{19}$] oligonucleotide shows intermediate behaviour.

The fluorescence-time profiles of d(pApA) were recorded at 14 wavelengths between 290 nm $\leq \lambda_{\text{fl}} \leq 470$ nm to probe the dynamics in the emission bands around 320 and 430 nm.

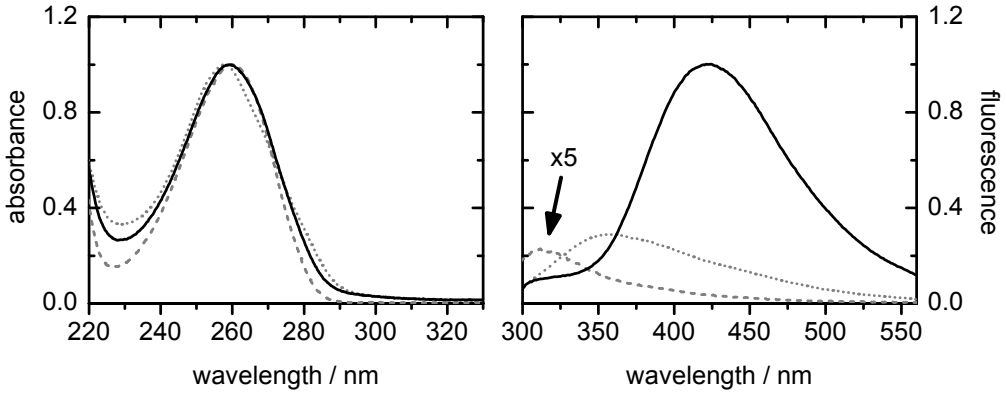

Fig. 3.1: Static absorption (left) and fluorescence spectra (right) of dAMP (gray, dashed), d(pApA) (black, solid), and d[A(pA)$_{19}$] (gray, dotted). The absorptions were normalised at $\lambda = 260$nm. The fluorescence intensity of dAMP has been amplified for better comparison.

Representative fluorescence decay curves in the UV and the visible wavelength regions together with the global fits and the individual exponential contributions are shown in Figure 3.2. In the UV, the time profiles of d(pApA) look quite similar to those of dAMP. The fitted time constants are $\tau_1 = 100$ fs (fixed) and $\tau_2 = 0.36 \pm 0.01$ ps. Accompanying measurements on dAMP for comparison gave a bi-exponential decay with $\tau_1 = 100$ fs (fixed) and $\tau_2 = 0.32 \pm 0.07$ ps at $\lambda_{\mathrm{fl}} = 320$ nm and a single-exponential decay with $\tau_2 = 0.32 \pm 0.07$ ps at $\lambda_{\mathrm{fl}} = 430$ nm. With increasing wavelengths, however, the fluorescence lifetime of d(pApA) becomes much longer than that of the monomer. The observed time profiles in the visible region are thus described using three exponentials with the additional time constants $\tau_3 = 5.1 \pm 0.4$ ps and $\tau_4 = 278 \pm 36$ ps next to the $\tau_2 = 0.36 \pm 0.01$ ps decay time also observed in the UV.

3.4 Discussion

The observed complex fluorescence dynamics of d(pApA) is assigned to two different electronic deactivation pathways. Which one the molecule follows will depend on the extent of base stacking. When the two nucleobases in the dinucleotide are dynamically unstacked, the excitation is localised in one of the bases, resulting in a deactivation as in the mononucleotide. The time constants τ_1 and τ_2 found in both the monomer and the dinucleotide are thus attributed to the ultrafast relaxation out of the initially excited Franck-Condon region and the established deactivation pathway through a conical intersection involving the C^2-H ring puckering motion.[7] Strong base stacking, however, leads to the formation of excimer states, which evidently are quite long-lived. Here, the observation of two longer time constants (τ_3 and τ_4) suggests a stepwise relaxation, during which the molecule visits different conformations. As the stability of the excimer states will depend on the orientation of the two nucleobases towards each other, one may speculate that the initial

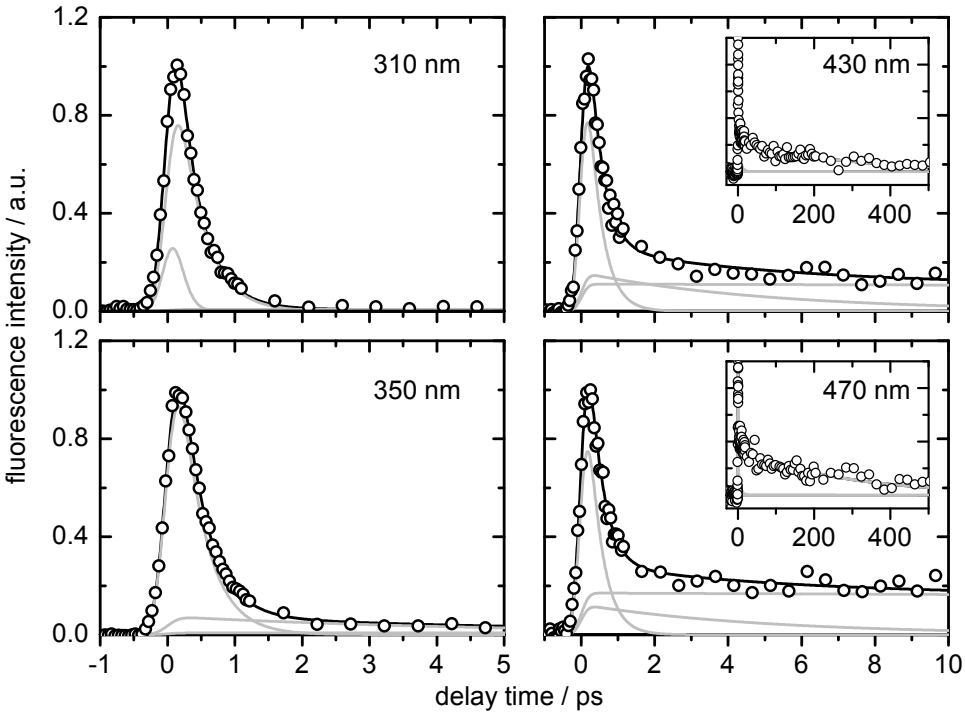

Fig. 3.2: Fluorescence-time profiles of d(pApA) measured at $\lambda_{\mathrm{fl}} = 310$, 350, 430, and 470 nm following excitation at $\lambda_{\mathrm{pump}} = 261$ nm. Open circles represent the data points, black lines the overall fits, gray lines the underlying contributions. Note the different time scales.

orientation of the chromophores at a helical angle of $\approx 36°$ as in B-DNA first leads to an excimer state with a lifetime of 5.1 ps (τ_3). However, the most stable excimer state is supposed to have a face-to-face conformation.[8] The bases could also be somewhat tilted towards each other, likely depending on a possible partial charge transfer in the excimer state. Such a structure should be less easily accessible in longer oligonucleotides, explaining the larger red-shift of the fluorescence of d(pApA) than d[A(pA)$_{19}$]. The return from the excimer state in the excited-state minimum energy configuration to the ground state is concluded to take ≈ 280 ps (τ_4). This experimentally derived picture nicely supports a recent CASPT2 theoretical study.[8]

There is the controversial issue, over how many bases the 'exciton' or 'excimer' character in a DNA oligonucleotide is delocalised.[1,9,10] The present results provide clear, convincing evidence for the formation of such excimer states in the adenosine dinucleotide. Referring to the established base sequence dependence of the electronic deactivation dynamics in DNA,[3] we conclude that the nature and lifetimes of the excited states under discussion depend strongly on the π-stack conformations of the nucleobases. The conformations in turn are highly dynamic, depending on the length of the oligonucleotide strand.

References

[1] D. Markovitsi, F. Talbot, T. Gustavsson, D. Onidas, E. Lazzarotto, S. Marguet, *Nature* **441**, E7 (2006).

[2] C. E. Crespo-Hernández, B. Cohen, B. Kohler, *Nature* **441**, E8 (2006).

[3] N. K. Schwalb, F. Temps, *Science* **322**, 243 (2008).

[4] C. T. Middleton, K. de La Harpe, C. Su, Y. K. Law, C. E. Crespo-Hernández, B. Kohler, *Annu. Rev. Phys. Chem.* **60**, 217 (2009).

[5] J. Eisinger, M. Guéron, R. G. Shulman, T. Yamane, *Proc. Natl. Acad. Sci. U.S.A.* **55**, 1015 (1966).

[6] T. Pancur, N. K. Schwalb, F. Renth, F. Temps, *Chem. Phys.* **313**, 199 (2005).

[7] L. Serrano-Andrés, M. Merchán, A. C. Borin, *Chem. Eur. J.* **12**, 6559 (2006).

[8] G. Olaso-González, M. Merchán, L. Serrano-Andrés, *J. Am. Chem. Soc.* **131**, 4368 (2009).

[9] I. Buchvarov, Q. Wang, M. Raytchev, A. Trifonov, T. Fiebig, *Proc. Natl. Acad. Sci. U.S.A.* **104**, 4794 (2007).

[10] T. Takaya, C. Su, K. de La Harpe, C. E. Crespo-Hernández, B. Kohler, *Proc. Natl. Acad. Sci. U.S.A.* **105**, 10285 (2008).

4

Spectral Signatures of Exciton and Excimer States in the Ultrafast Electronic Relaxation of the Adenine Dinucleotide Revealed by Femtosecond Measurements

Mayra C. Stuhldreier, Michal Malicki[†], Katharina Röttger, Carmen Schüler, Joscha Kleber, Tassilo Muskat, and Friedrich Temps[*]

Institut für Physikalische Chemie, Christian-Albrechts-Universität zu Kiel, Olshausenstr. 40, D-24098 Kiel, Germany

[†]Present address: Department of Chemistry, Northwestern University, Tech K345, 2145 Sheridan Rd, Evanston, IL 60208-3113, U.S.A.

[*]To whom correspondence should be addressed.
Electronic address: temps@phc.uni-kiel.de, URL: http://www.uni-kiel.de/phc/temps

to be submitted

Own contributions presented in this paper:

- Femtosecond time-resolved fluorescence up-conversion spectroscopy
- Femtosecond time-resolved absorption spectroscopy (together with K. Röttger)
- Writing of the data analysis software and data analysis of all presented data
- Writing of the publication

Abstract

The ultrafast electronic relaxation of the adenine dinucleotide [d(pApA) or d(ApA)] after 260 nm UV-photo-excitation has been investigated by means of femtosecond time-resolved fluorescence and absorption measurements, with single-colour and broadband detection in both cases. The results reveal characteristic wavelength-dependent spectral features and excited-state dynamics quite unique for the dinucleotide compared to the adenine mononucleotide and to longer adenine oligonucleotides. In particular, the recorded fluorescence and transient absorption maps and time profiles provide four distinctive time constants, from $\tau_1 \lesssim 0.1$ ps, $\tau_2 = 0.3 - 0.4$ ps, $\tau_3 = 8.30 \pm 0.60$ ps, to $\tau_4 = 380 \pm 40$ ps, which are associated with specific spectral features. Based on the evident spectral splitting and band positions, spectral evolutions and the temporal sequence, the observations are assigned in part to excitonic, transitional and trapped excimer-like excited states of the dinucleotide in stacked conformation and to monomer-like excitations in dynamically disordered dinucleotide configurations. Most importantly, two narrowly spaced excited-state absorption bands with different temporal evolutions are associated with the transformation of the excited initial excitonic state to the long-lived excimer state. The time-resolved fluorescence spectra show the formation of this metastable excimer in $\tau \approx 10 - 15$ ps. The excimer lifetime of $\tau_4 = 380 \pm 40$ ps observed in fluorescence and in transient absorption agrees with the slow component in the ground state recovery time profile measured at $\lambda = 250$ nm. Overall, these results project a comprehensive picture for the electronic relaxation in the dinucleotide as a model for understanding the dynamics in larger oligonucleotides.

4.1 Introduction

The understanding of the nature and dynamics of the excited electronic states in DNA is of paramount importance because of the vulnerability of the genomic information encoded by the nucleobases to photo-induced damage by ultraviolet radiation. Investigations of the underlying molecular and supramolecular mechanisms determining the photostability and photoreactivity of DNA and its building blocks have therefore been of prime interest for decades.[1–4] Several landmark discoveries exemplify the progress achieved over the years: Early studies in the 1970s demonstrated that the free DNA bases and their nucleosides or nucleotides in aqueous solution at room temperature after excitation in their strong first UV absorption bands around $\lambda = 260$ nm stand out for extremely low fluorescence quantum yields ($\phi \approx 10^{-4}$).[3,5] Some thirty years later, time-resolved measurements directly determined the excited electronic state lifetimes of the natural DNA and RNA bases and established their values in the several hundreds of femtoseconds to few picoseconds range.[6–9] These highly acclaimed results have been rationalised by the existence of extraordinarily efficient ultrafast radiationless electronic relaxation pathways, by which the energy of an absorbed UV photon is rapidly dissipated and converted to heat before the

bases are harmed by a photo-induced reaction.[4,10,11] The ultrashort excited-state lifetimes of the natural nucleobases have consequentially been considered as key factors leading to the relative immunity of the DNA to UV-photodamage. Surprisingly, however, measurements on single- and double-stranded DNA oligonucleotides revealed that the electronic lifetimes in these large macromolecular nucleobase assemblies can be some striking three to four orders of magnitude longer than in the monomers.[12–16] This huge discrepancy initiated intense debate, whether the long-lived excited electronic states in oligonucleotides are due to delocalised dipole-coupled 'excitons' extending over several bases,[13,14,17–20] or whether they originate from the formation of 'excimers'[21] by two π-stacked bases on the same strand with possible (partial) charge transfer (CT) character.[15,16,22–25] To complicate matters further, the excited electronic states and dynamics in DNA are affected in yet poorly understood ways by conformational disorder, strand length, and base sequence.[20,23,24,26–34]

In this paper, we report an in-depth study by femtosecond fluorescence and absorption spectroscopy of the photo-initiated dynamics in the adenine dinucleotide $d(A)_2$ (cf. Figure 4.1) as the smallest model system showcasing the effect of π-stacking interactions between two adjacent adenines on the excited electronic states in DNA. The investigation reveals so far unavailable explicit spectro-temporally resolved information on the evolution of the distinct monomer-, exciton- or excimer-like excited states in this model dimer.

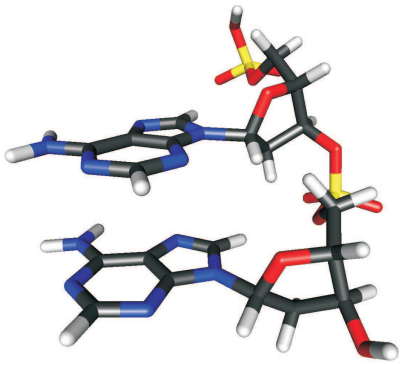

Fig. 4.1: Structure of the adenine DNA dinucleotide $d(A)_2$ in B-DNA conformation. The scheme displays the diphosphate d(pApA), which carries an extra phosphate group at the 5'-end and was employed in part of the present work, besides the monophosphate d(ApA) in the other part.

Considering the monomer adenine chromophore (i.e., 9*H*-Ade, Ado, AMP or dAdo, dAMP) in water under near-physiological conditions as reference, transient absorption experiments found excited-state lifetimes after excitation at $\lambda \approx 260$ nm of $\tau = 0.20 - 0.30$ ps,[6,7,15,35] while time-resolved fluorescence measurements hinted at biphasic decays with time constants in the range $\tau_1 \approx 0.10$ ps and $\tau_2 \approx 0.30 - 0.50$ ps.[8,9,15,36] To explain these results, theory suggested several barrierless electronic deactivation pathways *via* conical intersections (CIs) between the excited and the ground state along distinct internal coordinates.[11,37–53]

Turning to DNA oligonucleotides, however, Plessow *et al.* were among the first who measured long-lived fluorescence with picosecond time resolution and reported lifetimes for $d(A)_{15}$ of several 100 ps and 2 ns.[54] Transient absorption experiments by the Kohler group gave excited-state lifetimes with considerable amplitudes of $\tau = 126 \pm 8$ ps for $d(A)_{18}$, $\tau = 154 \pm 14$ ps for poly(rA) and poly(dA), and $\tau = 150 \pm 30$ ps for the $(dA)_{18}\cdot(dT)_{18}$ duplex.[12,55] Kwok *et al.* soon afterwards presented broadband fluorescence and absorption measurements on $d(A)_{20}$, from which they extracted lifetimes of $\tau \approx 0.39$ ps for adenine-like excited states versus $\tau \approx 4.3$ ps and $\tau \approx 182$ ps for two excimer-like states.[15] Fluorescence up-conversion measurements in our laboratory on single strands of different sequences including $d(A)_{20}$ analysed with a global model led to the determination of decay times of $\tau \approx 5.8 \pm 0.4$ ps and $\tau \approx 100 \pm 20$ ps assigned to excimer formation next to a monomer-like component of $\tau \approx 0.63 \pm 0.03$ ps.[16] Markovitsi and co-workers in contrast proposed that UV excitation populates collective (Frenkel) exciton states delocalised over several adjacent bases on the same or on opposite strands, followed by ultrafast intraband energy transfer to long-lived weakly fluorescent states at the bottom of the exciton stack.[13,14,17–19,56,57] Buchvarov *et al.* suggested the formation of excitons in a series of $d(A)_n$ oligonucleotides of different lengths n upon photo-excitation with a $1/e$ delocalisation length of 3.3 ± 0.5 bases.[20] Studying $r(A)_n$ oligomers, however, Takaya *et al.* found delocalisation over only two adjacent bases, with no hint at a longer delocalisation length.[23] They suggested a dynamic model, where initially populated excitons rapidly collapse to localised excimer states within at most a few ps. According to a subsequent global fitting analysis by Su *et al.*, the same lifetime constants of $\tau = 2.72$ ps and $\tau = 183$ ps describe the bi-exponential decays of the entire series of $d(A)_n$ oligomers from $n = 2 - 18$, but the amplitudes for the short and long components depend strongly on the strand length.[26] Delocalised excitons were concluded to be trapped on no more than two bases after less than 1 ps. From CD measurements on a series of $d(A)_n$ strands, Kadhane *et al.* concluded that only two adenine units couple when excited at $\lambda = 251$ nm, but that this number increases for shorter wavelengths.[58] Gas phase absorption spectra for $d(A)_2$, $d(A)_3$ and $d(A)_4$ by the same group confirmed additionally that the small blue-shift of the absorption maxima of the oligomers compared to the monomer arises predominantly due to excitonic coupling and not from the different micro-environment due to the solvent water molecules.[59] Eventually, temperature dependent transient absorption results led Konorov *et al.* to conclude that the initial excitation in stacked regions of $d(A)_{12}$ is cooperative and involves several bases, the number of which reduces with increasing temperature.[29] The collectively excited exciton should then rapidly decay to a long-lived excimer with lower energy. Considering different conformations, a high degree of base overlap was supposed to favour cooperative initial excitation.[28]

Theoretical work on model systems consisting of two or more adenines with DNA-like orientation underlined the existence of exciton and excimer/CT states,[25,60–71] but arrived at partially contradicting pictures regarding their energies relative to the optically bright

excited states. Particular importance is attributed to the ab initio calculations by Olaso-González *et al.*, who explored the relaxation pathway from the photo-excited state in B-DNA configuration to a neutral excimer with face-to-face structure at substantially lower energy.[70] Hydrogen bonding has been supposed to regulate the fast monomer-like non-radiative decay routes of an adenine in dsDNA.[72] QM/MM calculations of the absorption spectra of A·T DNA suggested that most excited states are delocalised over at most two bases and that CT states are at higher energy than the bright states in the Franck-Condon (FC) region, but coupling between local and CT states may lead to charge separation.[73] Based on time-dependent density functional theory (TD-DFT) calculations including solvation by the polarisable continuum model (PCM), Improta and Markovitsi and co-workers eventually argued in favour of a multi-pathway relaxation mechanism, involving excitons with lifetimes of a few ps, neutral excimers decaying on the sub-nanosecond time scale, and persistent CT states showing weak fluorescence for nanoseconds.[74,75]

Dinucleotides like $d(A)_2$ have been realised as model systems for the investigation of the excited electronic states in RNA and DNA early on.[76,77] Depending on base combination, significantly red-shifted emission bands have been found and interpreted as evidence for the formation of excimer states in dimers with well-stacked structures besides normal monomer-like fluorescence from dynamically unstacked molecules.[1,78–85] Figure 4.2 displays the UV absorption and fluorescence spectra of $d(A)_2$, which is of interest in this paper, compared to dAMP to illustrate the huge differences in excited-state properties between the dimer and the monomer. As can be seen, the strong $\pi\pi^*$ absorption by $d(A)_2$ peaks at slightly shorter wavelength than that of dAMP and is somewhat broader in the red wing (Figure 4.2a). The blue-shift and broadening are well expected and rationalised by excitonic coupling between the two adenines in the stacked configuration.[17,18,59,65] Moreover, the dinucleotide exhibits a weak residual absorption reaching to much longer wavelengths ($\lambda > 290$ nm) than in the dAMP case, hinting at optically nearly dark excimer/CT states at energies below the optically bright $\pi\pi^*$ states. Those relatively minor effects in absorption are left far behind, however, by the dramatic changes in fluorescence behaviour (Figure 4.2b), where the dinucleotide exhibits a strongly red-shifted intense additional emission band with maximum around $\lambda_{\mathrm{fl}} = 430$ nm besides weak fluorescence in the monomer region around $\lambda_{\mathrm{fl}} = 320$ nm. This shift corresponds to a considerable energy difference ($\Delta E \approx 1$ eV). Additionally, the much higher fluorescence intensity in the visible region of the spectrum suggests a much longer excited-state lifetime than in dAMP. This has indeed been demonstrated by a first femtosecond time-resolved measurement.[86] The prevalent stacked, B-DNA-like conformation of the dinucleotide has been confirmed by NMR,[87] CD[88] and ion mobility[89] spectra (cf. Figure 4.S1, Supplementary Information).

In the following, we present femtosecond UV/vis fluorescence up-conversion measurements, broadband UV/vis fluorescence spectra taken with a Kerr-gating setup, broadband UV/vis absorption maps, and single-colour deep-UV absorption measurements of $d(A)_2$ in buffered

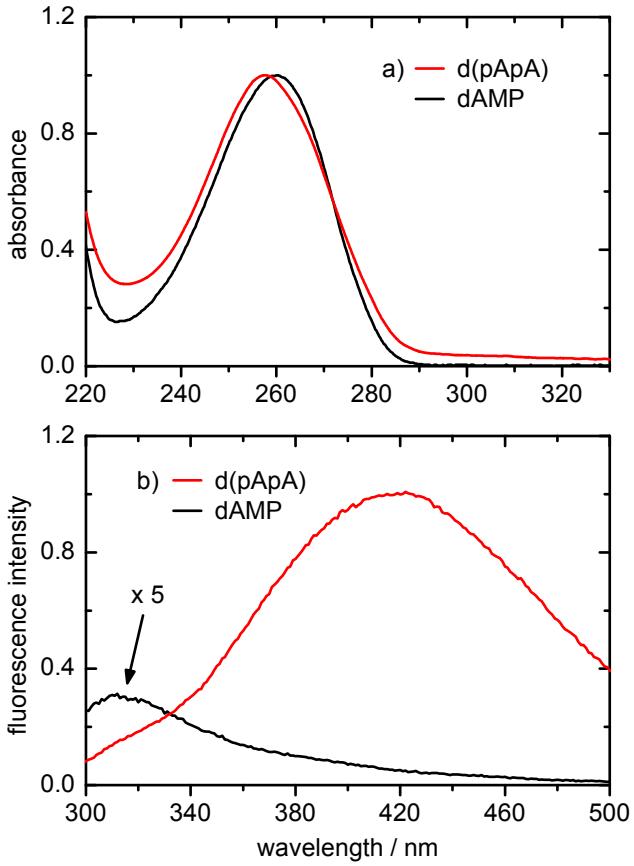

Fig. 4.2: a) Measured static UV/vis absorption and b) fluorescence spectra after excitation at $\lambda_{\text{pump}} = 260$ nm of the adenine dinucleotide d(pApA) (red) and monomer dAMP (black). The absorbances were normalised for better comparison. The fluorescence intensity of dAMP has been amplified for better comparison.

aqueous solution at pH 7.0 to elucidate the complex excited electronic state relaxation mechanisms in ssDNA oligonucleotides. The obtained data exhibit spectrally and temporally resolved evidence for the transformation from the photo-prepared initial exciton in B-DNA-like stacked dinucleotide molecules *via* ultrafast intraband relaxation and subsequent slower structural rearrangement to an energetically stabilised long-lived excimer. Distinctive steps are revealed in the time-resolved emission and/or transient absorption spectra. Additionally, the data indicate that the photo-excited states in unstacked dinucleotides are substantially perturbed by the nearby second adenine such that the supposed 'monomer-like' dynamics require some consideration.

4.2 Experimental Section

4.2.1 Materials

The experimental measurements were carried out in several successive stages with two slightly different $d(A)_2$ dinucleotide samples: Fluorescence decay curves at selected wavelengths and transient fluorescence spectra were recorded with the up-conversion and Kerr-gating techniques for d(pApA), broadband UV/vis and single-colour deep-UV transient absorption measurements were carried out for d(ApA). Both dinucleotide samples differ only by the extra 5'-phosphate group in d(pApA), which is not expected to alter the photophysical properties of the two π-stacked adenine bases by a notable amount because of the efficient shielding of the negative charge on the phosphates by the surrounding water molecules in solution. The compounds were supplied in several batches by Midland Certified Reagents (d(pApA)), biomers.net (d(ApA)) and Sigma-Aldrich (dAMP, AMP, Ado). The dinucleotides were certified by MALDI mass spectra. The integrity of the d(pApA) sample was furthermore checked by electrospray mass spectrometry (see SI, Figure 4.S2). No impurities could be detected other than a small amount of dAMP, which can arise by fragmentation of the dinucleotide in the mass spectrometer or may have already been present as background in the sample, but cannot have an effect on the experimental results regarding the long-lived excited states of the dinucleotide. All mono- and dinucleotide samples were subsequently dissolved in phosphate buffered (16 mM NaH_2PO_4, 34 mM Na_2HPO_4, 117 mM NaCl) ultrapure water (pH 7.0). The dinucleotide solutions were thermally annealed and allowed to slowly cool back down to room temperature before their measurements. UV absorption spectra were routinely taken on a Shimadzu UV-2401 desktop spectrometer. Static UV/vis fluorescence spectra of appropriately diluted solutions were measured using a Jobin-Yvon FluoroMax-4 spectrometer. CD spectra were recorded on a JASCO J-715 spectrometer.

4.2.2 Femtosecond Time-Resolved Measurements

All femtosecond measurements were performed using UV excitation pulses at $\lambda_{\text{pump}} = 260$ nm with magic-angle polarisation in flow cells of 0.1 or 1 mm optical path length with 0.2 mm fused silica windows. Peristaltic pumps between the sample reservoirs and flow cells ensured that the irradiated volumes were exchanged between successive laser shots. For the fluorescence experiments, the solutions were adjusted to optical densities at 1 mm path length of OD $\approx 0.3 - 0.5$, corresponding to concentrations per nucleobase of $\approx 0.2 - 0.3$ mM. The transient absorption measurements were made at 0.1 mm optical path length using solutions of OD ≈ 0.7 (d(ApA)) and OD ≈ 1.5 (dAMP), corresponding to concentrations per base of ≈ 4.4 and 10 mM, respectively. The integrity of the solutions before and after time-resolved measurement was checked by static absorption and fluorescence spectroscopy.

Fluorescence Up-Conversion Measurements

The excitation pulses for the fluorescence up-conversion measurements[36,90] were supplied by a frequency-doubled non-collinear optical parametric amplifier (NOPA) pumped by a regeneratively amplified 1 kHz, 775 nm Ti:Sa laser system (Clark CPA 2001) and focused into the sample cell by an $f = 200$ mm dielectric mirror. The pulse energies were kept at ≤ 100 nJ to prevent photodamage. The resulting fluorescence was collected and refocused into a BBO crystal by two 90° off-axis parabolic mirrors ($f = 119$ mm) for type I sum frequency generation (SFG) with the 775 nm gate pulses from the Ti:Sa laser. The obtained SFG light was monitored as function of pump-gate time delay after passage through an $f = 0.1$ m double monochromator by single-photon counting. The stability of the measurements was checked by recording two time scans per sample solution followed by repetition with a fresh sample. The instrument response function (IRF) and time-zero were determined by the cross-correlation signal of the gate and scattered pump light. The full width at half maximum (FWHM) of the IRF was ≈ 350 fs, resulting in a time resolution of the experiment after deconvolution of $\Delta t \approx 150$ fs.

Kerr-Gated Fluorescence Spectra

The laser pulses for the Kerr-gated transient fluorescence spectrometer designed similar to setups in the literature[91,92] were derived from an 800 nm Ti:Sa oscillator/amplifier system (Continuum Libra HE). The applied 260 nm NOPA pump pulse energies were slightly higher (≈ 350 nJ/pulse) than in the up-conversion experiment. The emitted fluorescence was focused onto a 1 mm cuvette containing benzene as Kerr medium between two doubled wire-grid polarisers (Moxtek UBB01) in crossed configuration. The Kerr shutter was temporally opened by time-delayed 800 nm Ti:Sa laser pulses (≈ 300 μJ) focused into the benzene cuvette at 45° polarisation. The transmitted fluorescence was dispersed by an $f = 0.15$ m spectrograph and recorded by an ICCD camera (Princeton Instruments SpectraPro 2150i + PI-MAX). Photometric corrections were made using a calibration curve generated by comparison of the static fluorescence spectra taken with slightly detuned Kerr-gate polarisers of tryptophan in water and 1,1,4,4-tetraphenyl-1,3-butadiene in cyclohexane with the calibrated fluorescence spectra of Gardecki *et al.* as standard.[93] The temporal chirp of the fluorescence spectra was corrected using AMP in phosphate buffered aqueous solution for reference.[15] The time resolution of the spectrometer was found to be $\Delta t \approx 350$ fs, limited mainly by the relaxation behaviour of the Kerr gate medium.

Transient Absorption Measurements

Our broadband UV/vis and single-colour deep-UV transient absorption spectrometer has been described in some detail elsewhere.[94] The sample solutions of d(ApA) and dAMP for comparison were excited as before at $\lambda_{\text{pump}} = 260$ nm ($\Delta t = 35$ fs, 300 nJ/pulse).

Broadband probe pulses between 320 nm $\leq \lambda_{\text{probe}} \leq$ 680 nm were obtained by supercontinuum generation in CaF_2. Single-colour probe pulses at $\lambda_{\text{probe}} = 250$ nm to monitor the ground-state recovery (GSR) of the molecules after UV excitation were provided by a second frequency-doubled NOPA. The probe pulses were time-delayed with respect to the pump, split into signal and reference, and focused into the sample cell, where the signal pulses were spatially and temporally overlapped with the pump pulses. The transmitted broadband probe pulses were dispersed in a calibrated prism spectrograph and detected by two FFT CCD cameras, the deep-UV probe pulses were measured by two matched photodiodes. The detected data were transferred to a desktop computer *via* a custom-designed controller board (Entwicklungsbüro Stresing Berlin). The experimental time resolutions were between $\Delta t \approx 50 - 60$ fs.

All measurements were repeated several times with each sample solution to ensure reproducibility and to check that no photodamage had taken place during the experiments. A background measurement on the neat aqueous buffer solution was made directly before or afterwards under the same conditions to account for coherent artefacts such as cross-phase modulation (XPM), stimulated Raman scattering (SRS) and weak longer-lived signal contributions from solvated electrons generated by multi-photon absorption of the pump pulses in water. The two-dimensional (2D) spectro-temporal transient absorption maps reproduced in Figure 4.S3 illustrate the high quality of the obtained raw data for a typical sample and a typical background measurement. As shown, all artefacts in the background map were very small and easily corrected for as usual.[95–97]

Data Collection and Analysis

All experiments were controlled by LabView scripts.[98] The obtained time profiles were analysed using Mathematica software[99] by non-linear least-squares fitting of model functions given by the sum of a suitable number of exponentials convoluted with a Gaussian for the IRF. Error limits of time constants given below are 2σ standard deviations unless noted otherwise.

4.3 Results

4.3.1 Time-Resolved Fluorescence Measurements

Fluorescence-Time Profiles at Selected Wavelengths

Figure 4.3 displays the fluorescence-time profiles of d(pApA) measured with the up-conversion setup at 14 distinct wavelengths in the range 290 nm $\leq \lambda_{\mathrm{fl}} \leq$ 470 nm. The selected wavelengths cover the best part of the fluorescence window of the dinucleotide (cf. Figure 4.2). For comparison, Figure 4.S4 gives corresponding results under similar conditions for dAMP.

As can be seen, the measurements reveal drastically different fluorescence dynamics of d(pApA) at UV wavelengths ($\lambda_{\mathrm{FL}} \lesssim 360$ nm) *vs.* longer wavelengths in the visible ($\lambda_{\mathrm{FL}} \gtrsim$ 420 nm). Between $\lambda_{\mathrm{fl}} = 290$ and ≈ 330 nm, the time profiles of d(pApA) look quite similar to those of dAMP (cf. Figure 4.S4). Beginning at $\lambda_{\mathrm{fl}} \gtrsim 340$ nm, however, weak longer-lived contributions start to grow in amplitude with increasing wavelength. At $\lambda_{\mathrm{fl}} \geq 420$ nm, eventually, the long-lived fluorescence not only gains considerably in importance, but also lasts for several hundred picoseconds. Referring to Figure 4.2, the observation of the long-lived fluorescence components at $\lambda_{\mathrm{fl}} \gtrsim 340$ nm coincides with the appearance of the red-shifted 'excimer-like' emission band in the static fluorescence spectrum.

For a quantitative analysis, the experimental fluorescence decay curves were evaluated by global least-squares fitting. To obtain satisfactory representations for the data at all wavelengths, model functions were needed consisting of a sum of four exponentials convoluted with the IRF. The resulting best-fit values for the excited-state fluorescence lifetimes of d(pApA) were found to be

$$\begin{aligned}
\tau_{\mathrm{FL1}} &= 0.10 \pm 0.05 \text{ ps}, \\
\tau_{\mathrm{FL2}} &= 0.41 \pm 0.05 \text{ ps}, \\
\tau_{\mathrm{FL3}} &= 8.30 \pm 0.60 \text{ ps}, \\
\tau_{\mathrm{FL4}} &= \ 380 \pm \ \ 40 \text{ ps},
\end{aligned}$$

with 2σ statistical uncertainties and added estimated systematical error limits for τ_{FL1} and τ_{FL2}. The quality of the fits with respect to the data curves can be seen from Figure 4.3. Apart from τ_{FL1}, the different decay times are well determined because they predominate the fluorescence profiles at distinctive wavelengths. The value for τ_{FL1}, which could not be omitted at shorter wavelengths, is below the resolution of our up-conversion experiment and was therefore kept fixed for the final fit. Decay-associated spectra of the amplitudes for the different components are given in Figure 4.S5.

For comparison, the fluorescence lifetimes for dAMP determined by a global fit to the data in Figure 4.S4 are $\tau_{\mathrm{FL1,dAMP}} = 0.10 \pm 0.05$ ps and $\tau_{\mathrm{FL2,dAMP}} = 0.32 \pm 0.07$ ps in excellent agreement with the literature.[8,9,15,36]

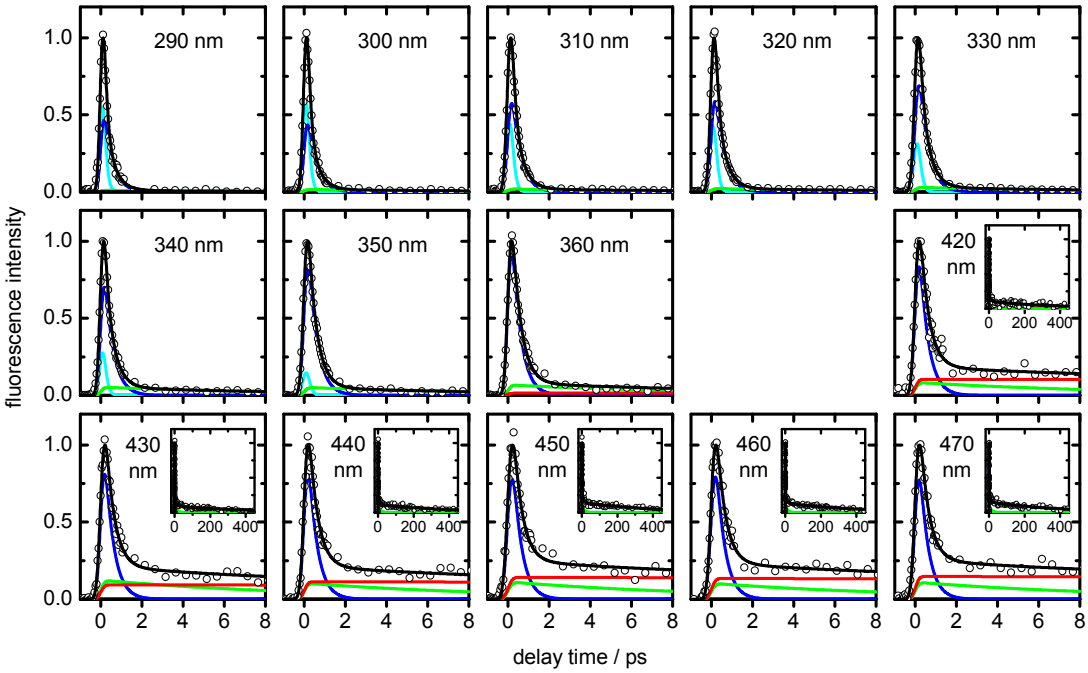

Fig. 4.3: Fluorescence-time profiles of d(pApA) in H_2O (pH 7.0) at 14 selected wavelengths between 290 nm $\leq \lambda_{FL} \leq$ 470 nm after excitation at $\lambda_{pump} = 260$ nm. Open circles represent the data points, black lines the overall fits, coloured lines the underlying contributions, whose decay constants are given in the text. The insets show the same data on a longer time scale. The gap from 370 to 410 nm is due to the high second harmonic intensity resulting from the 775 nm gate pulses in the up-conversion crystal.

Time-Dependent Fluorescence Spectra

The transient fluorescence spectra of d(pApA) measured by Kerr-gating are displayed in Figure 4.4 together with reference spectra for the mononucleoside adenosine (Ado). The spectra are given for selected delay times after the 260 nm excitation pulse for the wavelength range 330 nm $\leq \lambda_{fl} \leq$ 480 nm. At shorter wavelengths, the transmission of the Kerr gate was cut off by the wire-grid polarisers.

As expected from the sub-picosecond excited-state lifetime of Ado, which is basically the same as for AMP/dAMP,[8,9,15,36] the fluorescence of Ado decays very rapidly with time. At $\Delta t = 4$ ps after the pump pulse, the spectrum is no longer distinguishable from the background. In strong contrast, the fluorescence of d(pApA) at $\Delta t = 4$ ps is still quite intense (Figure 4.4b). Moreover, the distributions of the spectra after $\Delta t = 2$ and $\Delta t = 4$ ps are shifted to longer wavelengths compared to $\Delta t = 1$ ps. This slowly starting trend marks the onset of a pronounced spectral evolution that continues towards longer times up to $\Delta t \approx 65$ ps (Figure 4.4c). In particular, the long-lived emission in the visible region of the spectrum with maximum around $\lambda_{fl} = 420$ nm survives for $\Delta t > 100$ ps. On closer inspection, the red-shift of the fluorescence maximum becomes clearly discernible after $\Delta t \approx 10 - 15$ ps. This time thus seems to be the reaction time from the optically prepared

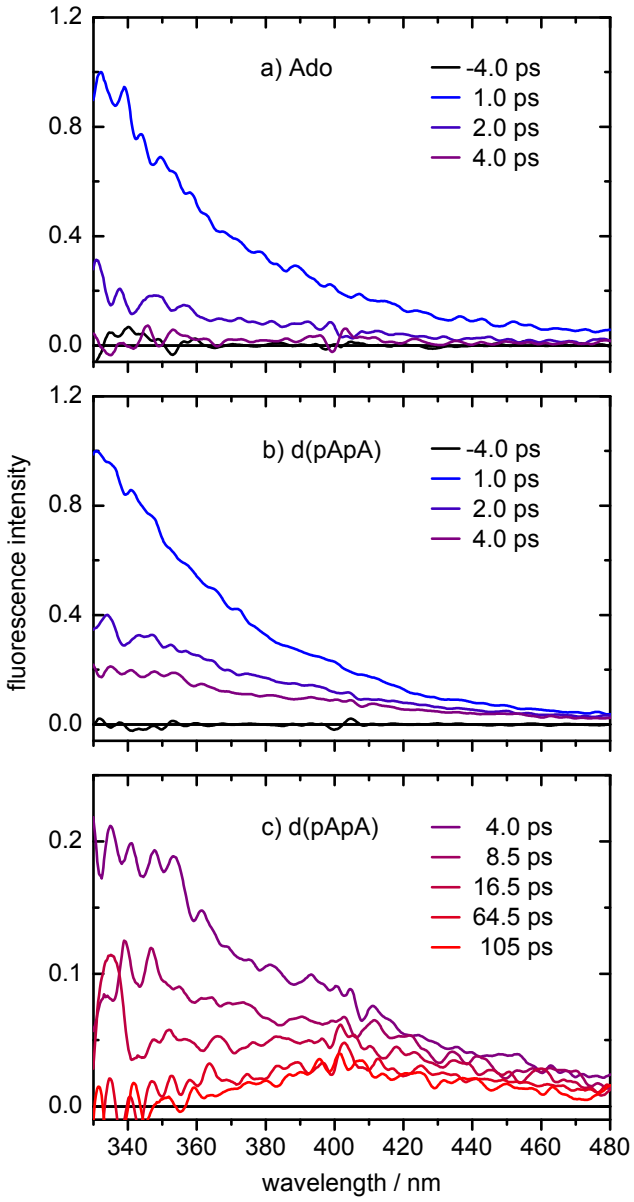

Fig. 4.4: Transient fluorescence spectra of a) Ado and b,c) d(pApA) in H_2O (pH 7.0) at selected delay times after the excitation pulses at $\lambda_{pump} = 260$ nm. The traces at $\Delta t = -4$ ps show the background. Note the different intensity scales in panels b) and c).

initial excited state of the dinucleotide to the long-lived state. At later times, the transient spectra showcase the characteristic broad 'excimer-like' fluorescence with maximum at $\lambda_{FL} \approx 420$ nm predominating in the static fluorescence spectrum (Figure 4.2). The UV fluorescence of d(pApA) around 350 nm, on the other hand, decays more slowly than in the Ado (or AMP/dAMP) cases, but drops to nearly zero after ≈ 30 ps, where the excimer-like emission around 420 nm is still pronounced (Figure 4.4c). These observations are in full agreement with the fluorescence up-conversion data above. They also ensure that no unexpected behaviour happens in the gap in the up-conversion measurements between $\lambda_{FL} = 360$ and 420 nm.

4.3.2 Transient Absorption Measurements

Figure 4.5 shows the 2D spectro-temporal transient absorption map measured for d(ApA) in H_2O (pH 7.0) as sample next to a transient absorption map for dAMP after 260 nm photo-excitation under the same experimental conditions. Both maps were corrected for artefacts from XPM, SRS or multi-photon absorption and the very weak solvated electron absorption (cf. Figure 4.S3) at $\lambda_{\text{probe}} \geq 500$ nm.

As can be seen immediately, the excited-state dynamics of the dinucleotide differ vastly from the mononucleotide. The data for dAMP affirm the sub-picosecond excited-state lifetime of the mononucleotide in agreement with the fluorescence results above and previously reported transient absorption results in the literature.[6,7,15,35] In strong contrast, the dinucleotide d(ApA) exhibits intense excited-state absorption (ESA) bands in the UV around $\lambda \approx 340$ nm and in the visible around $\lambda \approx 625$ nm surviving for hundreds of picoseconds. Thus, the observed excited states of d(ApA) have lifetimes up to three orders of magnitude longer than in dAMP. Moreover, the transient absorption map for d(ApA) reveals a pronounced spectral evolution as function of delay time that was not observed in the dAMP case. In particular, the initially quite broad ESA maximum from $\lambda_{\text{probe}} = 320$ to ≈ 450 nm that dominates the ESA spectrum of d(ApA) in the first picosecond after excitation as in dAMP can be seen to evolve to a rather narrow long-lived ESA band from $\lambda \approx 325 - 370$ nm with peak absorption at $\lambda = 345$ nm (and several 100 ps lifetime). The weaker absorption in the visible region of the spectrum between $\lambda \approx 500 - 650$ nm has a similar lifetime. That this long-lived visible absorption genuinely belongs to the dinucleotide is underlined by a comparison of the raw data maps for the d(ApA) sample

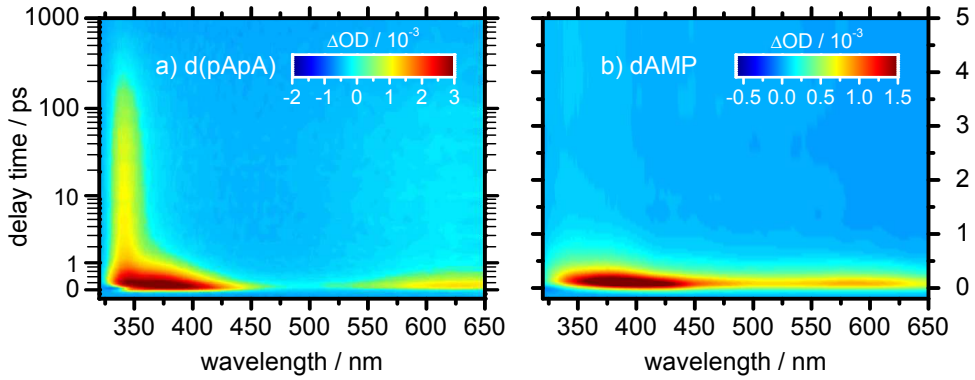

Fig. 4.5: Background-corrected two-dimensional spectro-temporal transient absorption maps of a) d(ApA) and b) dAMP in buffered H_2O (pH 7.0) after 260 nm photo-excitation as function of probe wavelength in the range 330 nm $\leq \lambda_{\text{probe}} \leq$ 650 nm. Note the different time scales in a) and b): The non-linear time scale used for d(ApA) in a) covers the full range from $\Delta t = 0.2$ to 1000 ps obtained by taking $\log(\Delta t + 1 \text{ ps})$ and subsequent relabelling of the axis. The linear time scale for dAMP in b) extends only up to $\Delta t = 5$ ps. The intensities are colour-coded as shown by the insets.

solution and the neat aqueous buffer solution in Figure 4.S3. The evident spectral evolution therefore reflects distinctive dynamical transformations in electronic character and in conformation of the photo-excited dinucleotide molecules as function of time. Eventually, the only region where an extremely short-lived stimulated emission (SE) signal from the initial optically excited state(s) is discernible, is around time-zero near $\lambda = 330$ nm, where the fluorescence up-conversion measurements showed intense fluorescence with ≈ 100 fs lifetime.

The transient spectra at different delay times after excitation displayed in Figure 4.6 illustrate the unusual, surprisingly structured excited-state absorption behaviour of the dinucleotide compared to the mononucleotide more clearly. For d(ApA), three ESA bands are immediately distinguished (Figure 4.6a), the first very broad one with maximum around $\lambda \approx 630$ nm, the second peaking at $\lambda \approx 375$ nm, and the third with sharp peak at $\lambda \approx 345$ nm. In the following, these bands will be referred to as ESA_{630}, ESA_{375}, and ESA_{345}, respectively. This behaviour is unique for d(ApA) as the comparison with dAMP (Figure 4.6c) reveals. The transient ESA spectrum of dAMP is more even with only a shallow minimum near 470 nm and just a single, broader band in the UV with maximum at $\lambda \approx 390 - 380$ nm. On closer inspection, the UV ESA bands of d(ApA) also show pronounced spectral evolution. Both ESA_{345} and ESA_{375} can be seen to shift to the blue within the first few picoseconds. Most importantly, however, ESA_{375} decays much faster (in $\lesssim 2$ ps) than ESA_{345} and ESA_{630}, which survive for several hundred picoseconds (cf. Figures 4.6a and b). Moreover, ESA_{345} seems to rise slightly delayed compared to ESA_{375}. In the dAMP case, one can observe only some spectral broadening of the ESA towards shorter wavelengths.

In order to extract the temporal dynamics encoded in the 2D absorption map of d(ApA), the time histories of the observed vis and UV ESA bands were first analysed in a global fashion after spectral integration between $\lambda_{\text{probe}} = 560 - 680$ nm and $\lambda_{\text{probe}} = 320 - 460$ nm, respectively. The resulting two temporal ESA profiles and the temporal profile of the ground state recovery (GSR) measurement provided by the single-colour deep-UV measurement at $\lambda_{\text{probe}} = 250$ nm are given in Figure 4.7. The data are shown on a linear time scale for the first 5 ps and a logarithmic time scale thereafter. From the fit to the three profiles, four time constants (with 2σ error limits) were extracted:

$$\begin{aligned}
\tau_{\text{TA1}} &= 0.30 \pm 0.08 \text{ ps}, \\
\tau_{\text{TA2}} &= 2.08 \pm 0.06 \text{ ps}, \\
\tau_{\text{TA3}} &= \quad 80 \pm \quad 23 \text{ ps}, \\
\tau_{\text{TA4}} &= 380 \pm \quad 40 \text{ ps}.
\end{aligned}$$

As can be seen, the fits give very good representations of the experimental curves. Considering the time constant values, however, several remarks are in order: First, the quoted τ_{TA1} value is the average of two slightly different values of 0.25 ± 0.08 ps for the ESA band from $560 - 680$ nm and 0.34 ± 0.03 ps for the integrated ESA between the $320 - 460$ nm

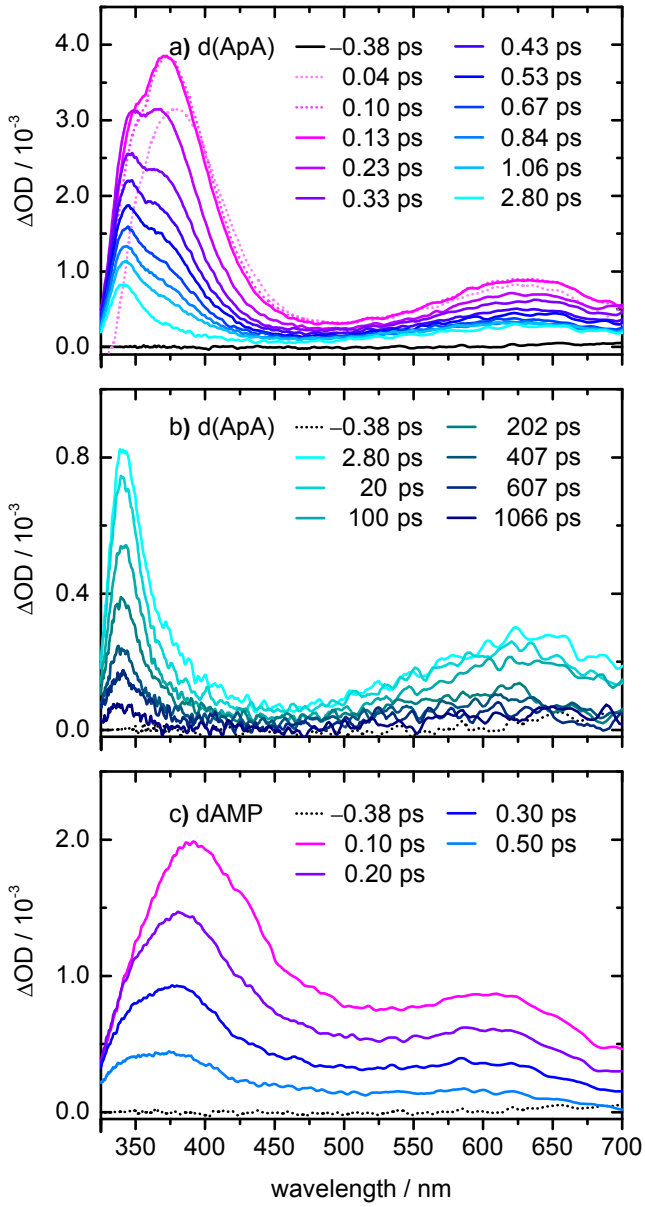

Fig. 4.6: Transient absorption spectra of d(ApA) and dAMP in H_2O (pH 7.0) at different delay times following excitation at $\lambda_{\mathrm{pump}} = 260$ nm. a) d(ApA) up to $\Delta t = 2.8$ ps, b) d(ApA) up to $\Delta t = 1066$ ps, c) dAMP up to $\Delta t = 0.50$ ps. Spectra for delay times before the transient absorption reaches its maximum value in a) are given by dotted lines for clarity.

and the 250 nm measurements, respectively (see Discussion). At 250 nm, on the other hand, τ_{TA1} may describe ESA or the slight time delay in the GSR expected by the sub-picosecond electronic deactivation process. Second, τ_{TA2} describes the vibrational cooling of the internally hot ground state molecules returned from the excited state in the time profile at 250 nm, where it predominates, while the small positive contributions ($\approx 6\%$, respectively) by τ_{TA2} to the ESA bands can only reflect excited-state dynamics. Third, τ_{TA3} and τ_{TA4} highlight the much slower electronic relaxation channels of the dinucleotide.

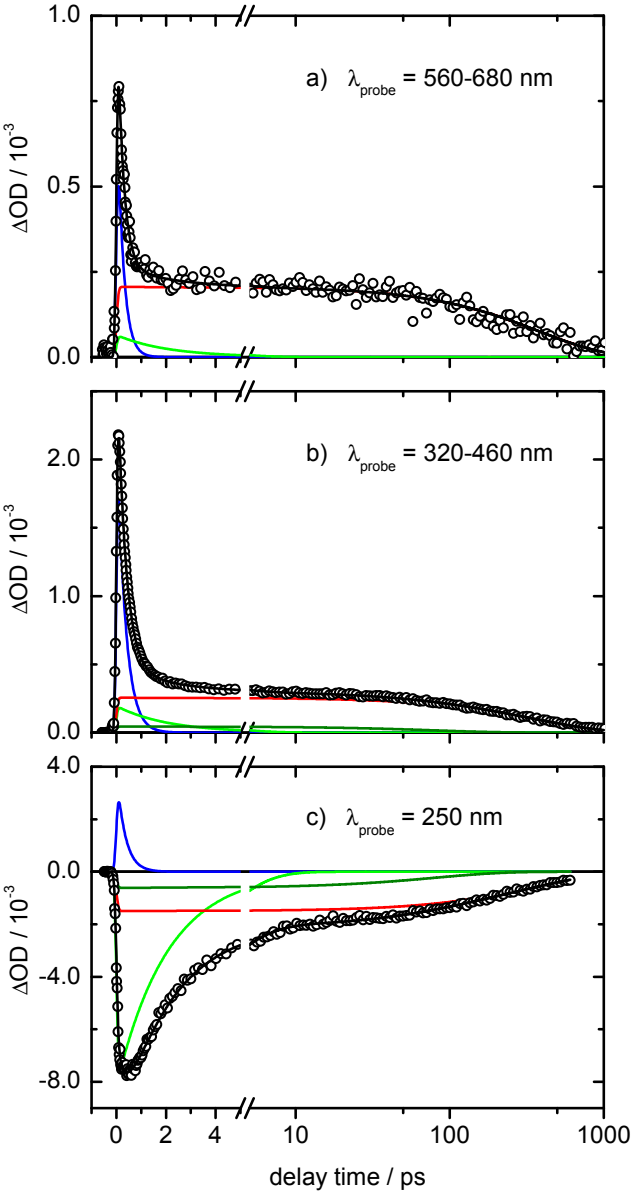

Fig. 4.7: Transient absorption-time profiles of d(ApA) in H_2O (pH 7.0) after excitation at $\lambda_{\mathrm{pump}} = 260$ nm a) in the visible from $\lambda_{\mathrm{probe}} = 560 - 680$ nm, b) in the UV from $\lambda_{\mathrm{probe}} = 320 - 450$ nm, and c) at $\lambda_{\mathrm{probe}} = 250$ nm. Open circles represent the data points, black lines the overall fits, coloured lines the underlying contributions, whose decay constants are given in the text. Note the linear time scale for the first 5 ps and the logarithmic time scale thereafter.

The value for τ_{TA4} was fixed in the fit to the transient absorption data at 250 nm at the value determined by the fluorescence up-conversion measurements because of the shorter observation range in the 250 nm experiment ($<$ 600 ps determined by the translation stage).

Spectro-Temporal Evolution of the UV ESA Bands

The spectro-temporal evolution of the two excited-state absorption bands in the UV region at $\lambda \approx 375$ and ≈ 345 nm ($\Delta t = 0$) reveals so far unprecedented information on the ensuing ultrafast electronic transitions and dynamical transformations which take place in the photo-excited dinucleotide molecules in the first $1 - 3$ ps. The total wavelength integrated UV absorption band cannot account for the eye-catchingly different dynamics of ESA_{345} and ESA_{375}. Therefore, all transient absorption spectra were fitted with three log-normal functions[100] to unravel the fast band-specific dynamics. Selected transient spectra together with the total fit (black line) and the underlying contributions (coloured lines) are displayed in Figure 4.8.

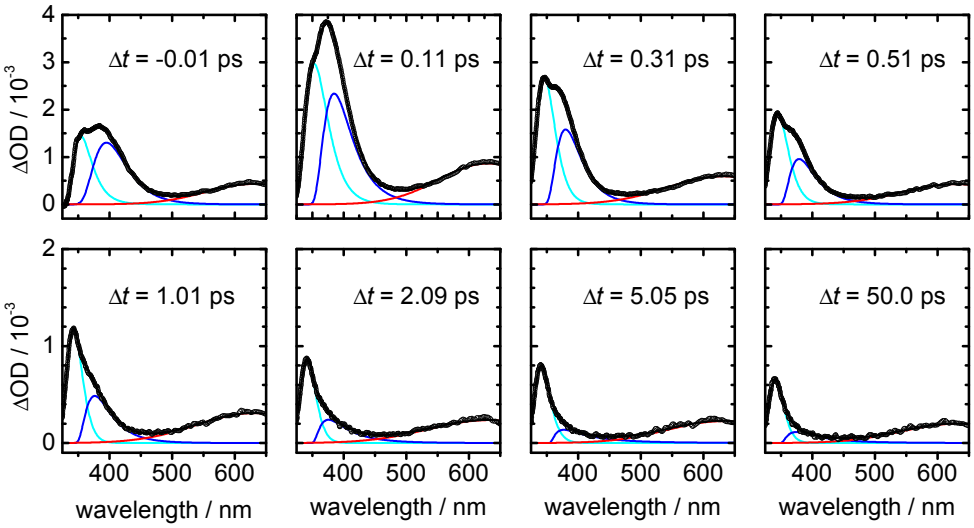

Fig. 4.8: Expanded views of the transient ESA spectra of d(ApA) at selected delay times Δt in the first 5 picoseconds after the 260 nm excitation pulse and at $\Delta t = 50$ ps together with the individual spectral bands (light blue, dark blue and red) from least-squares fits to the experimental spectra (open circles). The overall fits are shown by the black lines on top of the data.

The temporal behaviour of the band integrals for ESA_{345} and ESA_{375} is displayed in Figure 4.9a and b and describes how the entire ESA bands decay after excitation, independent of the wavelength shift. ESA_{630} does not shift temporarily and is therefore sufficiently described by the wavelength-integrated vis absorption band shown in Figure 4.7. The temporal evolution of both UV ESA bands can be described by three decaying exponential

functions, but the initial decay (blue) of ESA_{375} is considerably faster than that of ESA_{345}. The time constants needed to describe the data are

$$\tau_{ESA_{375},1} = 0.22 \pm 0.02 \text{ ps } (78\%) \textit{ vs.}$$
$$\tau_{ESA_{345},1} = 0.39 \pm 0.01 \text{ ps } (86\%).$$

The second time constant (green) is not necessarily comparable. A significant contribution of ESA_{375} decays with

$$\tau_{ESA_{375},2} = 1.0 \pm 0.2 \text{ ps } (18\%),$$

whereas for ESA_{345} a small contribution decaying with

$$\tau_{ESA_{345},2} = 19 \pm 8 \text{ ps } (3\%)$$

was needed in the fitting procedure to describe the data satisfyingly. However, $\tau_{ESA_{345},2}$ only accounts for 3% of the overall fit, therefore its physical meaning is debatable. Both bands then feature a long-lived contribution (red), which was fixed to $\tau = 380$ ps in the fitting procedure. About 4% of ESA_{375} and 11% of ESA_{345} decay on this time scale. It has to be noted that the longevity of ESA_{375} may also be misleading. When looking carefully at the transient spectra in Figure 4.8 one notes that the discernibility of both ESA bands vanishes after $1 - 5$ ps. Therefore the long-lived component in the temporal behaviour of ESA_{375} might well be an artefact of the fitting procedure, and the absorption band actually decays completely within the first few ps. However, it was not possible to model this scenario with appropriate accuracy without constraining nearly every fitting parameter.

The wavelength shift of ESA_{345} and ESA_{375} was quantified by a correlation function

$$C(t) = \frac{\tilde{\nu}(t) - \tilde{\nu}(\infty)}{\tilde{\nu}(0) - \tilde{\nu}(\infty),} \tag{4.1}$$

where $\tilde{\nu}(t)$ refers to the peak wavenumber of the absorption band as a function of delay time after excitation. $\tilde{\nu}(0)$ and $\tilde{\nu}(\infty)$ as peak wavenumber at 'time zero' and after completion of the wavelength shift merely serve as scaling factors. The data could be described by a biexponential decay for both ESA_{345} and ESA_{375} as shown together with the corresponding total fit (black lines) and the underlying contributions (coloured lines) in Figure 4.9c and d. The time constants of the biexponential fit for both ESA bands are

$$\tau_{C(t)_{375},1} = 0.05 \pm 0.04 \text{ ps } (69\%) \text{ and}$$
$$\tau_{C(t)_{375},2} = 0.32 \pm 0.09 \text{ ps } (31\%).$$

resp.

$$\tau_{C(t)_{345},1} = 0.04 \pm 0.01 \text{ ps } (87\%) \text{ and}$$
$$\tau_{C(t)_{345},2} = 0.70 \pm 0.03 \text{ ps } (13\%)$$

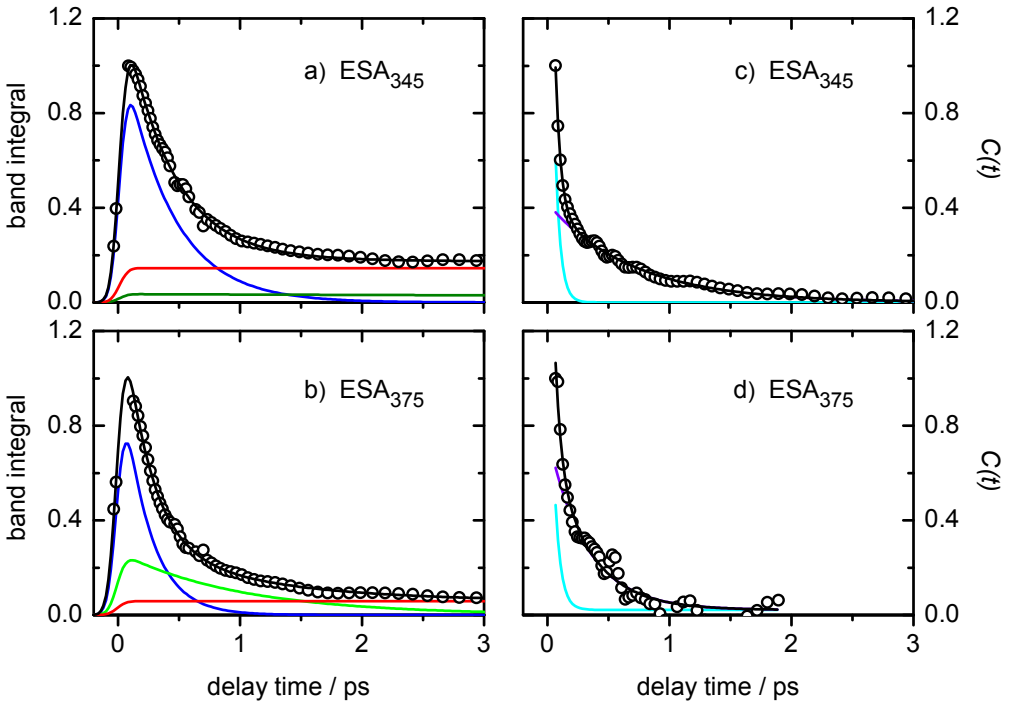

Fig. 4.9: Band integral-time profiles for a) ESA_{345} and b) ESA_{375}, together with peak wavenumber-time profiles, quantified as $C(t)$, for c) ESA_{345} and d) ESA_{375}. Open circles represent the data points, black lines the overall fits, coloured lines the underlying contributions, whose decay constants are given in the text.

The contribution of the faster component in both cases is denoted by a light blue line, the contributions of the slower component by a purple line. The fast peak wavenumber shift in both cases is virtually the same, although its relative amplitude is lower for ESA_{375}. The slower decay is twice as fast for ESA_{375} than for ESA_{345} within the experimental error limits.

4.4 Discussion

The obtained comprehensive experimental results illuminate the photo-initiated dynamics in the adenine dinucleotide from several viewpoints: The time-resolved fluorescence data reflect the properties of the excited states in the Franck-Condon window, the departure of the wavepacket from the FC region and the surviving weakly fluorescent states, which differ substantially from the initial states. The spectro-temporal absorption data probe the excited-state dynamics at short and long times *via* $S_1 \rightarrow S_n$ ESA even when the $S_1 \rightarrow S_0$ transition turns optically dark. The two distinct excited-state absorption bands with drastically different temporal dynamics in the near UV reveal the evolution of the exciton/excimer-like states in the dimer at yet unprecedented level. The eventual ground state bleach (GSB) recovery measured in the deep-UV demonstrates the return of the photo-excited molecules to the ground state and rules out persistent other optically dark states. These complementary data converged nicely. By all measures, the photophysical

behaviour of the dinucleotide differs drastically from the monomer nucleotide and showcases an intricate hierarchy of dynamical processes on vastly differing time scales, from $\tau \lesssim 100$ fs, *via* $\tau = 0.30 - 0.40$ ps and $\tau \approx 8$ ps, to $\tau = 380$ ps. This wide range of observed lifetimes spanning more than three orders of magnitude reflects quite distinct excited molecular states and configurations that are sampled in the course of the electronic relaxation from the photo-prepared initial (exciton) state back to the ground state.

To set the stage for the subsequent evaluation in view of the frequent debate about the interpretation of such multi-exponential dynamics, some general remarks are in order. In the first place, we realise that a wavepacket prepared by a femtosecond laser is not expected to decay exponentially when different regions on the respective potential energy hypersurface (PEHS) are sampled. This is true especially in multichromophore systems. When excited-state relaxation leads to changes in emission, for instance, this may indicate departure from the FC window, rapid intramolecular vibrational redistribution (IVR), change in electronic character, e.g., by mixing of $\pi\pi^*$ and $n\pi^*$ states when the molecule becomes non-planar, and/or change in solvation. Transitions like departure from the FC region, approach of an extended flat region on the PEHS, change in electronic character, or resolvation are well documented in the relaxation of DNA base monomers,[4,24] where they are supported by electronic structure and quantum dynamics calculations.[11,50,101] IVR and vibrational cooling in the excited state, on the other hand, are expected to be similar in the different purine bases. But since the measured lifetimes for, e.g., adenine,[6,7,9,15,36] guanine[6,7,9,102] and hypoxanthine[94,103,104] differ strongly, those effects should not predominate here. It has to be kept in mind, however, that proposed intermediate 'states' in the electronic relaxation may not necessarily correspond to true local minima on a PEHS. Instead, they may describe dynamically distinct transient configurations of the photo-excited molecules en route. Eventually, given the complexity of the relaxation dynamics even in single base monomers, it is unreasonable at this time to expect definitive explanations for all experimental findings. Comparison with the monomer nucleotide will nevertheless allow us to pinpoint critical steps in the unique photo-induced dynamics in the adenine dinucleotide.

The assignment of the various components of a multi-exponential decay curve to specific dynamical processes in the investigated molecules is in general not unproblematic as the motion of a photo-excited wavepacket on a complex multi-dimensional potential energy hypersurface may be inherently non-exponential. Moreover, the sample solutions consist of a quite inhomogeneous ensemble of dynamically more or less well stacked dinucleotide molecules. In the present case, however, where the comparison of the data for the dinucleotide and the mononucleotide revealed huge differences which can only arise by specific coupling mechanisms in the dinucleotide, the above aim appears justified. First, the well-defined values for the different time constants, which span more than three orders in magnitude from $\lesssim 0.1$ ps to ≈ 400 ps with rather small percentage error limits, strongly suggest that they belong to specific processes or mechanisms. This is true in particular,

where virtually identical values were found from the fluorescence and from the absorption data, as was the case both at the fast end ($\tau_{\mathrm{FL1}} \lesssim 0.10$ ps, $\tau_{\mathrm{FL2}} \approx 0.41$ ps *vs.* $\tau_{\mathrm{ESA1}} \approx 0.30$ ps) and at the slow end ($\tau_{\mathrm{FL4}} = \tau_{\mathrm{ESA4}} = 380$ ps). On the other hand, the observation of decay time constants exclusively either in fluorescence ($\tau_{\mathrm{FL3}} \approx 8$ ps) or absorption measurements ($\tau_{\mathrm{ESA2}} \approx 2$ ps and $\tau_{\mathrm{ESA3}} \approx 80$ ps) hints at deactivation pathways which are optically dark regarding either absorption to S_n states or fluorescence. Furthermore, the theoretical understanding of the excited electronic states and radiationless relaxation mechanisms in the DNA bases and small oligonucleotides has reached a state, where the various elementary steps may be quantitatively elucidated. With these premises, we may rationalise the observed excited-state dynamics of the adenine dinucleotide by at least two different electronic deactivation pathways. Which one the molecule follows will largely depend on the degree of base stacking. This property of course is a very dynamical one, allowing for a range of intermediate situations.

4.4.1 dAMP

As already noted, the measured excited-state lifetimes for dAMP agree well with available literature data.[4,6–9,36] The underlying deactivation mechanism has been addressed by quantum chemical excited-state calculations[37–46,49] and molecular dynamics simulations.[11,47,48,50–53,71,72,105,106] At $\lambda \approx 260$ nm, two $\pi\pi^*$ states (L_b and L_a) and one $n\pi^*$ state have to be taken into consideration. Solvation by water stabilises $\pi\pi^*(L_a)$, which carries the bulk of the oscillator strength from S_0, and destabilises $n\pi^*$. The intensely debated question of the correct ordering of those states at vertical excitation is somewhat artificial, however, because the answer depends strongly on the fluctuating surrounding water molecules.[52] Moreover, the excited determinants show significant configurational mixing. Thus, the optically bright photo-excited state ($\pi\pi^*(L_a)$) at $\lambda \approx 260$ nm may actually correspond to the first (S_1) or second (S_2) or even the third (S_3) vertically excited state at the ground-state equilibrium configuration of hydrated adenine. Consensus appears to emerge[9,11,47,50–53] that the short lifetime of $\tau_1 \lesssim 0.1$ ps seen in fluorescence is associated with the rapid departure of the excited wavepacket from the FC region of the photo-excited $\pi\pi^*(L_a)$ state and ultrafast $(S_3/S_2) \rightarrow S_1$ relaxation. Moving through a region, where the three excited states are strongly mixed, the wavepacket thus reaches the S_0 state within $\tau_2 \approx 0.3 - 0.4$ ps *via* two S_1/S_0 CIs. One route involves ring puckering at the C^2 atom, the other distortion of the pyrimidine ring at the C^6 position and NH_2 out-of-plane motion.[11,38–41,45,49–52] Unfortunately, a gap still exists between ab initio and semi-empirical multireference configuration interaction calculations regarding the relative contributions by those routes.[51,52] Simulations based on time-dependent density functional theory (TD-DFT) have been noted to be incompatible with the experimental data at present.[51]

4.4.2 Franck-Condon Excited States of $d(A)_2$

The dinucleotide exists in solution mainly in B-DNA conformation and the two stacked adenine sub-units in the B-type DNA helix configuration experience sizeable excitonic coupling. As is well known for adenine, two $\pi\pi^*$ and at least one $n\pi^*$ state per base have to be taken into consideration. This leads to a number of transitions accessible by a UV pump pulse, which is further increased by static and dynamic disorder. CT states originating from interbase transitions are in principle also possible, but they lie most likely at higher energies than the optically bright $\pi\pi^*$ states in the FC range.[64,65,67,74] Following the vertical photo-excitation process to the $\pi\pi^*$-type exciton state(s), we first expect relaxation within the (neutral) exciton stack of states. This process takes place within $\tau \lesssim 0.1$ ps and results in an energetically stabilised, $\pi\pi^*$-bound excimer $d(ApA)^*_{X(BDNA)}$ due to the excited-state electronic interaction of the two adenines in B-DNA stacked conformation.

4.4.3 Excited-State Pathway Towards Long-Lived Excimer States

The subsequent energetic stabilisation of the excimer is expected to be accompanied by conformational changes, especially in the helical angle and in the distance between the two adenines, but also in the solvation shell. In the final minimum energy configuration of the excited state, the electronic state structure of the dinucleotide will therefore differ substantially compared to the adenine monomer, resulting in the observed very different electronic deactivation dynamics after UV photo-excitation. Both fluorescence and absorption data reveal that eventually a long-lived excited state with a lifetime of $\tau = 380$ ps is populated. In the intermediate timescale, two main features have to be examined more closely. Firstly, time-resolved fluorescence exhibits a contribution decaying with $\tau \approx 8$ ps. Secondly, the spectro-temporal evolution of the specifically structured excited-state absorption band grants a lot of information regarding transformation processes in the excited state. In the following, we derive from these data a plausible picture of the relaxation pathway in the excited state. This explanation is not necessarily the only appropriate one, but it is internally consistent.

Initial Excited-State Transformations

Both ESA_{375} and ESA_{345} show a very fast contribution to the overall peak wavenumber shift, which can be rationalised by intra-exciton stack relaxation within $\tau \approx 50$ fs. We point out that the transient blue-shift monitors the energetic stabilisation of excited states, not their depopulation. The difference in the slower contribution to the dynamic blue-shift for both transient absorption bands consequently indicates that ESA_{375} and ESA_{345} monitor different excited states, or rather different regions on the PEHS. These two conformations evolve separately until reaching their respective minimum. The relaxation is completed

two times faster for ESA_{375} than for ESA_{345}. The two narrow UV ESA bands originating from different excited-state conformations stand in contrast to the spectral characteristics of dAMP (see Figure 4.6). As described above, dAMP deactivates ultrafast *via* a well-described barrierless excited-state pathway and cannot possibly be trapped on the excited-state surface. On the contrary, the initially prepared wavepacket in the excited state spreads out on the way towards conical intersections with the electronic ground state, thus leading to the broad, unstructured excited-state absorption. The broad UV transient absorption band seems to slightly blue-shift as well, but the shift is difficult to quantify.

After energetic stabilisation of the initially populated exciton states, their depopulation can be followed by ESA band integral-time profiles. The different excited-state lifetimes of ESA_{375} and ESA_{345} confirm their assignment to distinct excited-state conformations. In particular, we attribute ESA_{345} to a long-lived excimer state predicted by theory, where the two adenine subunits exhibit face-to-face (F2F) configuration at considerable shorter distance than in B-DNA ($\approx$ 2.9 Å *vs.* 3.4 Å).[70,74,107] This state is characterised by maximal orbital overlap and shared electron density between the two adenine subunits, and will in the following be denoted as $d(ApA)^*_{X(F2F)}$. This assignment is supported by the long lifetime of $\tau = 380$ ps of ESA_{345} and the observation of a similar 'excimer band' for the dinucleotide d(ApG).[108] The initial ESA_{345} decay with $\tau \approx 0.4$ ps indicates that besides the evolution towards the long-lived excimer, an ultrafast deactivation pathway is also accessible. Whether this deactivation can be regarded as 'monomer-like', has to be considered with caution and is discussed below.

The second ESA_{375} band seems to reflect mainly the dynamics of dynamically unstacked dinucleotides, which decay 'monomer-like' with $\tau \approx 0.2$ ps. One may speculate that the $\tau = 1$ ps component, which accounts for $\approx$ 18% of the overall signal, reflects the interconversion of an unstacked dinucleotide towards the more stable face-to-face excimer conformation. This transition would require rotation motions of the two chromophores, which is likely to take place in the ps region. However, the picosecond component may as well reflect 'perturbed-monomer-like' dynamics of one adenine subunit being influenced by the adjacent nucleobase (discussed below).

Excited-State Pathway Towards $d(ApA)^*_{X(F2F)}$

The energetic relaxation towards the F2F excimer state proceeds supposedly along a combined molecular torsion and intermonomer distance coordinate and visits several intermediate geometries.[70,107] With complementary time-resolved measurements we observed a hierarchy of three time constants ($\tau \approx 8$ ps, 80 ps and 380 ps), which backs the assumption of a sequential relaxation. The $\tau \approx 8$ ps decay component needed to model the fluorescence profiles at $\lambda_{FL} \geq 420$ nm is tentatively ascribed to an intermediate state or conformation (not necessarily a true local energy minimum) en route to the long-lived excimer. Broadband fluorescence spectra also showed a clear 'excimer fluorescence band'

after $\Delta t \approx 10 - 15$ ps. We therefore conclude that the excited-state population after $\Delta t \approx 10$ ps is located exclusively in the long-lived F2F excimer.

The much longer lifetimes of $\tau \approx 80$ ps and $\tau \approx 380$ ps evidently belong to $d(ApA)^*_{X(F2F)}$. That two values were needed to fit the data profiles is taken as a sign for structural inhomogeneity of the excimer rather than an indication for two distinctive states or structures. The combined amplitude of the two long-lived components accounts for 21% of the initial GSB, suggesting that such a fraction of dinucleotide molecules transform to long-lived excimers. Attributing the positive initial component with $\tau \approx 0.3$ ps (cf. Figure 4.7c) only to ESA instead of a delay in the GSR and assuming that any long-lived ESA components hidden under the GSB scale proportionately, the fraction of dinucleotides forming long-lived excimers increases to 25%. The fully relaxed excimer state with a lifetime of $\tau \approx 380$ ps was monitored by transient absorption and ground state recovery measurements, but could also be observed by the fluorescence up-conversion experiment. We therefore consider the excimer state as 'optically grey', and not plain black.

4.4.4 'Perturbed-Monomer-Like' Relaxation of $d(A)_2$

When the dinucleotide is dynamically mostly unstacked, even if the initially excited state is excitonically coupled, the excitation will localise on one of the bases. This is followed by a deactivation mechanism comparable to that for the mononucleotide. Following the line of arguments for Ado or AMP,[9,11,47,50–53] the $\tau \lesssim 0.1$ ps time constant observed in fluorescence might therefore be (partially) attributed to the departure of the excited wavepacket from the Franck-Condon region and/or the transition from the $\pi\pi^*(L_a)$ to the $\pi\pi^*(L_b)$ state in the excited base. However, one has to keep in mind that this possible deactivation pathway exists additionally to the ultrafast intraband relaxation of the exciton stack, as described above.

The $\tau \approx 0.3 - 0.4$ ps time constant encountered in the fluorescence decay curves and in the absorption-time profiles of the dinucleotide agrees with similar values for the monomer, where they were assigned to the direct radiationless electronic deactivation through two predominating $\pi\pi^*/S_0$ conical intersections (CIs) to the ground state (S_0).[11,38–41,45,49–52] Taking our data, which were obtained under the same experimental conditions as for the dinucleotide, the excited electronic state lifetime of the mononucleotide dAMP is between $\tau = 0.32$ and 0.20 ps depending on whether it was determined in absorption or in fluorescence, respectively. Both of the two known major relaxation channels in adenine, which involve an out-of-plane deformation of the NH_2 group and an out-of-plane ring puckering motion of the C^2, respectively, may contribute. The slightly longer ESA time constant for the dinucleotide than in the monomer case (0.20 ± 0.02 ps at 400 nm $\leq \lambda_{probe} \leq 700$ nm, cf. Figure 4.S6) may be rationalised by some steric hindering of the out-of-plane motions by the neighbouring base.

At first glance, the high amplitudes of the $0.3 - 0.4$ ps components in the fluorescence-

time and in the absorption-time profiles seem to indicate that a large fraction of the photo-excited dinucleotide molecules (between 80 and 90% based on the relative signal amplitudes) deactivates *via* monomer-like pathways. However, one has to account for the absorption transition dipole moments of the $S_1 \rightarrow S_n$ ESA process from dynamically unstacked dinucleotides on the one hand and the $d(ApA)^*_{X(F2F)}$ conformation on the other hand. The GSR measurement unambiguously demonstrate that $\approx 25\%$ of the excited molecule eventually form a long-lived excimer before returning to the ground state. Obviously, the F2F excimer is darker regarding absorption than dynamically unstacked molecules and the $d(ApA)^*_{X(BDNA)}$ configuration.

Tentatively, the slightly shorter value of $\tau \approx 0.3$ ps from the ESA measurement is preferred for the lifetime of the 'monomer-like' states of the dinucleotide molecules compared to the $\tau \approx 0.4$ ps from the fluorescence measurement, because the latter value is more likely to be affected by the beginning electronic and configurational changes towards excimer formation. However, we point out that the comparison of initial dinucleotide dynamics with the monomer deactivation dynamics has to be considered with caution.

Ground State Recovery

The transient time profile determined by the single-colour experiment at $\lambda = 250$ nm arises by a superposition of the ground-state bleach (GSB) signal resulting due to the photo-excitation of the molecules and possible ESA contributions. The measured negative amplitude shows that the GSB predominates. The temporal evolution thus reflects the recovery of the population in the S_0 state (i.e., the GSR). Accordingly, the time constant of $\tau \approx 2$ ps describing the best part of the 250 nm time profile belongs to the cooling of the vibrationally hot molecules returned to the S_0 state in only ≈ 0.3 ps *via* the nonadiabatic transitions through the CIs ('perturbed-monomer-like' relaxation pathway). About $\approx 38\,500$ cm^{-1} of vibrational energy have to be dissipated. A cooling time of ≈ 2 ps is fast compared to typical vibrational relaxation times in organic solvents,[109–111] but typical for the nucleobases or nucleotides in water.[7,102] For large photochromic dye molecules in organic solvents, for example, we have previously found vibrational cooling times of $\approx 5-10$ ps.[109,110] However, vibrational relaxation rates in liquids usually depend on the spectral density of low frequency modes of the solvent and on the coupling between the low frequency modes of the chromophore and the solvent.[111,112] For nucleobases in water, the strong hydrogen bonding networks appear to promote the very fast vibrational relaxation, such that even sub-picosecond times can be observed.[113]

4.4.5 Proposed Relaxation Scheme

Taking into account all the above mentioned features of the spectro-temporal evolution of the UV ESA bands, the fluorescence-time profiles and the GSB recovery, we propose the

following electronic relaxation scheme after photo-excitation: Firstly, relaxation within the initially populated exciton stack takes place with $\tau \lesssim 0.1$ ps (observed in fluorescence). The bottom of the exciton stack corresponds to the B-DNA stacked excimer conformation $\mathrm{d(ApA)}^*_{\mathrm{X(BDNA)}}$, which subsequently evolves within $\Delta t \approx 10$ ps to the energetically relaxed face-to-face excimer $\mathrm{d(ApA)}^*_{\mathrm{X(F2F)}}$. About $\approx 25\%$ of the initially excited molecules relax *via* this long-lived excimer ($\tau \approx 80$ ps and $\tau \approx 380$ ps), which exhibits a certain amount of conformational disorder.

Another possible deactivation route proceeds *via* 'perturbed-monomer-like' pathways in $\tau \approx 0.3$ ps. We emphasise that even if the excitation energy is localised on one adenine monomer, interaction between the neighbouring chromophores is present. The excited-state geometry of dynamically unstacked dinucleotides therefore differs from that of dAMP, which is confirmed by the strikingly different transient absorption spectra of d(ApA) and dAMP (see Figure 4.6).

4.4.6 Implications for Other Di- and Oligonucleotides

The adenine dinucleotide d(ApA) is a simple DNA model system, where a relaxed, energetically stable excimer state with face-to-face conformation is accessible. The 'perfect' orbital overlap in the $\mathrm{d(ApA)}^*_{\mathrm{X(F2F)}}$ geometry cannot be adopted by hetero-dinucleotides. However, long-lived excimer states have been found in a series of homo- and hetero-dinucleotides,[1,78–85] it is therefore of interest to compare their excited-state lifetimes and geometrical structures. In a preceding paper, we reported on the case of the mixed adenine-guanine DNA dinucleotide d(ApG), where between $25-35$ % of the photo-excited molecules were found to form a long-lived excimer $\mathrm{d(ApG)}^*_{\mathrm{X(\,min\,)}}$ with significant charge-transfer (CT) character and almost optically dark appearance regarding fluorescence, before returning to the ground state after a lifetime of $\tau \approx 124$ ps.[108] Two major differences can be stated between d(ApA) and d(ApG). Firstly, the excimer lifetime is longer for the homo-dinucleotide, where the face-to-face conformation is accessible. Secondly, the percentage of molecules forming the long-lived excimer seems to be higher for d(ApG). This may be explained by the CT character of the excimer, which leads to stabilisation in the aqueous environment. Besides, the larger molecular motion needed to reach the face-to-face geometry may result in a smaller fraction of molecules eventually forming the long-lived excimer $\mathrm{d(ApA)}^*_{\mathrm{X(F2F)}}$, while a part of the molecules is lost 'on the way' to the completely relaxed structure. This is backed by the observation of a contribution $\tau \approx 80$ ps, with which the GSB is refilled. Furthermore, the eventually formed long-lived exciplex of d(ApG) may be populated in part directly and is not only formed by excited-state transformations. The exciplex state may be considered as 'optically grey' regarding absorption, as the initially excited states of d(ApG) already possess (partial) CT character.[114]

A systematic study on further dinucleotides, followed by tri- and tetranucleotides, will hopefully shed more light onto this complex matter. As theory suggested significant dif-

ferences in the amount of stacking for d(ApG) and d(GpA),[114] the base sequence has to be considered too.

4.5 Conclusions

In summary, we presented femtosecond UV/vis fluorescence up-conversion measurements, broadband UV/vis fluorescence spectra taken with a Kerr-gating setup, broadband UV/vis absorption maps, and single-colour deep-UV absorption measurements of $d(A)_2$ in buffered aqueous solution at pH 7.0 to elucidate the complex excited electronic state relaxation mechanisms in ssDNA oligonucleotides. The adenine dinucleotide $d(A)_2$ is a simple DNA model system, which allowed us to assign the complex excited-state dynamics to excimer and 'perturbed-monomer-like' deactivation pathways. In contrast to the monomer dAMP, which exhibits an excited-state lifetime of $\tau \approx 0.2 - 0.3$ ps, $d(A)_2$ showcases an intricate hierarchy of dynamical processes on vastly differing time scales, from $\tau \lesssim 100$ fs, *via* $\tau = 0.30 - 0.40$ ps and $\tau \approx 8$ ps, to $\tau = 380$ ps. Based on these time scales and considering the complementary information granted by transient fluorescence and absorption spectroscopy, we propose a relaxation scheme which ranges from the ultrafast relaxation within the initially excited exciton stack to the formation of a stable, long-lived excimer state with face-to-face conformation on the one hand, and to 'perturbed-monomer-like' deactivation pathways on the other hand. The excimer state exhibits an astonishing spectral feature, namely a narrow, long-lived ESA band around $\lambda \approx 345$ nm. A similar band has already been identified as excimer signature for the hetero-dinucleotide d(ApG).[108]

As we assume the long-lived excimer state to possess face-to-face conformation, one may even say that the stable excimer state is accessible only in the dinucleotide. Actually, femtosecond time-resolved fluorescence measurements on the all-adenine DNA eicosamer $d(pA)_{20}$ yielded $\approx 100 - 200$ ps as the longest time constant,[15,16] supporting the assumption that longer strands are not flexible enough to adopt the stable face-to-face conformation entirely. The presented results provide clear, convincing evidence for the formation of stable exciton/excimer states already in the adenosine dinucleotide. Referring to the established base sequence dependence of the electronic deactivation dynamics in DNA,[16] we conclude that the nature and lifetimes of the excited states under discussion depend strongly on the π-stacking conformation of the nucleobases. The conformations in turn are highly dynamic, depending on the length of the oligonucleotide strand.

Supplementary Information

Electrospray mass spectra of d(pApA) in the negative ion mode, static CD spectra of d(pApA) compared with $d[A(pA)_{19}]$, transient absorption data of d(ApA) before solvent correction and respective data of pure solvent, fluorescence-time profiles of d(AMP), decay-associated fluorescence spectra for d(pApA), and ESA decay times of dAMP.

Acknowledgement

The financial support of this work by the Deutsche Forschungsgemeinschaft is gratefully acknowledged. Furthermore, the authors thank Prof. Dr. J. Grötzinger for allowing us to take the CD spectra.

References and Notes

[1] J. Eisinger, R. G. Shulman, *Science* **161**, 1311 (1968).

[2] J. Eisinger, *Photochem. Photobiol.* **7**, 597 (1968).

[3] P. R. Callis, *Annu. Rev. Phys. Chem.* **34**, 329 (1983).

[4] C. E. Crespo-Hernández, B. Cohen, P. M. Hare, B. Kohler, *Chem. Rev.* **104**, 1977 (2004).

[5] M. Daniels, W. W. Hauswirth, *Science* **171**, 675 (1971).

[6] J.-M. L. Pecourt, J. Peon, B. Kohler, *J. Am. Chem. Soc.* **122**, 9348 (2000).

[7] J.-M. L. Pecourt, J. Peon, B. Kohler, *J. Am. Chem. Soc.* **123**, 10370 (2001).

[8] J. Peon, A. H. Zewail, *Chem. Phys. Lett.* **348**, 255 (2001).

[9] D. Onidas, D. Markovitsi, S. Marguet, A. Sharonov, T. Gustavsson, *J. Phys. Chem. B* **106**, 11367 (2002).

[10] L. Serrano-Andrés, M. Merchán, *J. Photochem. Photobiol. C* **10**, 21 (2009).

[11] M. Barbatti, A. J. A. Aquino, J. J. Szymczak, D. Nachtigallovà, P. Hobza, H. Lischka, *Proc. Natl. Acad. Sci. U.S.A.* **107**, 21453 (2010).

[12] C. E. Crespo-Hernández, B. Cohen, B. Kohler, *Nature* **436**, 1141 (2005).

[13] D. Markovitsi, D. Onidas, T. Gustavsson, F. Talbot, E. Lazzarotto, *J. Am. Chem. Soc.* **127**, 17130 (2005).

[14] D. Markovitsi, F. Talbot, T. Gustavsson, D. Onidas, E. Lazzarotto, S. Marguet, *Nature* **441**, E7 (2006).

[15] W.-M. Kwok, C. Ma, D. L. Phillips, *J. Am. Chem. Soc.* **128**, 11894 (2006).

[16] N. K. Schwalb, F. Temps, *Science* **322**, 243 (2008).

[17] B. Bouvier, T. Gustavsson, D. Markovitsi, P. Millié, *Chem. Phys.* **275**, 75 (2002).

[18] B. Bouvier, J.-P. Dognon, R. Lavery, D. Markovitsi, P. Millie, D. Onidas, K. Zakrzewska, *J. Phys. Chem. B* **107**, 13512 (2003).

[19] E. Emanuele, D. Markovitsi, P. Millié, K. Zakrewska, *ChemPhysChem* **6**, 1387 (2005).

[20] I. Buchvarov, Q. Wang, M. Raytchev, A. Trifonov, T. Fiebig, *Proc. Natl. Acad. Sci. U.S.A.* **104**, 4794 (2007).

[21] Strictly speaking, the definition of an excimer implies formation of a bound excited dimer from two originally separate molecules in their ground state upon photo-excitation of one moiety. The nucleobases as the chromophores of interest in an oligonucleotide are of course linked *via* the sugar-phosphate backbone. In the electronic ground state, however, two neighbouring nucleobases can be considered as electronically isolated. The bound 'excimer' with shared π-electron density between two bases results only after electronic excitation of one of the chromophores so that the use of this term is justified. The extent of charge transfer between the two moieties will depend on the different bases.

[22] C. E. Crespo-Hernández, B. Cohen, B. Kohler, *Nature* **441**, E8 (2006).

[23] T. Takaya, C. Su, K. de La Harpe, C. E. Crespo-Hernández, B. Kohler, *Proc. Natl. Acad. Sci. U.S.A.* **105**, 10285 (2008).

[24] C. T. Middleton, K. de La Harpe, C. Su, Y. K. Law, C. E. Crespo-Hernández, B. Kohler, *Annu. Rev. Phys. Chem.* **60**, 217 (2009).

[25] E. B. Starikov, G. Cuniberti, S. Tanaka, *J. Phys. Chem. B* **113**, 10428 (2009).

[26] C. Su, C. T. Middleton, B. Kohler, *J. Phys. Chem. B* **116**, 10266 (2012).

[27] N. K. Schwalb, F. Temps, *J. Chem. Phys. A* to be submitted (2008).

[28] S. O. Konorov, H. G. Schulze, C. J. Addison, C. A. Haynes, M. W. Blades, R. F. B. Turner, *Open Spectrosc. J.* **3**, 9 (2009).

[29] S. O. Konorov, H. G. Schulze, C. J. Addison, C. A. Haynes, R. F. B. Turner, M. W. Blades, *Open Spectrosc. J.* **3**, 43 (2009).

[30] K. de La Harpe, B. Kohler, *J. Phys. Chem. Lett.* **2**, 133 (2011).

[31] I. Vayá, T. Gustavsson, F.-A. Miannay, T. Douki, D. Markovitsi, *J. Am. Chem. Soc.* **132**, 11834 (2010).

[32] D. Markovitsi, T. Gustavsson, I. Vayá, *J. Phys. Chem. Lett.* **1**, 3271 (2010).

[33] I. Vayá, J. Brazard, T. Gustavsson, D. Markovitsi, *Photochem. Photobiol. Sci.* **11**, 1767 (2012).

[34] I. Vayá, T. Gustavsson, T. Douki, Y. Berlin, D. Markovitsi, *J. Am. Chem. Soc.* **134**, 11366 (2012).

[35] B. Cohen, P. M. Hare, B. Kohler, *J. Am. Chem. Soc.* **125**, 13594 (2003).

[36] T. Pancur, N. K. Schwalb, F. Renth, F. Temps, *Chem. Phys.* **313**, 199 (2005).

[37] S. Perun, A. L. Sobolewski, W. Domcke, *Chem. Phys.* **313**, 107 (2005).

[38] S. Perun, A. L. Sobolewski, W. Domcke, *J. Am. Chem. Soc.* **127**, 6257 (2005).

[39] L. Serrano-Andrés, M. Merchán, A. C. Borin, *Chem. Eur. J.* **12**, 6559 (2006).

[40] C. M. Marian, *J. Chem. Phys.* **122**, 104314 (2005).

[41] L. Blancafort, *J. Am. Chem. Soc.* **128**, 210 (2006).

[42] L. Serrano-Andrés, M. Merchán, A. C. Borin, *Proc. Natl. Acad. Sci. U. S. A.* **103**, 8691 (2006).

[43] H. Chen, S. Li, *J. Phys. Chem. A* **109**, 8443 (2005).

[44] S. Yamazaki, S. Kato, *J. Am. Chem. Soc.* **129**, 2901 (2007).

[45] I. Conti, M. Garavelli, G. Orlandi, *J. Am. Chem. Soc.* **131**, 16108 (2009).

[46] I. Conti, E. D. Donato, F. Negri, G. Orlandi, *J. Phys. Chem. A* **113**, 15265 (2009).

[47] E. Fabiano, W. Thiel, *J. Phys. Chem. A* **112**, 6859 (2008).

[48] Y. Lei, S. Yuan, Y. Dou, Y. Wang, Z. Wen, *J. Phys. Chem. A* **112**, 8497 (2008).

[49] W. M. I. Hassan, W. C. Chung, N. Shimakura, S. Koseki, H. Kono, Y. Fujimura, *Phys. Chem. Chem. Phys.* **12**, 5317 (2010).

[50] M. Barbatti, H. Lischka, *J. Am. Chem. Soc.* **130**, 6831 (2008).

[51] M. Barbatti, Z. Lan, R. Crespo-Otero, J. J. Szymczak, H. Lischka, W. Thiel, *J. Chem. Phys* **137**, 22A503 (2012).

[52] Z. Lan, Y. Lu, E. Fabiano, W. Thiel, *ChemPhysChem* **12**, 1989 (2011).

[53] R. Mitrić, U. Werner, M. Wohlgemuth, G. Seifert, V. Bonačić-Koutecký, *J. Phys. Chem. A* **113**, 12700 (2009).

[54] R. Plessow, A. Brockhinke, W. Eimer, K. Kohse-Hoeinghaus, *J. Phys. Chem. B* **104**, 3695 (2000).

[55] C. E. Crespo-Hernández, B. Kohler, *J. Phys. Chem. B* **108**, 11182 (2004).

[56] D. Markovitsi, T. Gustavsson, F. Talbot, *Photochem. Photobiol. Sci* **6**, 717 (2007).

[57] D. Onidas, T. Gustavsson, E. Lazzarotto, D. Markovitsi, *J. Phys Chem. B* **111**, 9644 (2007).

[58] U. Kadhane, A. I. S. Holm, S. V. Hoffmann, S. B. Nielsen, *Phys. Rev. E: Stat., Nonlinear, Soft Matter Phys.* **77**, 021901 (2008).

[59] L. M. Nielsen, S. O. Pedersen, M.-B. S. Kirketerp, S. B. Nielsen, *J. Chem. Phys.* **136**, 064302 (2012).

[60] A. Czader, E. R. Bittner, *J. Chem. Phys* **128**, 035101 (2008).

[61] K. Hyeon-Deuk, Y. Tanimura, M. Cho, *J. Chem. Phys.* **128**, 135102 (2008).

[62] H.-H. Ritze, P. Hobza, D. Nachtigallovà, *Phys. Chem. Chem. Phys.* **9**, 1672 (2007).

[63] D. Nachtigallovà, P. Hobza, H.-H. Ritze, *Phys. Chem. Chem. Phys.* **10**, 5689 (2008).

[64] A. W. Lange, M. A. Rohrdanz, J. M. Herbert, *J. Phys. Chem. B* **112**, 6304 (2008).

[65] A. W. Lange, J. M. Herbert, *J. Am. Chem. Soc.* **131**, 3913 (2009).

[66] S. Tonzani, G. C. Schatz, *J. Am. Chem. Soc.* **130**, 7607 (2008).

[67] F. Santoro, V. V. Barone, R. Improta, *Proc. Natl. Acad. Sci. U.S.A.* **104**, 9931 (2007).

[68] F. Santoro, V. Barone, R. Improta, *ChemPhysChem* **9**, 2531 (2008).

[69] F. Santoro, V. Barone, R. Improta, *J. Am. Chem. Soc.* **131**, 15232 (2009).

[70] G. Olaso-González, M. Merchán, L. Serrano-Andrés, *J. Am. Chem. Soc.* **131**, 4368 (2009).

[71] I. Conti, P. Altoè, M. Stenta, M. Garavelli, G. Orlandi, *Phys. Chem. Chem. Phys.* **12**, 5016 (2010).

[72] Y. Lu, Z.-G. Lan, W. Thiel, *Angew. Chem., Int. Ed.* **50**, 6864 (2011).

[73] F. Plasser, A. J. A. Aquino, W. L. Hase, H. Lischka, *J. Phys. Chem. A* **116**, 11151 (2012).

[74] R. Improta, V. Barone, *Angew. Chem. Int. Ed.* **50**, 12016 (2011).

[75] A. Bànyàsz, T. Gustavsson, D. Onidas, P. Changenet-Barret, D. Markovitsi, R. Improta, *Chem. Eur. J.* **19(11)**, 3762 (2013).

[76] M. M. Warshaw, I. T. Jr., *J. Mol. Biol.* **13**, 54 (1965).

[77] M. Y. Warshaw, I. Tinoco, *J. Mol. Biol.* **20**, 29 (1966).

[78] J. Eisinger, M. Guéron, R. G. Shulman, T. Yamane, *Proc. Natl. Acad. Sci. U.S.A.* **55**, 1015 (1966).

[79] M. Daniels, J. P. Morgan, *Chem. Phys. Lett.* **58**, 283 (1978).

[80] M. Daniels, J. P. Morgan, *J. Luminescence* **18/19**, 593 (1979).

[81] J. P. Morgan, P. R. Callis, *Photochem. Photobiol.* **29**, 1107 (1979).

[82] J. P. Morgan, M. Daniels, *Photochem. Photobiol.* **31**, 101 (1980).

[83] J. P. Morgan, M. Daniels, *Photochem. Photobiol.* **31**, 207 (1980).

[84] C. S. Shaar, J. P. Morgan, M. Daniels, *Photochem. Photobiol.* **39**, 747 (1984).

[85] M. Daniels, C. S. Shaar, J. P. Morgan, *Biophys. Chem.* **32**, 229 (1988).

[86] M. Stuhldreier, C. Schüler, J. Kleber, F. Temps, *Ultrafast Phenomena XVII*, M. Chergui, D. M. Jonas, E. Riedle, R. W. Schoenlein, A. J. Taylor, Eds. (Oxford University Press, Inc., 2011), pp. 553–555.

[87] C.-H. Lee, F. S. Ezra, N. S. Kondo, R. H. Sarma, S. S. Danyluk, *Biochemistry* **15**, 3627 (1976).

[88] C. S. M. Olsthoorn, L. J. Bostelaar, J. F. M. De Rooij, J. H. van Boom, C. Altona, *Eur. J. Biochem.* **115**, 309 (1981).

[89] J. Gidden, M. T. Bowers, *Eur. Phys. J. D* **20**, 409 (2002).

[90] N. K. Schwalb, F. Temps, *J. Phys. Chem. A* **113**, 13113 (2009).

[91] B. Schmidt, S. Laimgruber, W. Zinth, P. Gilch, *Appl. Phys. B* **76**, 809 (2003).

[92] C. Ma, W. M. Kwok, W. S. Chan, P. Zuo, J. T. W. Kan, P. H. Toy, D. L. Phillips, *J. Am. Chem. Soc.* **127**, 1463 (2005).

[93] J. A. Gardecki, M. Maroncelli, *Appl. Spectrosc.* **52**, 1179 (1998).

[94] K. Röttger, R. Siewertsen, F. Temps, *Chem. Phys. Lett.* **536**, 140 (2012).

[95] M. Lorenc, M. Ziolek, R. Naskrecki, J. Karolczak, J. Kubicki, A. Maciejewski, *Appl. Phys. B* **74**, 19 (2002).

[96] A. L. Dobryakov, S. A. Kovalenko, N. P. Ernsting, *J. Chem. Phys.* **119**, 988 (2003).

[97] A. L. Dobryakov, S. A. Kovalenko, N. P. Ernsting, *J. Chem. Phys.* **123**, 044502 (2005).

[98] *LabView 8.0* (National Instruments, 2006).

[99] *Mathematica Version 8.0* (Wolfram Research, Inc., 2011).

[100] D. B. Siano, D. E. Metzler, *J. Chem. Phys.* **51**, 1856 (1969).

[101] M. Barbatti, J. J. Szymczak, A. J. A. Aquino, D. Nachtigallová, H. Lischka, *J. Chem. Phys.* **134**, 014304 (2011).

[102] V. Karunakaran, K. Kleinermanns, R. Improta, S. A. Kovalenko, *J. Am. Chem. Soc.* **131**, 5839 (2009).

[103] J. Chen, B. Kohler, *Phys. Chem. Chem. Phys.* **14**, 10677 (2012).

[104] J. P. Villabona-Monsalve, R. Noria, S. Matsika, J. Péon, *J. Am. Chem. Soc.* **134**, 7820 (2012).

[105] A. N. Alexandrova, J. C. Tully, G. Granucci, *J. Phys Chem. B* **114**, 12116 (2010).

[106] Y. Lu, Z. Lan, W. Thiel, *J. Comput. Chem.* **33**, 1225 (2012).

[107] N. Öksüz, F. Temps, *unpublished results* .

[108] M. C. Stuhldreier, F. Temps, *Faraday Discuss.* doi: 10.1039/c3fd00003f (2013).

[109] R. Siewertsen, J. B. Schönborn, B. Hartke, F. Renth, F. Temps, *Phys. Chem. Chem. Phys.* **13**, 1054 (2011).

[110] R. Siewertsen, F. Strübe, J. Mattay, F. Renth, F. Temps, *Phys. Chem. Chem. Phys.* **13**, 3800 (2011).

[111] T. Elsaesser, W. Kaiser, *Annu. Rev. Phys. Chem.* **42**, 83 (1991).

[112] J. C. Owrutsky, D. Raftery, R. M. Hochstrasser, *Annu. Rev. Phys. Chem.* **45**, 519 (1994).

[113] M. Yang, L. Szyc, K. Röttger, H. Fidder, E. T. J. Nibbering, T. Elsaesser, F. Temps, *J. Phys Chem. B* **115**, 5484 (2011).

[114] F. Santoro, V. Barone, A. Lami, R. Improta, *Phys. Chem. Chem. Phys.* **12**, 4934 (2010).

Spectral Signatures of Exciton and Excimer States in the Ultrafast Electronic Relaxation of the Adenine Dinucleotide Revealed by Femtosecond Measurements

Supplementary Information

Mayra C. Stuhldreier, Michal Malicki[†], Katharina Röttger, Carmen Schüler, Joscha Kleber, Tassilo Muskat, and Friedrich Temps[*]

Institut für Physikalische Chemie, Christian-Albrechts-Universität zu Kiel, Olshausenstr. 40, D-24098 Kiel, Germany

[†]Present address: Department of Chemistry, Northwestern University, Tech K345, 2145 Sheridan Rd, Evanston, IL 60208-3113, U.S.A.

[*]To whom correspondence should be addressed.
Electronic address: temps@phc.uni-kiel.de, URL: http://www.uni-kiel.de/phc/temps

to be submitted

4.SI.1 Circular Dichroism Spectrum of d(pApA)

The measured circular dichroism (CD) spectrum of the dinucleotide d(pApA) in buffered H_2O (pH 7.0) in Figure 4.S1 closely resembles that of the much longer eicosanucleotide d[A(pA)$_{19}$], which points at very similar conformations.[1,2] In particular, the complex band contour around 260 nm with a positive w-shaped peak from 260 – 280 nm and a negative peak around 250 nm is characteristic for a prevalent B-DNA-like helical conformation. Further, the strong positive band below 240 nm shows the presence of π-stacked adenine subunits. The spectra agree well with a series of temperature- and strand-length dependent CD measurements on adenine oligonucleotides by Olsthoorn *et al.*[3] Accordingly, the stability of the B-DNA helix in solution can be estimated by the more or less pronounced w-shape of the 260 – 280 nm band. For d(pApA), Olsthoorn *et al.* found a significant decrease of the band around 260 nm with increasing temperature. The spectrum at high temperature eventually resembles that of the monomer dAMP. For longer polyadenosine strands, in contrast, the decrease with increasing temperature is not very pronounced. This illustrates the increased structural flexibility of d(pApA) compared to d[A(pA)$_{19}$]. The single-strand helix is only stabilised by π-stacking interactions between the adjacent nucleobases, which makes the conformation less stable than in the case of the hydrogen-bonded double helix.

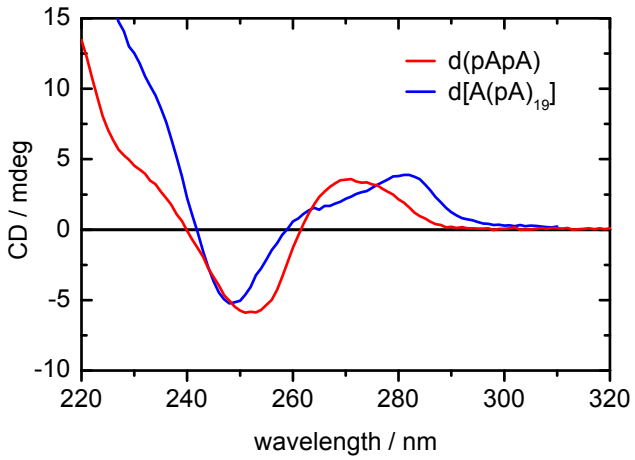

Fig. 4.S1: Circular dichroism spectra of d(pApA) (red, this work) and d[A(pA)$_{19}$] (blue, taken from reference[4]) in solution in H_2O (pH 7.0) at room temperature.

4.SI.2 ESI Mass Spectrum of d(pApA)

The electrospray ionisation (ESI) mass spectrum of d(pApA) was recorded on a Bruker Daltonics APEX-Qe Fourier Transform Ion Cyclotron Resonance mass spectrometer with 9.4 T magnet and a Combi Ion Source. The sample was dissolved in a 1:1 mixture of ultrapure water and methanol. Spectra were recorded in negative and in positive ion mode. The ESI mass spectrum in negative ion mode is displayed in Figure 4.S2.

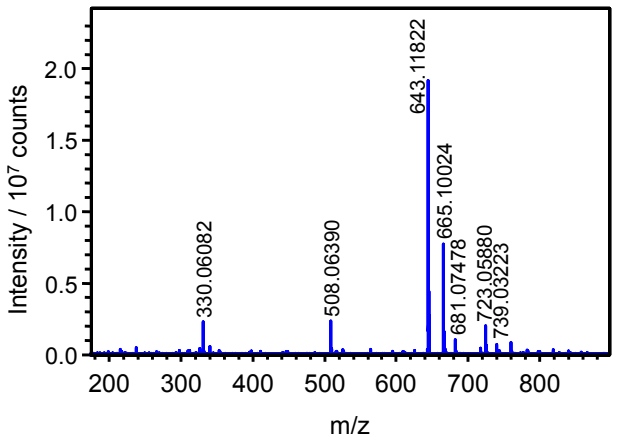

Fig. 4.S2: ESI mass spectrum of the 5'-d(pApA)-3' sample recorded in negative ion mode.

The observed main peak at $m/z = 643.11822$ was immediately assigned to the molecular formula $C_{20}H_{25}N_{10}O_{11}P_2$ ($m/z_{calc} = 643.11795$), which corresponds to the dinucleotide d(pApA). The neighbouring peaks at $m/z = 665.10024$ and 681.07478 arise from the respective sodium ($m/z_{calc} = 665.09989$) and potassium salts ($m/z_{calc} = 681.07383$). The sodium salt of the dinucleotide also forms a sodium chloride adduct, which can be observed at $m/z = 723.05880$ ($C_{20}H_{24}N_{10}O_{11}P_2Na_2{}^{35}Cl$, $m/z_{calc} = 723.05852$) and $m/z = 725.05488$ ($C_{20}H_{24}N_{10}O_{11}P_2Na_2{}^{37}Cl$, $m/z_{calc} = 725.05557$, not labelled in Figure 4.S2). The observed mass-to-charge ratios $m/z = 739.03223$ and $m/z = 741.03009$ (not labelled in Figure 4.S2) correspond to the molecular formulas $C_{20}H_{24}N_{10}O_{11}P_2NaK^{35}Cl$ ($m/z_{calc} = 739.03245$) and $C_{20}H_{24}N_{10}O_{11}P_2NaK^{37}Cl$ ($m/z_{calc} = 741.02950$), respectively, and are due to the potassium chloride adduct of the sodium salt or the sodium chloride adduct of the potassium salt of the dinucleotide.

At lower mass-to-charge ratio, the signal at $m/z = 330.06082$ belongs to the molecular formula $C_{10}H_{13}N_5O_6P$ ($m/z_{calc} = 330.06034$) and accordingly to the monomer dAMP. Likewise, $m/z = 508.06390$ was assigned to the molecular formula $C_{15}H_{20}N_5O_{11}P_2$ ($m/z_{calc} = 508.06345$), which corresponds to a fragment where the dinucleotide d(pApA) has split off one adenine molecule. This coincides with the well-known loss of a neutral 5'-terminus nucleobase in oligonucleotides.[5,6] As no corresponding mass-to-charge ratio was observed in the positive ion mode spectrum, we conclude that the fragmentation takes place in the

ESI process, not in the sample solution, and is limited to the negative ion mode process.

Analogous sodium adducts observed in the positive ion mode ESI spectrum for all mass-to-charge ratios were assigned to the nucleotide monomer and the dinucleotide. MS/MS measurements at $m/z = 723.05880$, 643.11822, and 508.06390 confirmed the assignments. The ion with $m/z = 723.05880$ decomposes predominantly to $m/z = 665.10024$, thus giving the sodium salt of the adenine dinucleotide by elimination of sodium chloride. From the dinucleotide ($m/z = 643.11822$), fragments are split off with $m/z = 508.06390$ and $m/z = 330.06082$, which again correspond to the loss of one adenine molecule and the monomer, respectively. The secession of the 3'-monomer has also been observed by Rodgers *et al.*[5] This indicates that at least part of the observable dAMP signal originates from the ESI process. Therefore, we can safely conclude that the primary mononucleotide content in the sample solution is well below 6 %. Such a small trace of dAMP cannot affect the conclusions on excimer state formation in the electronically excited dinucleotide. MS/MS measurements of the fragment with $m/z = 508.06390$ again gave rise to a monomer signal at $m/z = 330.06082$.

4.SI.3 Two-Dimensional Spectro-Temporal Transient Absorption Maps

In order to separate the signals by the nucleotide samples from interfering solvent contributions and experimental artefacts in the transient absorption measurements, a measurement on the pure solvent was performed directly before or after each sample measurement in the same flow cell under the same experimental conditions. Two typical raw transient absorption maps for the d(ApA) sample in the aqueous phosphate buffer obtained with the 0.1 mm path length flow cell and for the neat buffer solution on the same time and intensity scale are shown in Figure 4.S3.

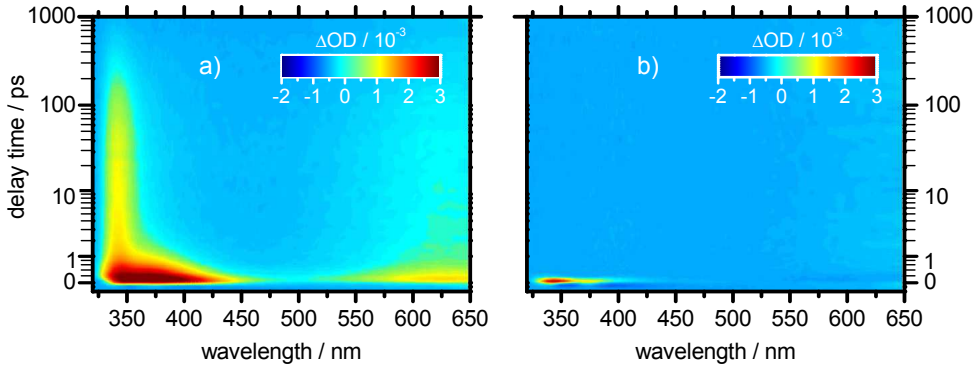

Fig. 4.S3: Measured transient absorption maps after excitation at $\lambda_{\text{pump}} = 260$ nm in the 0.1 mm flow cell as function of probe wavelength and delay time for a) d(ApA) in aqueous phosphate buffer (pH 7) without solvent correction and b) the neat phosphate buffer solution.

As can be seen, coherent artefacts or background contributions by the solvent were much smaller than the absorptions by the sample under all conditions. A solvent contribution due to cross phase modulation (XPM) and multi-photon absorption appears mainly around time zero at probe wavelengths of $\lambda \leq 400$ nm.[7–9] Furthermore, a weak transient absorption can be observed in the solvent measurement at $\lambda_{\text{probe}} \geq 500$ nm after $\Delta t \approx 1$ ps. This contribution is due to the absorption from solvated electrons generated in neat water by two-photon absorption[10]. The XPM and multi-photon absorption signals and the contributions by solvated electrons were subsequently subtracted from the transient absorption map of the sample solutions with suitable scaling factors as described[8,9] to obtain solvent-corrected transient absorption maps for the samples given in the main paper.

4.SI.4 Fluorescence-Time Profiles of dAMP

The fluorescence time profiles for dAMP at λ_{fl} = 320, 350 and 430 nm in Figure 4.S4 provide the reference, with which the corresponding data for the dinucleotide d(pApA) can be compared.

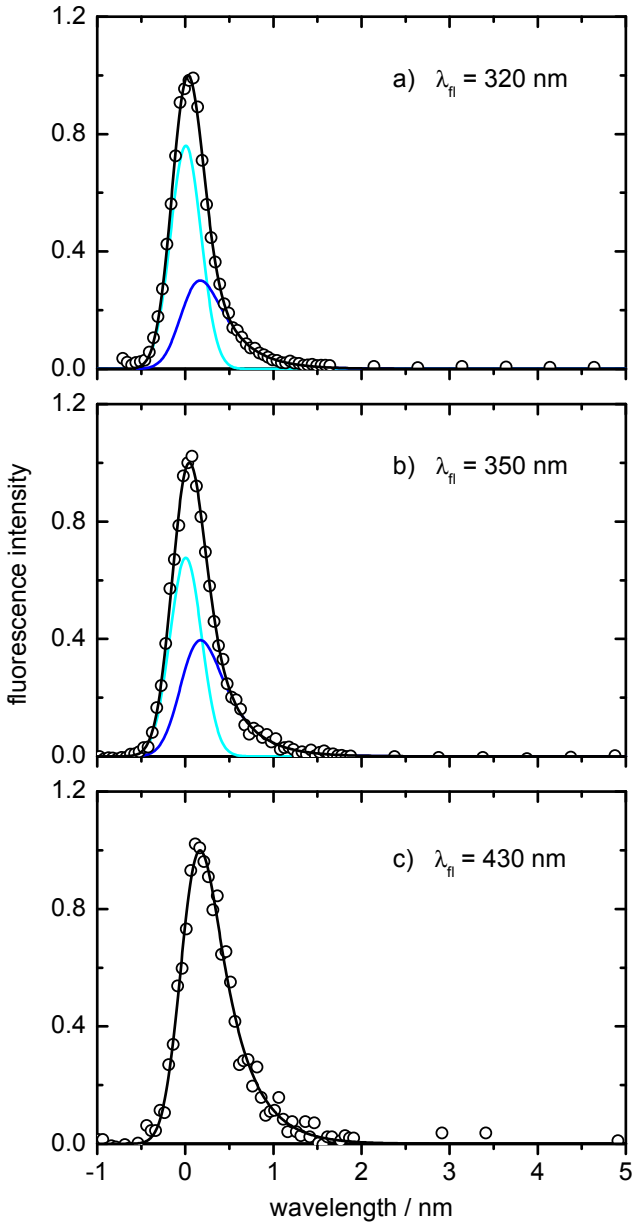

Fig. 4.S4: Measured fluorescence decay curves for dAMP in H_2O (pH 7.0) after excitation at λ_{pump} = 260 nm at three selected fluorescence wavelengths. Open circles represent the data points, black lines the overall fits, coloured lines the underlying contributions (λ_{fl} = 320 and 350 nm only), whose decay constants are given in the text.

As shown, the measured decay curves could be nicely modelled using two time constants,

τ_{FL1}(dAMP) = 0.10±0.05 ps and τ_{FL2}(dAMP) = 0.32±0.07 ps, determined by a global fit. A single exponential with decay time τ_{FL2} would suffice to describe the data at λ_{fl} = 430 nm, but the fits to the λ_{fl} = 320 and 350 nm data unambiguously required the faster additional τ_{FL1} component. As all trial values for τ_{FL1} came out below the ≈ 150 fs experimental time resolution with relatively large error limits, its exact magnitude has to be treated with some caution. For simplicity, and to reduce the uncertainty in τ_{FL2} in the final analysis, the value for τ_{FL1} was eventually kept fixed. The above results for dAMP are in excellent agreement with the available literature data.[11–14]

4.SI.5 Decay-Associated Fluorescence Spectra for d(pApA)

The decay-associated spectra extracted from the single-colour fluorescence decay profiles recorded by the up-conversion technique (see Figure 4.3 in the main paper) are displayed in Figure 4.S5.

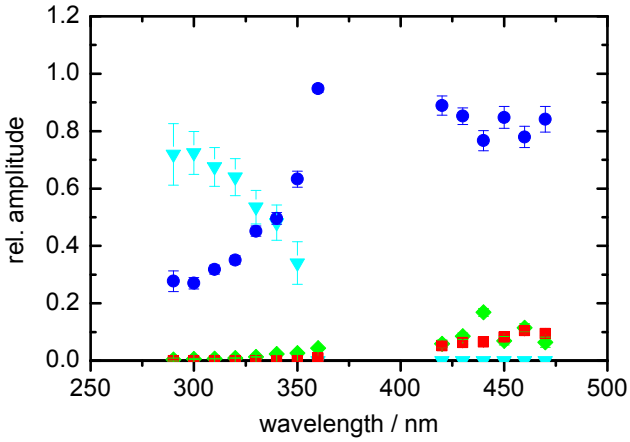

Fig. 4.S5: Decay associated spectra belonging to the single-colour fluorescence decay profiles of d(pApA) in H_2O (pH 7.0) after excitation at λ_{pump} = 260 nm. Light blue triangles: τ_1 = 0.10 ps, dark blue circles: τ_2 = 0.41 ps, green diamonds: τ_3 = 8.30 ps, red squares: τ_4 = 380 ps.

They are in excellent agreement with the broadband fluorescence spectra recorded by the Kerr gating technique (see Figure 4.4 in the main paper). The main contribution in the UV is an ultrafast decaying component with τ_1 = 0.10 ps, whose amplitude decreases with increasing λ_{fl}. The relative amplitude of τ_2 = 0.41 ps is ≈ 30% in the UV and rises to ≈ 80% in the visible wavelength range. The longer-lived contributions with τ_3 = 8.30 ps and τ_4 = 380 ps are observed for $\lambda_{fl} \gtrsim$ 360 nm and account each for ≈ 10% in the visible wavelength range.

4.SI.6 Excited-State Absorption Decay Times of dAMP

The measured transient absorption data for dAMP displayed in Figure 4.5 in the main paper affirm the sub-picosecond excited-state lifetime of the mononucleotide. Within our experimental errors, the time profiles at all investigated probe wavelengths were found to decay nicely single-exponential.

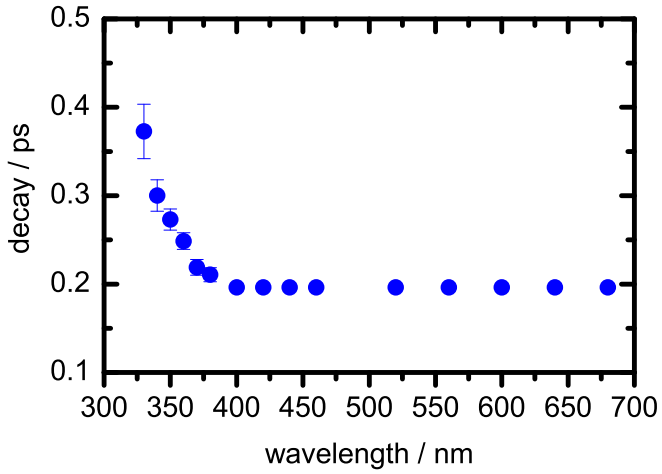

Fig. 4.S6: Plot of the effective transient absorption decay constants of dAMP *vs.* probe wavelength determined from Figure 4.5 in the main paper.

Figure 4.S6 shows the obtained effective time constants as function of probe wavelength. The wavelength-independent ESA decay times in the range 400 nm $\leq \lambda_{\text{probe}} \leq$ 700 nm give the excited-state lifetime for dAMP in H_2O (pH 7.0) after 260 nm photo-excitation of $\tau = 0.20 \pm 0.02$ ps, in good agreement with the fluorescence up-conversion results above and preceding transient absorption results in the literature.[15]. The increase of the values at $\lambda_{\text{probe}} \leq 380$ nm is known to arise due to the onset of HGSA by the vibrationally hot S_0 molecules from the ultrafast internal conversion of the photo-excited state.[10,16] The virtually complete ultrafast GSR was further confirmed by the measured 250 nm time profile, which showed the refilling of the GSB signal by the ensuing electronic relaxation with two time constants, $\tau = 0.6 \pm 0.1$ ps and 1.9 ± 0.2 ps. As expected, the first component is slightly longer than the lifetime of the photo-excited state determined by the ESA decay, because the 250 nm measurement catches the molecules at a later stage in time, after their return to S_0. The second component describes the subsequent cooling of the vibrationally hot S_0 molecules, which is known to be quite fast in aqueous solution.[10,16–18]

References

[1] W. Johnson, I. Tinoco, *Biopolymers* **7**, 727 (1969).

[2] V. A. Bloomfield, D. M. Crothers, I. Tinoco, *Nucleic Acids: Structures, Properties and Functions* (University Science Books, Sausalito, 2000).

[3] C. S. M. Olsthoorn, L. J. Bostelaar, J. F. M. De Rooij, J. H. van Boom, C. Altona, *Eur. J. Biochem.* **115**, 309 (1981).

[4] N. K. Schwalb, F. Temps, *Science* **322**, 243 (2008).

[5] M. T. Rodgers, S. Campbell, E. M. Marzluff, J. L. Beauchamp, *Int. J. Mass Spectrom. Ion Processes* **137**, 121 (1994).

[6] S. A. McLuckey, G. Vaidyanatban, S. Habibi-Goudarzi, *J. Mass Spectrom.* **30**, 1222 (1995).

[7] M. Lorenc, M. Ziolek, R. Naskrecki, J. Karolczak, J. Kubicki, A. Maciejewski, *Appl. Phys. B* **74**, 19 (2002).

[8] A. L. Dobryakov, S. A. Kovalenko, N. P. Ernsting, *J. Chem. Phys.* **119**, 988 (2003).

[9] A. L. Dobryakov, S. A. Kovalenko, N. P. Ernsting, *J. Chem. Phys.* **123**, 044502 (2005).

[10] J.-M. L. Pecourt, J. Peon, B. Kohler, *J. Am. Chem. Soc.* **123**, 10370 (2001).

[11] J. Peon, A. H. Zewail, *Chem. Phys. Lett.* **348**, 255 (2001).

[12] D. Onidas, D. Markovitsi, S. Marguet, A. Sharonov, T. Gustavsson, *J. Phys. Chem. B* **106**, 11367 (2002).

[13] T. Pancur, N. K. Schwalb, F. Renth, F. Temps, *Chem. Phys.* **313**, 199 (2005).

[14] W.-M. Kwok, C. Ma, D. L. Phillips, *J. Am. Chem. Soc.* **128**, 11894 (2006).

[15] C. E. Crespo-Hernández, B. Cohen, P. M. Hare, B. Kohler, *Chem. Rev.* **104**, 1977 (2004).

[16] K. Röttger, R. Siewertsen, F. Temps, *Chem. Phys. Lett.* **536**, 140 (2012).

[17] C. T. Middleton, B. Cohen, B. Kohler, *J. Phys. Chem. A* **111**, 10460 (2007).

[18] V. Karunakaran, K. Kleinermanns, R. Improta, S. A. Kovalenko, *J. Am. Chem. Soc.* **131**, 5839 (2009).

5

Ultrafast Photo-Initiated Molecular Quantum Dynamics in the DNA Dinucleotide d(ApG) Revealed by Broadband Transient Absorption Spectroscopy

Mayra C. Stuhldreier and Friedrich Temps*

Institute of Physical Chemistry, Christian-Albrechts-University Kiel,
Olshausenstr. 40, D-24098 Kiel, Germany

*To whom correspondence should be addressed.
E-mail: temps@phc.uni-kiel.de; Web: http://www.uni-kiel.de/phc/temps

Faraday Discuss. 163, doi:10.1039/C3FD00003F, **2013**

Own contributions presented in this paper:

- Femtosecond time-resolved fluorescence up-conversion and absorption spectroscopy
- Writing of the data analysis software and data analysis of all presented data
- Writing of the publication

Abstract

The ultrafast photo-initiated quantum dynamics of the adenine-guanine dinucleotide d(ApG) in aqueous solution (pH 7) has been studied by femtosecond time-resolved spectroscopy after excitation at $\lambda = 260$ nm. The results reveal a hierarchy of processes on time scales from $\tau < 100$ fs to $\tau > 100$ ps. Characteristic spectro-temporal signatures are observed indicating the transformation of the molecules in the electronic relaxation from the photo-excited state to a long-lived exciplex. In particular, broadband UV/vis excited-state absorption (ESA) measurements detected a distinctive absorption by the excited dinucleotide around $\lambda = 335$ nm, ≈ 0.5 eV to the blue compared to the maximum of the broad and unstructured ESA spectrum after excitation of an equimolar mixture of the mononucleotides dAMP and dGMP. A similar feature has been identified as signature of the excimer in the dynamics of the adenine dinucleotide d(ApA). The lifetime of the d(ApG) exciplex was found to be $\tau = 124 \pm 4$ ps both from the ESA decay time and from the ground-state recovery time, far longer than the sub-picosecond lifetimes of excited dAMP or dGMP. Fluorescence-time profiles measured by the up-conversion technique indicate that the exciplex state is reached around ≈ 6 ps after excitation. Very weak residual fluorescence at longer times red-shifted to the emission from the photo-excited state shows that the exciplex is almost optically dark, but still has enough oscillator strength to give rise to the dual fluorescence of the dinucleotide in the static fluorescence spectrum.

5.1 Introduction

The understanding of the photophysical and photochemical properties of the DNA and its building blocks is of fundamental scientific interest because of the sensitivity of the genetic information to UV light-induced chemical reactions which may result in mutagenic and potentially lethal lesions.[1–3] Stimulated by the huge advances in ultrafast time-resolved spectroscopy, the lifetimes and radiationless deactivation dynamics of the excited electronic states of the DNA bases and their nucleosides or nucleotides, isolated base pairs, and single- and double-stranded oligonucleotides have been measured in the last ten to fifteen years with the help of femtosecond pump-probe spectroscopy.[3,4] Following the measurement of highly efficient, ultrafast electronic deactivation processes in the free nucleobases on the sub-picosecond time scale,[3,5–7] experiments on DNA model strands revealed that the excited-state lifetimes in these large base assemblies can be some surprising three to four orders of magnitude longer than for the base monomers.[8] These striking observations created substantial controversy, whether the long-lived excited states of oligonucleotides originate from the formation of excimers or exciplexes[9] with (partial) charge transfer (CT) character between two neighbouring π-stacked bases of a strand[10] or whether they should be understood as (Frenkel) excitons delocalised over several bases.[10,11] Soon afterwards, the peculiar photo-initiated quantum molecular dynamics of the oligonucleotides turned

out as the rule rather than exception.[4,12–18] Furthermore, first quantum chemical results became available for model systems consisting of two or more nucleobases with DNA-like orientation.[19–28] Both from the experimental and theoretical point of view, however, oligonucleotides with more than two bases are still too large for complete understanding of the excited-state structures and dynamics. Further, experiments on long oligonucleotides are hampered by structural inhomogeneities washing out more specific information that might be hidden in excited-state spectra.

In order to elucidate the photo-initiated quantum molecular dynamics in DNA oligonucleotides in more detail, we initiated a series of investigations by femtosecond time-resolved fluorescence and absorption spectroscopy of the ultrafast electronic relaxations of selected short di-, tri- and tetranucleotides.[29] These fragments are the smallest model systems showing the effect of π-stacking interactions between adjacent bases on the nature and dynamics of the excited electronic states. Although the molecules are dynamically disordered, circular dichroism (CD) and nuclear magnetic resonance (NMR) studies confirmed high fractions of stacked (B-DNA like) configurations.[30–39] Further, early static emission spectra suggested the formation of excimer/exciplex-like states upon UV excitation of stacked conformations for several dinucleotides.[1,40–46] Nevertheless, there have yet been few time-resolved experimental studies on dinucleotides.[47–50] Buchvarov *et al.* reported excited-state absorption (ESA) spectra for a series of $d(A)_n$ oligomers ($2 \leq n \leq 18$) and attributed the > 100 ps lifetimes to delocalised, electronically relaxed excitons.[47] Takaya *et al.* determined electronic relaxation rates for several ribose dinucleotides after 267 nm excitation from measurements of the ground-state recovery (GSR) times at $\lambda = 252$ nm and identified the long-lived states as excimers/exciplexes.[48] More recently, Su *et al.* analysed the GSR time profiles of adenosine and 2'-deoxyadenosine oligonucleotides $(A)_n$ and $d(A)_n$ as function of length and correlated the quantum yields for excimer formation with the fractions of stacked bases in the strands.[49] In our laboratory, we investigated the fluorescence decay dynamics of the adenine dinucleotide.[50]

In this paper, we report on a comprehensive study of the ultrafast excited-state dynamics of the adenine-guanine dinucleotide d(ApG) (see Figure 5.1) in aqueous solution at pH 7 by femtosecond UV/vis fluorescence up-conversion, broadband UV/vis absorption and single-colour deep-UV absorption measurements.

In contrast to the extremely weak fluorescence in the UV region from the respective mononucleotides, d(ApG) exhibits a broad, red-shifted second emission maximum around $\lambda = 460$ nm typical for the alleged 'excimers' in addition to 'monomer-like' emission in the UV (cf. Figure 5.2). Similar spectra have been observed for the adenine dinucleotide d(ApA), where the excimer state revealed itself by its exceptionally long ($\approx 300 - 400$ ps) fluorescence lifetime. The selection of the mixed dinucleotide d(ApG) for investigation was further motivated by the observed large effects on the fluorescence lifetimes upon substitution of an increasing number of adenines in a $d(A)_{20}$ strand by guanines.[12] The performed time-resolved measurements on d(ApG) are compared to data for the mononucleotides de-

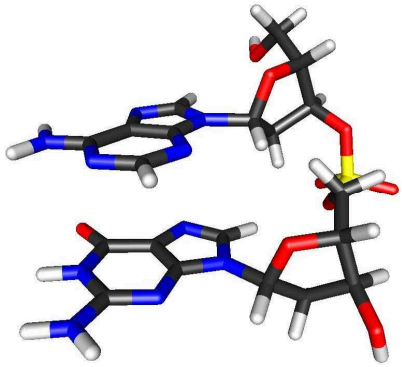

Fig. 5.1: Structure of d(ApG) in B-DNA conformation.

oxyadenosine monophosphate (dAMP) and deoxyguanosine monophospate (dGMP) and to the recently obtained detailed picture for the excited-state dynamics of d(ApA).[29] The results reveal clear spectro-temporal signatures of the elusive excimers in the excited-state absorption spectra that allow us to assess their fast formation and subsequent slow relaxation.

5.2 Experimental

The femtosecond fluorescence and absorption experiments have been described in some detail elsewhere.[51,52] The required UV pump and probe pulses were derived from the output of a regeneratively amplified Ti:Sa laser system (Clark-MXR CPA2001, 775 nm, 150 fs, 1 mJ, 1 kHz) in home-built non-collinear optical parametric amplifiers with frequency doubling crystals. Broadband supercontinuum probe pulses ($320-700$ nm) were generated from a small fraction of the 775 nm beam in a CaF_2 plate. The investigated nucleotides were purchased from biomers.net (5'-d(ApG)-3') and Sigma-Aldrich (dAMP, dGMP) and dissolved in phosphate buffered ultrapure water (16 mM NaH_2PO_4, 34 mM Na_2HPO_4, 117 mM NaCl).

All time-resolved experiments were carried out in flow cells with 0.2 mm fused silica windows. The excitation wavelength was $\lambda = 260$ nm with magic-angle polarisation in all cases. Fluorescence up-conversion measurements were performed on sample solutions of ≈ 0.2 mM concentration in 1 mm flow cells. The decay curves after photo-excitation were measured at three selected wavelengths ($\lambda_{FL} = 310$, 350 and 430 nm). The 775 nm gate pulses of the experiment limited the time resolution after deconvolution to $\Delta t \approx 150$ fs. Better time resolution ($\Delta t \approx 50$ fs) was reached by the transient absorption experiments which were performed in flow cells of 0.1 mm optical path length using sample concentrations of $\approx 3 - 10$ mM. The two-dimensional (2D) transient spectro-temporal absorption maps were recorded for delay times up to $\Delta t = 1.3$ ns after excitation. The short optical path length and higher sample concentrations resulted in smaller than usual coherent artefacts from cross-phase modulation (XPM) and stimulated Raman scattering (SRS) and very weak signal contributions from solvated electrons generated by multi-photon absorp-

tion of the pump pulses in water which were readily subtracted as described.[29,52] GSR time profiles were followed at $\lambda = 244$ nm up to a delay time of $\Delta t = 600$ ps. To ensure reproducibility, all measurements were repeated several times. Error limits given below correspond to the 2σ standard deviation.

UV absorption spectra were taken on a Shimadzu UV-2401 desktop spectrometer. Fluorescence spectra of the mononucleotides dAMP, dGMP and the dinucleotide d(pApG) (Midland Certified Reagents) were measured with a Jobin-Yvon FluoroMax-4 spectrometer. The additional phosphate group at the 5'-end of d(pApG) compared to d(ApG) is not expected to have any significant effect here.[1,40–46]

5.3 Results

5.3.1 Steady-State Spectra

The static absorption and fluorescence spectra of the dinucleotide and the two mononucleotides are given in Figure 5.2. The absorption of d(ApG) matches that of an equimolar mixture of dAMP and dGMP in the red wing, but is slightly stronger towards the blue (Figure 5.2a). The absorption maximum of the dinucleotide is blue-shifted by ≈ 2.5 nm. The fluorescence spectra, on the other hand, differ strongly both in intensity and in shape (Figure 5.2b). As can be seen, the dinucleotide exhibits the aforementioned 'dual fluorescence' with a roughly 0.55 : 0.45 intensity ratio between the 'monomer-like' emission in the UV and the 'excimer-like' emission in the VIS region.

5.3.2 Transient Fluorescence Measurements

Figure 5.3 displays the observed fluorescence-time profiles for d(ApG) at two wavelengths, $\lambda_{\mathrm{FL}} = 310$ nm and $\lambda_{\mathrm{FL}} = 430$ nm. The data could be nicely modelled using a sum of up to four exponential decay functions. The time constants increased gradually with the emission wavelength. The fluorescence decay curves for dAMP and dGMP under the same experimental conditions required at most two exponentials for fitting.

In the UV ($\lambda_{\mathrm{FL}} = 310$ nm), the emissions by the dinucleotide and the two monomers differ little (Figure 5.3a). The fluorescence decays in the sub-picosecond range in all cases. The obtained best-fit lifetimes for d(ApG) are (amplitudes in parentheses)

$$\begin{aligned} \tau_{\mathrm{FL1}} &\leq 0.10 \text{ ps}, \\ \tau_{\mathrm{FL2}} &= 0.41 \pm 0.05 \text{ ps } (90\,\%), \\ \tau_{\mathrm{FL3}} &= 2.10 \pm 0.50 \text{ ps } (10\,\%). \end{aligned}$$

The monomer decay curves (measured at $\lambda_{\mathrm{FL}} = 320$ nm) are bi-exponential and described by lifetimes of $\tau_{\mathrm{FL1}} \leq 0.10$ ps, $\tau_{\mathrm{FL2}} = 0.34 \pm 0.11$ ps for dAMP and $\tau_{\mathrm{FL1}} = 0.12 \pm 0.07$ ps, $\tau_{\mathrm{FL2}} = 0.68 \pm 0.11$ ps for dGMP.

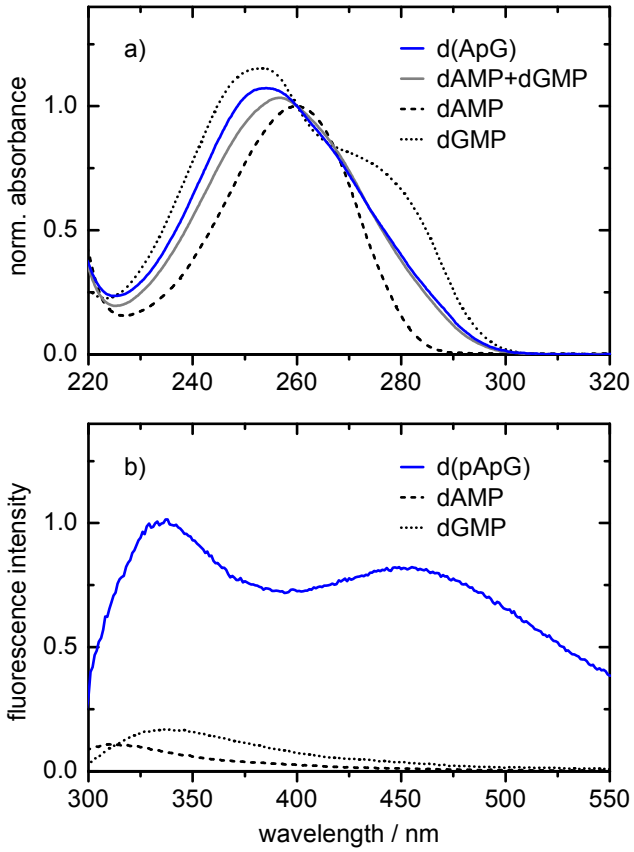

Fig. 5.2: a) UV absorption spectra of d(ApG), dAMP, dGMP and an equimolar mixture of dAMP and dGMP normalised at $\lambda = 260$ nm for better comparison of the band shapes. Relative to the mixture of dAMP and dGMP, the unnormalised spectrum of d(ApG) shows a normal hypochromic effect of ≈ 7 %. b) Static fluorescence spectra of d(pApG), dAMP and dGMP after 260 nm excitation.[53] As noted in the text (cf. Section 5.2), the extra phosphate of d(pApG) compared to d(ApG) does not alter the relevant dual fluorescence properties of the dinucleotide.[1,40–46]

The time profiles for d(ApG) at $\lambda_{FL} = 350$ were similar to those at the shorter wavelength except for the virtual absence of the ≤ 0.10 ps component. At $\lambda_{FL} = 430$ nm, in contrast, the dinucleotide was observed to emit for much longer times than the nucleotide monomers (Figure 5.3b, inset). The fitted d(ApG) fluorescence lifetimes in this 'excimer' emission region[40–46] are

$$\tau'_{FL2} = 0.46 \pm 0.01 \text{ ps } (46\,\%),$$
$$\tau'_{FL3} = 1.20 \pm 0.30 \text{ ps } (43\,\%),$$
$$\tau'_{FL4} = 5.90 \pm 1.40 \text{ ps } (10\,\%),$$
$$\tau'_{FL5} = 118 \pm 60 \text{ ps } (1\,\%),$$

without ultrashort (≤ 0.10 ps) component. Under the same conditions, the monomers feature $\tau'_{FL2} = 0.32 \pm 0.07$ ps (dAMP) and $\tau'_{FL2} = 0.53 \pm 0.16$ ps, $\tau'_{FL3} = 1.8 \pm 0.8$ ps (dGMP). The data for GMP could also be approximated by a single exponential with $\tau'_{FL2} = 0.86 \pm 0.10$ ps. These lifetimes for the monomers are in good agreement with

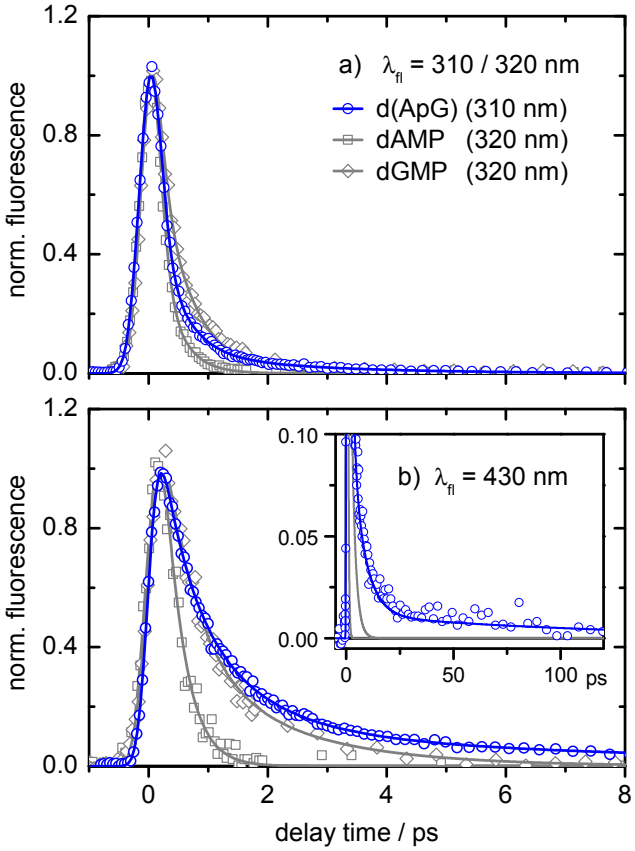

Fig. 5.3: Fluorescence-time profiles of d(ApG), dAMP and dGMP at a) $\lambda_{fl} = 310$ nm (320 nm for dAMP and dGMP) and at b) $\lambda_{fl} = 430$ nm after excitation at $\lambda = 260$ nm. Open symbols are data points, solid lines represent the best-fit decay curves. The inset in b) show the data for d(ApG) on an expanded time scale.

available literature data.[6,54,55] For d(ApG), on the other hand, the slow (though not very precisely determined) component with $\tau'_{FL5} = 118$ ps hints at the existence of a long-lived excited state, but this state appears to be only barely observable in fluorescence.

5.3.3 Transient Absorption Measurements

The measured two-dimensional spectro-temporal transient absorption maps after excitation of d(ApG), dAMP, dGMP and an equimolar mixture of the two monomer nucleotides are displayed for delay times up to $\Delta t = 5$ ps in Figure 5.4.

Considering first the two monomers (Figs. 5.4c–d), dAMP has an intense ESA band with maximum around ≈ 380 nm for $\Delta t \lesssim 0.5$ ps,[3,5,56] whereas dGMP features two ESA bands with maxima at ≈ 340 nm and ≈ 450 nm that decay within $\Delta t \approx 2$ ps after excitation,[57] slightly more slowly than for dAMP. The sum spectrum for both monomers therefore shows broad ESA over the entire wavelength range with no clear maximum at all and an effective lifetime of $1 - 2$ ps. The measured map for the equimolar dAMP/dGMP mixture in Figure 5.4b indeed equals the weighted sum of the two monomer maps.

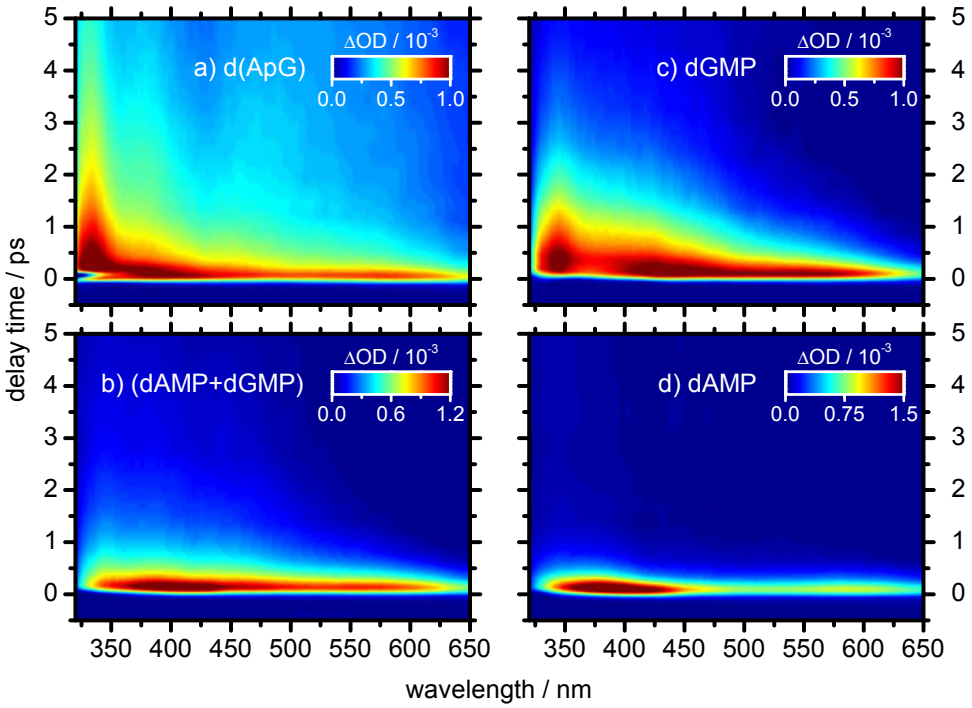

Fig. 5.4: Two-dimensional spectro-temporal transient absorption maps after 260 nm photo-excitation for a) d(ApG) ($c = 3.2$ mM), b) an equimolar mixture of dAMP and dGMP ($c = 4.8$ mM for each monomer), c) dGMP ($c = 9.1$ mM) and d) dAMP ($c = 9.7$ mM) for delay times up to $\Delta t = 5$ ps. Note the different concentrations of the dinucleotide and the mononucleotides and the different intensity scales (colour codes) in the respective panels.

The 2D transient absorption map for the dinucleotide in Figure 5.4a differs strongly from the other three. First, it is the only one with a negative feature near time zero at $\lambda \approx 325$ nm from stimulated emission (SE). Second, the broad positive ESA extending over the entire wavelength range decays mainly within the first 4 ps after excitation, but residues of this ESA are observable well up to $\Delta t \approx 300$ ps after excitation (see Figure 5.5 below). Moreover, the ESA appears to be weakly structured. A remarkable feature is the distinctive narrow absorption band with maximum at $\lambda \approx 330 - 340$ nm, which remains distinguishable from the broad background for ≈ 300 ps (Figure 5.6 below).

To determine the excited-state lifetimes for d(ApG), time profiles were extracted from the 2D maps at 15 wavelengths distributed across the spectrum from $\lambda = 330 - 680$ nm and analysed by global fitting with up to three decaying exponentials. Three representative data curves and their fits are given in Figs. 5.5a–c. From the analysis, the d(ApG) decay times (and amplitudes depending on wavelength in parentheses) were found to be

$$\tau_{\mathrm{ESA1}} = 0.24 \pm 0.01 \text{ ps } (40 - 80\,\%),$$
$$\tau_{\mathrm{ESA2}} = 2.44 \pm 0.14 \text{ ps } (45 - 10\,\%),$$
$$\tau_{\mathrm{ESA3}} = 124 \pm 4 \text{ ps } (\approx 15\,\%).$$

Also shown in the ESA decay diagram is the time profile of the ground state recovery (GSR) followed at $\lambda = 244$ nm (Figure 5.5d). A similar fit using three exponentials

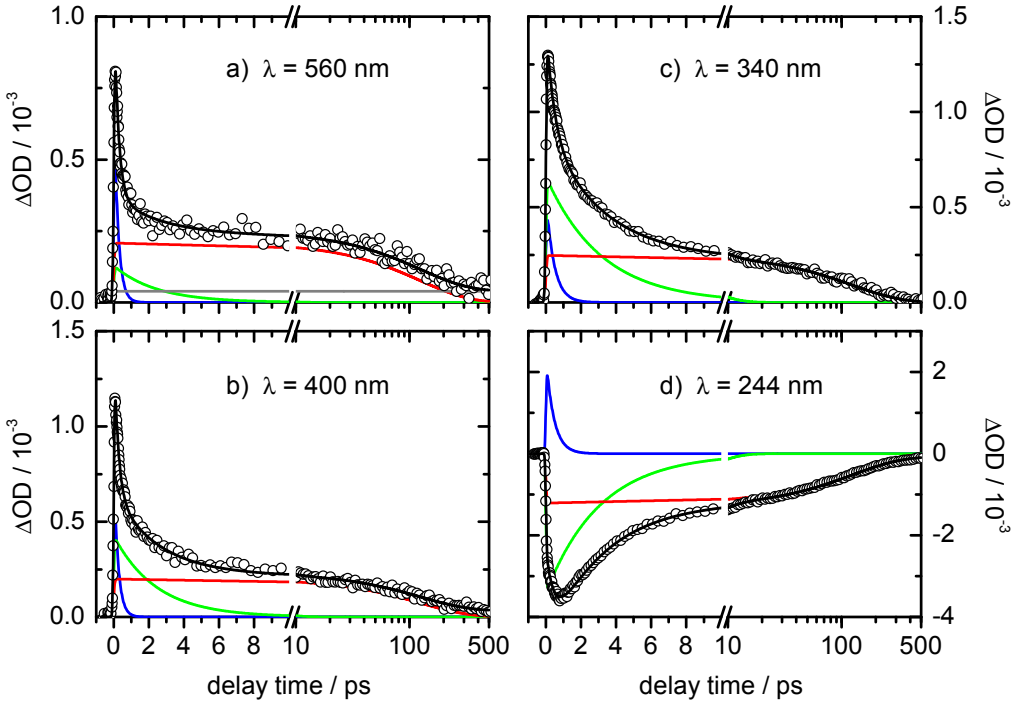

Fig. 5.5: Transient absorption-time profiles of d(ApG) after 260 nm excitation at a) $\lambda = 560$ nm (ESA), b) $\lambda = 400$ nm (ESA), c) $\lambda = 340$ nm (ESA) and d) $\lambda = 244$ nm (GSR). Open circles show data, solid lines the overall fits (black) and their components (coloured). The small constant offset in the fit at $\lambda = 560$ nm is attributed to the solvated electron absorption.

yielded a lifetime constant of $\tau_{\mathrm{GSR1}} = 0.45 \pm 0.02$ ps describing the fast initial evolution of the experimental signal likely due to dynamics of the excited state and two time constants of

$$\tau_{\mathrm{GSR2}} = 3.10 \pm 0.10 \text{ ps } (74\,\%),$$
$$\tau_{\mathrm{GSR3}} = 124 \pm 4 \text{ ps } (26\,\%)$$

representing the recovery of the electronic ground state (GSR) as evident by the refilling of the ground state bleach (GSB) signal appearing immediately after excitation. Judged from the relative amplitudes of τ_{GSR2} and τ_{GSR3}, the fraction of long-lived excited states is at least about 26 %, but may be as high as $\approx 35\,\%$ if the amplitude of the fast positive component (τ_{GSR1}) is taken as a measure for longer-lived ESA obscured by the strong GSB at the detection wavelength.

Within experimental errors, the electronic relaxation of d(ApG) seems to be practically complete within ≤ 500 ps after excitation.

5.4 Discussion

The comprehensive results above demonstrate the advantages of approaching the complex excited-state dynamics in DNA building blocks strategically by several complementary

experimental techniques at the same time. Namely, the time-resolved fluorescence measurements reflect mainly the properties of the photo-excited state(s) in the Franck-Condon (FC) region, the departure of the wavepacket from the FC window and the fate of surviving optically bright states at later stages in time. The transient spectro-temporal UV/vis absorption maps probe the excited-state dynamics as function of wavelength for longer times *via* observable $S_1 \rightarrow S_n$ ESA even when the $S_1 \rightarrow S_0$ emission turns optically dark. Last but not least, the GSB measurements in the deep-UV check for unknown long-lived optically dark states and showcase the eventual recovery of the electronic ground state. The experiments revealed a hierarchy of processes happening on time scales ranging from $\tau < 100$ fs *via* $\tau = 0.2/0.4 - 2.5$ ps *via* $\tau \approx 6 - 10$ ps to $\tau > 100$ ps. The complementary data thus allow for an in-depth assessment of the distinctive radiationless electronic decay mechanisms of the d(ApG) dinucleotide as opposed to the mononucleotides dAMP and dGMP and in comparison to the dynamics of the adenine dinucleotide d(ApA).

5.4.1 dAMP and dGMP

As already noted, the measured excited-state lifetimes for dAMP and dGMP agree well with available literature data.[3,5,6,54–57] Regarding the ensuing mechanisms, we can discuss only a few selected references next to some overview articles.[4,58–60]

For dAMP,[61–66] consensus appears to have emerged that the ultrashort lifetime of $\tau_1 \leq 0.1$ ps seen in fluorescence is associated with the rapid departure of the excited wavepacket from the FC region of the photo-excited $\pi\pi^*(L_a)$ state, which actually corresponds to the second (S_2) or third excited state (S_3) at the ground-state equilibrium configuration in solution and carries the bulk of the oscillator strength from S_0. Moving through a region, where the $S_3(\pi\pi^*)$, $S_2(\pi\pi^*)$ and $S_1(n\pi^*)$ states are strongly mixed, the wavepacket can reach the S_0 state *via* conical intersections (CIs) of the excited-state and ground-state potential energy hypersurfaces (PEHSs) along two main pathways, which are still intensely debated.[67] One route involves ring puckering at the C^2 atom, the other a distortion of the pyrimidine ring at the C^6 position and NH_2 out-of-plane motion.

Three pathways have been proposed for the nonadiabatic dynamics of dGMP, ring distortion, out-of-plane displacement of the NH_2 group and out-of-plane motion of the CO group.[68–74] dGMP has two spectrally resolved bright $\pi\pi^*$ transitions. The observed biphasic decay dynamics have been assigned to ultrafast $\pi\pi^*(L_b \rightarrow L_a)$ relaxation and subsequent slower motion to the CIs with S_0 across a plateau-like region on L_a.

5.4.2 Franck-Condon Excited States of d(ApG)

Compared to a single A or G, the complexity of the excited-state structure in a homo- or heterodimer such as d(ApA) or d(ApG) increases exponentially. Each purine base has two accessible $\pi\pi^*$ states (L_a and L_b). For a perfectly stacked homodimer with face-to-

face orientation of the two chromophores, an exciton model predicts two allowed and two forbidden $\pi\pi^*$-type transitions. Helical distortion in the B-DNA like conformation and static and dynamic disorder lift this simple picture. Nevertheless, the coupling of the transition dipole moments explains the blue-shift of the UV absorption maximum and the hypochromicity of di- and oligonucleotides compared to their monomers. However, the picture is further complicated by the presence of at least one $n\pi^*$ state per monomer in the vicinity of the first $\pi\pi^*$ states and by the possibility of CT transitions. The latter connect, e.g., the highest occupied molecular orbital (HOMO) of one monomer to the lowest unoccupied molecular orbital (LUMO) of the other.

In d(ApA) and longer dA_n strands, the first CT states most likely lie at significantly higher energies than the optically bright $\pi\pi^*$-type states in the FC range.[19,22,23,27] An ultrashort (< 50 fs) pump pulse tuned to the first UV absorption band is expected to prepare a neutral exciton delocalised over both bases of the stacked dimer (or delocalised over a few bases in a longer strand). The subsequent temporal evolution of the photo-excited exciton towards to relaxed, energetically stabilised and therefore long-lived excimer involves fast intraband scattering followed by large-amplitude motions of the two adenines forming a neutral excimer (see below).

In heterodimers like d(ApG) and mixed-sequence strands in the FC range, the exciton concept is less useful unless the coupling strength reaches and exceeds the splitting between the excited states of the two chromophores. Using time-dependent density functional theory (TD-DFT) including solvent effects by the polarisable continuum model (PCM), Santoro *et al.* predicted that four of the first ten excited states of d(ApG) in the FC region carry most of the oscillator strength.[75] The lowest CT states were found to be strongly mixed and close in energy with the bright dimer excited states. With the 6-31G(d) basis set, the S_1 and S_7 transitions were identified as $\pi\pi^*(G_{L_a})$ and $\pi\pi^*(G_{L_b})$, respectively, while S_2 and S_4 were of mixed $\pi\pi^*(A_{L_a}/G{\rightarrow}A_{CT})$ character. S_3, S_5 and S_8 were of $n\pi^*$ character, S_6 was the $\pi\pi^*(A_{L_b})$ transition with low oscillator strength, and S_9 and S_{10} led to energetically higher CT states.

At higher levels of theory, the calculated four $\pi\pi^*$-related transitions were strongly mixed, with significant CT character in all four, and more evenly distributed oscillator strengths.[75] Thus, a pronounced exciplex/CT character of the excited states of d(ApG) in the FC range is expected. Moreover, it appears quite likely that the flexibility of d(ApG) allows for a structural transformation to an energetically trapped exciplex with correspondingly prolonged lifetime at significantly lower energy than the bright $\pi\pi^*$-type excited dimer states.

5.4.3 Monomer-Like Excited Dinucleotides

The 0.2 to ≈ 1 ps excited-state lifetimes observed by the fluorescence up-conversion and transient absorption experiments ($\tau_{ESA1} = 0.24$ ps, $\tau_{FL2}, \tau'_{FL2} = 0.4 - 0.5$ ps, $\tau'_{FL3} = 1.2$ ps) are very similar to corresponding values for the mononucleotides and are there-

fore attributed to fast electronic relaxation of unstacked, 'monomer-like' excited dimers [$d(ApG)^*_m$]. The measured $\tau_{ESA2} = 2.44$ ps, however, already appears slightly long for simple 'monomer-like' decay dynamics. It may belong to slower, sterically hindered dimers or to dimers just entering the slow lane to the excimer/exciplex (see below).

By comparison with earlier work,[52,56] the $\tau_{GSR2} = 3.10$ ps value is attributed to the electronic relaxation of monomer-like excited dinucleotide molecules and identified as cooling time of 'vibrationally hot' $d(ApG)^{\#}_{(S_0)}$ molecules after their return to S_0. Remarkably, this time is about 50 % longer than observed elsewhere[52,56] despite of the lower vibrational temperature from one-photon excitation of a dinucleotide compared to a monomer. An explanation by slower electronic deactivation of hindered dinucleotides seems likely from this point of view.

5.4.4 Relaxation to Excimer/Exciplex States

Theory predicted the existence of a relaxed, energetically stabilised neutral excimer after photo-excitation of d(ApA) and longer dA_n strands with two chemically 'bound' adenines at considerably shorter distance than in B-DNA ($\approx$ 2.9 Å *vs.* 3.4 Å) with face-to-face (F2F) orientation in the minimum energy configuration.[24,27,76] In this neutral excimer state, denoted as $d(ApA)^*_{X(F2F)}$ here, the two adenine subunits lie on top of each other with maximal orbital overlap and significant π-electron density between the two purine rings. A similar configuration is likely for the relaxed exciplex of d(ApG) in its minimum energy state $d(ApG)^*_{X(min)}$ as well,[76] although a perfect face-to-face orientation is not possible in this case with two chemically different subunits. Obviously, the transformations of the photo-excited dimers from their FC states [$d(ApA)^*_{(FC)}$ and $d(ApG)^*_{(FC)}$] to the excimer/exciplex [$d(ApA)^*_{X(F2F)}$ and $d(ApG)^*_{X(min)}$] in local potential energy minima well below the bright $\pi\pi^*$-type dimer states require a great deal of large-amplitude motion of the two subunits relative to each other besides solvent displacement and (re)solvation. Judged from the isomerisation times of photochromic switches, e.g., azobenzenes,[77] where the internal forces steering the molecules are far stronger than in the weakly attractive case of two nucleobases, we expect time scales for relaxation to the excimer/exciplex of several picoseconds. Our experimental data give some insight here:

First, the ultrafast disappearance of the stimulated emission (SE) at $\lambda \approx 330$ nm close to time-zero in the transient 2D absorption map (Figure 5.4a) on the same time scale as the fastest fluorescence decay component ($\tau_{FL1} \leq 0.1$ ps) at about the same wavelength shows that the earliest transitions in the photo-excited dinucleotide happen in ≤ 0.1 ps. These transitions were first observed[29,50] for $d(ApA)^*$ and now also for $d(ApG)^*$. It is unclear, whether the SE and fastest fluorescence arise more from 'monomer-like' or from 'stacked' dinucleotides, but it is striking that no significant SE was found in the 2D maps for the monomers (Figs. 5.4b–d). This suggests (partial) relaxation within the photo-excited $\pi\pi^*$ stacks to 'relaxed' excited dimers [$d(ApA)^*_{(FCrelax)}$ and $d(ApG)^*_{(FCrelax)}$] as mechanism. To

some extent, this is related to the supposed $S_3 \rightarrow S_2 \rightarrow S_1$ transitions in the monomers in ≤ 0.1 ps. That time appears too short for large-amplitude motions of the entire purine rings. Further, the 'relaxed' excited states remain observable in fluorescence (lifetime τ_{FL2}, see above). As has been noted, however, the FC and relaxed FC states of d(ApG)* are expected to have pronounced CT character, in contrast to the exciton situation for d(ApA)*. In longer strands, the intraband exciton relaxation leads to a localisation of the excitation on two bases within 1 to at most a few ps.[12]

Next, as briefly introduced above, the relaxation from the $\mathrm{d(ApA)}^*_{(\mathrm{FCrelax})}$ resp. $\mathrm{d(ApG)}^*_{(\mathrm{FCrelax})}$ states to the final excimer/exciplex states involves torsional motion from the B-DNA to an F2F conformation and relative motion of the two chromophore units towards each other next to solvent displacement and (re)solvation. The time window, within which these processes occur, must range from between $\Delta t \approx 0.5$ ps (τ'_{FL2}) or ≈ 2.5 ps (τ_{ESA2}) after excitation to $\Delta t \approx 6$ ps (τ'_{FL3}) after excitation in the d(ApG) case and to $\Delta t \approx 8 - 10$ ps[29] in the d(ApA) case. The intermediate states in this $\Delta t \approx 10$ ps window after excitation are unlikely to correspond to local energy minima, as the downhill motion on the PEHS should be more or less continuous. During this process, on the other hand, they likely gain in excimer/exciplex character, which is why they will be referred to as $\mathrm{d(ApA)}^*_{\mathrm{X(BDNA)}}$ and $\mathrm{d(ApG)}^*_{\mathrm{X(BDNA)}}$ in the following. Since CT states are nominally optically dark in emission, the very weak residual fluorescence of d(ApG) at long delay times (cf. Figure 5.3b) despite of the fact that $\approx 25 - 35\,\%$ (see results) of the photo-excited molecules have not yet returned to the ground state indicates that the CT/exciplex minimum is reached after $\Delta t \approx 6$ ps (τ_{FL3}) at the earliest. We consider the long-lived $\mathrm{d(ApG)}^*_{\mathrm{X(min)}}$ CT/exciplex as optically 'dark grey' here, and not plain black. Judged from the more intense fluorescence with > 100 ps lifetime in the d(ApA) case,[50] the neutral $\mathrm{d(ApA)}^*_{\mathrm{X(F2F)}}$ excimer is labelled as 'bright grey' in this context. The long lifetimes naturally account for the higher fluorescence quantum yields of π-stacked dinucleotides compared with the monomers.

Eventually, Figure 5.6 depicts transient spectra extracted from the 2D maps at selected delay times for d(ApG) in the center compared to d(ApA) above and the equimolar mixture of dAMP and dGMP below. Showing distinctive, rather narrow, long-lived absorption bands around $\lambda = 330$ nm in the d(ApG) case and between $\lambda \approx 330$ and 375 nm in the d(ApA) case, these transient spectra reveal features that appear to be characteristic and unique for the excimer/exciplex states of the stacked dinucleotides.

For d(ApA), two partially overlapping UV ESA bands are observed which peak at $\lambda \approx 348$ and at $\lambda \approx 368$ nm in addition to the weaker broad ESA in the VIS region with maximum at $\lambda = 630$ nm (Figure 5.6a). The intense 386 nm ESA band disappears in only ≈ 1 ps and may therefore be attributed to 'monomer-like' excited states or to a short-lived higher $\pi\pi^*$ excited state of the stacked dimer, while the spectral narrowing and blue-shift of the 348 nm ESA band within $\approx 5 - 10$ ps hints at the above-mentioned intermediate $\mathrm{d(ApA)}^*_{\mathrm{X(BDNA)}}$-type states en route to the long-lived $\mathrm{d(ApA)}^*_{\mathrm{X(F2F)}}$ excimer.

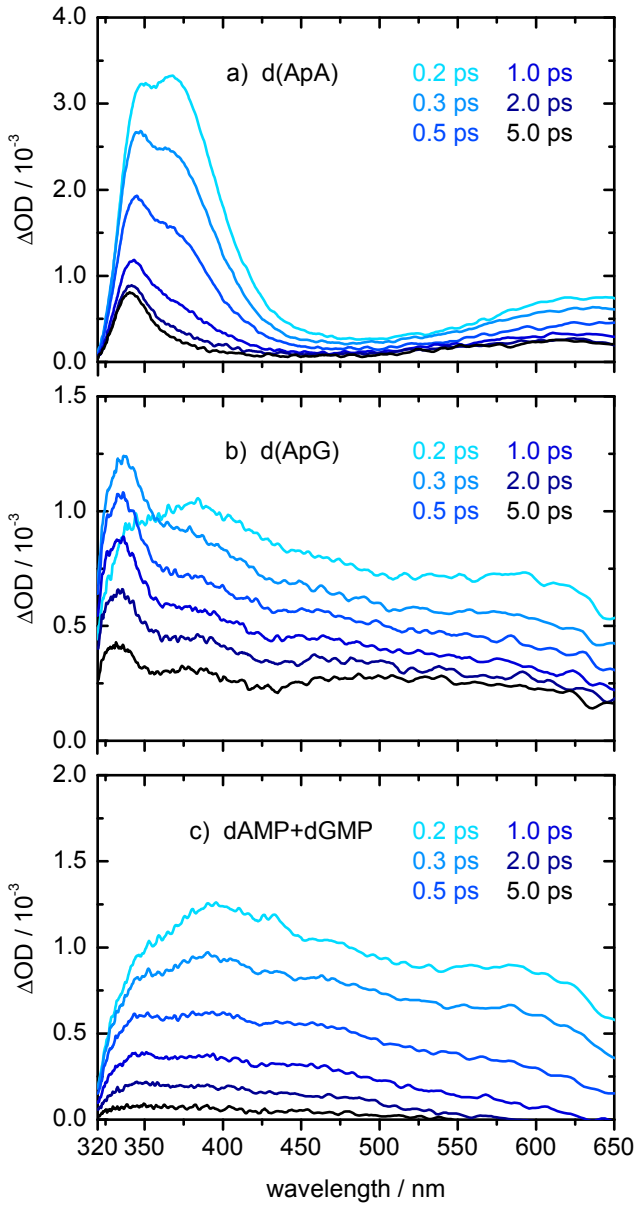

Fig. 5.6: Transient excited-state absorption spectra at selected delay times after excitation for a) d(ApA)[29], b) d(ApG) and c) an equimolar mixture of dAMP and dGMP.

Being trapped in a potential energy minimum on the excited PEHS, the latter has a lifetime of $\tau = 380$ ps according to the observed ESA decay time, the longest fluorescence lifetime and the ground state recovery time.[29] Su *et al.* interpreted their similar results for the GSR after 267 nm photo-excitation of d(ApA) in terms of $\approx 46\,\%$ of stacked and $\approx 64\,\%$ of unstacked dimers in thermal equilibrium.[49] We did, however, notice differences between the transient spectra of d(ApA) and dAMP at short delay times, which indicate that the excited-state absorption properties of 'unstacked' dimers and dAMP are not quite the same.[29]

In the case of d(ApG) (Figure 5.6b), the $\lambda \approx 330$ nm 'exciplex' band peaks ≈ 0.5 eV to

the blue compared to the maximum of the broad ESA after excitation of the equimolar dAMP/dGMP mixture. Although this $d(ApG)^*_X$ band appears less pronounced than for $d(ApA)^*_X$, the shape of the spectrum in the $\lambda = 320 - 400$ nm region is very different from that of the dAMP/dGMP mixture. Regrettably, the SE observed immediately after UV excitation may obscure a possible delayed rise of the exciplex feature. Compared to d(ApA), however, the lack of spectral evolution in the d(ApG) spectrum in the first few ps after excitation is striking. This may be related to the pronounced CT character of the bright excitation transitions for d(ApG) explained above. The lifetime of $\tau = 124$ ps of the eventually formed long-lived CT/exciplex state $d(ApG)^*_{X(\,\mathrm{min}\,)}$ and the time for its slow return to the ground state is shorter by a factor of about 3 compared to d(ApA) and in good agreement with a measurement for the ribose nucleotide ApG ($\tau = 105$ ps) by Takaya *et al.*[48] Regarding the mechanism, Olaso-Gonzaléz *et al.* proposed thermal activation followed by nonadiabatic decay along the known monomer-like pathways.[24]

5.4.5 Implications for Other Di- and Oligonucleotides

The extent of π-stacking between neighbouring bases in DNA oligonucleotides is highly dependent on strand length, exact base sequence, and experimental conditions such as pH, temperature and ion concentration. Their effect on the overall excited-state dynamics is therefore hard to quantify. Disturbed π-stacking likely accounts for many of the current problems in the interpretation and comparison of time-resolved measurements of different oligonucleotides.[4,10–18,47–49]

Here, we pinpointed common characteristics, but also differences between the dinucleotides d(ApG) and d(ApA). Both are supposed to adopt B-DNA conformations in thermal equilibrium in neutral aqueous solution, but are flexible enough to relax to non-B-DNA like (e.g., 'face-to-face') excimer structures with lower energy relative to the $\pi\pi^*$-type bright states upon photo-excitation. Remarkably, even the relatively minor exchange of one purine base with another led to a pronounced decrease in the excited-state lifetime. Naturally, the partial 'locking' of the bases in a longer B-DNA oligonucleotide strand should lead to less well stabilised excimers and thereby a decrease in the excited-state lifetime. This effect is countered by the higher stacking fractions in longer strands,[49] but enhanced by varying base sequence.[12] Correlations of the exciplex decay rates with the thermodynamic driving force estimated from the ionisation energy of the donor minus the electron affinity of the acceptor have met some success,[48] while the stacking fractions in a comparison of a series of $d(A)_n$ oligonucleotides provided rather good guidance.[49]

Systematic studies of additional model systems, preferably other dinucleotides, followed by tri- and tetranucleotides and by short self-complementary hairpins, will presumably shed more light onto this complex matter. Since theoretical calculations suggested significant differences between the AG and GA sequences regarding the extent of stacking, the nature of the FC excited states and their coupling with the exciplex/CT states,[75] it will be

interesting to compare the dynamics of d(ApG) and d(GpA) and additional dinucleotides. The so far missing d(GpG) and the differences between RNA and DNA dinucleotides should be checked next.

5.5 Conclusions

In summary, we have studied the complex electronic relaxation dynamics of the DNA dinucleotide d(ApG) by means of femtosecond time-resolved fluorescence and absorption spectroscopy. The most pronounced difference between the dinucleotide and its monomer nucleotides that was found is the strikingly longer excited-state lifetime of the former. The observed multi-exponential decay dynamics hint at step-wise transitions along complex pathways. We found evidence in the spectra for the formation of an excimer state on the stacked dinucleotide d(ApG) with lifetime $\tau = 124 \pm 4$ ps. This is shorter compared with d(ApA), whose excimer state presumably adopts a face-to-face conformation. We attribute this difference to less orbital overlap in d(ApG) and thereby weaker stabilisation. Nevertheless, both dinucleotides exhibit a common spectral 'excimer feature', the narrow excited-state absorption band around $\lambda = 330$ nm. The ≈ 0.5 eV blue-shift compared to the broad ESA maximum of a mixture of the mononucleotides shows considerable energetic stabilisation. This feature may be of great help in future studies of the photo-initiated quantum molecular dynamics of other di- and oligonucleotides. We attributed our observation to the formation of the excimer in its minimum energy configuration below the bright $\pi\pi^*$-type excited states in a time of $\Delta t \approx 5-10$ ps after excitation. The subsequent slow return to the ground state in several hundred picoseconds refills the initial ground state bleach signal. Little to no room appears left for additional other, longer-lived dark states in the dynamics. The nucleotide monomers dAMP and dGMP exhibit only weak transient absorption around $\lambda = 330$ nm, and both decay to their electronic ground states within $< 1 - 2$ ps. Time-resolved emission measurements confirmed the picture derived from the transient absorption experiments and revealed that the excimer state of d(ApG) is nearly optically dark regarding fluorescence.

Acknowledgements

This work has been supported by the Deutsche Forschungsgemeinschaft. The authors thank J. Kleber for taking the emission spectra of dAMP, dGMP and d(pApG).

References and Notes

[1] J. Eisinger, R. G. Shulman, *Science* **161**, 1311 (1968).

[2] P. R. Callis, *Annu. Rev. Phys. Chem.* **34**, 329 (1983).

[3] C. E. Crespo-Hernández, B. Cohen, P. M. Hare, B. Kohler, *Chem. Rev.* **104**, 1977 (2004).

[4] C. T. Middleton, K. de La Harpe, C. Su, Y. K. Law, C. E. Crespo-Hernández, B. Kohler, *Annu. Rev. Phys. Chem.* **60**, 217 (2009).

[5] J.-M. L. Pecourt, J. Peon, B. Kohler, *J. Am. Chem. Soc.* **122**, 9348 (2000).

[6] J. Peon, A. H. Zewail, *Chem. Phys. Lett.* **348**, 255 (2001).

[7] T. Gustavsson, A. Sharonov, D. Markovitsi, *Chem. Phys. Lett.* **351**, 195 (2002).

[8] C. E. Crespo-Hernández, B. Cohen, B. Kohler, *Nature* **436**, 1141 (2005).

[9] As is customary in the literature on DNA, the terms 'excimer' and 'exciplex' will be used essentially synonymously in this text to describe the formation of a (comparatively long-lived) bound complex of two nucleobases upon excitation with shared electron density between them regardless of whether the two nucleobases are identical or not. Strictly speaking, the definition of an excimer or exciplex (as 'excited homodimer' or 'excited heterodimer', respectively) describes the formation of a bound dimer in the excited electronic state from two units that are not connected in their ground state, while the nucleobases as the chromophores of interest in a di- or oligonucleotide are linked *via* the sugar-phosphate backbone. But the important point in the present case is the formation of a bound complex with shared electron density between the two bases on excitation. Accordingly, the two nucleobase chromophores can be regarded as electronically unbound in the ground state, the bound state arises on electronic excitation of a subunit only. An exciplex with two different chromophores usually implies at least some charge transfer (CT) character of the excited state due to the different ionisation energies and electron affinities of the subunits, an excimer may be neutral regarding the charges on two identical subunits.

[10] C. E. Crespo-Hernández, B. Cohen, B. Kohler, *Nature* **441**, E8 (2006).

[11] D. Markovitsi, F. Talbot, T. Gustavsson, D. Onidas, E. Lazzarotto, S. Marguet, *Nature* **441**, E7 (2006).

[12] N. K. Schwalb, F. Temps, *Science* **322**, 243 (2008).

[13] W.-M. Kwok, C. Ma, D. L. Phillips, *J. Phys. Chem. B* **113**, 11527 (2009).

[14] S. O. Konorov, H. G. Schulze, C. J. Addison, C. A. Haynes, M. W. Blades, R. F. B. Turner, *Open Spectrosc. J.* **3**, 9 (2009).

[15] B. Kohler, *J. Phys. Chem. Lett.* **1**, 2047 (2010).

[16] I. Vayá, T. Gustavsson, F.-A. Miannay, T. Douki, D. Markovitsi, *J. Am. Chem. Soc.* **132**, 11834 (2010).

[17] I. Vayá, J. Brazard, T. Gustavsson, D. Markovitsi, *Photochem. Photobiol. Sci.* **11**, 1767 (2012).

[18] D. Markovitsi, T. Gustavsson, I. Vayá, *J. Phys. Chem. Lett.* **1**, 3271 (2010).

[19] F. Santoro, V. V. Barone, R. Improta, *Proc. Natl. Acad. Sci. U.S.A.* **104**, 9931 (2007).

[20] D. Nachtigallovà, P. Hobza, H.-H. Ritze, *Phys. Chem. Chem. Phys.* **10**, 5689 (2008).

[21] E. B. Starikov, G. Cuniberti, S. Tanaka, *J. Phys. Chem. B* **113**, 10428 (2009).

[22] A. W. Lange, M. A. Rohrdanz, J. M. Herbert, *J. Phys. Chem. B* **112**, 6304 (2008).

[23] A. W. Lange, J. M. Herbert, *J. Am. Chem. Soc.* **131**, 3913 (2009).

[24] G. Olaso-González, M. Merchán, L. Serrano-Andrés, *J. Am. Chem. Soc.* **131**, 4368 (2009).

[25] I. Conti, P. Altoè, M. Stenta, M. Garavelli, G. Orlandi, *Phys. Chem. Chem. Phys.* **12**, 5016 (2010).

[26] Y. Lu, Z.-G. Lan, W. Thiel, *Angew. Chem., Int. Ed.* **50**, 6864 (2011).

[27] R. Improta, V. Barone, *Angew. Chem. Int. Ed.* **50**, 12016 (2011).

[28] F. Plasser, A. J. A. Aquino, W. L. Hase, H. Lischka, *J. Phys. Chem. A* **116**, 11151 (2012).

[29] M. C. Stuhldreier, M. Malicki, K. Röttger, C. Schüler, J. Kleber, T. Muskat, F. Temps, *to be submitted* (2013).

[30] M. Y. Warshaw, I. Tinoco, *J. Mol. Biol.* **20**, 29 (1966).

[31] C. R. Cantor, M. M. Warshaw, H. Shapiro, *Biopolymers* **9**, 1059 (1970).

[32] J. L. Sussman, I. Barzilav, M. Keren-Zur, Y. Lapidot, *Biochim. Biophys. Acta* **308**, 189 (1973).

[33] N. P. Johnson, T. Schleich, *Biochemistry* **13**, 981 (1974).

[34] C.-H. Lee, F. S. Ezra, N. S. Kondo, R. H. Sarma, S. S. Danyluk, *Biochemistry* **15**, 3627 (1976).

[35] C. S. M. Olsthoorn, C. A. G. Haasnoot, C. Altona, *Eur. J. Biochem.* **106**, 85 (1980).

[36] C. S. Olsthoorn, L. J. Bostelaar, J. H. Van Boom, C. Altona, *Eur. J. Biochem.* **112**, 95 (1980).

[37] C. S. M. Olsthoorn, L. J. Bostelaar, J. F. M. De Rooij, J. H. van Boom, C. Altona, *Eur. J. Biochem.* **115**, 309 (1981).

[38] C. S. M. Olsthoorn, J. Doornbos, H. P. M. De Leeuw, C. Altona, *Eur. J. Biochem.* **125**, 367 (1982).

[39] Z. Vokáčová, M. Budášínský, I. Rosenberg, B. Schneider, J. Šponer, V. Sychrovský, *J. Phys. Chem. B* **113**, 1182 (2009).

[40] J. Eisinger, M. Guéron, R. G. Shulman, T. Yamane, *Proc. Natl. Acad. Sci. U.S.A.* **55**, 1015 (1966).

[41] M. Daniels, J. P. Morgan, *Chem. Phys. Lett.* **58**, 283 (1978).

[42] J. P. Morgan, P. R. Callis, *Photochem. Photobiol.* **29**, 1107 (1979).

[43] J. P. Morgan, M. Daniels, *Photochem. Photobiol.* **31**, 101 (1980).

[44] J. P. Morgan, M. Daniels, *Photochem. Photobiol.* **31**, 207 (1980).

[45] C. S. Shaar, J. P. Morgan, M. Daniels, *Photochem. Photobiol.* **39**, 747 (1984).

[46] M. Daniels, C. S. Shaar, J. P. Morgan, *Biophys. Chem.* **32**, 229 (1988).

[47] I. Buchvarov, Q. Wang, M. Raytchev, A. Trifonov, T. Fiebig, *Proc. Natl. Acad. Sci. U.S.A.* **104**, 4794 (2007).

[48] T. Takaya, C. Su, K. de La Harpe, C. E. Crespo-Hernández, B. Kohler, *Proc. Natl. Acad. Sci. U.S.A.* **105**, 10285 (2008).

[49] C. Su, C. T. Middleton, B. Kohler, *J. Phys. Chem. B* **116**, 10266 (2012).

[50] M. Stuhldreier, C. Schüler, J. Kleber, F. Temps, *Ultrafast Phenomena XVII*, M. Chergui, D. M. Jonas, E. Riedle, R. W. Schoenlein, A. J. Taylor, Eds. (Oxford University Press, Inc., 2011), pp. 553–555.

[51] N. K. Schwalb, F. Temps, *J. Phys. Chem. A* **113**, 13113 (2009).

[52] K. Röttger, R. Siewertsen, F. Temps, *Chem. Phys. Lett.* **536**, 140 (2012).

[53] J. Kleber, Diploma Thesis (Kiel, 2009).

[54] D. Onidas, D. Markovitsi, S. Marguet, A. Sharonov, T. Gustavsson, *J. Phys. Chem. B* **106**, 11367 (2002).

[55] T. Pancur, N. K. Schwalb, F. Renth, F. Temps, *Chem. Phys.* **313**, 199 (2005).

[56] J.-M. L. Pecourt, J. Peon, B. Kohler, *J. Am. Chem. Soc.* **123**, 10370 (2001).

[57] V. Karunakaran, K. Kleinermanns, R. Improta, S. A. Kovalenko, *J. Am. Chem. Soc.* **131**, 5839 (2009).

[58] L. Serrano-Andrés, M. Merchán, *J. Photochem. Photobiol. C* **10**, 21 (2009).

[59] T. Gustavsson, R. Improta, D. Markovitsi, *J. Phys. Chem. Lett.* **1**, 2025 (2010).

[60] M. Barbatti, A. J. A. Aquino, J. J. Szymczak, D. Nachtigallovà, P. Hobza, H. Lischka, *Proc. Natl. Acad. Sci. U.S.A.* **107**, 21453 (2010).

[61] C. M. Marian, *J. Chem. Phys.* **122**, 104314 (2005).

[62] S. Perun, A. L. Sobolewski, W. Domcke, *J. Am. Chem. Soc.* **127**, 6257 (2005).

[63] L. Blancafort, *J. Am. Chem. Soc.* **128**, 210 (2006).

[64] L. Serrano-Andrés, M. Merchán, A. C. Borin, *Chem. Eur. J.* **12**, 6559 (2006).

[65] M. Barbatti, H. Lischka, *J. Am. Chem. Soc.* **130**, 6831 (2008).

[66] I. Conti, M. Garavelli, G. Orlandi, *J. Am. Chem. Soc.* **131**, 16108 (2009).

[67] M. Barbatti, Z. Lan, R. Crespo-Otero, J. J. Szymczak, H. Lischka, W. Thiel, *J. Chem. Phys* **137**, 22A503 (2012).

[68] H. Chen, S. Li, *J. Chem. Phys.* **124**, 154315 (2006).

[69] C. M. Marian, *J. Phys. Chem. A* **111**, 1545 (2007).

[70] S. Yamazaki, W. Domcke, *J. Phys. Chem. A* **112**, 7090 (2008).

[71] S. Yamazaki, W. Domcke, A. L. Sobolewski, *J. Phys. Chem. A* **112**, 11965 (2008).

[72] L. Serrano-Andrés, M. Merchán, A. C. Borin, *J. Am. Chem. Soc.* **130**, 2473 (2008).

[73] M. Barbatti, J. J. Szymczak, A. J. A. Aquino, D. Nachtigallová, H. Lischka, *J. Chem. Phys.* **134**, 014304 (2011).

[74] B. Heggen, Z. Lan, W. Thiel, *Phys. Chem. Chem. Phys.* **14**, 8137 (2012).

[75] F. Santoro, V. Barone, A. Lami, R. Improta, *Phys. Chem. Chem. Phys.* **12**, 4934 (2010).

[76] N. Öksüz, F. Temps, *unpublished results* .

[77] T. Pancur, F. Renth, F. Temps, B. Harbaum, A. Krueger, R. Herges, C. Naether, *Phys. Chem. Chem. Phys.* **7**, 1985 (2005).

6

Structural Characterisation and Time-Resolved Electronic Deactivation Dynamics of a Self-Complementary Oligonucleotide Loop as Model for DNA Double Strands

This Chapter deals with the pairing properties and the ultrafast dynamics of a short self-complementary oligonucleotide loop, consisting of two complementary oligonucleotide trimers connected with a hexaethylene glycol spacer (d[5'-GpGpGp-HEG-pCpCpC-3']). This molecule turned out to be an excellent model system for hydrogen-bonded DNA double strands in aqueous solution. Due to its small size it is also accessible by theoretical investigations. Static UV/vis absorption spectra and a thorough NMR spectroscopic investigation revealed the nature and extent of base pairing between the two trimer-'arms', which agree nicely with molecular dynamics simulations. Femtosecond time-resolved fluorescence spectroscopy corroborates initial electronic deactivation dynamics consistent with those of a single G-C base pair in $CHCl_3$, whereas transient absorption measurements excluded the population of long-lived, optically dark states.

6.1 Introduction

Nucleobase pairs, single and double strands have quite different excited-state geometries and therefore the electronic deactivation dynamics differ considerably (see Chapter 1). To unravel the different contributions of base pairing, π-stacking and base sequence influence, a variety of model systems is needed to account for each effect separately. In the Chapters 3, 4 and 5, two closely related model systems for π-stacking interactions were discussed; in the present Chapter a model system for hydrogen bonded nucleobase pairs is introduced

and characterised. Whereas Watson-Crick single base-pairs are accessible in $CHCl_3$,[1,2] the natural aqueous environment exhibits several problems when short oligonucleotides ($\leq$ 6 base pairs) are involved, such as hydrogen bonding of the nucleobases with water. The flexibility of DNA strands at room temperature hinders the formation of a base-paired duplex for such short oligonucleotides. As the hydrogen bonds may statistically break at ambient temperatures especially at the ends of the duplex, a minimal number of base pairs is needed to hold two single strands 'in place' so the outer base pairs can re-form the broken hydrogen bonds. The opening and re-forming of hydrogen bonds happens relatively fast. Leroy *et al.* determined the lifetime of an individual base pair, e.g., the time it needs to open in an oligonucleotide double strand, to lie in the range of a few milliseconds to a few tens of milliseconds.[3] Due to these effects, base strands with at least $10-20$ consecutive bases are usually needed at room temperature to form a stable double helix in water, shorter strands do not associate on their own. This leads to an overwhelming contribution from π-stacking effects to the overall dynamics of the respective double strands. Additionally, a huge number of base sequences needs to be considered when dealing with long oligonucleotides. These disadvantages can be avoided with the system presented in this Chapter, an oligonucleotide hairpin. The term 'DNA hairpin' is used somewhat ambiguously for both naturally self-complementary oligonucleotide sequences which spontaneously form an intrastrand loop,[4–8] and artificial, synthesised loops.[9–17] The latter molecules feature two complementary base sequences connected by a spacer, which consists often of stilbene derivatives,[9–15] fused aromatic ring systems,[15–17] or rarely an aliphatic chain.[13,14] If the spacer has the right length, the nucleotide-'arms' are pre-orientated to ensure pairing between them even if they consist only of few base pairs. Combined NMR and molecular modelling studies of synthetic self-complementary oligonucleotide loops featuring an aliphatic linker revealed a stable B-DNA structure of the formed duplexes, which consisted of $6-10$ base pairs.[13,18–20] In this context, Altmann *et al.* observed that a penta- or hexaethylene glycol spacer leads to better paring of the nucleobase pair adjacent to the linker than a shorter propylene-phosphate-propylene linker.[18] Siegmund *et al.* found a similar effect within a range of aliphatic carbon chain linkers ($C8-C16$): A C14 chain led to the most stable duplex, longer and shorter chain lengths decreased its stability.[13] It seems as if a chain length of about 14 atoms (or a pentaethylene glycol linker) is optimal to hold two oligonucleotide-'arms' together. A study of Tuma *et al.* compared static circular dichroism spectra of $d(C)_x$-linker-$d(G)_x$ oligonucleotides with two different linkers (stilbene and hexaethylene glycol (HEG)) in aqueous solution with a calculated one for an ideal B-DNA form.[14] They made three major observations: *(i)* The stilbene-linked loops were much more stable than the HEG-linked systems. *(ii)* The HEG-linked dimers formed a weak, the HEG-linked trimers already a stable B-DNA helical structure. *(iii)* The lowest unoccupied molecular orbital of the stilbene-linked systems is delocalised over the stilbene and the adjacent guanine, thus distorting the helical structure and altering the electronic properties of the molecule.

The femtosecond time-resolved dynamics of relatively long DNA double strands have been studied by several groups.[21–26] However, the results are subject to discussions, as the dynamics depend crucially on the base sequence and on the exact experimental conditions. The Kohler group investigated a series of G·C nucleobase double strands and self-complementary hairpins by transient absorption spectroscopy in aqueous solution, namely $d(GC)_9 \cdot d(CG)_9$, $d(C_4G_4) \cdot d(G_4C_4)$, $d(C_5A_4G_5)$, and $d(G_5T_4C_5)$.[22,23] All double strands adopted a B-DNA helical form, the $d(GC)_9 \cdot d(CG)_9$ double strand was additionally measured in Z-DNA and Hoogsteen configuration.[23] They found for all hydrogen bonded double helices slower dynamics ($\tau \approx 4.1 - 7.6$ ps) than for the single nucleotides dGMP and dCMP and attributed this observation to the population of dark states which cannot be observed by time-resolved emission spectroscopy.[22] These findings are supported by a theoretical QM/MM study of a G·C base pair embedded in a dodecamer DNA duplex in water of Zeleny *et al.*[27] They found the dynamics to slow down in the base pair compared to to free G and C and attributed this finding to the hindered G-NH_2 out-of-plane motion which is needed to reach a conical intersection with the ground state. Although Zeleny *et al.* attributed the slower decay dynamics of the G·C base pair exclusively to the restraints arising from the hydrogen bonds, the above experimental and theoretical studies mainly illustrate the need for shorter hydrogen bonded model systems, as for the investigated systems the effects of π-stacking in the rather long DNA strands and interstrand hydrogen bonding cannot be separated. It is well established that π-stacking leads to prolonged decay dynamics (cf. Chapters 1, 3, 4, and 5), which might conceal effects from hydrogen bonding in the above mentioned studies.

Considering all this, we designed a self-complementary short oligonucleotide strand, whose oligonucleotide-'arms' consist of a guanosine and a cytidine trimer, respectively, their deoxyribose backbones being connected *via* a hexaethylene glycol (HEG) linker. This linker is assumed to have the ideal length to ensure pairing,[13,18] and it does not absorb UV light as aromatic linkers, which may lead to an alteration of the involved molecular orbitals and the stacking properties.[14] The structural formula of this molecule is d[5'-GpGpGp-HEG-pCpCpC-3'], in the following also denoted as $d(G)_3$-HEG-$d(C)_3$ or 'loop'. Please note the position of phosphate groups - they are missing at the open 5'- and 3'-end of the oligonucleotide, whereas the linker is connected *via* phosphate groups to both the guanosine and the cytidine trimer. In Figure 6.1, the Watson-Crick paired G-C base pair together with the atom numbering is depicted, as well as a schematic drawing of the investigated oligonucleotide loop.

The atom numbering follows the pattern commonly used for nucleotides, although in Figure 6.1 only the positions where hydrogen atoms are located are labelled. This is because their positions become important for the structure determination *via* NMR spectroscopy. The R indicate the binding sites to the rest of the oligonucleotide strand. To distinguish the respective three guanosine and cytosine 'sister' nucleobases, the base pairs are denominated as $x/y/z$, where the z-base pair is located at the open end of the oligonucleotide

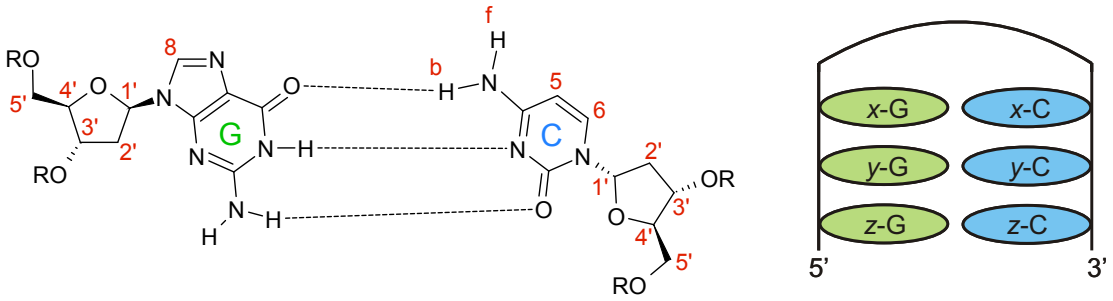

Fig. 6.1: Left: Chemical structure and atom numbering of the Watson-Crick paired G-C base pair. R indicates the phosphate group the nucleosides are linked with, except at the open 5'- and 3'-ends, where R=H. Right: Schematic drawing of the investigated d[5'-GpGpGp-HEG-pCpCpC-3'] loop. The labelling according to x-/y-/z-base pair will be used throughout the text.

duplex, the x-base pair sits next to the HEG spacer and the y-base pair lies in between the two others.

6.2 Structural Characterisation

A number of different spectroscopic techniques was applied for the structural characterisation of the self-complementary oligonucleotide loop d(G)$_3$-HEG-d(C)$_3$ (cf. Chapter 2). In the following, the experimental results from NMR spectroscopy, static absorption, fluorescence and circular dichroism spectroscopy performed on the studied molecule are presented and discussed. The conclusions drawn from the data are then compared with the picture that emerges from molecular mechanics simulations.

6.2.1 NMR Spectroscopy

NMR spectroscopic data for a 1 μM solution of d(G)$_3$-HEG-d(C)$_3$ were acquired on a Bruker Avance 600 MHz spectrometer in the group of Prof. Dr. F. D. Sönnichsen (Otto Diels Institute of Organic Chemistry, CAU Kiel). 1D-^{1}H-NMR spectra as well as 2D-^{1}H-NMR spectra (Nuclear Overhauser Effect Spectroscopy, NOESY, and Total Correlation Spectroscopy, TOCSY) were recorded at 275.2 K and pH 7.2 (90% H_2O/10% D_2O) and at 278 K and pH 7.0 (D_2O). The ^{1}H-NMR spectrum of the loop at pH 7.2 and 275.2 K together with the hydrogen atom assignment is shown in Figure 6.2. Equivalent hydrogen atoms belonging to sister nucleobases are labelled in the same colour, the atom numbering was done according to Figure 6.1.

As the oligonucleotide possesses many hydrogen atoms which are chemically alike and partially overlap in the spectrum, the assignment of the H atoms could only be accomplished by analysing the 2D-NMR spectra. In the spectra taken at pH 7.2, the amino and imino protons of the nucleobases can be observed nicely. In the spectra taken at pH 7.0 on the other hand, the respective signals are absent due to exchange with the solvent D_2O. The

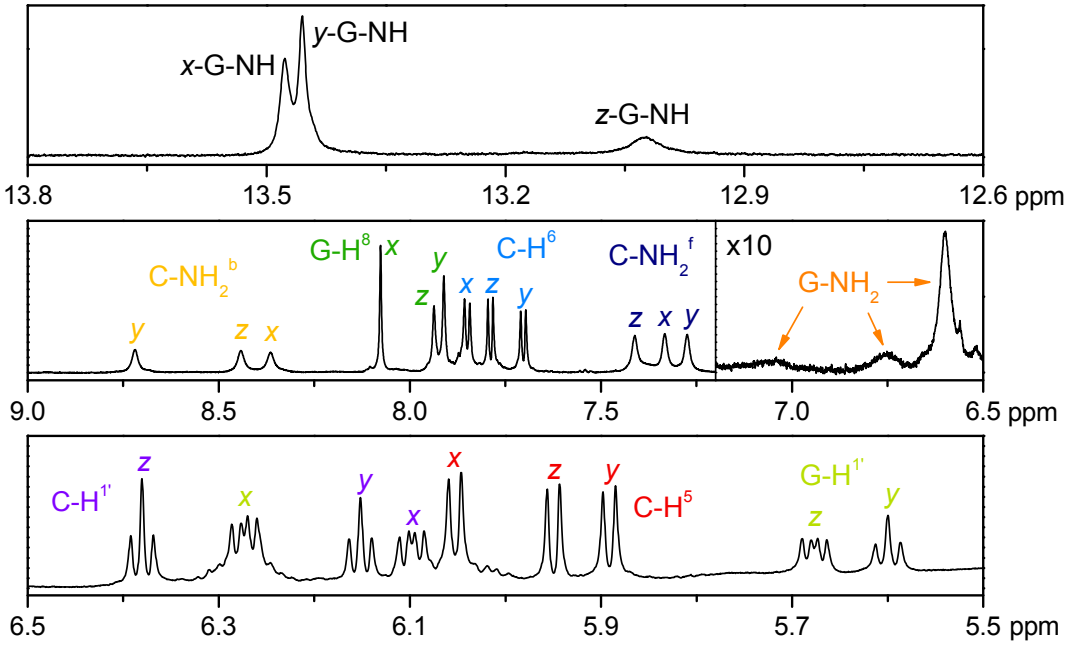

Fig. 6.2: ^{1}H-NMR spectrum of d[5'-GpGpGp-HEG-pCpCpC-3'] (600 MHz, 275.2 K, 1 µM in 90% H_2O/10% D_2O, pH 7.2). The assignment (see also Figure 6.1) is coloured to facilitate the recognition of the hydrogen atoms belonging to sister nucleobases. The region from 7.2-6.5 ppm in the middle panel has been amplified 10 times.

deoxyribose protons lie in the region around $2.5 - 5.0$ ppm (except $H^{1'}$) and vanish in the water suppression ($\delta_{H_2O} \approx 4.3$ ppm). Consequently, the pH 7.0 spectra in D_2O were used to assign the sugar protons. But even here some assignment difficulties remained, as the sugar protons lie quite closely to each other, exhibit a complex multiplet structure and overlap partially. The coupling patterns are rather complicated and the $H^{3'}$ protons still vanish in the water suppression. It was not possible to integrate the ribose proton peaks as there are baseline issues due to the water suppression and the quantity of close lying and overlapping signals. However, cross peaks for all ribose protons (even for the $H^{3'}$ protons) could be found in the 2D spectra. In the end, all hydrogen atoms of the nucleobases and the sugar moieties (except z-C-$H^{5'}$) could be found, assigned and related to each other. The assignments are as follows:

> ^{1}H-NMR (600 MHz, 275.2 K, 90% H_2O/10% D_2O, pH 7.2): δ = 13.48 (s, 1H, x-G-NH), 13.45 (s, 1H, y-G-NH), 13.02 (s, br, 1H, z-G-NH), 8.72 (s, 1H, y-C-NH_2^b), 8.44 (s, 1H, z-C-NH_2^b), 8.36 (s, 1H, x-C-NH_2^b), 8.07 (s, 1H, x-G-H^8), 7.93 (s, 1H, z-G-H^8), 7.91 (s, 1H, y-G-H^8), 7.85 (d, 1H, ^3J = 8.0 Hz, x-C-H^6), 7.79 (d, 1H, ^3J = 7.7 Hz, z-C-H^6), 7.70 (d, 1H, ^3J = 7.7 Hz, y-C-H^6), 7.41 (s, 1H, z-C-NH_2^f), 7.33 (s, 1H, x-C-NH_2^f), 7.27 (s, 1H, y-C-NH_2^f), 6.38 (t, 1H, ^3J = 7.0 Hz, z-C-$H^{1'}$), 6.27 (dd, 1H, ^3J = 9.7, 5.8 Hz, x-G-$H^{1'}$), 6.15 (t, 1H, ^3J = 7.0 Hz, y-C-$H^{1'}$), 6.10 (dd, 1H, ^3J = 9.5, 5.8 Hz, x-C-$H^{1'}$), 6.05 (d, 1H, ^3J = 7.8 Hz, x-C-H^5), 5.95 (d, 1H, ^3J = 7.8 Hz, z-C-H^5), 5.89 (d, 1H, ^3J = 7.8

Hz, y-C-H^{5}), 5.67 (dd, 1H, ^{3}J = 9.7, 5.6 Hz, z-G-H$^{1'}$), 5.60 (t, 1H, ^{3}J = 7.8 Hz, y-G-H$^{1'}$) ppm.

^{1}H-NMR (600 MHz, 278 K, D_2O, pH 7.0): δ = 8.07 (s, 1H, x-G-H^{8}), 7.93 (s, 1H, z-G-H^{8}), 7.91 (s, 1H, y-G-H^{8}), 7.85 (d, 1H, ^{3}J = 8.3 Hz, x-C-H^{6}), 7.78 (d, 1H, ^{3}J = 7.9 Hz, z-C-H^{6}), 7.71 (d, 1H, ^{3}J = 8.0 Hz, y-C-H^{6}), 6.38 (t, 1H, ^{3}J = 7.2 Hz, z-C-H$^{1'}$), 6.27 (dd, 1H, ^{3}J = 9.4, 5.9 Hz, x-G-H$^{1'}$), 6.15 (t, 1H, ^{3}J = 7.0 Hz, y-C-H$^{1'}$), 6.10 (dd, 1H, ^{3}J = 9.5, 5.9 Hz, x-C-H$^{1'}$), 6.05 (d, 1H, ^{3}J = 7.8 Hz, x-C-H^{5}), 5.93 (d, 1H, ^{3}J = 7.9 Hz, z-C-H^{5}), 5.89 (d, 1H, ^{3}J = 7.8 Hz, y-C-H^{5}), 5.69 (dd, 1H, ^{3}J = 9.5, 6.0 Hz, z-G-H$^{1'}$), 5.62 (t, 1H, ^{3}J = 7.9 Hz, y-G-H$^{1'}$), 5.05 (m, x-G-H$^{3'}$), 5.02 (m, y-G-H$^{3'}$), 4.89 (m, x-C-H$^{3'}$), 4.87 (m, y-C-H$^{3'}$), 4.83 (m, z-G-H$^{3'}$), 4.65 (m, z-C-H$^{3'}$), 4.44 (m, x-G-H$^{4'}$), 4.39 (m, y-G-H$^{4'}$), 4.24 (m, x-C-H$^{4'}$), 4.22 (m, y-C-H$^{4'}$, z-G-H$^{5'}$), 4.19 (m, z-G-H$^{4'}$), 4.16 (m, y-C-H$^{5'}$), 4.14 (m, y-G-H$^{5'}$), 4.11 (m, z-C-H$^{4'}$), 4.07 (m, y-G-H$^{5'}$), 4.04 (m, y-C-H$^{5'}$), 4.02 (m, x-C-H$^{5'}$), 3.99 (m, x-C-H$^{5'}$), 3.68 (m, z-G-H$^{5'}$), 3.60 (ddd, ^{2}J = 18.5, ^{3}J = 11.8, 5.5 Hz, PEG-H) 2.74 (m, x-G-H$^{2'}$), 2.68 (m, y-G-H$^{2'}$), 2.66 (m, z-G-H$^{2'}$), 2.56 (m, x-C-H$^{2'}$, y-C-H$^{2'}$), 2.50 (m, z-G-H$^{2'}$), 2.43 (m, x-C-H$^{2'}$), 2.36 (m, z-C-H$^{2'}$), 2.29 (m, y-C-H$^{2'}$) ppm.

The nucleobases guanosine and cytidine next to the hexaethylene glycol spacer are denoted as x-G and x-C (top), the following as y-G and y-C (middle), and the two bases at the open end of the loop are referred to as z-G and z-C (bottom), respectively, as depicted in Figure 6.1. The Figure also gives the atom numbering used throughout this Chapter. The amino and imino protons of the nucleobases are denoted as G-NH, G-NH_2, and C-NH_2. In the latter case, the amino proton involved in the hydrogen bond towards guanosine is denoted as C-NH_2^b, the free proton as C-NH_2^f. The deoxyribose atom numbers are labelled with a prime for distinction from the nucleobase atom numbers, as is common for nucleosides. At the 2'- and 5'-positions, two diastereotopic hydrogen atoms are present, respectively. Although usually these two hydrogens have a different chemical shift (but may accidentally have the same), an unambiguous assignment was not possible in the present case. Therefore, in the above assignment the labels H$^{2'}$ and H$^{5'}$ refer to both diastereotopic hydrogen atoms, whether or not they show the same chemical shift.

The interpretation of the 2D-^{1}NMR spectra yielded clear structural information about the investigated oligonucleotide loop. Accordingly, it forms a paired, B-DNA like double helix. To illustrate how this conclusion was achieved, Figure 6.3 and Figure 6.4 display two different regions of the overlayed 2D-^{1}H-NMR spectra of the investigated loop at 275.2 K and pH 7.2, recorded with the TOCSY (black) and NOESY (red) methods. The TOCSY spectrum shows couplings through bonds, whereas the NOESY spectrum reveals couplings through space, i.e., spatial proximity. The latter of course usually indicates also couplings between bond-connected protons, as they are intrinsically spatially near. The intensity of the NOESY cross peaks decreases with the sixth power of the distance. At the axes, the

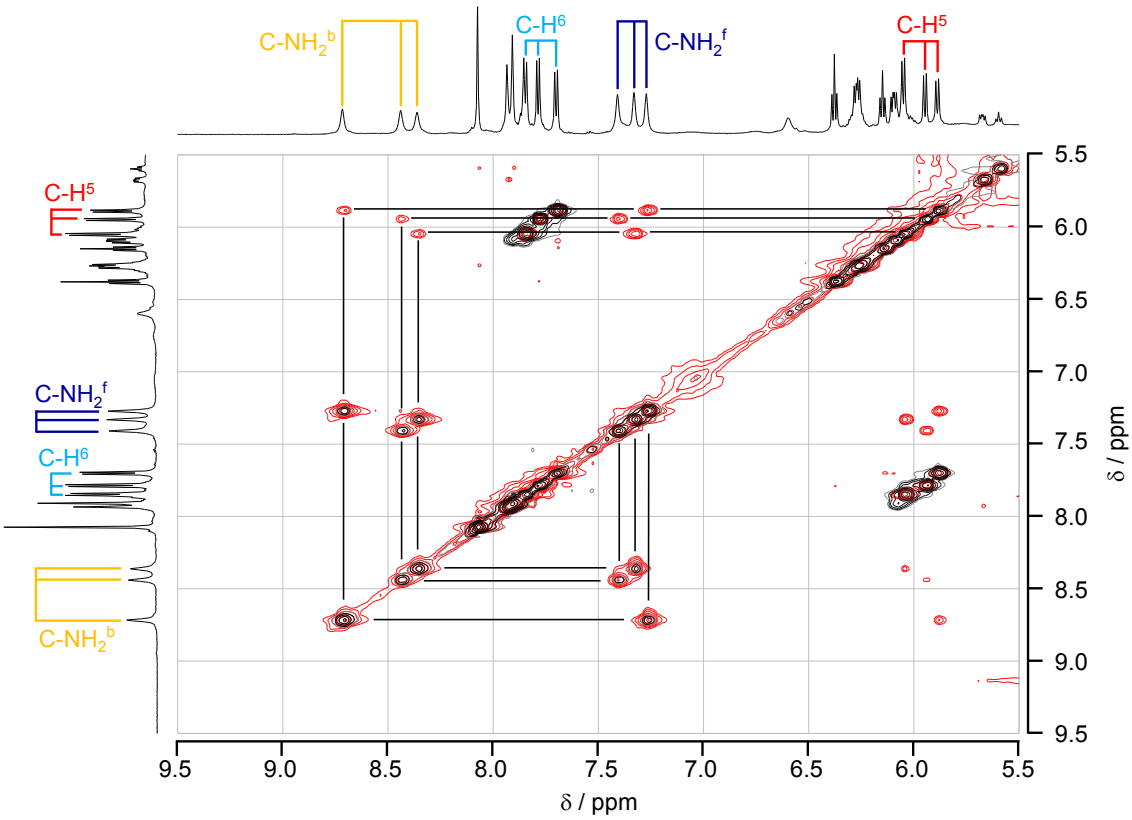

Fig. 6.3: Overlayed 2D-^{1}H-NMR spectra of d[5'-GpGpGp-HEG-pCpCpC-3'] (275.2 K, 1 µM in 90% H_2O/10% D_2O, pH 7.2), recorded with the TOCSY (black) and NOESY (red) method. The spectra are shown from 5.5 to 9.5 ppm on both axes. The coloured lines and labels help identify the protons mentioned in the text (see also Figure 6.2), the thin black lines are drawn to mark the proton coupling through bonds (TOCSY, black) and space (NOESY, red).

^{1}H-NMR spectrum is displayed, coloured lines and labels guide the eye to the hydrogen atoms of special interest in the respective case.

In Figure 6.3, the area of couplings between cytidine amino and ring protons has been amplified. Firstly, cross peaks in the TOCSY spectrum (black) show which ring and amino hydrogens belong together, i.e., pairs of C-H^5/C-H^6 and C-NH$_2^b$/C-NH$_2^f$ can be spotted. Secondly, cross peaks in the NOESY spectrum (red) allow one to correlate the ring protons and amino protons, which gives three sets of hydrogens which belong to one cytidine, respectively. Thirdly, weak NOESY cross peaks (sometimes mere shoulders of a broader peak) reveal further coupling between the cytidine subunits. From these, the middle cytidine can be distinguished easily, as it exhibits couplings to both other cytidines. The discrimination of top and bottom cytidine is more complicated, but can eventually be achieved by analysing the cross peaks of the ring protons to the deoxyribose moieties (not visible in Figure 6.3, but in the 2D-^{1}H-NMR spectra at pH 7.0). In particular, the *z*-C-H$^{3'}$ proton shows an upfield shift. It is located at the 3' end of the oligonucleotide, where no

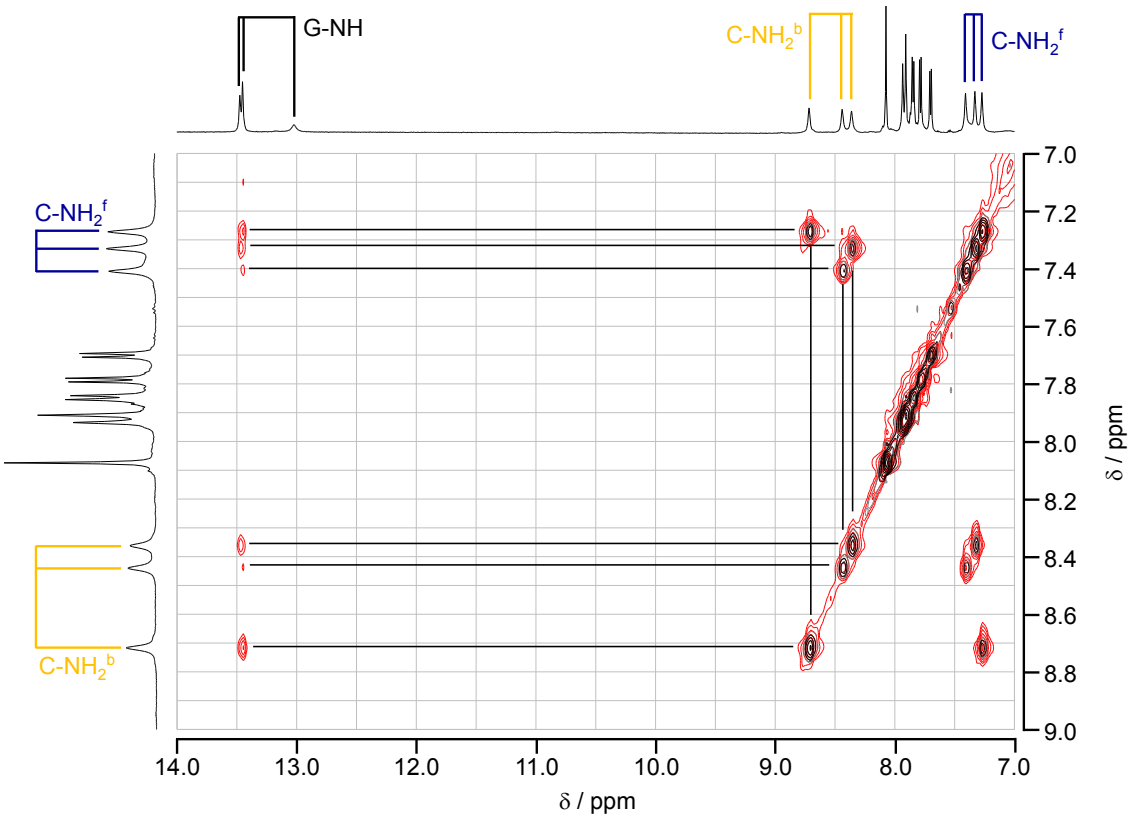

Fig. 6.4: Overlayed 2D-^{1}H-NMR spectra of d[5'-GpGpGp-HEG-pCpCpC-3'] (600 MHz, 275.2 K, 1 µM in 90% H_2O/10% D_2O, pH 7.2), recorded with the TOCSY (black) and NOESY (red) method. The spectra are shown from 7.0 to 14.0 ppm on the abscissa and from 7.0 to 9.0 ppm on the ordinate. The coloured lines and labels help identify the protons mentioned in the text (see also Figure 6.2), the thin black lines are drawn to mark the proton coupling through bonds (TOCSY, black) and space (NOESY, red).

phosphate group is attached. The electron-withdrawing phosphate groups attached to the deoxyribose in 3'- and 5'-position in the sugar-phosphate backbone de-shield the respective sugar-protons and cause a downfield shift for *x*- and *y*-C-H$^{3'}$. The replacement of the 3'-phosphate group with a hydroxy group consequently causes a relative upfield shift for the 'open end' deoxyribose protons. With the same considerations, the guanosine protons and their respective sugar protons could be assigned. At the 5'-end of the oligonucleotide, the *z*-G-H$^{5'}$ protons also show a strong upfield shift due to the lacking 5'-phosphate group.

In Figure 6.4, the main interest lies in the NOESY cross peaks between the G-NH and both C-NH_2 protons, which originate from spatial proximity ensured by a stable hydrogen bond between G and C. The *z*-G-NH exhibits only a very weak (though existing) coupling to its cytidine counterpart, which cannot be seen at the displayed amplification. This indicates a rather weak hydrogen bond between the base pair at the open end of the loop, as may be expected due to the highest flexibility there. The top and middle base pair also

show couplings to the cytidine next to their respective hydrogen bonding partner.

As mentioned above, the 2D-^{1}H-NMR spectra strongly suggest a B-DNA like double helix. Several observations support this surmise. The B-helical form of a DNA strand (be it paired or unpaired) constitutes of nucleobases describing a right-handed ascending curve, with an interbase distance of 0.34 nm and an intrabase angle of 36°. This leads inevitably to an asymmetric coupling pattern. As the nucleobases are horizontally displaced, the proton distances and therefore NOE intensities depend on the direction of the helical turn. As an example, in the 2D-^{1}H-NOESY spectrum cross peaks between z-C-H^6/y-C-H$^{2'}$ and y-C-H^6/x-C-H$^{2'}$ could be observed, while y-C-H^6/z-C-H$^{2'}$ and x-C-H^6/y-C-H$^{2'}$ cross peaks are missing. Considering the 3D structure and therefore the distances between the involved protons, this agrees perfectly with the assumed B-DNA helix. An illustration of the sterical reasons for the observed coupling pattern is given in Figure 6.5. The displayed B-DNA helical structure of the d(C)$_3$ trimer-'arm' of the oligonucleotide loop shows unambiguously the asymmetric distances between C-H^6 atoms (depicted in yellow) and C-H$^{2'}$ hydrogens (shown in green), which result from the right-handedness of the helix. Observed 2D-^{1}H-NOESY couplings are denoted with solid arrows, missing coupling peaks are indicated by dotted arrows. Similar patterns were found for the guanosine nucleobase sequence. Unfortunately, the NOE couplings were too scarce and too weak to calculate the structure from the cross peak intensities. Nevertheless, the qualitative analysis is rather certain.

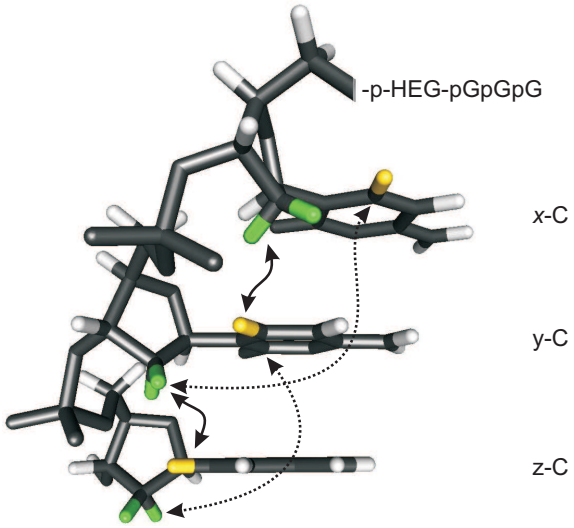

Fig. 6.5: B-DNA structure of the d(C)$_3$ trimer-'arm' of the oligonucleotide loop. C-H^6 atoms are depicted in yellow, C-H$^{2'}$ protons in green. The remaining hydrogen atoms are shown in light gray, all other atoms in dark grey. The occurrence of 2D-^{1}H-NOESY cross peaks between ribose and cytosine protons is asymmetric, due to the sterical implications of the B-DNA helical form. The arrows denote observed (solid lines) and missing (dotted lines) 2D-^{1}H-NOESY cross peaks.

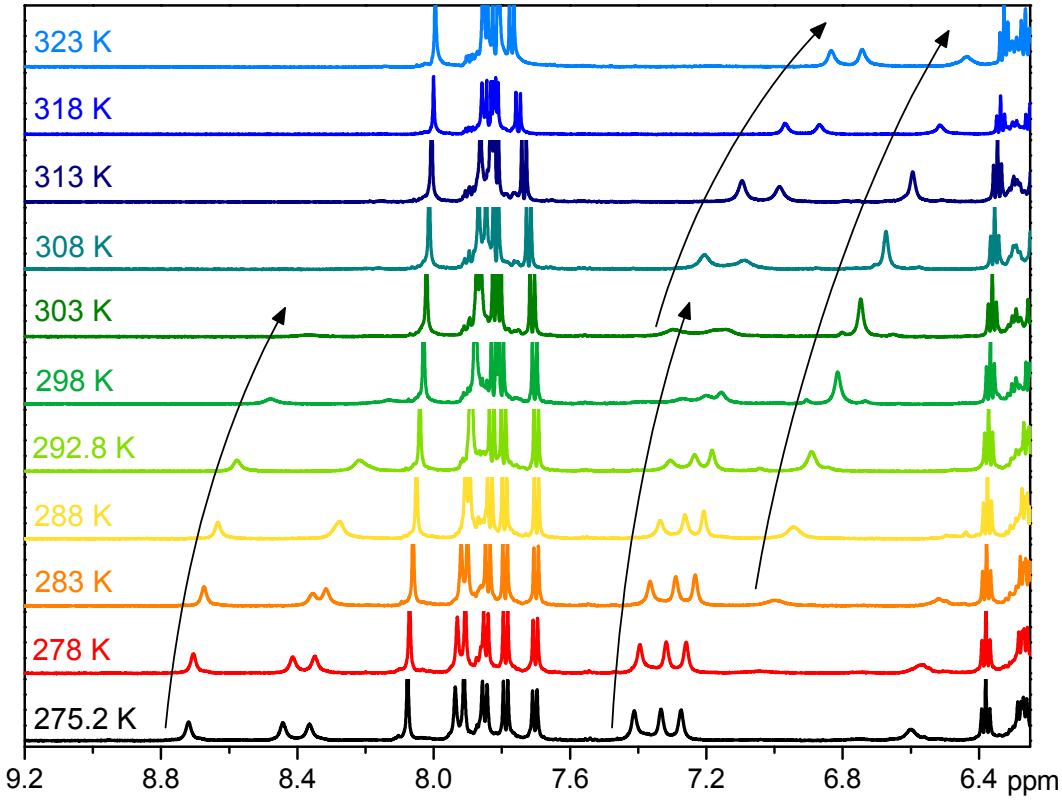

Fig. 6.6: Temperature-dependent ^{1}H-NMR spectra of d[5'-GpGpGp-HEG-pCpCpC-3'] (600 MHz, 275.2 K, 1 µM in 90% H_2O/10% D_2O, pH 7.2). The arrows are drawn to guide the eye to the upfield shift and vanishing splitting of the cytidine amino protons due to decreasing base pairing with rising temperature and flexibility.

Additionally to the above discussed NMR spectra near the solvent freezing point, a series of temperature-dependent ^{1}H-NMR spectra at pH 7.2 have been recorded to monitor the increasing flexibility of the oligonucleotide strand. The region from 9.0 to 6.25 ppm at eleven different temperatures is shown in Figure 6.6. The main focus in the displayed region lies on the shift and vanishing splitting of the cytidine amino protons. At low temperatures, the loop is quite frozen in a B-DNA helical form, as described above. With increasing temperature, however, the overall strand flexibility increases and the two oligonucleotide 'arms' eventually open up. This behaviour is reflected by the gradual upfield shift of both the bound (C-NH_2^b, $\delta \approx 8.7 - 8.4$ ppm) and unbound (C-NH_2^f, $\delta \approx 7.4 - 7.3$ ppm) cytidine amino proton. When the hydrogen bonds break due to the melting of the double helix form, only three peaks can be observed for the three cytidine amino groups. When the amino group is not engaged in a hydrogen bond, it can rotate freely - the two amino hydrogen atoms are no longer different, but chemically equivalent and thus have the same chemical shift. The melting process or 'opening up' of the loop is gradually. At ambient temperature (around 20 °C), where all other experiments where carried out, a notable amount of loop molecules is already open. But the temperature-dependent spectra let us safely conclude that there still are sufficient molecules paired, even if they are rather

flexible and likely to move quite freely. In fact, their amount may even be underestimated by looking at the ^{1}H-NMR spectrum at 292.8 K, as the bound amino proton signals are broadening with increasing temperature and therefore seem to vanish more quickly as they really do.

6.2.2 Static Absorption, Fluorescence and Circular Dichroism Spectra

In this Section, the static absorption, fluorescence and circular dichroism spectra of $d(G)_3$-HEG-$d(C)_3$ are shown and compared to those of the respective nucleotides dGMP and dCMP and the nucleotide trimers $d(G)_3$ and $d(C)_3$. All samples were dissolved in aqueous phosphate buffer (pH 7.0). The static spectra were recorded as described in Chapter 2.

Static Absorption Spectra

In Figure 6.7a, the static UV/vis absorption spectra of the oligonucleotide loop (green) and its constituent nucleotide-trimers $d(G)_3$ (grey) and $d(C)_3$ (dark grey) are shown, as well as the sum of the two latter (black). For the sum spectrum, the respective trimer concentrations of the sample solutions were considered, to ensure comparability with the $d(G)_3$-HEG-$d(C)_3$ loop. For comparison, the static absorption of the mononucleotides dGMP (grey) and dCMP (dark grey) is given by dotted lines. All absorption spectra are normalised at $\lambda = 260$ nm, which is the excitation wavelength in the static and time-resolved emission experiments.

It is immediately obvious that the absorption spectrum of the loop differs from the sum of $d(G)_3$ and $d(C)_3$. In particular, a hypochromism around 275 nm is clearly visible. The gradual decrease of the hypochromism with increasing temperature can be followed in the temperature-dependent absorption spectra in Figure 6.7b, which are taken from the Thesis of Nina K. Schwalb.[28] Upon heating, the oligonucleotide gains flexibility which eventually leads to the breakup of the base-paired double helix. Accordingly, the absorption spectrum at 75 °C and higher temperatures is consistent with the sum spectrum of $d(G)_3$ and $d(C)_3$. In the small insets in Figure 6.7b, melting curves for two different absorption wavelengths are shown. Although the melting curves are rather smeared out and a melting temperature cannot be precisely determined, it lies below 50 °C. This implicates as well as the temperature-dependent ^{1}H-NMR spectra a substantial amount of paired loop at room temperature.

The comparison of the absorption spectra of the nucleotide trimers $d(G)_3$ and $d(C)_3$ with those of their respective monomers dGMP and dCMP shows hypochromism due to π-stacking of the three adjacent nucleobases in the wavelength range $\lambda_{abs} = 265 - 290$ nm in both cases. This underlines the importance of comparing the spectroscopic properties of the oligonucleotide loop with those of its constituent trimers to account for base stacking interactions within the trimer-'arms'.

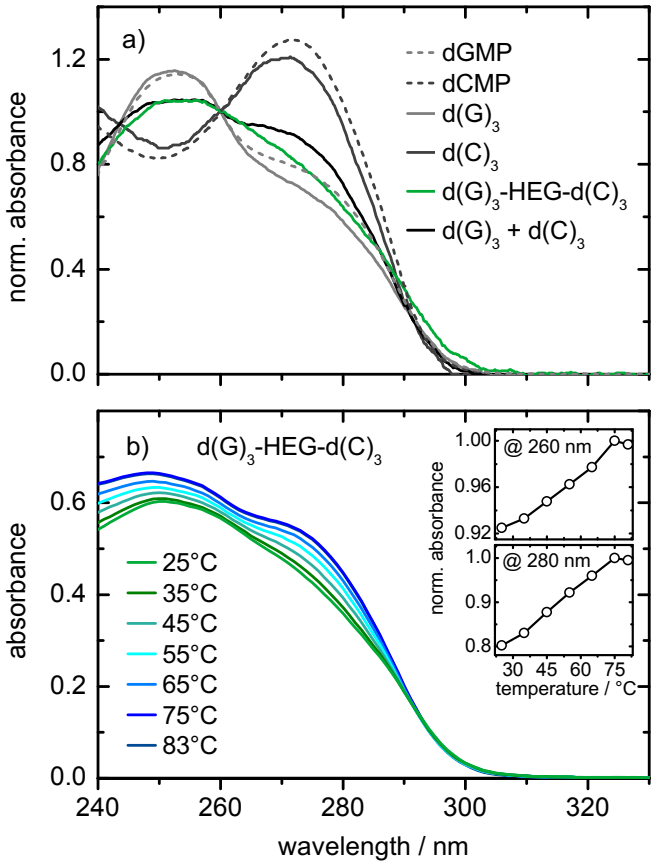

Fig. 6.7: a) Static absorption spectra of the oligonucleotide loop $d(G)_3$-HEG-$d(C)_3$ (green) and its constituent nucleotide-trimers $d(G)_3$ (grey) and $d(C)_3$ (dark grey). The sum of the two latter is denoted by the black solid line. The respective spectra of the mononucleotides dGMP (grey) and dCMP (dark grey) are given by dotted lines. The absorbance was normalised at λ = 260 nm. b) Temperature-dependent absorption spectra of $d(G)_3$-HEG-$d(C)_3$.[28] The insets show melting curves at the two absorption wavelength λ = 260 nm and λ = 280 nm.

Static Fluorescence and Circular Dichroism Spectra

The static fluorescence and circular dichroism spectra shown in Figure 6.8 are taken from the Thesis of Nina K. Schwalb.[28] In Figure 6.8a, static emission spectra after excitation with λ = 260 nm of the oligonucleotide loop $d(G)_3$-HEG-$d(C)_3$ (green) and its constituent nucleotide-trimers $d(G)_3$ (grey) and $d(C)_3$ (dark grey) in aqueous buffer solution are shown. They exhibit quite different shapes, as may be expected for molecules with rather different excited-state geometries. It is evident that the loop emission spectrum cannot be described as a sum of the constituent nucleobase trimers.

The circular dichroism spectra of a 0.01 mM loop solution (green) compared to a 0.02 mM solution of a $d(G)_{10}$·$d(C)_{10}$ B-DNA double helix (black) shown in Figure 6.8b are similar to each other. They both show a clear B-DNA signature, which is characterised by a negative contribution around 245 nm and a positive band around 275 nm.[29] We can

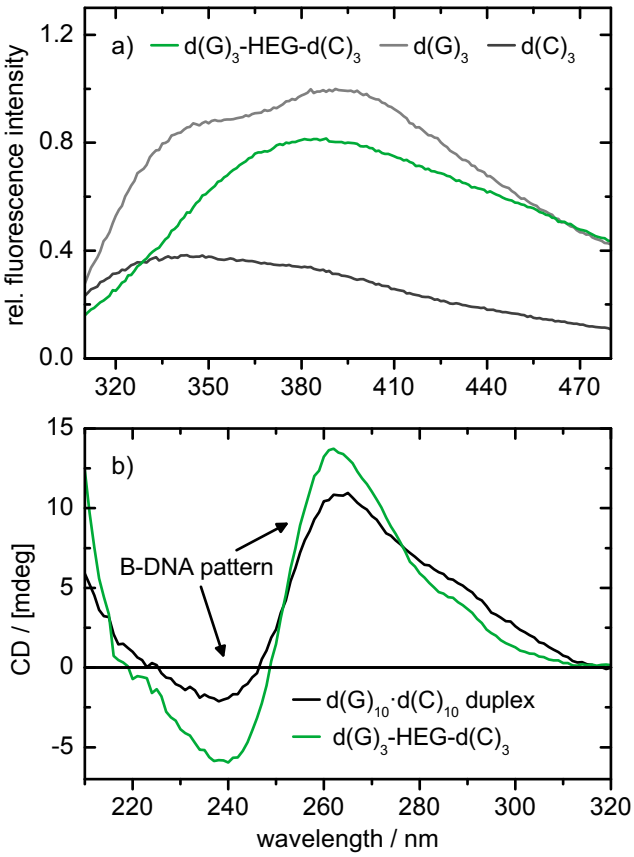

Fig. 6.8: a) Static fluorescence spectra after excitation with $\lambda = 260$ nm of the oligonucleotide loop $d(G)_3$-HEG-$d(C)_3$ (green) and its constituent nucleotide-trimers $d(G)_3$ (grey) and $d(C)_3$ (dark grey) in aqueous buffer solution.[28] b) Circular dichroism spectra of $d(G)_3$-HEG-$d(C)_3$ (green) and a $d(G)_{10}{\cdot}d(C)_{10}$ B-DNA double helix in aqueous buffer solution taken from reference[28].

therefore conclude also from CD spectroscopy that the $d(G)_3$-HEG-$d(C)_3$ oligonucleotide adopts a stable B-DNA helical form, apparently even more stable than the short decameric G·C double helix, as may be deduced from the circular dichroism intensities.

6.2.3 Molecular Mechanics Simulations

As has been observed by a number of different spectroscopic techniques, the investigated oligonucleotide d[5'-GpGpGp-HEG-pCpCpC-3'] forms a B-DNA like double helix, which is stable at room temperature, albeit quite flexible. As this molecule is comparatively small, it is accessible to theoretical investigations. Preliminary molecular dynamics simulations in water at 300 K were performed by Mats Eriksson in the group of Prof. Dr. B. Hartke (Institute of Physical Chemistry, CAU Kiel).[30] He investigated a series of oligonucleotide loops d[5'-GpGpG-$(C_2H_4O)_x$-CpCpC-3'] with varying linker length (x = 4, 5, 6, 7), but lacking the two phosphate groups adjacent to the ethylene glycol linker. The results showed

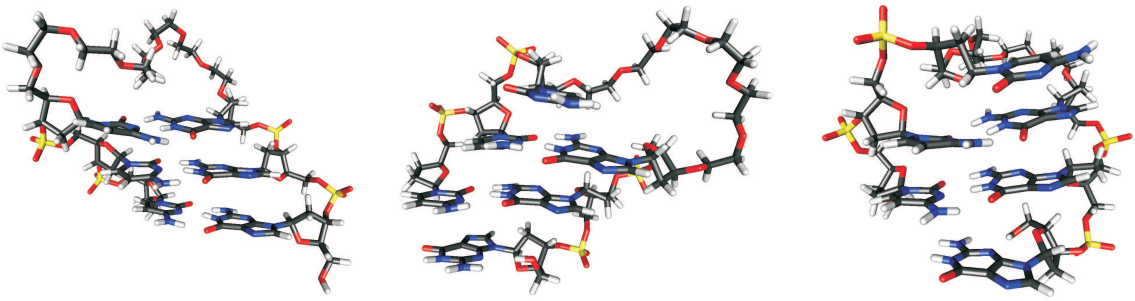

Fig. 6.9: Snapshots of the molecular dynamics calculations of three different d[5'-GpGpG-$(C_2H_4O)_x$-CpCpC-3'] loops in water at 300 K. The water molecules have been omitted for clarity. Left: Base paired x = 7 structure with only minor tilting of the nucleobase chromophores. Center: 'Register shifted' x = 6 loop, the spacer is still flexible. Right: 'Register shifted' x= 4 system, the HEG linker is quite constrained and bent behind the G·C base stack.

the molecule to stay mainly in the B-DNA structure at least for the simulation time up to 12 ns. However, the adopted B-DNA helix structure is slightly distorted compared to the textbook values of 36° turn per base pair and 0.34 nm interbase distance, namely it exhibits a $\approx 27°$ turn and ≈ 0.41 nm distance for the d[5'-GpGpG-$(C_2H_4O)_6$-CpCpC-3'] molecule. Another interesting observation was the forming of a hydrogen-bonded double strand with a 'register shift' in some of the trajectories (see Figure 6.9). In this mismatched structure, only two base pairs are hydrogen bonded (y-G with z-C and x-G with y-C), whereas z-G and x-C are free. The linker length has a high influence on the correct base pairing geometry as it pre-orientates the two trimer-'arms'. For the x = 7 bridged loop mostly the completely hydrogen bonded structure was observed, although the base pair at the open end is quite flexible and did break and re-form repeatedly in the simulation trajectories. The 'register shift' geometry observed in the x = 6 system may already be a hint that the system becomes unstable with a linker length shorter than $18 - 20$ atoms, although this loop also was mostly in the 'designed' base pairing geometry during the simulation time. Loosening and breaking of the initial three base pairs is supposedly initiated by the movement of the linker 'behind' the base stack, as if it is too constrained when positioned like a handle. The shorter-bridged $x = 4, 5$ structures exhibit predominantly mismatched, 'register shifted' structures with the linker 'behind' the base stack and competing with the x-base pair for the same space. Base tilting fluctuations have been observed for all systems, as expected for this small oligonucleotide at room temperature.

Altogether, the performed molecular mechanics simulations provide a valuable tool for estimating the influence of the linker system on the stability of the paired loop. It has to be noted that the chain length of the mostly stable x = 7 system closely resembles the experimentally investigated $d(G)_3$-HEG-$d(C)_3$ because of the additional phosphate groups in the structure of the latter. It is therefore unlikely that the 'register shift' plays a role in the presented static and femtosecond time-resolved measurements, but for different loop systems with shorter chain lengths it may need to be considered. In these cases, the

^{1}H-NMR spectra should feature additionally 'free' C-NH_2 and G-NH protons from the unbound *z*-G and *x*-C, which would show a considerable upfield shift compared to the respective protons engaged in a hydrogen bond. In the case of d(G)$_3$-HEG-d(C)$_3$, no hint for the presence of the mismatched structure was observed *via* ^{1}H-NMR spectroscopy.

6.3 Femtosecond Time-Resolved Spectroscopy

Fluorescence-time profiles after excitation with $\lambda_{\text{pump}} = 260$ nm at the emission wavelength $\lambda_{\text{fl}} = 350$ nm have been recorded for the nucleotide dGMP, the trimers d(G)$_3$ and d(C)$_3$ and their equimolar mixture, the decamers d(G)$_{10}$ and d(C)$_{10}$ and their equimolar mixture, and the oligonucleotide loop d(G)$_3$-HEG-d(C)$_3$. All measurements were performed with several batches and repeated $2-3$ times on the same sample solution to ensure reproducibility and to check that no photo-induced damage had taken place during the measurement. The experimental setup of the fluorescence up-conversion as well as the fitting of the time profiles is described in Chapter 2.

6.3.1 Results

In Figure 6.10, fluorescence-time profiles of the oligonucleotide loop d(G)$_3$-HEG-d(C)$_3$ (green) and its constituent nucleotide-trimers d(G)$_3$ (grey) and d(C)$_3$ (dark grey) in aqueous buffer solution are shown, together with the overall fit functions, whose decay constants are given in Table 6.1. It can clearly be seen that the loop leaves the optically bright state faster than its constituent nucleobase trimers. This effect must be due to base pairing, as the equimolar mixture of d(G)$_3$ and d(C)$_3$ shows exactly the same temporal behaviour as the mathematical sum (weighted by the extinction coefficient) of the d(G)$_3$- and d(C)$_3$-transients. This is in agreement with the assumption that the trimers cannot pair in aqueous solution because the strands are too short and the complex forming with water is preferred. Only the pre-orientation induced by the linker enables nucleobase pairing of the oligonucleotide loop. In Figure 6.11, the fluorescence-time profile of the (d(G)$_3$+d(C)$_3$) equimolar mixture is shown and compared with the corresponding time-profile of the loop. The faster fluorescence decay of d(G)$_3$-HEG-d(C)$_3$ is again clearly observable. It has to be noted that at the excitation wavelength $\lambda_{\text{pump}} = 260$ nm the extinction coefficient of d(G)$_3$ is higher than that of d(C)$_3$, so that d(G)$_3$ absorbs $\approx 60\%$ of the initial excitation light. Accordingly, the temporal behaviour of the (d(G)$_3$+d(C)$_3$) mixture rather resembles that of d(G)$_3$.

The fitted time constants and relative amplitudes for all investigated molecules can be found in Table 6.1. The absolute values of the decay times do not have an immediate physical meaning and are hard to compare. Therefore, the amplitude weighted average time constants $\langle\tau\rangle$ have been calculated, which describe the overall deactivation dynamics. They give a good impression on how fast the excited molecule leaves the initially excited

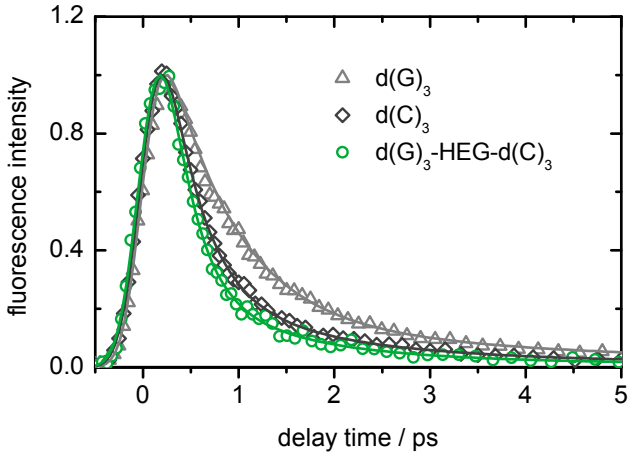

Fig. 6.10: Fluorescence-time profiles of the oligonucleotide loop $d(G)_3$-HEG-$d(C)_3$ (green) and its constituent nucleotide-trimers $d(G)_3$ (grey) and $d(C)_3$ (dark grey) in aqueous buffer solution at $\lambda_{fl} = 350$ nm after excitation with $\lambda_{pump} = 260$ nm. Symbols represent the data points, solid lines the overall fit functions, whose decay constants are given in Table 6.1.

optically bright state. The $\langle\tau\rangle$ values confirm that the emission of the $d(G)_3$-HEG-$d(C)_3$ loop deactivates fastest, as the qualitative examination of the fluorescence-time profiles already suggested.

	$\langle\tau\rangle$ / ps
dGMP	0.64±0.15
$d(G)_3$	1.14±0.01
$d(G)_{10}$	7.62±0.04
$d(C)_3$	0.65±0.05
$d(C)_{10}$	0.70±0.06
$(d(G)_3+d(C)_3)$	0.95±0.21
$d(G)_{10}\cdot d(C)_{10}$	2.87±0.06
loop	0.53±0.03

When comparing the deactivation times of the guanosine monomer and its trimer and decamer, the increase of lifetime is obvious. This is even better observed in the fluorescence-time profiles, which are shown in Figure 6.12. Evidently, the increasing number of G units leads to a much longer excited-state lifetime. There are two possible explanations for this effect. Firstly, the π-systems of neighbouring purine bases overlap to a considerable extent, thus forming long-lived excited states (compare also the adenine dinucleotide in Chapters 3 and 3, as well as the adenine-guanine hetero-dinucleotide in Chapter 5). In the case of the cytosine series this effect cannot be observed, presumably the π-systems of pyrimidine bases overlap to a lesser extent. Secondly, G-rich DNA strands have a tendency to form non-canonical four-stranded structures, so-called G-quadruplexes.[31] We cannot

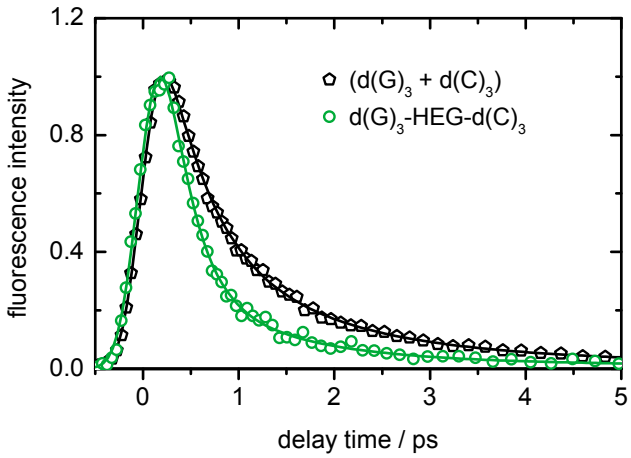

Fig. 6.11: Fluorescence-time profiles of $d(G)_3$-HEG-$d(C)_3$ (green) and an equimolar mixture of $d(G)_3$ and $d(C)_3$ (black) in aqueous buffer solution at $\lambda_{fl} = 350$ nm after excitation with $\lambda_{pump} = 260$ nm together with the overall fit functions, whose decay constants are given in Table 6.1.

be sure, whether the guanosine decamer exists in solution in a B-DNA single-stranded helical form, or if a more complex superstructure is formed. The electronically excited states and deactivation pathways may differ considerably for single-strand helix and G-quadruplex structure, which in turn might inhibit the comparability of dGMP, $d(G)_3$ and $d(G)_{10}$. This observation again emphasises the necessity for a model system which can mimic very short oligonucleotide duplexes, so as not to mix the effects of nucleobase pairing and π-stacking on the excited-state dynamics. The shortest possible duplex formed by 'free' oligonucleotides without linker consists of decamers, which obviously already exhibit a large amount of π-stacking, and in the case of guanine-rich sequences the possibility of G-quadruplex forming.

Table 6.1: Decay constants τ_i in ps and their relative amplitudes A_i fitted to the fluorescence-time profiles of the investigated molecules in aqueous buffer solution at $\lambda_{fl} = 350$ nm after excitation with $\lambda_{pump} = 260$ nm. The errors correspond to the 2σ standard deviation.

	τ_1 / ps	A_1	τ_2 / ps	A_2	τ_3 / ps	A_3
dGMP	0.53±0.08	0.94±0.08	2.3±1.9	0.06±0.07		
$d(G)_3$	0.71±0.02	0.87±0.02	4.1±0.4	0.13±0.02		
$d(G)_{10}$	0.71±0.02	0.30±0.02	4.1±0.4	0.28±0.03	15.0±0.7	0.42±0.03
$d(C)_3$	0.35±0.03	0.81±0.04	1.2±0.3	0.16±0.04	5.9±2.5	0.03±0.02
$d(C)_{10}$	0.35±0.03	0.74±0.06	1.2±0.3	0.23±0.05	5.9±2.5	0.03±0.02
$(d(G)_3+d(C)_3)$	0.45±0.09	0.65±0.14	1.3±0.5	0.32±0.13	6.3±3.7	0.04±0.04
$d(G)_{10}\cdot d(C)_{10}$	0.47±0.03	0.67±0.02	2.9±0.7	0.19±0.02	14.5±1.9	0.14±0.02
loop	0.27±0.02	0.81±0.03	1.1±0.2	0.17±0.03	6.7±2.4	0.02±0.01

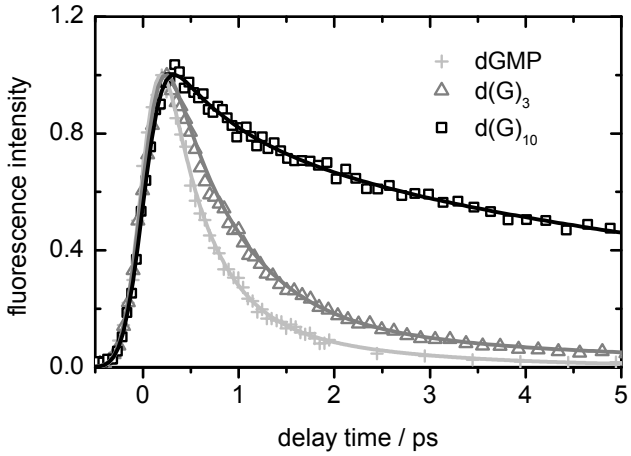

Fig. 6.12: Fluorescence-time profiles of dGMP (light grey), $d(G)_3$ (grey), and $d(G)_{10}$ (black) in aqueous buffer solution at the emission wavelength $\lambda_{fl} = 350$ nm after excitation with $\lambda_{pump} = 260$ nm. Symbols represent the data points, solid lines the overall fit functions, whose decay constants are given in Table 6.1.

6.3.2 Discussion

The femtosecond time-resolved emission experiments after excitation with $\lambda_{pump} = 260$ nm confirmed that the initially excited optically bright excited states of the hydrogen bonded system depopulate very rapidly, even faster than those of the constituent nucleotide trimers. A similar effect was observed for the Watson-Crick paired G·C base pair in $CHCl_3$ by Schwalb *et al.*[1,2] They observed a 'pure' G·C deactivation time of the optically bright states of $\tau = 0.30 \pm 0.03$ ps.[2] However, transient absorption spectroscopy results by K. Röttger in our group on G·C in $CHCl_3$ revealed that the base pair does not return directly to the ground state, but that most likely optically dark (charge transfer) states are populated.[32] $CHCl_3$ as a solvent has of course different properties than water, so the systems and especially the involved dark excited electronic states cannot be equalised.

Preliminary transient absorption measurements on the self-complementary loop in aqueous solution gave in fact no hints to the presence of long-lived states. In Figure 6.13, absorption-time profiles at $\lambda_{abs} = 400$ nm and $\lambda_{abs} = 245$ nm after excitation with $\lambda_{pump} = 260$ nm of $d(G)_3$-HEG-$d(C)_3$ and an equimolar mixture of $d(G)_3$ and $d(C)_3$ are shown.[32] From the ground state recovery (GSR) measurement at $\lambda_{abs} = 245$ nm, we may safely conclude that no long-lived, optically dark states are populated after leaving the initially excited optically bright states. The hydrogen-bonded hairpin returns to the electronic ground state quite fast, with a time constant of $\tau \approx 5$ ps. In contrast, the initial ground state bleach of the equimolar mixture ($d(G)_3$+$d(C)_3$) is refilled with $\tau \approx 12$ ps. The positive excited-state absorption monitored at $\lambda_{abs} = 400$ nm decays biexponentially. A contribution with $\tau \approx 1$ ps was observed in both cases, additionally to the respective time constants from the GSR measurements. The relative amplitude of the

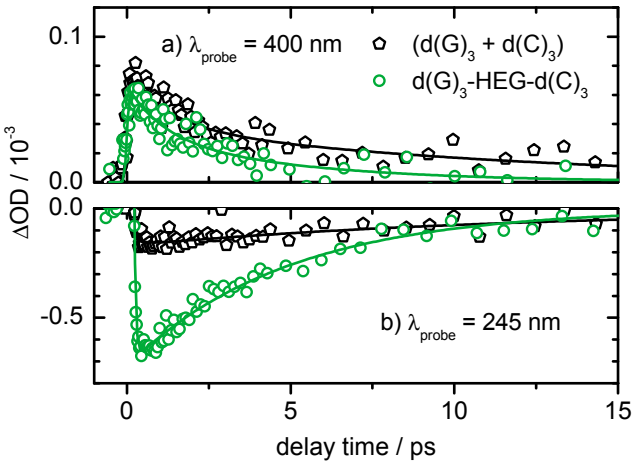

Fig. 6.13: Absorption-time profiles of $d(G)_3$-HEG-$d(C)_3$ (green) and an equimolar mixture of $d(G)_3$ and $d(C)_3$ (black) in aqueous buffer solution at the absorption wavelengths a) $\lambda_{abs} = 400$ nm and b) $\lambda_{abs} = 245$ nm after excitation with $\lambda_{pump} = 260$ nm.[32] Symbols represent the data points, solid lines the overall fit functions.

picosecond component was $\approx 50\%$, respectively, and corresponds to τ_2 derived from the fluorescence-time profiles.

Theoretical investigations by Sobolewski and Domcke yielded an explanation for the fast deactivation dynamics in a hydrogen bonded base pair.[33,34] They found an electron-transfer from the photo-excited guanosine to its cytosine counterpart, directly followed by a proton transfer from G to C. The minimum energy pathway on the excited-state surface leads barrierless to a conical intersection with the ground state *via* a coupled electron-proton transfer. In the ground state, the initial Watson-Crick structure is restored. In contrast, Biemann *et al.* concluded from transient absorption measurements of the G·C Watson-Crick base pair in $CHCl_3$ combined with a TD-DFT study, that no proton transfer between the pairing nucleosides takes place.[35] However, this is probably due to the fact that they excited the sample solution with $\lambda_{pump} = 284$ nm, where mainly the cytosine absorbs. Accordingly, the proton transfer which stems from the photo-excited guanosine may very well not be observable with the used excitation wavelength.

6.4 Conclusion

In summary, it can be stated that the presented short oligonucleotide loop is an excellent model for short DNA double strands. Even at ambient temperatures it forms a stable double helix, which allows for the investigations of hydrogen bonded Watson-Crick base pairs in aqueous solution. Transient absorption spectroscopy results indicate that no long-lived dark states are involved in the relaxation pathway, but rather that the base-paired short strand returns to the ground state faster than its constituent single strands.[32] This result and the time-resolved fluorescence measurements presented in this Chapter are in

good agreement with a theoretical model which involves a coupled electron-proton transfer in the G·C Watson-Crick base pair, thus allowing for very fast excited-state dynamics.[33,34]

References

[1] N. K. Schwalb, F. Temps, *J. Am. Chem. Soc.* **129**, 9272 (2007).

[2] N. K. Schwalb, T. Michalak, F. Temps, *J. Phys. Chem. B* **113**, 16365 (2009).

[3] J. L. Leroy, M. Kochoyan, H. D. Tam, M. Gueron, *J. Mol. Biol.* **200**, 223 (1988).

[4] T. Gelot, P. Touron-Touceda, O. Cregut, J. Leonard, S. Haacke, *J. Phys. Chem. A* **116**, 2819 (2012).

[5] T. Heinlein, J.-P. Knemeyer, O. Piestert, M. Sauer, *J. Phys. Chem. B* **107**, 7957 (2003).

[6] J. Jung, A. Van Orden, *J. Am. Chem. Soc.* **128**, 1240 (2006).

[7] M. M. Lin, L. Meinhold, D. Shorokhov, A. H. Zewail, *Phys. Chem. Chem. Phys.* **10**, 4227 (2008).

[8] K. Siegmund, P. Daublain, Q. Wang, A. Trifonov, T. Fiebig, F. D. Lewis, *J. Phys. Chem. B* **113**, 16276 (2009).

[9] G. S. Blaustein, F. D. Lewis, A. L. Burin, *J. Phys. Chem. B* **114**, 6732 (2010).

[10] F. C. Grozema, S. Tonzani, Y. A. Berlin, G. C. Schatz, L. D. A. Siebbeles, M. A. Ratner, *J. Am. Chem. Soc.* **130**, 5157 (2008).

[11] F. C. Grozema, S. Tonzani, Y. A. Berlin, G. C. Schatz, L. D. A. Siebbeles, M. A. Ratner, *J. Am. Chem. Soc.* **131**, 14204 (2009).

[12] F. D. Lewis, Y. Wu, X. Liu, *J. Am. Chem. Soc.* **124**, 12165 (2002).

[13] K. Siegmund, M. Hariharan, F. D. Lewis, *J. Phys. Chem. B* **115**, 3740 (2011).

[14] J. Tuma, S. Tonzani, G. C. Schatz, A. H. Karaba, F. D. Lewis, *J. Phys. Chem. B* **111**, 13101 (2007).

[15] F. D. Lewis, R. S. Kalgutkar, Y. Wu, X. Liu, J. Liu, R. T. Hayes, S. E. Miller, M. R. Wasielewski, *J. Am. Chem. Soc.* **122**, 12346 (2000).

[16] R. Carmieli, T. A. Zeidan, R. F. Kelley, Q. Mi, F. D. Lewis, M. R. Wasielewski, *J. Phys. Chem. A* **113**, 4691 (2009).

[17] M. Wenninger, D. Fazio, U. Megerle, C. Trindler, S. Schiesser, E. Riedle, T. Carell, *Chem. Bio. Chem.* **12**, 703 (2011).

[18] S. Altmann, A. M. Labhardt, D. Bur, C. Lehmann, W. Bannwarth, M. Billeter, K. Wuethrich, W. Leupin, *Nucleic Acids Res.* **23**, 4827 (1995).

[19] J. P. Bartley, T. Brown, A. N. Lane, *Biochemistry* **36**, 14502 (1997).

[20] L. Kozerski, A. P. Mazurek, R. Kawecki, W. Bocian, P. Krajewski, E. Bednarek, J. Sitkowski, M. P. Williamson, A. J. G. Moir, P. E. Hansen, *Nucleic Acids Res.* **29**, 1132 (2001).

[21] N. K. Schwalb, F. Temps, *Science* **322**, 243 (2008).

[22] C. E. Crespo-Hernández, K. de La Harpe, B. Kohler, *J. Am. Chem. Soc.* **130**, 10844 (2008).

[23] K. de La Harpe, C. E. Crespo-Hernández, B. Kohler, *ChemPhysChem* **10**, 1421 (2009).

[24] C. E. Crespo-Hernández, B. Cohen, B. Kohler, *Nature* **436**, 1141 (2005).

[25] D. Markovitsi, F. Talbot, T. Gustavsson, D. Onidas, E. Lazzarotto, S. Marguet, *Nature* **441**, E7 (2006).

[26] C. E. Crespo-Hernández, B. Cohen, B. Kohler, *Nature* **441**, E8 (2006).

[27] T. Zeleny, M. Ruckenbauer, A. J. A. Aquino, T. Muller, F. Lankas, T. Drsata, W. L. Hase, D. Nachtigallova, H. Lischka, *J. Am. Chem. Soc.* **134**, 13662 (2012).

[28] N. K. Schwalb, Ultrafast Electronic Deactivation Dynamics in DNA Model Systems by Femtosecond UV Fluorescence Spectroscopy, Ph.D. Thesis, Christian-Albrechts-Universität zu Kiel (2009).

[29] I. T. Victor A. Bloomfield, Donald M. Crothers, *Nucleic Acids: Structures, Properties, and Functions* (University Science Books, 2000).

[30] M. Eriksson, *unpublished results* .

[31] J. T. Davis, *Angew. Chem., Int. Ed.* **43**, 668 (2004).

[32] K. Röttger, *unpublished results* .

[33] A. L. Sobolewski, W. Domcke, *Phys. Chem. Chem. Phys.* **6**, 2763 (2004).

[34] A. L. Sobolewski, W. Domcke, C. Hättig, *Proc. Natl. Acad. Sci. U.S.A.* **102**, 17903 (2005).

[35] L. Biemann, S. A. Kovalenko, K. Kleinermanns, R. Mahrwald, M. Markert, R. Improta, *J. Am. Chem. Soc.* **133**, 19664 (2011).

7

Ultrafast Solvation Dynamics of Ferulic Acid in Bulk Aqueous Solution and in a Micellar Environment

Mayra C. Stuhldreier[†], Hendrik Böhnke[†], Michal Malicki[°], Nina K. Schwalb[§], Nevin Öksüz[†], Kathleen Oehlke[‖], Julia Keppler[‡], Karin Schwarz[‡], and Friedrich Temps[†*]

[†]Institute of Physical Chemistry, University of Kiel, Germany
[‡]Institute of Human Nutrition and Food Science, University of Kiel, Germany
[°]Present address: Department of Chemistry, Northwestern University, Evanston, U.S.A.
[§]Present address: Bayer Technology Services GmbH, Leverkusen, Germany
[‖]Present address: Max-Rubner Institute, Karlsruhe, Germany

[*]To whom correspondence should be addressed.
E-mail: temps@phc.uni-kiel.de; Web: http://www.uni-kiel.de/phc/temps

manuscript

Own contributions presented in this paper:

- Femtosecond time-resolved fluorescence up-conversion and Kerr gating spectroscopy
- Static absorption and emission spectroscopy
- Writing of the data analysis software and data analysis of all presented data
- Writing of the publication

Abstract

The solvation dynamics of ferulic acid (FA) in acetate buffered bulk water (pH 5.0) and in a micellar solution of cetyltrimethylammonium bromide (CTAB) in aqueous buffer solution (pH 5.0) have been investigated by means of femtosecond time-resolved fluorescence spectroscopy after photo-excitation at $\lambda = 320$ nm. The solvation processes around photo-excited FA in micellar solution are slower than in bulk water, reflecting the constrained environment and much reduced molecular mobilities around the chromophore at the interfacial layer. The amplitude-weighted time constants have been determined to $\langle\tau_{\mathrm{s,aq}}\rangle = 19 \pm 2$ ps and $\langle\tau_{\mathrm{s,CTAB}}\rangle = 30 \pm 2$ ps. FA leaves the excited state with $\tau_{\mathrm{FL}} = 19 \pm 2$ ps in bulk aqueous solution and $\tau_{\mathrm{FL}} = 33 \pm 7$ ps at the micellar interface. The prolongation of excited-state lifetime might be explained by the involvement of a conical intersection 'on the way' to the $E \rightarrow Z$ isomerisation of the vinylic double bond into the electronic deactivation pathway. The necessary molecular motion to reach this conical intersection is assumed to be slowed down in a constricted environment. Quantum chemical calculations at the TD-DFT level of theory support this assumption, as they found the destination orbital upon UV photo-excitation to feature a node through the vinylic double bond.

7.1 Introduction

To gain insight into the micro-environment of a solute in a restricted environment such as the micellar surface, it is useful to monitor the mobility of the solvent shell surrounding the investigated molecule. This is best done by recording the time dependent Stokes shift of the fluorescence spectrum which derives from the reorganisation of the solvent shell around a molecule whose dipole moment has changed upon electronic excitation. The reorganisation can be monitored by recording the emission spectra shortly after excitation, as these spectra show a time-dependent red-shift according to the stabilisation of the solvated excited molecule.[1] The time that is needed to reach the equilibrium structure of the solvated excited molecule and hence to complete the fluorescence shift is directly related to the mobility of the solvent molecules and therefore to the structure of the micro-environment of the solvated molecule. Two different cases have to be considered: If the solvent dynamics are relatively fast in comparison with the fluorescence lifetime (which is the case for most fluorescence dye molecules), the rearrangement of solvent molecules can be followed easily up to completion and the emission spectrum after finishing the re-solvation matches the static fluorescence. On the other hand, if the fluorescence lifetime is comparable to the time scale of the solvent dynamics, the fluorescence spectra decay in intensity while red-shifting, which makes the complete determination of the solvation dynamics difficult. In the latter case, the static spectrum as the sum of all emitted photons is blue-shifted in comparison with the spectrum which is emitted from the minimum of the potential energy surface (PES) of the solvated excited molecule, as the early transient

spectra contribute significantly to the overall emission.

In pure water, the solvent response is known to be quite fast. For different molecules in aqueous solution, a biexponential decay with $\tau \approx 0.2$ ps and $\tau \approx 1$ ps was experimentally[2–12] and theoretically[13–15] observed. The faster component is assigned to reflect the librational modes of the water molecules, the slower to their diffusive or translational motion. On the other hand, several studies observed that the mobility of water molecules is severely slowed down in various organised environments.[4,5,10,16–21] For example, Vajda *et al.* studied the mobility of water molecules surrounding coumarin dyes inside cyclodextrin cavities as a highly constrained environment.[17] The observed time scales range from < 50 fs to 1.2 ns, whereupon the slower time scales appear only in the restricted environment, not in bulk water. The Levinger group investigated water solvation dynamics inside reverse micelles by fluorescence up-conversion spectroscopy. They could determine the stepwise acceleration of the solvation dynamics with increasing water pool size inside the micelles.[4,20] Additionally, the stronger effect of steric restriction by the micellar environment on the water mobility compared to the deceleration of water molecules 'only' bound to K^+ or Ca^{2+} was revealed.[5] Mitra *et al.* followed the alteration of the solvation dynamics around a hydrated coumarin dye in inverse micelles as function of hydration degree and temperature.[10] They could observe faster solvation dynamics with increasing hydration degree and temperature, along with a simultaneous decrease of rotational restriction and assigned this finding to the higher mobility of 'bulk' water compared to surface-bound water molecules. Others dealt with the water dynamics of a coumarin dye in reverse micelles[18] and in the Stern layer of CTAB micelles.[19] Due to limited time resolution ($\geq$ 20ps) they could not observe fast initial dynamics, but found the respective water solvation dynamics to decay within several ns in the reverse micelles and within a few hundred ps in the aqueous micelles. A remarkable observation by Benderskii *et al.* was the acceleration of water dynamics around a coumarin dye at an air/water interface covered with stearic acid compared to the dynamics at a pure air/water interface.[6] They concluded that the rearrangement and disruption of the hydrogen bonding network of water at a biologically relevant interface allows for the water molecules to move more freely. Kim *et al.* reported hydration dynamics of tryptophan in aqueous nanochannels ($\approx$ 50 Å).[21] They could distinguish three different solvation time scales, for water molecules at the confining lipid interface, the adjacent water layer which is more loosely bound, and finally bulk-like hydration dynamics in the channel center. Their work nicely visualises the complexity of water solvation dynamics in natural systems. The solvation dynamics around large hydrated biomolecules such as DNA double strands is accessible by introducing a 'microsolvation probe' molecule in the double strand, where it replaces a native base pair and can therefore monitor the water mobility inside the DNA double strand.[22,23] Examples are a planar dibenzofuran derivative[23] or a coumarin dye.[22] The latter revealed a continuous fluorescence red-shift up to 40 ns after excitation and the authors concluded that motions of ions, DNA backbone and nucleobases play an important role

in the solvation response.[22]

In the present work, we studied the mobility in the water solvent shell around the cinnamic acid derivative ferulic acid (FA, see Figure 7.1) in both aqueous solution and in the palisade layer of CTAB micelles. Ferulic acid is a weak acid with $pK_a = 4.56$.[24] It is also an natural antioxidant, which acts as radical catcher by being oxidised itself. Especially unsaturated fatty acids are prone to radical oxidation as one of the most important deterioration reactions. An application of the antioxidant ability of FA is its addition to oil-in-water (o/w) emulsions. Emulsions as the surfactant-stabilised form of otherwise immiscible liquids play a major role in, e.g., pharmaceutical formulations and food. The location and mobility of the antioxidant molecule and its surrounding solvation shell within the emulsion system affect its reactivity significantly.[25–29] FA is located directly at the interface of an o/w emulsion stabilised by the emulsifier cetyltrimethylammonium bromide (CTAB, see Figure 7.1), which was observed *via* ^{1}H-NMR spectroscopy.[30] Because the micro-environment of the interface, the so-called palisade layer, of CTAB micelles and CTAB stabilised emulsion droplets is very similar, it is possible to model the o/w interface by CTAB micelles. Consequently, the investigation of molecular mobility and solvent shell characteristics of FA at a water-micelle interface presented in this work is of interest when designing and improving antioxidant-protected o/w emulsion systems.

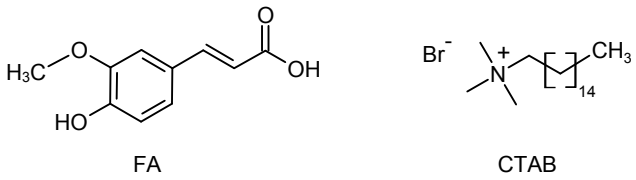

FA CTAB

Fig. 7.1: Chemical structure of ferulic acid (FA, left) and cetyltrimethylammonium bromide (CTAB, right).

In the following, we report on femtosecond time-resolved broadband fluorescence measurements which allow us to follow the dynamic Stokes shift in real time. The results suggest that the steric constraints at the water/micelle interface and the electrostatic interactions with the polar headgroups of the emulsifier alter both the fluorescence lifetime of ferulic acid and the water solvent shell mobility.

7.2 Experimental

The sample solutions of FA in acetic buffer solution (pH = 5.0) and in CTAB micelles in acetic buffer solution (c_{CTAB} = 30 mM, pH = 5.0) were prepared according to Oehlke *et al.*[24] In the following, ferulic acid dissolved in aqueous buffer solution will be denoted as FA/H_2O, ferulic acid in the micellar solution will be referred to as FA/CTAB. The concentration of ferulic acid was adjusted to c_{FA} = 50 μM or c_{FA} = 400 μM in both solutions. Upon the employed emulsifier concentration of 30 mM, at least 83% of the FA

molecules are incorporated in the micelle/water interface.[24] In a former work, Oehlke *et al.* determined the radius of the CTAB micelles, which leads to a maximum number of 120 CTAB molecules per micelle and a micelle concentration of $\geq$ 250 μM in the solution.[31] This value is in good agreement with a study of CTAB aggregation numbers in dependence of salt concentration in the solvent.[32] For c_{FA} = 50 μM, the micelle concentration exceeds the FA concentration at least fivefold. In the c_{FA} = 400 μM case, the FA:micelle ratio is $\leq$ 1.6 : 1. However, as the micelles are large compared to the ferulic acid molecule, and fluorescence-time profiles from single-colour and broadband measurements did not differ visibly, we can safely exclude monitoring of cooperative effects between two or more FA molecules. This is particularly true when ferulic acid exists in its anionic form, due to electrostatic repulsion. The logarithmic acid dissociation constant of FA in aqueous solution was determined by Oehlke *et al.* to $\mathrm{pK_a}$ = 4.56,[24] which is in good agreement with other literature values.[33,34] At a pH value of 5.0, this leads to 73% dissociation of ferulic acid to the respective carboxylate anion form. In the micellar interface, the ratio of carboxylate anion equals the respective value in acetic buffer (72% anion form),[24] we can therefore safely conclude to monitor the same species as well in aqueous environment as at the micellar surface. The second dissociation constant of FA is much higher ($\mathrm{pK_{a,2}}$ = 8.8),[33,34] the formation of the phenolate anion form can therefore be neglected.

Fluorescence Up-Conversion Setup

The experimental setup of the femtosecond time-resolved fluorescence up-conversion spectroscopy in our laboratory has been described previously.[35,36] In short, the respective sample solution was pumped through a flow cell with 1 mm optical path length and the molecules were excited by a pump pulse at λ_{pump} = 321 nm generated by a Ti:Sa pumped home-built frequency-doubled non-collinear optical parametric amplifier (NOPA). The excitation power was $\approx$ 0.1 mW and the pulse duration $\approx$ 50 fs (Gaussian FWHM). The fluorescence at 12 different emission wavelengths in the range of λ_{fl} = 410 − 520 nm was collected and focused into a 1 mm BBO crystal for type I sum frequency generation (θ_N = 54.4°). The Ti:Sa fundamental at λ = 775 nm with a pulse duration of $\approx$ 150 fs (Gaussian FWHM) was used as gate pulse. Temporal resolution was achieved by a computer-controlled delay stage carrying a retroreflector in the gate beam path. The time zero of the experiment was defined by the simultaneous arrival of gate and pump pulse in the BBO crystal and determined by the cross correlation signal with scattered pump light. The full width at half maximum (FWHM) of the cross peak was determined to be $\approx$ 350 fs, resulting in a time resolution of $\approx$ 150 fs after deconvolution. All measurements were repeated several times with fresh sample solutions to ensure reproducibility. The ferulic acid concentration was c_{FA} = 50 μM for all measurements.

Broadband Fluorescence Kerr Gating Setup

To record broadband fluorescence spectra, the sample solution contained in a 1 mm flow cell was excited as in the fluorescence up-conversion setup, at $\lambda_{\text{pump}} = 320$ nm pulses resulting from a frequency-doubled, Ti:Sa pumped home-built NOPA. The emitted fluorescence was focused onto the Kerr medium (benzene) contained in a 1 mm path length cuvette. The Kerr medium was placed between two pairs of sheet polarisers (Moxtek, UBB01) in a cross-polarisation configuration. The laser fundamental at $\lambda = 800$ nm, which could be delayed temporarily *via* a translation stage, was focused onto the Kerr medium without passing the polarisers. The transmitted fluorescence then was focused on the entrance slit of a grating spectrograph (2150i, Princeton Instruments) and recorded spectrally resolved with a CCD camera (PI-MAX, Princeton Instruments). The recorded fluorescence spectra were spectrally corrected using a calibration curve generated by comparing static fluorescence spectra of 2-aminopyridine in water, measured with the Kerr-cell polarisers slightly detuned from the cross-polarisation configuration, with the spectral profile reported by Melhuish.[37] The time resolution of the setup was found to be ≈ 350 fs. The ferulic acid concentration was $c_{\text{FA}} = 400$ μM for all measurements.

Data Processing

The single-colour transient fluorescence spectroscopy yielded intensity-time profiles at the given fluorescence wavelength. The obtained time profiles were described by a sum of two decaying exponential functions, one of them rising with τ_{rise}, and both convoluted with a Gaussian $G_{\text{IRF}}(t)$ describing the instrument response function (IRF). For the fitting procedure, a non-linear least-squares routine based on the Levenberg-Marquardt algorithm implemented in Mathematica[38] was used.

In the case of the broadband experiment, transient spectra at different delay times were extracted from the recorded 2D map. They were fitted with a log-normal function[39] to quantify the dynamic Stokes shift. The temporal evolution of the respective fluorescence peak position can be described by the so-called solvation-correlation function[1,40,41]

$$C(t) = \frac{\tilde{\nu}(t) - \tilde{\nu}(\infty)}{\tilde{\nu}(0) - \tilde{\nu}(\infty)}. \tag{7.1}$$

In our case, the $\tilde{\nu}$'s refer to the maximum of the time-dependent emission spectra in wavenumbers, but the equation is also valid for other characteristics of the spectrum. The difficulty consists in determining precisely the transient spectrum in the moment of excitation, to give the peak position $\tilde{\nu}(0)$ before any solvent shell reorganisation has taken place. One possibility to calculate this 'time-zero spectrum' has been described by Fee and Maroncelli.[42] Here, we extrapolated the values for $\tilde{\nu}(0)$ from the $C(t)$ curves. As the fluorescence shift is not completed within the fluorescence lifetime of FA/H_2O and only hardly for FA/CTAB, the asymptotic baseline of $C(t)$ was taken as $\tilde{\nu}(\infty)$.[43]

7.3 Experimental Results

Static Absorption and Fluorescence Spectra

In Figure 7.2, the normalised static absorption and fluorescence spectra of ferulic acid in acetic buffer solution, CTAB micelles, $CHCl_3$, and *n*-hexane are shown. The first two absorption bands of ferulic acid are visible in all solvents, but the intensity of the second absorption band around 290 nm decreases with the solvent polarity until only a shoulder is visible in *n*-hexane. Both absorption bands show a slight blue-shift with increasing solvent polarity. The static emission spectra, however, show simultaneously a significant red-shift (56 nm from *n*-hexane to aqueous solution) as is expected for a polar solute.

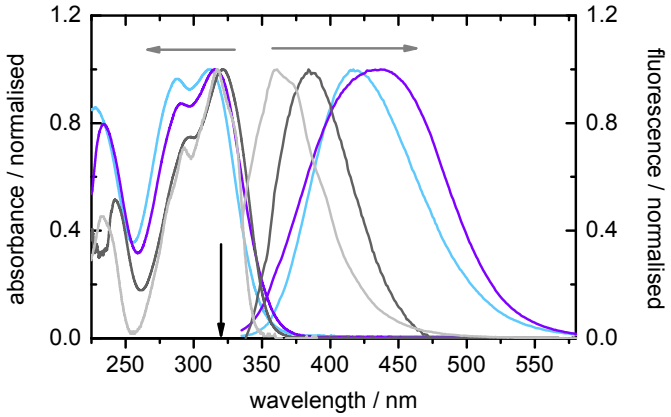

Fig. 7.2: Normalised static absorption ($\lambda < 350$ nm) and emission ($\lambda > 350$ nm) spectra of FA in CTAB micelles (violet), aqueous acetic buffer solution at pH 5.0 (light blue), $CHCl_3$ (grey) and *n*-hexane (light grey). The excitation wavelength $\lambda_{pump} = 320$ nm is indicated by with a vertical black arrow. The grey horizontal arrows denote the direction of band shifts with increasing solvent polarity.

Fluorescence-Time Profiles at Selected Wavelengths

Single-colour fluorescence-time profiles at three representative fluorescence wavelengths (λ_{fl} = 420, 460, and 500 nm) together with the overall fits and the underlying contributions for FA in aqueous solution and in micelles are displayed in Figure 7.3. The respective fit parameters are summarised in Table 7.1. The comparison of wavelength-dependent fluorescence-time profiles of FA/H_2O with FA/CTAB easily demonstrates the significantly longer excited-state lifetime for ferulic acid at the micellar surface. Additionally, the delayed rise of the emission is more distinct for FA/CTAB. Both effects grows more pronounced with increasing fluorescence wavelength. This can be seen even more clearly in Figure 7.4, where the overall fit functions describing the single-colour fluorescence-time profiles in the range from $\lambda_{fl} = 420 - 520$ nm in 10 nm steps are shown up to 20 ps after

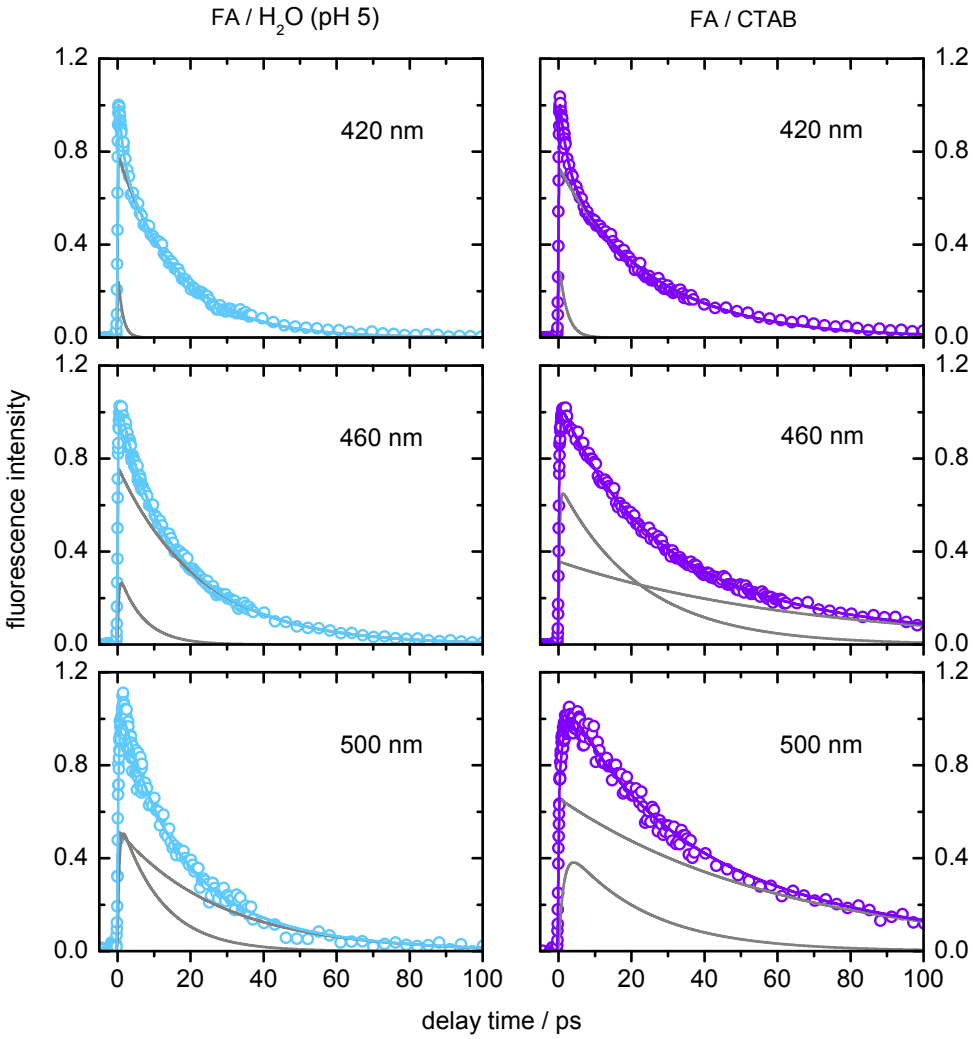

Fig. 7.3: Fluorescence-time profiles of FA at λ_{fl} = 420, 460, and 500 nm in acetic buffer solution at pH 5.0 (left column) and CTAB (right column) after excitation with $\lambda_{\mathrm{pump}} = 321$ nm. Circles represent the data points, coloured lines the overall fit functions and grey lines the underlying contributions. The respective time constants are given in Table 7.1.

Table 7.1: Decay constants τ_i in ps and their relative amplitudes A_i fitted to the fluorescence-time profiles of of FA/H_2O and FA/CTAB in aqueous buffer solution at λ_{fl} = 420, 460, and 460 nm after excitation with λ_{pump} = 320 nm. The errors correspond to the 2σ standard deviation.

	λ_{fl} / nm	A_1	τ_1 / ps	A_2	τ_{rise} / ps	τ_2 / ps
	420	0.72	16.2±0.3	0.28		1.3±0.1
FA/H_2O	460	0.71	23±1	0.29	0.31±0.06	7±1
	500	0.47	28±5	0.53	0.46±0.12	12±3
	420	0.69	25±1	0.31	0.09±0.04	2.1±0.2
FA/CTAB	460	0.34	67±8	0.66	0.28±0.02	22±2
	500	0.59	61±3	0.41	1.4±0.2	22±3

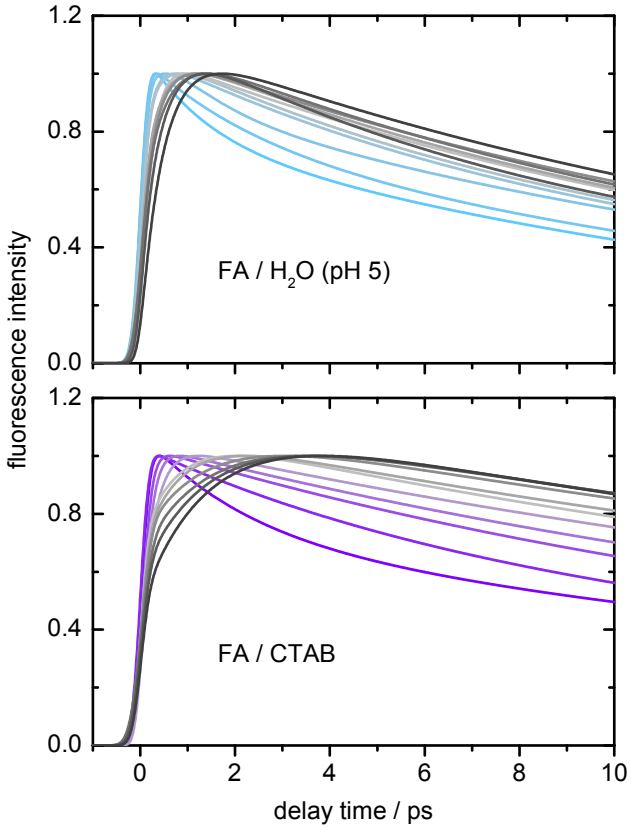

Fig. 7.4: Overall fit functions describing the fluorescence-time profiles of FA in acetic buffer solution at pH 5.0 (top, light blue to dark gray) and CTAB (bottom, violet to dark gray) after excitation with $\lambda_{\text{pump}} = 321$ nm. The emission range is $\lambda_{\text{fl}} = 420 - 520$ nm in 10 nm steps, whereupon the shorter wavelengths are depicted in colour and the longer wavelengths in dark gray. The data points have been left out for clarity.

excitation. The increase in fluorescence lifetime and the delayed rise of the fluorescence-time profile with increasing emission wavelength is observed for both FA in buffered water and at the micellar surface. However, for FA/CTAB the effect is significantly enhanced compared to FA/H_2O. From the fluorescence up-conversion data, a clear alteration of the deactivation dynamics due to steric hindrances can be deduced. But as the emission band shifts significantly to the red, resulting in apparently gradually longer lifetimes for the red fluorescence wavelengths, the fitted time constants at single emission wavelengths do not have a direct physical meaning.

Transient Fluorescence Spectra

In Figure 7.5, the recorded broadband fluorescence spectra of FA/H_2O (left column) and FA/CTAB (right column) are displayed as two-dimensional spectro-temporal maps. The wavelength is displayed on the abscissa, the delay time on the ordinate, and the fluorescence intensity is colour-coded. The upper maps are shown up to delay times $\Delta t = 10$ ps, the lower maps monitor the fluorescence up to $\Delta t = 100$ ps.

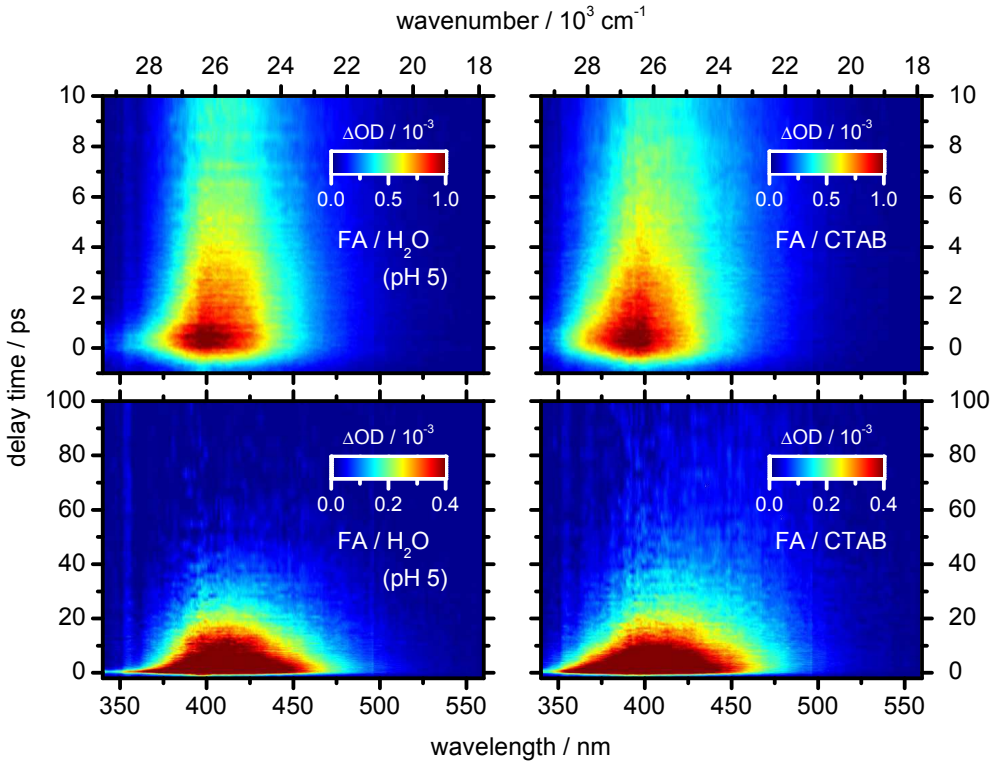

Fig. 7.5: Two-dimensional spectro-temporal fluorescence maps of FA in solution in acetic buffer solution (left) and CTAB (right) after excitation with $\lambda_{\text{pump}} = 320$ nm up to delay times $\Delta t = 10$ ps (top) and $\Delta t = 100$ ps (bottom).

The comparison reveals that ferulic acid in bulk aqueous solution emits fluorescence up to ≈ 50 ps after excitation, whereas for FA at the micellar interface emission can be detected up to ≈ 100 ps after excitation. The FA/H_2O spectrum is also narrower and shifts faster within the first few ps than its FA/CTAB counterpart.

The differences can more clearly be observed in the transient fluorescence spectra at different delay times displayed in Figure 7.6. The transient fluorescence spectra are depicted in colour, the respective static emission spectrum (grey) is depicted for comparison. The transient spectra emphasise the difference in emission between FA in the bulk phase and the interface nicely:

(i) The FA/H_2O systems emits fluorescence only half as long as the FA/CTAB sample (≈ 40 ps *vs.* ≈ 90 ps).
(ii) The emission spectrum of FA/CTAB is broader over the whole observation time.
(iii) The initial blue-shift of the fluorescence is faster for FA/H_2O.

An interesting feature for both sample solutions consists in the observation of transient fluorescence spectra which peak at longer wavelength than the respective static emission spectrum. As the fluorescence lifetime of ferulic acid is short, the quite blue transient spectra directly after excitation contribute to a significant amount to the static spectrum, which is defined as the sum of all transient spectra up to infinite times.

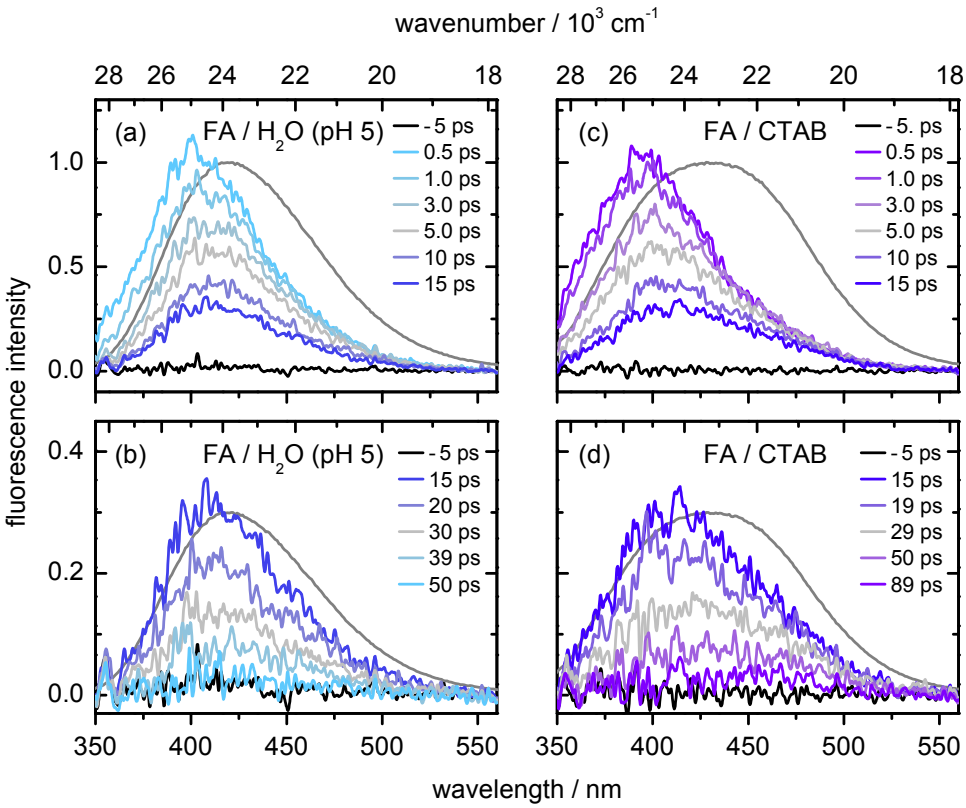

Fig. 7.6: Transient fluorescence spectra of FA in solution in acetic buffer solution (left) and CTAB (right) at different delay times Δt after excitation with $\lambda_{\text{pump}} = 320$ nm. Note the different Δt values in the lower panels. The grey spectrum corresponds to the respective static emission spectrum. The energy scale is given in nm (bottom) and cm^{-1} (top).

Fluorescence Lifetimes and Solvation Correlation Functions

To quantify the total fluorescence lifetime, omitting effects from fluorescence band shifts, the total emission from $340 - 560$ nm recorded by the Kerr gating spectrometer was spectrally integrated and described by a multi-exponential decay. The data points together with the overall fits and the underlying contributions are shown in Figure 7.7. For the description of the emission decay of ferulic acid in both aqueous solution and at the micellar surface, three exponentials were required. A very fast component with τ_{FL1} below our time resolution of ≈ 150 fs was necessary to describe the data in both cases. In addition, for FA in aqueous buffer solution the decay constants

$$\tau_{\text{FL2,aq}} = 2.8 \pm 1.9 \text{ ps and}$$
$$\tau_{\text{FL3,aq}} = 19 \pm 2 \text{ ps}$$

were found. For FA at the micellar surface the respective values were

$$\tau_{\text{FL2,CTAB}} = 6.4 \pm 1.9 \text{ ps and}$$
$$\tau_{\text{FL3,CTAB}} = 33 \pm 7 \text{ ps.}$$

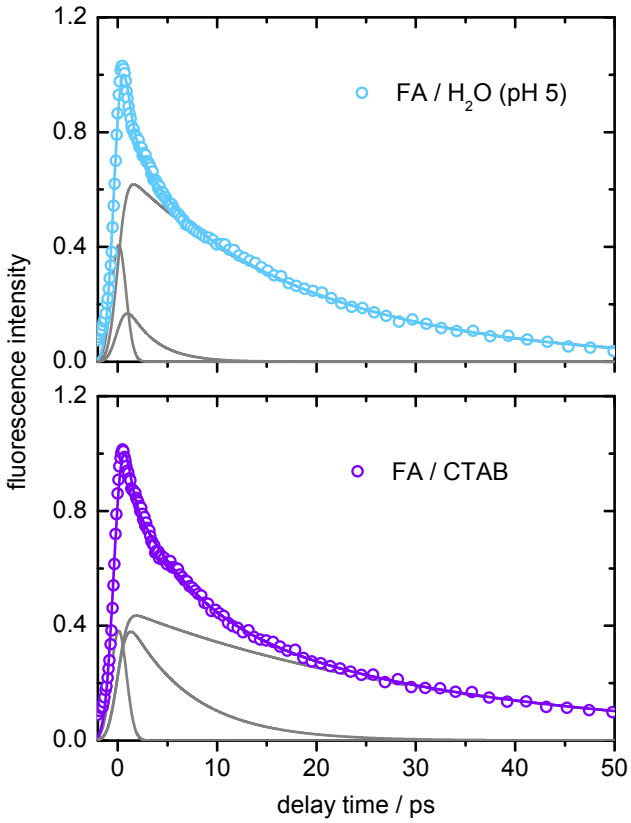

Fig. 7.7: Spectrally integrated fluorescence-time profiles of FA in solution in acetic buffer solution (top) and CTAB (bottom) after excitation with $\lambda_{\mathrm{pump}} = 320$ nm. Circles represent the data points, coloured lines the overall fit functions and grey lines the underlying contributions. The apparent dip at $\Delta t \approx 5$ ps in the lower panel is merely an artefact of the spectral integration and does not have a physical meaning.

The lifetime of ferulic acid at the micellar surface is altogether approximately twice as long as in aqueous solution. The ratio of the relative amplitudes of the decay constants τ_{FL2} and τ_{FL3} was determined to 1 : 2.7 for FA/H_2O and 1 : 1 for FA/CTAB.

For calculating the solvation-correlation function $C(t)$ according to Eq. 7.2, only the peak position $\tilde{\nu}(t)$ in wavenumbers of the emission spectrum was needed, not the shape. As it was not possible to obtain a transient fluorescence spectrum at 'time zero' of the experiment due to the limited time resolution of our experiment, $\tilde{\nu}(0)$ was extrapolated from the initial $C(t)$ decay (cf. Figure 7.8 below). We chose this approximation as $\tilde{\nu}(0)$ is merely a scaling factor, and little variations did not affect the temporal behaviour of $C(t)$ significantly. In the present case, the solvation dynamics timescale is comparable to the fluorescence lifetime, and the correct value for $\tilde{\nu}(\infty)$ cannot be taken from the static spectrum, but from the asymptotic baseline of $C(t)$.[43] The resulting solvation correlation functions together with the underlying fits are displayed in Figure 7.8.

The clear time-dependent red-shift of the transient fluorescence spectra already observable in the transient spectra shown in Figure 7.6 is described quantitatively by Eq. 7.2. The

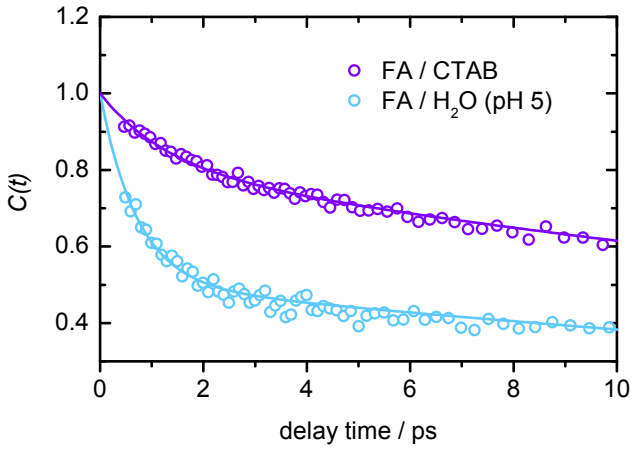

Fig. 7.8: Solvation correlation functions $C(t)$ for FA in acetic buffer solution (light blue) and in CTAB micelles (violet) after excitation with $\lambda_{\mathrm{pump}} = 320$ nm. Symbols represent the data points, solid lines the overall fit functions.

respective data could be fitted by two independent exponential decay functions to give the time constants

$$\tau_{\mathrm{s1,aq}} = 0.7 \pm 0.3 \text{ ps } (50\,\%) \text{ and}$$
$$\tau_{\mathrm{s2,aq}} = 37 \pm 5 \text{ ps } (50\,\%)$$

for FA in aqueous buffer solution and

$$\tau_{\mathrm{s1,CTAB}} = 1.3 \pm 0.9 \text{ ps } (20\,\%) \text{ and}$$
$$\tau_{\mathrm{s2,CTAB}} = 37 \pm 3 \text{ ps } (80\,\%)$$

for FA at the surface of CTAB micelles (see Figure 7.8). Additionally to the prolonged time constant τ_{s1}, the relative amplitude of the two components change. Whereas for FA/H_2O τ_{s1} and τ_{s2} contribute equally to the overall decay, at the micellar surface the longer component τ_{s2} clearly dominates the dynamics. The amplitude weighted average time constants

$$\langle \tau_{\mathrm{s,aq}} \rangle = 19 \pm 2 \text{ ps and}$$
$$\langle \tau_{\mathrm{s,CTAB}} \rangle = 30 \pm 2 \text{ ps}$$

illustrate the profound difference in solvent shell mobility quite clearly.

7.4 DFT Calculations

Calculations on the TD-DFT level of theory employing the B3LYP functional and the cc-pVDZ basis set were performed to determine the nature of the first excited states of ferulic acid and to possibly gain insight into the decay mechanism. The ground and the first

three excited states S_1 ($\pi\pi_1^*$), S_2 ($n\pi^*$) and S_3 ($\pi\pi_2^*$) were optimised without constraints. Having identified the respective minimum geometries $S_{x,min}$ for each state S_x, the vertical excitation energies, total energies in relation to S_0 in the optimised ground state, dipole moments and oscillator strengths for the ground state and the first three excited states were calculated and can be found in Table 7.2.

Upon vertical excitation, there is a large change in dipole moment from the ground to the first excited state ($\mu = 2.86$ D $\rightarrow \mu = 8.78$ D), which indicates a certain charge separation. For all optimised geometries, the dipole moments of the excited states follow the order $\mu(S_1) > \mu(S_3) > \mu(S_2) > \mu(S_0)$, except for $S_{2,min}$ ($n\pi^*$), where S_0 and S_2 change places. Furthermore, the energetic splitting between the first and the third excited state was found to be 37 nm, which is in reasonable agreement with the experimental finding of the splitting of the first two absorption bands of $30-36$ nm in all solvents. The experimental splitting has been taken from the fitting of the absorption spectrum with two Gaussian functions as the two bands overlap to a large extent, thus distorting the band maxima. The second excited state shows no oscillator strength, indicating an optically dark state. This assignment is supported by the involved molecular orbitals. The transitions could be assigned as follows: S_1 corresponds to a HOMO $\rightarrow$ LUMO excitation and therefore to a $\pi\pi^*$ state. The HOMO-2 $\rightarrow$ LUMO transition conforms with S_2 and a $n\pi^*$ state, finally S_3

Table 7.2: Vertical excitation energies (VEE, in eV), total energies (TE in eV, in relation to S_0 in the optimised ground state), oscillator strengths f and dipole moments μ in Debye of the ground and the first three excited states of ferulic acid in the gas phase at four different geometries $S_{x,min}$ according to TD-B3LYP/cc-pVDZ calculations.

geometry	State	VEE	TE	f	μ
$S_{0,min}$ (gs)	gs		0.00		2.86
	S_1	3.92	3.92	0.44	8.78
	S_2	4.40	4.40	0.00	5.38
	S_3	4.44	4.44	0.11	6.03
$S_{1,min}$ ($\pi\pi_1^*$)	gs		0.19		3.82
	S_1	3.55	3.74	0.36	9.51
	S_2	4.04	4.23	0.00	4.54
	S_3	4.27	4.46	0.18	6.73
$S_{2,min}$ ($n\pi^*$)	gs		0.86		4.94
	S_1	3.53	4.39	0.55	8.37
	S_2	2.77	3.63	0.00	3.12
	S_3	4.05	4.91	0.13	7.34
$S_{3,min}$ ($\pi\pi_2^*$)	gs		0.16		3.46
	S_1	3.75	3.90	0.41	8.91
	S_2	4.06	4.22	0.00	4.91
	S_3	4.14	4.30	0.20	7.16

is allocated to the HOMO-1 → LUMO transition which is again a $\pi\pi^*$ state. The LUMO, which is the destination orbital in all cases, features a node through the vinylic double bond, thus indicating its weakening.

After geometry optimisation in the excited state, the orbital order changes. Most importantly, S_2 now lies lower than S_1. The total energies of the discussed states are shown in Figure 7.9. From this sketch, a deactivation pathway along the geometric relaxation of the initially excited $\pi\pi^*$ to the $n\pi^*$ state seems feasible.

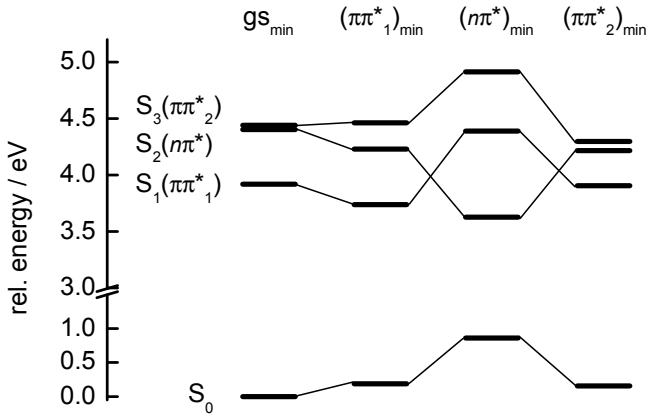

Fig. 7.9: Total energies according to TD-B3LYP/cc-pVDZ calculations of the ground and the first three excited states of ferulic acid at different geometries. $S_{x,min}$ stands for the minimum energy geometry after optimisation of the respective state S_x.

7.5 Discussion

The experimental findings of static and time-resolved measurements and theoretical calculations can be summarised as follows:

(i) Static emission spectra of ferulic acid in different solvents revealed an increasing Stokes shift with increasing solvent polarity. The emission maximum difference between FA in *n*-hexane and water amounts to 3700 cm^{-1}, which demonstrates the pronounced difference in excited-state stabilisation.

(ii) The fluorescence lifetime of ferulic acid at the micellar surface is nearly twice as long as the corresponding value for FA in bulk buffer solution ($\tau_{FL3,aq} = 19 \pm 2$ ps *vs.* $\tau_{FL3,CTAB} = 33 \pm 7$ ps).

(iii) The amplitude weighted average time constants for the solvation response are comparable to the fluorescence lifetimes ($\langle\tau_{s,aq}\rangle = 19 \pm 2$ ps *vs.* $\langle\tau_{s,CTAB}\rangle = 30 \pm 2$ ps). In particular, the initial solvation dynamics differ strongly. FA/H_2O exhibits a bulk-water like response ($\tau_{s1,aq} = 0.7 \pm 0.3$ ps, 50% relative amplitude), whereas the respective value for FA/CTAB is prolonged and decreased in amplitude ($\tau_{s1,aq} = 1.3 \pm 0.9$ ps, 20% relative amplitude).

(iv) TD-DFT calculations of FA in the gas phase revealed huge differences in the dipole moments of the ground and the first three electronically excited states and found the destination orbital for the first three transitions to possess a node through the vinylic double bond.

Fluorescence Lifetime

The observed fluorescence lifetime monitors the depopulation of the initially populated bright $\pi\pi^*$ state. The molecule subsequently returns to the electronic ground state either *via* an optically dark state or directly through conical intersections of the initially excited state with the ground state. The first possibility is rationalised by calculations on ferulic acid in the gas phase on the TD-DFT level of theory, which found an $n\pi^*$ state without oscillator strength with respect to the ground state. Upon geometry optimisation, the $n\pi^*$ state lies lower in energy than the initially excited $\pi\pi^*$ state, thus suggesting a deactivation pathway involving the optically dark $n\pi^*$ state. In contrast, Vengris *et al.* found an excited-state lifetime of 19 ps for FA in aqueous phosphate buffer (pH 7) by transient absorption measurements after excitation at $\lambda_{pump} = 318$ nm and no hint at the population of longer-lived states.[44] However, they did not follow the ground state recovery directly, therefore a definite exclusion of the involvement of longer-lived states is not possible.

Another possible deactivation pathway involves the $E \rightarrow Z$ isomerisation of ferulic acid upon UV irradiation.[45,46] Fast direct electronic deactivation in the picosecond range through conical intersections is typical for isomerising molecules.[47–49] In these cases, the conical intersection of the initially excited state with the ground state is reached after a

certain amount of torsion around the isomerising single or double bond has already taken place. The involvement of an isomerisation motion in the electronic deactivation pathway nicely explains the prolongation of the fluorescence lifetime of FA at the micellar surface: Most likely, the chromophore is sterically hindered by the close proximity of emulsifier headgroups, which presumably slows down the rotation around the vinylic double bond. The performed TD-DFT calculations support this assumption, as the destination orbital after UV excitation with $\lambda = 320$ nm features a node through the vinylic double bond.

The manipulation of excited-state surfaces by sterically hindering the molecular motions associated with the electronic deactivation pathway has also been shown in the case of *p*-coumaric acid, for which the excited-state lifetime was increased considerably by blocking the $E \rightarrow Z$ movement.[50] It has to be noted that Vengris *et al.* did not observe product absorption bands of the *Z*-isomer upon excitation of FA at $\lambda_{\mathrm{pump}} = 318$ nm.[44] Either the isomerisation quantum yield lies below the detection limit of $\approx 3\%$, or the respective bands might lie outside the employed detection window in the respective study ($\lambda_{\mathrm{probe}} = 370-650$ nm).

Solvent Shell Mobility

The amplitude weighted average time constants of the solvation response are quite similar to those of the fluorescence lifetime for both FA/H_2O and FA/CTAB. This finding has no direct physical meaning and merely illustrates the difficulties upon investigating the solvent shell mobility around a very short-lived chromophore. More precisely, the transient fluorescence spectra decay quite fast while still red-shifting, making it impossible to determine unambiguously the fluorescence spectrum emitted after completion of the solvent shell reorganisation. The temporal behaviour of the biphasic solvation correlation function $C(t)$ has therefore to be considered with care after the first few picoseconds. This is especially true for FA/H_2O, where the minimum of the PES of the solvated excited molecule is not reached within the fluorescence lifetime. At the micellar surface, the completion of the solvent shell rearrangement is presumably just completed within the accessible dynamic range of our experimental setup, although the weak intensities of the fluorescence spectra after $\Delta t = 50$ ps demand caution with this statement.

The initial solvation dynamics around FA, however, are clearly observable and quite dependent on the micro-environment. In bulk aqueous solution, the observed fast initial decay $\tau_{\mathrm{s1,aq}} = 0.7 \pm 0.3$ ps accounts for 50% of the overall solvation response and is in good agreement with literature.[2–8,10–15] For FA/CTAB, the initial response is clearly slowed down ($\tau_{\mathrm{s1,aq}} = 1.3 \pm 0.9$ ps) and only accounts for a fifth of the overall solvation correlation function. The rearrangement of the second or further solvation shells is monitored by the solvation dynamics after the first few picoseconds. As mentioned above, the determination of an unambiguous time constant for the slower dynamics is difficult. The overall decay dynamics are therefore best analysed by comparing the respective amplitude

weighted average time constants ($\langle\tau_{s,aq}\rangle = 19 \pm 2$ ps *vs.* $\langle\tau_{s,CTAB}\rangle = 30 \pm 2$ ps). Both the initial as well as the overall solvation response indicate a severely restricted solvent shell at the micellar surface. This is most likely due to electrostatic interactions of the polar water molecules with the charged ammonium headgroups of the emulsifier molecules.

In conclusion, the incorporation of FA at the water/micelle interface led to clearly observable differences in both fluorescence lifetime and solvent shell mobility compared with a bulk water environment. The monitoring of the fluorescence Stokes shift in emission by femtosecond time-resolved broadband fluorescence proved to be a very sensitive and straightforward tool to analyse the micro-environment of ferulic acid. Consequently, the investigation of alterations in the water solvent shell mobility around a fluorescence chromophore within, e.g., varying micellar systems should directly elucidate the penetration depth into the palisade layer and the strength of electrostatic interactions with different headgroups.

7.6 Conclusion

In summary, we presented the ultrafast solvation dynamics of the natural antioxidant ferulic acid in aqueous buffer solution and in a micellar environment with *sub*-picosecond time resolution. The time-dependent Stokes shift could be observed by broadband transient fluorescence spectroscopy and was described with a solvation-correlation function to give the amplitude weighted average time constants $\langle\tau_{s,aq}\rangle = 19 \pm 2$ ps for FA in aqueous solution and $\langle\tau_{s,CTAB}\rangle = 30 \pm 2$ ps for FA at the surface of CTAB micelles. We assign the clearly observable difference in solvent shell mobility to the restraints at the micellar surface, which most likely arise due to electrostatic interactions of water molecules with the polar headgroups of emulsifier molecules. The recorded fluorescence lifetime monitors the fast depopulation of the excited state and has been determined to $\tau_{FL3,aq} = 19 \pm 2$ ps and $\tau_{FL3,CTAB} = 33 \pm 7$ ps. The prolongation of excited-state lifetime at the water/micelle interface and calculations on the TD-DFT level of theory indicate the involvement of an (uncompleted) $E \rightarrow Z$ isomerisation of the vinylic double bond in the deactivation pathway.

References

[1] M. Maroncelli, J. MacInnis, G. R. Fleming, *Science* **243**, 1674 (1989).

[2] W. Jarzeba, G. C. Walker, A. E. Johnson, M. A. Kahlow, P. F. Barbara, *J. Phys. Chem.* **92**, 7039 (1988).

[3] R. Jimenez, G. R. Fleming, P. V. Kumar, M. Maroncelli, *Nature* **369**, 471 (1994).

[4] R. E. Riter, D. M. Willard, N. E. Levinger, *J. Phys. Chem. B* **102**, 2705 (1998).

[5] D. Pant, R. E. Riter, N. E. Levinger, *J. Chem. Phys.* **109**, 9995 (1998).

[6] A. V. Benderskii, K. B. Eisenthal, *J. Phys. Chem. B* **104**, 11723 (2000).

[7] X. Shen, J. R. Knutson, *J. Phys. Chem. B* **105**, 6260 (2001).

[8] D. Zhong, S. K. Pal, D. Zhang, S. I. Chan, A. H. Zewail, *Proc. Natl. Acad. Sci. U.S.A.* **99**, 13 (2002).

[9] W. Lu, J. Kim, W. Qiu, D. Zhong, *Chem. Phys. Lett.* **388**, 120 (2004).

[10] R. K. Mitra, S. S. Sinha, S. K. Pal, *Langmuir* **24**, 49 (2008).

[11] Y. Rao, N. J. Turro, K. B. Eisenthal, *J. Phys. Chem. C* **114**, 17703 (2010).

[12] M. Sajadi, M. Weinberger, H.-A. Wagenknecht, N. P. Ernsting, *Phys. Chem. Chem. Phys.* **13**, 17768 (2011).

[13] M. Maroncelli, G. R. Fleming, *J. Chem. Phys.* **89**, 5044 (1988).

[14] S. Roy, B. Bagchi, *J. Chem. Phys.* **99**, 9938 (1993).

[15] N. Nandi, S. Roy, B. Bagchi, *J. Chem. Phys.* **102**, 1390 (1995).

[16] K. Bhattacharyya, *J. Photosci.* **6**, 123 (1999).

[17] S. Vajda, R. Jimenez, S. J. Rosenthal, V. Fidler, G. R. Fleming, J. Castner, Edward W., *J. Chem. Soc., Faraday Trans.* **91**, 867 (1995).

[18] N. Sarkar, K. Das, A. Datta, S. Das, K. Bhattacharyya, *J. Phys. Chem.* **100**, 10523 (1996).

[19] N. Sarkar, A. Datta, S. Das, K. Bhattacharyya, *J. Phys. Chem.* **100**, 15483 (1996).

[20] D. M. Willard, R. E. Riter, N. E. Levinger, *J. Am. Chem. Soc.* **120**, 4151 (1998).

[21] J. Kim, W. Lu, W. Qiu, L. Wang, M. Caffrey, D. Zhong, *J. Phys. Chem. B* **110**, 21994 (2006).

[22] D. Andreatta, J. L. P. Lustres, S. A. Kovalenko, N. P. Ernsting, C. J. Murphy, R. S. Coleman, M. A. Berg, *J. Am. Chem. Soc.* **127**, 7270 (2005).

[23] F. Berndt, I. Ioffe, A. A. Granovsky, R. Mahrwald, S. Tannert, S. A. Kovalenko, N. P. Ernsting, *J. Photochem. Photobiol., A* **234**, 164 (2012).

[24] K. Oehlke, A. Heins, H. Stöckmann, K. Schwarz, *Food Chemistry* **118(1)**, 48 (2009).

[25] K. Schwarz, E. N. Frankel, J. B. German, *Fett/Lipid* **98**, 115 (1996).

[26] H. Stockmann, K. Schwarz, T. Huynh-Ba, *J. Am. Oil Chem. Soc.* **77**, 535 (2000).

[27] W. A. Pryor, J. A. Cornicelli, L. J. Devall, B. Tait, B. K. Trivedi, D. T. Witiak, M. Wu, *J. Org. Chem.* **58**, 3521 (1993).

[28] S. S. Pekkarinen, H. Stoeckmann, K. Schwarz, I. M. Heinonen, A. I. Hopia, *J. Agric. Food Chem.* **47**, 3036 (1999).

[29] A. Heins, D. B. McPhail, T. Sokolowski, H. Stoeckmann, K. Schwarz, *Lipids* **42**, 573 (2007).

[30] A. Heins, T. Sokolowski, H. Stoeckmann, K. Schwarz, *Lipids* **42**, 561 (2007).

[31] K. Oehlke, V. M. Garamus, A. Heins, H. Stoeckmann, K. Schwarz, *J. Colloid Interface Sci.* **322**, 294 (2008).

[32] K. Kuperkar, L. Abezgauz, K. Prasad, P. Bahadur, *J. Surfactants Deterg.* **13**, 293 (2010).

[33] S. P. Ozkorucuklu, J. L. Beltrán, G. Fonrodona, D. Barrón, G. Alsancak, J. Barbosa, *J. Chem. Eng. Data* **54**, 807 (2009).

[34] F. Z. Erdemgil, S. Şanli, N. Şanli, G. Özkan, J. Barbosa, J. Guiteras, J. L. Beltrán, *Talanta* **72**, 489 (2007).

[35] T. Pancur, F. Renth, F. Temps, B. Harbaum, A. Krueger, R. Herges, C. Naether, *Phys. Chem. Chem. Phys.* **7**, 1985 (2005).

[36] T. Pancur, N. K. Schwalb, F. Renth, F. Temps, *Chem. Phys.* **313**, 199 (2005).

[37] W. H. Melhuish, *J. Res. Nat. Bur. Stand., Sect. A* **76**, 547 (1972).

[38] Wolfram Research, *Mathematica Edition: Version 7.0* (Wolfram Research, Inc., Champaign, Illinois, 2008).

[39] D. B. Siano, D. E. Metzler, *J. Chem. Phys.* **51**, 1856 (1969).

[40] G. Van der Zwan, J. T. Hynes, *J. Phys. Chem.* **89**, 4181 (1985).

[41] B. Bagchi, D. W. Oxtoby, G. R. Fleming, *Chem. Phys.* **86**, 257 (1984).

[42] R. S. Fee, M. Maroncelli, *Chem. Phys.* **183**, 235 (1994).

[43] K. Hara, H. Kuwabara, O. Kajimoto, *J. Phys. Chem. A* **105**, 7174 (2001).

[44] M. Vengris, D. S. Larsen, M. A. Van der Horst, O. F. A. Larsen, K. J. Hellingwerf, R. Van Grondelle, *J. Phys. Chem. B* **109**, 4197 (2005).

[45] G. Kahnt, *Phytochemistry* **6**, 755 (1967).

[46] A. M. Brouwer, S. M. Fazio, N. Haraszkiewicz, D. A. Leigh, C. M. Lennon, *Photochem. Photobiol. Sci.* **6**, 480 (2007).

[47] R. Siewertsen, J. B. Schoenborn, B. Hartke, F. Renth, F. Temps, *Phys. Chem. Chem. Phys.* **13**, 1054 (2011).

[48] S. A. Kovalenko, A. L. Dobryakov, I. Ioffe, N. P. Ernsting, *Chem. Phys. Lett.* **493**, 255 (2010).

[49] R. Siewertsen, F. Renth, F. Temps, F. Soennichsen, *Phys. Chem. Chem. Phys.* **11**, 5952 (2009).

[50] M. Vengris, M. A. van der Horst, G. Zgrablic, I. H. M. van Stokkum, S. Haacke, M. Chergui, K. J. Hellingwerf, R. van Grondelle, D. S. Larsen, *Biophys. J.* **87**, 1848 (2004).

8

Summary and Outlook

This Thesis dealt with two main topics: the electronic deactivation dynamics of small DNA building blocks and the ultrafast solvation dynamics of the natural antioxidant ferulic acid. In the following, the respective results and conclusions as presented in Chapters 3 – 7 shall be summarised briefly. A short outlook will then be given on ongoing work, desirable further investigations, and possible improvements of the Kerr gating setup.

8.1 Electronic Deactivation Dynamics of Small DNA Building Blocks

The electronic deactivation dynamics after UV excitation of DNA, its monomers and small building blocks are complex. The observed excited-state lifetimes span several orders of magnitude and the deactivation pathways are hotly debated. Deoxyribonucleic acid as a huge biopolymer is difficult to understand without unravelling the contributions and interplay of different characteristics, such as base sequence, hydrogen bonding and π-stacking. During the course of this Thesis, several small DNA building blocks were investigated, namely the π-stacked dinucleotides d(ApA) (cf. Chapters 3 and 4) and d(ApG) (cf. Chapter 5) and the hydrogen-bonded self-complementary DNA hairpin d[5'-GpGpGp-HEG-pCpCpC-3'] (cf. Chapter 6). With these systems, all three above mentioned effects can be monitored and compared.

The influence of base stacking interactions was studied with two of the simplest possible model systems, the adenine homo-dinucleotide d(ApA) and the hetero-dinucleotide d(ApG). A thorough combined femtosecond time-resolved fluorescence and absorption investigation led to a complete picture of the overall electronic deactivation dynamics. In particular, the pathway in the electronically excited state could be monitored from the population of the initially excited bright $\pi\pi^*$ states *via* relaxed Franck-Condon states and

a long-lived excimer state back to the electronic ground state. An astonishing feature is the observation of an 'excimer band' around 340 nm observed for both dinucleotides in transient absorption measurements. For d(ApA), the longevity of the respective band and the very narrow band structure allowed for the assignment to the newly-formed, energetically stabilised excimer, in contrast to a second narrow absorption band which monitors the relaxation in the initially excited, 'perturbed-monomer-like' Frank-Condon states. The excimer signature was then also found in the transient absorption spectra of d(ApG), besides a more unstructured absorption band reflecting the complicated excited-state geometry introduced by two different interacting subunits. To the best of our knowledge, the exceptional structure of the transient absorption spectra was observed and presented for the first time in this Thesis.

The excimer state is relatively stable, its lifetime was determined to $\tau = 380$ ps for d(ApA) and $\tau = 124$ ps for d(ApG). It is reached within at most a few ps after excitation in both cases. The different stabilities of the formed excimer states shed light on the base sequence effect. Theoretical investigations of the adenine homodimer suggest that at least two excimer states with different interbase orientations can be formed.[G. Olaso-González *et al.*, *J. Am. Chem. Soc.* **131**, 4368 (2009)] The most stable excimer state was found to exhibit a face-to-face configuration, in which the two subunits lie directly on top of each other. An excimer state with intermediate stability and lifetime possesses a B-DNA like configuration. This assumption agrees well with the observed base sequence dependence of the excited-state lifetime: For the hetero-dinucleotide d(ApG) the stable face-to-face conformation like in the homo-dinucleotide is not accessible, as the orbital overlap cannot be as perfect as with to identical subunits, the excimer lifetime in d(ApG) accordingly is about three times shorter ($\tau_{\mathrm{d(ApG)}} = 124$ ps *vs.* $\tau_{\mathrm{d(ApA)}} = 380$ ps). It has to be taken into account that the excimer state in d(ApG) likely possesses a partial charge-transfer character due to the different electron affinity of adenosine and guanosine. In the time-resolved fluorescence spectroscopy, only small contributions of the long-lived state were monitored, thus indicating that the excimer state is nearly optically dark. However, in transient absorption measurements which monitored the return to the electronic ground state, approximately a third of the initially excited molecules was found to deactivate *via* the excimer state. No additional long-lived states are populated. The weak long-lived emission on the other hand is intense enough to give rise to a pronounced, red-shifted emission band in the static fluorescence spectra.

The effect of hydrogen bonding is a little difficult to monitor. Single nucleobases, nucleosides or nucleotides dissolved in aqueous buffer solution will not pair, but are solvated individually by water molecules. One possibility to circumvent this obstruction is the change of solvent. However, it has to be considered that the stabilisation of excited electronic states differs depending on the solvent. For the Watson-Crick G·C base pair in $CHCl_3$ for example, a radical state $(\mathrm{G\text{-}H})^{\bullet}\cdot(\mathrm{C{+}H})^{\bullet}$ with a lifetime of $\tau \approx 3$ ps may be formed in $CHCl_3$,[K. Röttger, *unpublished results*] which might exhibit a different lifetime

in an aqueous environment. If one wants to stick to water as a solvent, a certain length of two complementary single strands of at least $10 - 20$ bases also ensures pairing. The resulting number of hydrogen bonds holds the strands in place while single base pairs may open and re-form. However, the required lengths of the single strands introduce a certain amount of π-stacking interactions. To break free from this dilemma, we designed a short, self-complementary DNA loop, which consists only of three base pairs. This molecule forms a stable, albeit quite flexible double strand in aqueous solution, while π-stacking interactions are minimised (cf. Chapter 6). A thorough NMR study together with static absorption, fluorescence and circular dichroism spectroscopy and molecular mechanics simulations confirmed the hydrogen-bonded double helical structure of the hairpin. Femtosecond time-resolved fluorescence measurements revealed very short excited-state lifetimes, consistent with a theoretical model which suggests an electron-driven proton transfer in the excited state along a barrierless pathway from the initially excited states to the electronic ground state.[A. L. Sobolewski and W. Domcke, *Phys. Chem. Chem. Phys.* **6**, 2763 (2004), A. L. Sobolewski *et al.*, *Proc. Natl. Acad. Sci. U.S.A.* **102**, 17903 (2005)] Preliminary transient absorption results excluded the population of long-lived dark excited states in the case of the loop model system.[K. Röttger, *unpublished results*] In contrast, π-stacking interactions led to prolonged excited-state lifetimes, probably due to excimer formation, for the short single stranded oligonucleotide $d(G)_3$. We therefore conclude that the presented DNA hairpin is an excellent model to investigate hydrogen-bonding effects in aqueous solution without the interfering superposition of π-stacking.

8.2 Solvation Dynamics of Ferulic Acid

The cinnamic acid derivative ferulic acid (FA) occurs naturally mainly in plants and exhibits antioxidant activity, i.e., it may protect unsaturated fatty acids against oxidation by acting as a radical catcher. The extent and mobility of a water solvent shell surrounding the polar molecule FA at an interfacial layer may reveal insights into how the steric constraints influence molecular motion and reactivity. During this Thesis, solvation dynamics studies of FA in bulk aqueous phase and at a micellar surface were performed and are presented in detail in Chapter 7.

The steric constraints which are exerted on FA at the water/micelle interface lead to two main effects: *(i)* the prolongation of total fluorescence lifetime compared to FA in bulk aqueous solution and *(ii)* the considerable distortion of solvent shell mobility, monitored by the time-dependent red-shift in the transient fluorescence spectra. The first point may be rationalised by assuming an electronic deactivation pathway involving the $E \rightarrow Z$ isomerisation of the vinylic double bond. Calculations on the TD-DFT level of theory suggest the deactivation to proceed from the initially excited optically bright $\pi\pi^*$ states to the ground state *via* an optically dark $n\pi^*$ state. The three lowest excited states have in common that an electron is brought to the LUMO, which is a π^* state featuring a node

through the vinylic double bond. The steric hindrance of the large-amplitude motion of the $E \rightarrow Z$ isomerisation approximately doubles the time which is needed the return to the electronic ground state.

Even more insight in the micro environment of ferulic acid at the micellar surface may be drawn from the observed changes in the solvation dynamics, visualised by time-dependent Stokes shift. At the interface, FA still possesses a water solvent shell, but its movement is severely hindered. The first water layer around FA at the micellar surface moves not only much slower than in bulk water, its relative contribution to the overall solvation dynamics also decreases. One may speculate that this is due to a partial destruction of the initial, 'bulk-water-like' solvent shell. The rearrangement of the second or further solvation shells is monitored by the solvation dynamics after the first few picoseconds and are best analysed by comparing the respective amplitude weighted average time constants ($\langle\tau_{\mathrm{s,aq}}\rangle = 19\pm2$ ps *vs.* $\langle\tau_{\mathrm{s,CTAB}}\rangle = 30\pm2$ ps). One can conclude that both the initial as well as the overall solvation response indicate a severely restricted solvent shell at the micellar surface. This is most likely due to electrostatic interactions of the polar water molecules with the charged ammonium headgroups of the emulsifier molecules. Overall, the used broadband fluorescence Kerr gating setup proved an excellent experiment to track the distortion of an excited-state surface by sterically hindering the molecular motion which is associated with the electronic deactivation pathway.

8.3 Outlook

Further measurements on DNA model systems will hopefully give even more detailed insight in the interplay of π-stacking interactions and base sequence. To this end, the comparison of d(ApG) with d(GpA) might be interesting, as through the right-handedness of the B-DNA helical structure the resulting orbital overlap is different, which should influence the excimer formation. In first preliminary fluorescence up-conversion measurements, no significant differences in the excited lifetimes were observed.[M. C. Stuhldreier, *unpublished results*] However, as the emission contribution of the nearly optically dark excimer state is quite small, transient absorption measurements may provide more information here. The comparison with the d(GpG) dimer is also promising, as in that case the face-to-face conformation analogue to the stable d(ApA) excimer conformation should be accessible. The respective measurements should be taken out with care, as the guanosine subunit is easily oxidised. The investigation of the dinucleotides d(CpC), d(TpT), d(CpT) and d(TpC) may reveal some information on the extent of base stacking between homo- or hetero-pyrimidine subunits, and additionally on the formation of cyclo-pyrimidine dimers, which are a major photolesion in DNA. However, as this topic opens up a widely spread set of questions, a thorough understanding of the purine dinucleotides should be aimed at first.

Fluorescence up-conversion measurements on a series of $\mathrm{d(A)}_n$ ($n = 1, 2, 4, 8, 20$) oligonu-

cleotides hint at a gradually decreasing accessibility of the stable face-to-face excimer conformation due to an increasingly stabilised B-DNA helical geometry.[M. C. Stuhldreier, *unpublished results*] Again transient absorption measurements especially on the short $d(A)_3$ and $d(A)_4$ molecules would be essential to follow the fate of the narrow 'excimer transient absorption band'. The change and evolution of the narrow excited-state absorption band structure observed for d(ApA) in a series of $d(A)_n$ oligonucleotides might settle some of the controversy regarding the localisation length of excitation energy upon UV excitation. To improve the time resolution of the transient absorption setup and to minimise unwanted coherent artefacts which stem from the glass windows of the sample cell, the implementation of a laminar flow jet is under way.[U. C. Stange, *unpublished results*] Hopefully, this allows for the unambiguous decision whether or not the 'excimer band' rises delayed after UV excitation.

Regarding the hydrogen bonded model system, NMR studies on further oligonucleotide loops are planned, which might improve the duplex forming. First preliminary results for a 'tetramer' $d(G)_2$-HEG-$d(C)_2$ and an 'octamer' $d(G)_4$-HEG-$d(C)_4$ correspondent to the investigated loop are promising. Both show base pairing, although in case of the tetramer it is rather weak. Temperature-dependent UV/vis and NMR spectra on the octamer will hopefully yield a sharper melting temperature, and 2D-NMR spectra of this system may allow us to calculate the helical structure with the help of NOESY cross peaks. Time-resolved measurements on the relatively stable paired octamer and even longer systems may indicate the strand length, at which π-stacking effects are more pronounced than the G·C deactivation pathway. At the beginning, pure G·C stacks may facilitate the interpretation of the observed deactivation time scales, but in the medium term mixed oligonucleotide hairpins such as d(GpCpGp-HEG-pCpGpC) or even d(GpApCpGp-HEG-pCpGpTpC) are better model systems, in which no 'register shift' as suggested by molecular dynamics simulations [M. Eriksson, *unpublished results*] should occur. Additionally, further molecular dynamics simulations on the investigated system(s) to investigate the probability of a 'register shift' as a function of linker length and oligonucleotide strand length could be useful.

The broadband fluorescence Kerr gating setup has proved to be suitable for monitoring the solvation dynamics around short-lived excited molecules. Corresponding measurements of ferulic acid in different solvents were performed in the course of a Diploma Thesis in our work group.[J. Wiese, *Diploma Thesis*, CAU Kiel (2012)] The experimental setup might be interesting for measurements related to the SFB 677 *Function by Switching*. Photo-switches such as azobenzenes, which undergo an $E \rightarrow Z$ isomerisation upon UV excitation, might be studied in various solvents with different viscosities to mimic embedding in constraining environments. Understanding the implications of constraining the large-amplitude isomerisation motion on the overall switching efficiency may be important regarding the future implementation of the respective molecules in materials.

The Kerr gating setup itself might be improved by a few small alterations:

(i) The search for a Kerr medium other than benzene would improve the time resolution significantly. For a moderately fluorescing molecule, CCl_4 might be tested, especially if the setup is already properly aligned and optimised.

(ii) Improvement of the signal intensity might be achieved by replacing the two aluminium-coated parabolic mirrors for the collection, collimation and refocusation of the emitted fluorescence light by silver-coated ones. Unfortunately, the use of reflecting mirrors is not recommendable, as the reflection angle would be too big for achieving an acceptable time resolution. A Cassegrain reflector might be an alternative, but is difficult to align.

(iii) The intensity of the pump pulse could be optimised by replacing all silver-coated focusing mirrors after frequency-doubling with HR266 coated ones, as in the fluorescence up-conversion setup. The same is true for the mirror focusing the gate beam into the Kerr medium. A high reflective coating at this point might prevent blurring of the polarisation angle, thus improving the S/N ratio.

Danksagung

An dieser Stelle möchte ich allen danken, die auf die eine oder andere Weise zum Gelingen dieser Doktorarbeit beigetragen haben:

- An erster Stelle möchte ich mich bei meinem Doktorvater Prof. Dr. Friedrich Temps für die Möglichkeit bedanken, auf einem so spannenden und anspruchsvollen Forschungsgebiet tätig sein zu dürfen. Seine stete Unterstützung, Anregung und konstruktive Kritik, seine mitreißende Begeisterung für die Forschung sowie zahllose wissenschaftliche Diskussionen haben maßgeblich zum Gelingen dieser Arbeit beigetragen.
- Mein besonderer Dank gilt meinen lieben Freundinnen/Kolleginnen (geht das überhaupt zusammen?) Katharina und Julia, ohne die die letzten Jahre weder innerhalb noch außerhalb der Uni auch nur halb so schön und lustig gewesen wären. Sowohl fachlich als auch persönlich möchte ich euch nicht missen!
- Ron und Nina danke ich für die Begleitung der ersten Schritte im Labor, ohne euch wäre der experimentelle Teil dieser Arbeit nicht möglich gewesen. Ron danke ich zudem noch sehr herzlich dafür, ein langjähriger wunderbarer Bürokollege gewesen zu sein, mit allzeit offenen Ohren für Fragen, Probleme oder einfach nur Quatschen...
- Prof. Dr. Frank Sönnichsen aus der spektroskopischen Abteilung der Organischen Chemie verdanke ich die umfassende NMR-spektroskopische Untersuchung des Oligonukleotid-Loops sowie unschätzbare Hilfe bei deren Auswertung.
- Mats und Prof. Dr. Bernd Hartke gebührt Dank für die Molekulardynamik-Rechnungen zum Oligonukleotid-Loop, sowie für die Geduld mit der sie mir diese näher gebracht haben.
- Kathleen, Julia und Prof. Dr. Karin Schwarz aus der Abteilung Lebensmitteltechnologie danke ich für das Kooperationsprojekt Ferulasäure sowie die Versorgung mit den entsprechenden Proben.
- Für die Bereitstellung von theoretischen Rechnungen zu Ferulasäure, $d(A)_2$ und d(ApG) sowie deren Diskussion danke ich Nevin.
- Tassilo hat mit der ESI-massenspektrometrischen Untersuchung von d(pApA) einen wertvollen Beitrag zu dessen Charakterisierung geleistet.
- Für die Mitarbeit bei $d(A)_2$ danke ich Carmen. Hendrik hat mit seiner Hilfe und unermüdlich guten Laune die Anfänge des Ferulasäure-Projektes unterstützt, zu welchem Joss ebenfalls viel beigetragen hat.
- Den gesamten Arbeitskreisen Temps und Friedrichs (aktuelle und frühere Mitglieder) gebührt herzlicher Dank für eine entspannte, lustige und produktive Arbeitsatmosphäre.

- Ein sehr großer Dank geht an das gesamte Werkstatt-Team sowie Klaus und Michael für die Geduld angesichts diverser Spezialanfertigungswünsche und -Probleme und deren meist blitzschnelle Lösung. Joachim war eine große Hilfe bei allen chemisch-synthetisch und statisch-spektroskopischen Fragen. Für die Unterstützung bei sämtlichen Computer-Fragen danke ich Uwe sehr herzlich.
- Frau von der Heydt und Tanja danke ich für die Hilfe bei diversen organisatorischen Fragen und Problemen.
- Viele weitere Freunde haben dafür gesorgt, dass ich die letzten Jahre nicht nur mit Wissenschaft beschäftigt war - dafür danke ich euch!
- Nicht zuletzt danke ich meiner Familie, für die finanzielle, ideelle und überhaupt jede denkbare Unterstützung.
- Sven danke ich für seine Geduld mit mir, seine bedingungslose Unterstützung in allen Lebenslagen und seine Liebe.